A NEW METHODOLOGY FOR CLIMATE MODEL SELECTION AND APPLICATION TO TEMPERATURE, HEAT WAVE, WBGT AND LABOR PRODUCTIVITY ANALYSIS

by

Hamza Altınsoy

M.S., Physics, Boğaziçi University, 2008

Submitted to the Institute for Graduate Studies in
Science and Engineering in partial fulfillment of
the requirements for the degree of
Doctor of Philosophy

Graduate Program in Physics

Boğaziçi University

2018

ACKNOWLEDGEMENTS

First, I would like to thank my advisor, Professor Levent Kurnaz, for giving me the chance to do my thesis work under his supervision. I am grateful for the opportunity he gave me to conduct research in the fascinating field of climate change and for the problem he proposed, which led me into many interesting and interrelated subjects of the field. This thesis would not have been possible without his scientific guidance and especially moral support.

I am also thankful to Sevil Acar Aytekin, Teoman Turgut, Mete Tayanç and Ahmet Öztopal for the critical reading of this thesis. I would like to thank the administrative staff of the Physics Department in Bogaziçi University for providing very friendly and fruitful environment for doing research and Hacı Ahmet Yıldırım for comments on some of the published articles.

I acknowledge the World Climate Research Programme's Working Group on Regional Climate, and the Working Group on Coupled Modelling, former coordinating body of CORDEX and responsible panel for CMIP5. I also thank the climate modelling groups for producing and making available their model output. I also acknowledge the Earth System Grid Federation infrastructure an international effort led by the U.S. Department of Energy's Program for Climate Model Diagnosis and Intercomparison, the European Network for Earth System Modelling and other partners in the Global Organization for Earth System Science Portals (GO-ESSP). I acknowledge the E-OBS dataset from the EU-FP6 project ENSEMBLES and the data providers in the ECA&D project.

Last but not least, I thank my family, my wife Işık, my son Musa Ayaz, my family and my friend Murat who have been supporting me and sharing my burden all the way in this journey, without them I would not be able to write these words. I am deeply grateful.

ABSTRACT

A NEW METHODOLOGY FOR CLIMATE MODEL SELECTION AND APPLICATION TO TEMPERATURE, HEAT WAVE, WBGT AND LABOR PRODUCTIVITY ANALYSIS

In this thesis, the answers to four main research questions are sought. The first effort is about the finding the most accurate model combinations to project intended climate variables. A new methodology is proposed and testified to achieve this purpose. CORDEX Project is the main model data source and monthly temperature is the observed climate variable over Europe, Africa, West Asia, Central and South America. The suggested methodology outreaches the favorite EWA (Equally Weighted Average) approach in climate studies. It is found that CSIRO as GCM and CLM as RCM is the best choice to simulate temperature patterns. Besides, another methodology is proposed to select daily data sets of the most successful model combinations. Moreover, a new definition of "extremely hot day" is proposed. The selected model combinations, new definition of extremely hot day and TLVs of NIOSH are used to estimate the future heat waves, Wet Bulb Globe Temperature (WBGT) and labor productivity. It is found that adverse effects of climate change over the Northern Europe, the Mediterranean Coastal, the Sub-Saharan and Northern Africa, the southern Arabian Peninsula, Brazil, Iran, Afghanistan, Pakistan and the eastern Turkey will be more devastating than the remaining parts of the World.

ÖZET

İKLİM MODELİ SEÇİMİ İÇİN YENİ BİR YÖNTEM ÖNERİSİ VE SICAKLIK, ISI DALGASI, ÇALIŞAN VERİMLİLİĞİ ANALİZİNE UYGULAMALARI

Bu tezde, dört araştırma sorusuna cevaplar aranacaktır. İlk çaba, incelenen iklim değişkenini en doğru şekilde tahmin eden model kombinasyonunu bulmakla ilgilidir. Bu amacı gerçekleştirmek için yeni bir metot önerilmiş ve test edilmiştir. CORDEX Projesi ana veri kaynağıdır ve Avrupa, Afrika, Batı Asya, Orta ve Güney Amerika üzerindeki aylık sıcaklıklar gözlemlenen iklim değişkenidir. Önerilen metot, iklim çalışmalarında kullanılan eşit ağırlıklı ortalama yaklaşımından daha iyi sonuçlar vermektedir. Küresel iklim Modeli olarak CSIRO ve Bölgesel İklim Modeli olarak CLM sıcaklık desenlerinin simülasyonlarını yapmak için en iyi seçeneklerdir. Bunun yanı sıra, en başarılı model kombinasyonunun günlük verilerini seçmek için başka bir metot daha önerilmiştir. Dahası, aşırı sıcak gün için yeni bir tanım önerilmiştir. Seçilen model kombinasyonu, yeni aşırı gün tanımı, NIOSH'un sınır değerleri gelecekteki ısı dalgalarını, Islak Hazne Küre Sıcaklığı (WBGT)' yi ve işçi verimliliğini tahmin etmek için kullanılmıştır. İklim değişikliğinin olumsuz etkilerinin, Kuzey Avrupa, Akdeniz Sahilleri, Sahra Altı ve Kuzey Afrika, Güney Arap Yarımadası, Brezilya, İran, Pakistan ve Türkiye'nin doğusu için dünyanın kalanından daha yıkıcı olacağı bulunmuştur.

TABLE OF CONTENTS

ACKNOWLEDGEMENTS iii
ABSTRACT iv
ÖZET v
LIST OF FIGURES x
LIST OF TABLES xxvi
LIST OF SYMBOLS xxxii
LIST OF ACRONYMS/ABBREVIATIONS xxxiii
1. INTRODUCTION 1
2. LITERATURE REVIEW 4
2.1. Monthly Climate Variables 7
2.2. Heat Waves 17
2.3. Thermal Comfort 21
2.3.1. Thermal Comfort Methods 21
2.3.2. The Relation between Thermal Comfort and Labor Productivity 22
2.3.3. Thermal Comfort Standards 23
2.3.3.1. ISO 7730 Standard 23
2.3.3.2. ISO 11079 Standard 25
2.3.3.3. ISO 7243 Standard 25
3. DATA 41
3.1. Historical and Observed Monthly Temperature Data Set 41
3.2. Future Monthly Temperature Data Set 50
3.3. Historical, Observed and Future Daily Maximum Temperature Data Set 50
3.4. Historical and Future Daily Relative Humidity 54
4. METHODOLOGY 55
4.1. Method 1: GCM-RCM Combination Selection with respect to Monthly Temperature Data Set 55
4.1.1. Statistical Method 1: AAE as Indicator and Monthly Average Temperature as Data Set 55

4.1.2. Statistical Method 2: RMSE as Indicator and Monthly Average Temperature as Data Set 64
4.1.3. Statistical Method 3: T-Test as Indicator and Monthly Average Temperature as Data Set 65
4.1.4. Statistical Method 4: T-Test as Indicator and Annual Average Temperature as Data Set 66
4.2. Method 3: Future Projections of Temperature 66
4.3. Method 4: GCM-RCM Combination Selection with respect to Daily Maximum Temperature Data Set and Application to Heat Waves 67
4.4. Method 5: Application to WBGT and Labor Productivity 70
5. RESULTS 73
5.1. Application of Statistical Methodologies to the Monthly Temperature Data 73
5.1.1. Application of Statistical Methodology 1 to the Monthly Temperature Data: The Case of Europe 73
5.1.2. Application of Statistical Methodology 2 to the Monthly Temperature Data: The Case of Europe 102
5.1.3. Application of Statistical Methodology 3 to the Monthly Temperature Data: The Case of Europe 104
5.1.4. Application of Statistical Methodology 4 to the Monthly Temperature Data: The Case of Europe 107
5.1.5. Evaluation of Statistical Methodologies over Europe Temperature 111
5.1.6. Application of Statistical Methodology 1 to the Monthly Temperature Data: The Case of Africa 121
5.1.7. Application of Statistical Methodology 2 to the Monthly Temperature Data: The Case of Africa 126
5.1.8. Application of Statistical Methodology 3 to the Monthly Temperature Data: The Case of Africa 127
5.1.9. Application of Statistical Methodology 4 to the Monthly Temperature Data: The Case of Africa 135
5.1.10. Evaluation Of Statistical Methodologies Over Africa Temperature 136

5.1.11. Application of Statistical Methodology 1 to the Monthly Temperature Data: The Case of Central America 136
5.1.12. Application of Statistical Methodology 2 to the Monthly Temperature Data: The Case of Central America 143
5.1.13. Application of Statistical Methodology 3 to the Monthly Temperature Data: The Case of Central America 144
5.1.14. Application of Statistical Methodology 4 to the Monthly Temperature Data: The Case of Central America 148
5.1.15. Evaluation Of Statistical Methodologies Over Central America Temperature 155
5.1.16. Application of Statistical Methodology 1 to the Monthly Temperature Data: The Case of South America 155
5.1.17. Application of Statistical Methodology 2 to the Monthly Temperature Data: The Case of South America 156
5.1.18. Application of Statistical Methodology 3 to the Monthly Temperature Data: The Case of South America 159
5.1.19. Application of Statistical Methodology 4 to the Monthly Temperature Data: The Case of South America 164
5.1.20. Evaluation Of Statistical Methodologies Over South America Temperature 165
5.1.21. Application of Statistical Methodology 1 to the Monthly Temperature Data: The Case of West Asia 168
5.1.22. Application of Statistical Methodology 2 to the Monthly Temperature Data: The Case of West Asia 171
5.1.23. Application of Statistical Methodology 3 to the Monthly Temperature Data: The Case of West Asia 172
5.1.24. Application of Statistical Methodology 4 to the Monthly Temperature Data: The Case of West Asia 178
5.1.25. Evaluation of Statistical Methodologies Over West Asia Temperature 179
5.1.26. Overall Evoluation Application of Statistical Methodologies . . 181

5.2. Future Projection of Temperature 183
5.2.1. Future Projection of Temperature: The Case for Europe 183
5.2.2. Future Projection of Temperature: The Case for Africa 184
5.2.3. Future Projection of Temperature: The Case for Central America 189
5.2.4. Future Projection of Temperature: The Case for South America 189
5.2.5. Future Projection of Temperature: The Case for West Asia . . . 192
5.3. Application of the Methodology of Daily Maximum Temperature Selection 198
5.3.1. Application of the Methodology of Daily Maximum Temperature Selection: The Case of Europe 198
5.3.2. Application of the Methodology of Daily Maximum Temperature Selection: The Case of Africa 205
5.3.3. Application of the Methodology of Daily Maximum Temperature Selection: The Case of Central America 212
5.3.4. Application of the Methodology of Daily Maximum Temperature Selection: The Case of South America 218
5.3.5. Application of the Methodology of Daily Maximum Temperature Selection: The Case of West Asia 223
5.4. WBGT and Labor Productivity Alteration 229
5.4.1. WBGT and Labor Productivity Alteration: The Case of Europe 229
5.4.2. WBGT and Labor Productivity Alteration: The Case of Africa 231
5.4.3. WBGT and Labor Productivity Alteration: The Case of Central America 237
5.4.4. WBGT and Labor Productivity Alteration: The Case of South America 237
5.4.5. WBGT and Labor Productivity Alteration: The Case of West Asia 239
6. CONCLUSION 245
REFERENCES 249

LIST OF FIGURES

Figure 2.1. The GHG Emissions with respect to RCP 2.6, RCP 4.5 and RCP 8.5 5

Figure 2.2. The Observed CORDEX Regions in this Thesis 6

Figure 4.1. Mean of the model combination (MPI–M– MPI– ESM –LR- CLM–CCLM4–8–17–v1) and observation (E-OBS) data set in summer season in the period between the years 1976 and 2005 56

Figure 4.2. The difference between model combination and observation (AE), Absolute Value of The difference between model combination and observation (AAE), The Mean of 26 Models AAEs in each grid (MAAE) 56

Figure 4.3. The comparison of model combination (MPI–M–MPI–ESM–LR-CLM–CCLM4–8–17–v1) with MAAE in each grid 58

Figure 4.4. The comparison of the sum of comparisons of all seasons (SDAAE) of model combination (MPI–M–MPI–ESM–LR-CLM–CCLM4–8–17 –v1) with MSDAAE in each grid 59

Figure 4.5. The map of all second comparison (DSDAAE) of model combination (MPI–M–MPI–ESM–LR-CLM–CCLM4–8–17–v1) with MSDAAE in each grid 61

Figure 5.1. The Annual Absolute Value of The Average Temperature Errors of The Representative Models in The Statistical Methodology 1 in the period between the years 1976 and 2005 75

Figure 5.2. The Annual Absolute Value of The Average Temperature Errors of The Unrepresentative Models in The Statistical Methodology 1 in the period between the years 1976 and 2005 76

Figure 5.3. The Absolute Value of The Average Temperature Errors of The Representative Models in Statistical Methodology 1 in the period between the years 1976 and 2005 in Winter Season 77

Figure 5.4. The Absolute Value of The Average Temperature Errors of The Unrepresentative Models in Statistical Methodology 1 in the period between the years 1976 and 2005 in Winter Season 78

Figure 5.5. The Absolute Value of The Average Temperature Errors of The Representative Models in Statistical Methodology 1 in the period between the years 1976 and 2005 in Spring Season 79

Figure 5.6. The Absolute Value of The Average Temperature Errors of The Unrepresentative Models in Statistical Methodology 1 in the period between the years 1976 and 2005 in Spring Season 80

Figure 5.7. The Absolute Value of The Average Temperature Errors of The Representative Models in Statistical Methodology 1 in the period between the years 1976 and 2005 in Summer Season 81

Figure 5.8. The Absolute Value of The Average Temperature Errors of The Unrepresentative Models in Statistical Methodology 1 in the period between the years 1976 and 2005 in Summer Season 82

Figure 5.9. The Absolute Value of The Average Temperature Errors of The Representative Models in Statistical Methodology 1 in the period between the years 1976 and 2005 in Autumn Season 83

Figure 5.10. The Absolute Value of The Average Temperature Errors of The Unrepresentative Models in Statistical Methodology 1 in the period between the years 1976 and 2005 in Autumn Season 84

Figure 5.11. Mean of the Absolute Value of Average Error Values of 26 Model (MAEE) in each season and annually over Europe in the period between 1976 and 2005 85

Figure 5.12. Annual DAEE of the Representative Models in the Statistical Methodology 1 in the period between 1976 and 2005 86

Figure 5.13. Annual DAEE of the Unrepresentative Models in the Statistical Methodology 1 in the period between 1976 and 2005 87

Figure 5.14. DAEE of the Representative Models in the Statistical Methodology 1 in the period between the years 1976 and 2005 in Winter Season 88

Figure 5.15. DAEE of the Unrepresentative Models in the Statistical Methodology 1 in the period between the years 1976 and 2005 in Winter Season 89

Figure 5.16. DAEE of the Representative Models in the Statistical Methodology 1 in the period between the years 1976 and 2005 in Spring Season 90

Figure 5.17. DAEE of the Unrepresentative Models in the Statistical Methodology 1 in the period between the years 1976 and 2005 in Spring Season 91

Figure 5.18. DAEE of the Representative Models in the Statistical Methodology 1 in the period between the years 1976 and 2005 in Summer Season 92

Figure 5.19. DAEE of the Unrepresentative Models in the Statistical Methodology 1 in the period between the years 1976 and 2005 in Summer Season 93

Figure 5.20. DAEE of the Representative Models in the Statistical Methodology 1 in the period between the years 1976 and 2005 in Autumn Season 94

Figure 5.21. DAEE of the Unrepresentative Models in the Statistical Methodology 1 in the period between the years 1976 and 2005 in Autumn Season 95

Figure 5.22. The "SDAEE"s of the Representatıve Models in the Statistical Methodology 1 in the perıod between the years 1976 and 2005 . . 96

Figure 5.23. The "SDAEE"s of the Unrepresentatıve Models in the Statistical Methodology 1 in the perıod between the years 1976 and 2005 . . 97

Figure 5.24. The "MSDAEE of the Model Combinations in the Statistical Methodology 1 in the period between the years 1976 and 2005 98

Figure 5.25. The "DSDAEE of the Representative Model Combinations in the Statistical Methodology 1 in the period between the years 1976 and 2005 98

Figure 5.26. The "DSDAEE of the Unrepresentative Model Combinations in the Statistical Methodology 1 in the period between the years 1976 and 2005 99

Figure 5.27. The "DSDAEE of the Representative Model Combinations in the Statistical Methodology 2 in the period between the years 1976 and 2005 104

Figure 5.28. The "DSDAEE of the Unrepresentative Model Combinations in the Statistical Methodology 2 in the period between the years 1976 and 2005 105

Figure 5.29. The "DSDAEE of the Representative Model Combinations in the Statistical Methodology 3 in the period between the years 1976 and 2005 108

Figure 5.30. The "DSDAEE of the Unrepresentative Model Combinations in the Statistical Methodology 3 in the period between the years 1976 and 2005 109

Figure 5.31. The "DSDAEE of the Representative Model Combinations in the Statistical Methodology 4 in the period between the years 1976 and 2005 112

Figure 5.32. The "DSDAEE of the Unrepresentative Model Combinations in the Statistical Methodology 4 in the period between the years 1976 and 2005 113

Figure 5.33. AAE of various Test Types and EWA (Equally Weighted Ensemble) over Europe in the period between the years 1976 and 2005 in winter season. 116

Figure 5.34. AAE of various Test Types and EWA (Equally Weighted Ensemble) over Europe in the period between the years 1976 and 2005 in spring season. 117

Figure 5.35. AAE of various Test Types and EWA (Equally Weighted Ensemble) over Europe in the period between the years 1976 and 2005 in summer season. 118

Figure 5.36. AAE of various Test Types and EWA (Equally Weighted Ensemble) over Europe in the period between the years 1976 and 2005 in autumn season. 119

Figure 5.37. AAE of various Test Types and EWE (Equally Weighted Ensemble) over Europe in the period between the years 1976 and 2005 annually 120

Figure 5.38. The "DSDAEE of the Most Representative Model Combinations in Statistical Methodology 1 in the period between the years 1976 and 2005 123

Figure 5.39. The "DSDAEE of the Unrepresentative Model Combinations in Statistical Methodology 1 in the period between the years 1976 and 2005 124

Figure 5.40. The "DSDAEE of the Most Representative Model Combinations in Statistical Methodology 2 in the period between the years 1976 and 2005 128

Figure 5.41. The "DSDAEE of the Unrepresentative Model Combinations in Statistical Methodology 2 in the period between the years 1976 and 2005 129

Figure 5.42. The "DSDAEE of the Most Representative Model Combinations in Statistical Methodology 3 in the period between the years 1976 and 2005 132

Figure 5.43. The "DSDAEE of the Unrepresentative Model Combinations in Statistical Methodology 3 in the period between the years 1976 and 2005 133

Figure 5.44. The "DSDAEE of the Most Representative Model Combinations in Statistical Methodology 4 in the period between the years 1976 and 2005 137

Figure 5.45. The "DSDAEE of the Unrepresentative Model Combinations in Statistical Methodology 4 in the period between the years 1976 and 2005 138

Figure 5.46. The "DSDAEE of the Most Representative Model Combinations in Statistical Methodology 1 in the period between the years 1976 and 2005 141

Figure 5.47. The "DSDAEE of the Unrepresentative Model Combinations in Statistical Methodology 1 in the period between the years 1976 and 2005 142

Figure 5.48. The "DSDAEE of the Most Representative Model Combinations in Statistical Methodology 2 in the period between the years 1976 and 2005 145

Figure 5.49. The "DSDAEE of the Unrepresentative Model Combinations in Statistical Methodology 2 in the period between the years 1976 and 2005 146

Figure 5.50. The "DSDAEE of the Most Representative Model Combinations in Statistical Methodology 3 in the period between the years 1976 and 2005 148

Figure 5.51. The "DSDAEE of the Unrepresentative Model Combinations in Statistical Methodology 3 in the period between the years 1976 and 2005 149

Figure 5.52. The "DSDAEE of the Most Representative Model Combinations in Statistical Methodology 4 in the period between the years 1976 and 2005 152

Figure 5.53. The "DSDAEE of the Unrepresentative Model Combinations in Statistical Methodology 4 in the period between the years 1976 and 2005 153

Figure 5.54. The "DSDAEE of the Most Representative Model Combinations in Statistical Methodology 1 in the period between the years 1976 and 2005 157

Figure 5.55. The "DSDAEE of the Unrepresentative Model Combinations in Statistical Methodology 1 in the period between the years 1976 and 2005 158

Figure 5.56. The "DSDAEE of the Most Representative Model Combinations in Statistical Methodology 2 in the period between the years 1976 and 2005 160

Figure 5.57. The "DSDAEE of the Unrepresentative Model Combinations in Statistical Methodology 2 in the period between the years 1976 and 2005 161

Figure 5.58. The "DSDAEE of the Most Representative Model Combinations in Statistical Methodology 3 in the period between the years 1976 and 2005 162

Figure 5.59. The "DSDAEE of the Unrepresentative Model Combinations in Statistical Methodology 3 in the period between the years 1976 and 2005 163

Figure 5.60. The "DSDAEE of the Most Representative Model Combinations in Statistical Methodology 4 in the period between the years 1976 and 2005 166

Figure 5.61. The "DSDAEE of the Unrepresentative Model Combinations in Statistical Methodology 4 in the period between the years 1976 and 2005 167

Figure 5.62. The "DSDAEE of the Most Representative Model Combinations in Statistical Methodology 1 in the period between the years 1976 and 2005 170

Figure 5.63. The "DSDAEE of the Unrepresentative Model Combinations in Statistical Methodology 1 in the period between the years 1976 and 2005 171

Figure 5.64. The "DSDAEE of the Most Representative Model Combinations in Statistical Methodology 2 in the period between the years 1976 and 2005 173

Figure 5.65. The "DSDAEE of the Unrepresentative Model Combinations in Statistical Methodology 2 in the period between the years 1976 and 2005 174

Figure 5.66. The "DSDAEE of the Most Representative Model Combinations in Statistical Methodology 3 in the period between the years 1976 and 2005 176

Figure 5.67. The "DSDAEE of the Unrepresentative Model Combinations in Statistical Methodology 3 in the period between the years 1976 and 2005 177

Figure 5.68. The "DSDAEE of the Most Representative Model Combinations in Statistical Methodology 4 in the period between the years 1976 and 2005 180

Figure 5.69. The "DSDAEE of the Unrepresentative Model Combinations in Statistical Methodology 4 in the period between the years 1976 and 2005 181

Figure 5.70. The map of spatial distribution of differences of monthly temperature averages of Europe region in seasons (Winter; Spring; Summer and Autumn) for 2050s (2036-2065 - 1976 – 2005) according to RCP 2.6, RCP 4.5 and RCP 8.5 Scenario 185

Figure 5.71. The map of spatial distribution of differences of monthly temperature averages of Europe region in seasons (Winter; Spring; Summer and Autumn) for 2080s (2066-2095 - 1976 – 2005) according to RCP 2.6 , RCP 4.5 and RCP 8.5 Scenario 186

Figure 5.72. The map of spatial distribution of differences of monthly temperature averages of Africa region in seasons (Winter; Spring; Summer and Autumn) for 2050s (2036-2065 - 1976 – 2005) according to RCP 2.6, RCP 4.5 and RCP 8.5 Scenario 187

Figure 5.73. The map of spatial distribution of differences of monthly temperature averages of Africa region in seasons (Winter; Spring; Summer and Autumn) for 2080s (2066-2095 - 1976 – 2005) according to RCP 2.6 , RCP 4.5 and RCP 8.5 Scenario 188

Figure 5.74. The map of spatial distribution of differences of monthly temperature averages of Central America region in seasons (Winter; Spring; Summer and Autumn) for 2050s (2036-2065 - 1976 – 2005) according to RCP 2.6, RCP 4.5 and RCP 8.5 Scenario 190

Figure 5.75. The map of spatial distribution of differences of monthly temperature averages of Central America region in seasons (Winter; Spring; Summer and Autumn) for 2080s (2066-2095 - 1976 – 2005) according to RCP 2.6 , RCP 4.5 and RCP 8.5 Scenario 191

Figure 5.76. The map of spatial distribution of differences of monthly temperature averages of South America region in seasons (Winter; Spring; Summer and Autumn) for 2050s (2036-2065 - 1976 – 2005) according to RCP 2.6, RCP 4.5 and RCP 8.5 Scenario 193

Figure 5.77. The map of spatial distribution of differences of monthly temperature averages of South America region in seasons (Winter; Spring; Summer and Autumn) for 2080s (2066-2095 - 1976 – 2005) according to RCP 2.6 , RCP 4.5 and RCP 8.5 Scenario 194

Figure 5.78. The map of spatial distribution of differences of monthly temperature averages of West Asia region in seasons (Winter; Spring; Summer and Autumn) for 2050s (2036-2065 - 1976 – 2005) according to RCP 2.6, RCP 4.5 and RCP 8.5 Scenario 196

Figure 5.79. The map of spatial distribution of differences of monthly temperature averages of West Asia region in seasons (Winter; Spring; Summer and Autumn) for 2080s (2066-2095 - 1976 – 2005) according to RCP 2.6 , RCP 4.5 and RCP 8.5 Scenario 197

Figure 5.80. Extremely Hot Day Amounts in a year over Europe in 2050s with respect to RCP4.5 and RCP8.5 scenario 200

Figure 5.81. Extremely Hot Day Amounts in a year over Europe in 2080s with respect to RCP4.5 and RCP8.5 scenario 201

Figure 5.82. Consecutive Extremely Hot Day Amounts in a year over Europe in 2050s with respect to RCP4.5 and RCP8.5 scenario 202

Figure 5.83. Consecutive Extremely Hot Day Amounts in a year over Europe in 2080s with respect to RCP4.5 and RCP8.5 scenario 203

Figure 5.84. Extremely Hot Day Amounts in a year over Africa in 2050s with respect to RCP4.5 and RCP8.5 scenario 207

Figure 5.85. Extremely Hot Day Amounts in a year over Africa in 2080s with respect to RCP4.5 and RCP8.5 scenario 209

Figure 5.86. Consecutive Extremely Hot Day Amounts in a year over Africa in 2050s with respect to RCP4.5 and RCP8.5 scenario 210

Figure 5.87. Consecutive Extremely Hot Day Amounts in a year over Africa in 2080s with respect to RCP4.5 and RCP8.5 scenario 211

Figure 5.88. Extremely Hot Day Amounts in a year over Central America in 2050s and 2080s with respect to RCP8.5 scenario 215

Figure 5.89. Consecutive Extremely Hot Day Amounts in a year over Central America in 2050s and 2080s with respect to RCP8.5 scenario . . . 216

Figure 5.90. Extremely Hot Day Amounts in a year over South America in 2050s with respect to RCP4.5 and RCP8.5 scenario 219

Figure 5.91. Extremely Hot Day Amounts in a year over South America in 2080s with respect to RCP4.5 and RCP8.5 scenario 220

Figure 5.92. Consecutive Extremely Hot Day Amounts in a year over South America in 2050s with respect to RCP4.5 and RCP8.5 scenario . . 221

Figure 5.93. Consecutive Extremely Hot Day Amounts in a year over South America in 2080s with respect to RCP4.5 and RCP8.5 scenario . . 222

Figure 5.94. Extremely Hot Day Amounts in a year over West Asia in 2050s with respect to RCP4.5 and RCP8.5 scenario 224

Figure 5.95. Extremely Hot Day Amounts in a year over West Asia in 2080s with respect to RCP4.5 and RCP8.5 scenario 226

Figure 5.96. Consecutive Extremely Hot Day Amounts in a year over West Asia in 2050s with respect to RCP4.5 and RCP8.5 scenario 227

Figure 5.97. Consecutive Extremely Hot Day Amounts in a year over West Asia in 2080s with respect to RCP4.5 and RCP8.5 scenario 228

Figure 5.98. The map of spatial distribution of WBGT averages in Europe region in a year in Winter and Spring in each period (1976 - 2005 and 2066 – 2095) according to RCP 2.6s, RCP 4.5 and RCP 8.5 Scenario229

Figure 5.99. The map of spatial distribution of WBGT averages in Europe region in a year in Summer and Autumn in each period (1976 - 2005 and 2066 – 2095) according to RCP 2.6 , RCP 4.5 and RCP 8.5 Scenario 230

Figure 5.100. The reduction in labor productivity in Europe region in a year in Winter and Spring in each period (1976 - 2005 and 2066 – 2095) according to RCP 2.6 , RCP 4.5 and RCP 8.5 Scenario 230

Figure 5.101. The reduction in labor productivity in Europe region in Summer and Autumn in each period (1976 - 2005 and 2066 – 2095) according to RCP 2.6 , RCP 4.5 and RCP 8.5 Scenario 231

Figure 5.102. The map of spatial distribution of WBGT averages in Africa region in a year in Winter and Spring in each period (1976 - 2005 and 2066 – 2095) according to RCP 2.6 , RCP 4.5 and RCP 8.5 Scenario . . 232

Figure 5.103. The map of spatial distribution of WBGT averages in Africa region in a year in Summer and Autumn in each period (1976 - 2005 and 2066 – 2095) according to RCP 2.6, RCP 4.5 and RCP 8.5 Scenario 233

Figure 5.104. The reduction in labor productivity in Africa region in a year in Winter and Spring in each period (1976 - 2005 and 2066 – 2095) according to RCP 2.6 , RCP 4.5 and RCP 8.5 Scenario 234

Figure 5.105. The reduction in labor productivity in Africa region in a year in Summer and Autumn in each period (1976 - 2005 and 2066 – 2095) according to RCP 2.6 , RCP 4.5 and RCP 8.5 Scenario 235

Figure 5.106. The map of spatial distribution of WBGT averages in Central America region in a year in seasons (Winter, Spring, Summer and Autumn) in each period (1976 - 2005; 2036 - 2065 and 2066 – 2095) according to RCP 8.5 Scenario 236

Figure 5.107. The reduction in labor productivity in Central America region in a year in seasons (Winter, Spring, Summer and Autumn) in each period (1976 - 2005; 2036 - 2065 and 2066 – 2095) according to RCP 8.5 Scenario 238

Figure 5.108. The map of spatial distribution of WBGT averages in South America region in a year in Winter and Spring in each period (1976 - 2005 and 2066 – 2095) according to RCP 2.6 , RCP 4.5 and RCP 8.5 Scenario 239

Figure 5.109. The map of spatial distribution of WBGT averages in South America region in a year in Summer and Autumn in each period (1976 - 2005 and 2066 – 2095) according to RCP 2.6 , RCP 4.5 and RCP 8.5 Scenario 240

Figure 5.110. The reduction in labor productivity in South America region in a year in Winter and Spring in each period (1976 - 2005 and 2066 – 2095) according to RCP 2.6 , RCP 4.5 and RCP 8.5 Scenario . . . 241

Figure 5.111. The reduction in labor productivity in South America region in a year in Summer and Autumn in each period (1976 - 2005 and 2066 – 2095) according to RCP 2.6 , RCP 4.5 and RCP 8.5 Scenario . . 242

Figure 5.112. The map of spatial distribution of WBGT averages in West Asia region in a year in seasons (Winter, Spring, Summer and Autumn) in each period (1976 - 2005 and 2066 – 2095) according to RCP 4.5 and RCP 8.5 Scenario 243

Figure 5.113. The reduction in labor productivity in West Asia region in a year in seasons (Winter, Spring, Summer and Autumn) in each period (1976 - 2005 and 2066 – 2095) according to RCP 4.5 and RCP 8.5 Scenario 244

LIST OF TABLES

Table 2.1. Determined rest durations of NIOSH with respect to the metabolic rate and WBGT for light clothing 23

Table 3.1. The Names and Abbreviations of GCMs 43

Table 3.2. The Names and Abbreviations of RCMs 44

Table 3.3. The Names and Abbreviations of RCM / GCM model combinations for the monthly temperature of Europe 46

Table 3.4. The Names and Abbreviations of RCM / GCM model combinations for the monthly temperature of Africa 47

Table 3.5. The Names and Abbreviations of RCM / GCM model combinations for the monthly temperature of Central America 48

Table 3.6. The Names and Abbreviations of RCM / GCM model combinations for the monthly temperature of South America 48

Table 3.7. The Names and Abbreviations of RCM / GCM model combinations for the monthly temperature of West Asia 49

Table 3.8. The Names and Abbreviations of RCM / GCM model combinations for the daily maximum temperature of Europe 51

Table 3.9. The Names and Abbreviations of RCM / GCM model combinations for the daily maximum temperature of Africa 52

Table 3.10. The Names and Abbreviations of RCM / GCM model combinations for the daily maximum temperature of Central America 53

Table 3.11. The Names and Abbreviations of RCM / GCM model combinations for the daily maximum temperature of South America 53

Table 3.12. The Names and Abbreviations of RCM / GCM model combinations for the daily maximum temperature of West Asia 54

Table 5.1. The Names and Abbreviations of unrepresentative RCM / GCM model combinations 74

Table 5.2. The Names and Abbreviations of representative RCM / GCM model combinations 75

Table 5.3. The coefficients of The Most Representative Models 100

Table 5.4. The coefficients of The Unrepresentative Models 100

Table 5.5. The coefficients of The Most Representative Models 105

Table 5.6. The coefficients of The Unrepresentative Models 106

Table 5.7. The coefficients of The Most Representative Models 108

Table 5.8. The coefficients of The Unrepresentative Models 110

Table 5.9. The coefficients of The Most Representative Models 111

Table 5.10. The coefficients of The Unrepresentative Models 114

Table 5.11. The Amount of Total and successful GCM – RCMs 115

Table 5.12. The coefficients of The Most Representative Models 124

Table 5.13. The coefficients of The Unrepresentative Models 125

Table 5.14. The coefficients of The Most Representative Models 127

Table 5.15. The coefficients of The Unrepresentative Models 130

Table 5.16. The coefficients of The Most Representative Models 131

Table 5.17. The coefficients of The Unrepresentative Models 134

Table 5.18. The coefficients of The Most Representative Models 136

Table 5.19. The coefficients of The Unrepresentative Models 139

Table 5.20. The Amount of Total and successful GCM – RCMs 140

Table 5.21. The coefficients of The Most Representative Models 142

Table 5.22. The coefficients of The Unrepresentative Models 143

Table 5.23. The coefficients of The Most Representative Models 144

Table 5.24. The coefficients of The Unrepresentative Models 147

Table 5.25. The coefficients of The Most Representative Models 150

Table 5.26. The coefficients of The Unrepresentative Models 150

Table 5.27. The coefficients of The Most Representative Models 151

Table 5.28. The coefficients of The Unrepresentative Models 154

Table 5.29. The Amount of Total and successful GCM – RCMs 154

Table 5.30. The coefficients of The Most Representative Models 156

Table 5.31. The coefficients of The Unrepresentative Models 156

Table 5.32. The coefficients of The Most Representative Models 159

Table 5.33. The coefficients of The Unrepresentative Models 159

Table 5.34. The coefficients of The Most Representative Models 164

Table 5.35. The coefficients of The Unrepresentative Models 164

Table 5.36. The coefficients of The Most Representative Models 165

Table 5.37. The coefficients of The Unrepresentative Models 165

Table 5.38. The Amount of Total and successful GCM – RCMs 168

Table 5.39. The coefficients of The Most Representative Models 169

Table 5.40. The coefficients of The Unrepresentative Models 169

Table 5.41. The coefficients of The Most Representative Models 172

Table 5.42. The coefficients of The Unrepresentative Models 175

Table 5.43. The coefficients of The Most Representative Models 175

Table 5.44. The coefficients of The Unrepresentative Models 178

Table 5.45. The coefficients of The Most Representative Models 179

Table 5.46. The coefficients of The Unrepresentative Models 179

Table 5.47. The Amount of Total and successful GCM – RCMs 182

Table 5.48. The Amount of Total and successful GCMs 182

Table 5.49. The Amount of Total and successful RCMs 183

Table 5.50. The coefficients of The Most Representative Models 205

Table 5.51. The coefficients of The Unrepresentative Models 206

Table 5.52. The coefficients of The Most Representative Models 213

Table 5.53. The coefficients of The Unrepresentative Models 213

Table 5.54. The coefficients of The Most Representative Models 217

Table 5.55. The coefficients of The Unrepresentative Models 217

Table 5.56. The coefficients of The Most Representative Models 223

Table 5.57. The coefficients of The Unrepresentative Models 223

Table 5.58. The coefficients of The Most Representative Models 225

Table 5.59. The coefficients of The Unrepresentative Models 225

LIST OF SYMBOLS

$a_{i,j}$	Description of $a_{i,j}$
$a_{i,j,n}$	Description of $a_{i,j,n}$
$a_{m,k,i,j}$	Description of $a_{m,k,i,j}$
$a_{k,i,j}$	Description of $a_{k,i,j}$
$\sum_{i=1}^{n}$	Description of Sum in One Dimension
$\sum_{i=1,j=1}^{n,l}$	Description of Sum in Two Dimension

LIST OF ACRONYMS/ABBREVIATIONS

A1B	Balanced Emission Scenario
A2	Worst Emission Scenario
AAE	Absolute Average Error
AE	Average Error
AR4	Forth Assessment Report
AR5	Fifth Assessment Report
BC	Boundary Condition
CMIP3	Coupled Model Intercomparison Project 3
CMIP5	Coupled Model Intercomparison Project 5
CNC	Computer Numerical Control
CORDEX	Coordinated Regional Climate Downscaling Experiment
CPHD	Consecutive Period of Hot Day
CRU	Climate Research Unit
E-OBS	E-OBS Gridded Data Set
EHD	Extremely Hot Day
ENSEMBLES	EU-funded FP6 Integrated Project
ERA40	ECMWF re-analysis data for 45 years
ESI	Environmental Stress Index
EURO	Europe
EWA	Equally Weighted Average
GCM	Global Climate Model
HWDI	Heat Wave Duration Index
IC	Initial Condition
IPCC	Intergovernmental Panel on Climate Change
IREQ	Required Thermal Insulation
ISO	International Organization for Standardization
JFMA	January- February-March-April
JJAS	June-July-August-September

MENA	Middle East and Northern Africa
NIOSH	The National Institute for Occupational Safety and Health
OM	Percentile Value of Observation
OSHA	Occupational Safety and Health Administration
PDF	Probability Density Function
PES	Proposed Ensembles
PM	Percentile Value of Model
PMV	Predicted Mean Vote
PRUDENCE	Prediction of Regional scenarios and Uncertainties for Defining EuropeaN Climate change risks and Effects
RCM	Regional Climate Model
RCP	Representative Concentration Pathways
RCP 2.6	Radiative forcing level being 2.6 W/m2 by 2100
RCP 4.5	Radiative forcing level being 4.5 W/m2 by 2100
RCP 8.5	Radiative forcing level being 8.5 W/m2 by 2100
RMSE	Root Mean Square Error
SRES	Special Report on Emissions Scenarios
TAR	Third Assessment Report
TLV	Threshold Limit Value
USA	United States of America
WBGT	Wet Bulb Globe Temperature
WCRP	The World Climate Research Programme
WHO	World Health Organization

1. INTRODUCTION

It is essential to estimate the climate of the World as accurate as possible since it affects not only physical, social, economic life of human beings but also politics, security of states and life of species. There have been tremendous efforts in recent years to achieve this purpose. Global Climate Models (GCMs) are inevitable tools for researchers to estimate the climate of World. They produce several climatic outputs but the resolution is very low. In other words, the distance between the grid points, containing climatic outputs, are very high. Hence specific regions can not be examined or more detailed studies can not be carried out. Regional Climate Models (RCMs) fill this gap and they take some variables, generated by GCMs, as input and produce climate outputs in very high resolution. The dynamical performance of RCMs and the quality of GCMs variables are reciprocally significant to estimate the climatic variables of a specific region. In recent years, the number of studies in which several RCM and GCM combinations are used for projection has been tremendously increased. The most important constraint in these types of studies is the selection of accurate GCM-RCM combination(s).

In this thesis, one of the main research questions is the following. Which GCM-RCM combination(s) and ensemble method is more/the most accurate to represent the monthly temperature and precipitation patterns of observed areas and also the whole world? The quality and capability of further efforts like future projections, heat wave analysis and Wet Bulb Globe Temperature (WBGT) calculations in this thesis depends on the accuracy of GCMs and RCMs. The accuracy and reliability of several types of researches in the academic literature, containing climatic information from these climate models using the climatological variables of them are also dependent to the accuracy of selected GCMs and RCMs.

There are several advantages of this suggested methodology in climate studies. Researchers focus on the average of errors such as absolute values of difference between climate models and observation data set, Root Mean Square Error (RMSE)s

or correlation coefficients over a focused area. But in this way, they miss the certain deficiencies and huge errors of models in specific small parts of the observed regions since these errors and deficiencies vanish by averaging the errors over the whole region. It is claimed by researchers that the small spatial average errors of an observed area signals the trueness of climate model at the whole area. First of all, our proposed methodology to find the answer to this research question in this thesis objects to this claim and also offers a more appropriate approach to use in climate studies. The errors of the grid points in the observed regions are not neglected by averaging and the accurate GCM-RCM combinations are selected by taking into account all of the errors in grid points. The distribution of the errors are portrayed and translated into basic mathematical/statistical equations. This is the first advantage of our methodology.

The climate studies center upon the four climatic seasons. The climatic outputs are separated in these climatic studies and accuracy, sensitivity tests are applied in each season separately and then acquired results are given season by season. Therefore, it is difficult to determine the most/more accurate model(s) because they produce various errors in these four seasons. One model may have the least error in one season but it can be in the set of unrepresentative models in the following season because it may produce one of the worst results in the following season. Hence, it can be impossible to ignore or totally include this model in further studies. Second usefulness of our methodology is to dispatch this problem. All of the seasons are integrated into the study with equal importance and they are illustrated in a unique map to use for further calculations.

Third advantage of our methodology is that it shows the success of RCMs and GCMs over various regions to the scientific world. By this way, further improvements and developments can be carried out by analyzing the errors and the reasons behind these errors of climate models in the unsuccessful areas. The leading factors behind the errors over unsuccessful areas can be determined by analyzing the climatology of the unsuccessful areas in detail. Forth advantage of our methodology is determining the best RCM-GCM combinations over specific areas for researchers. By this means, they may determine the models which give reliable outcomes and the ones which risk their research.

In the second part of our thesis, 2050s (the period between 2036 and 2065) and 2080s (the period between 2066 and 2095) are chosen as the future periods. The temperature and precipitation alterations in these periods with respect to reference period (between 1976 and 2005) are analyzed via our methodology and the most representative GCM-RCM combinations.

Another research question in this thesis is the following. Which daily maximum temperature of model combinations is convenient to represent the distribution of observed maximum temperature which may be used for further heat wave analysis? A new methodology is proposed in contradistinction to the ones in the literature to find more/the most convenient model combinations. This methodology can also be used to select the appropriate daily minimum temperature and precipitation data set for the cold wave, drought and flood analysis.

The last research question in this thesis is to find the current and further labor productivity alteration in several parts of the World in the light of thermal comfort of the workers. WBGT is used as the thermal comfort index for the outdoor workers occupied in heavy works.

The organization of this thesis is as follows. In the second section of this thesis, the literature review will be presented. In the third section, the information about data sets used in this thesis will be given. In the fourth section, the newly proposed methodology will be theoretically discussed. In the fifth section, the results of the application of methods, defined in previous sections, will be presented. In the last section, the answers to aforementioned research questions and findings will be discussed and an overall evaluation will be presented. All of the sections will be divided to corresponding sub sections (according to the research questions) and data sets, methodologies and outcomes will be separately presented in these subsections.

2. LITERATURE REVIEW

GCM is designed to project the climatology of the whole World and hence they simulate the climate with very low resolution. GCM takes same variables like solar radiation, Green House Gas (GHG) concentrations, etc. as input and hindcast the previous period. Various parametrization are tried to estimate the historical climatology of the Earth.

Population and economic growths, social interactions, etc. are modelled by scientists and future emission scenarios are attained. The type and strength of these variables determines the value of GHG emissions. A2 is the most pessimistic one which forsees the continual increase of these gasses. B1 is the most optimistic one and predicts the decline of emissions in the future. A1B is the midway one between A2 and B1.

Coupled Model Intercomparison Project (CMIP) adds up all of the GCM simulation outputs in a common environment. In CMIP3, various climatic outcomes of several GCMs were collected during the years 2005 and 2006 and they were the latest ones until 2009. These outputs are one of the scientific infrastructure of Forth Assessment Report (AR4) of Intergovernmental Panel of Climate Change (IPCC). GCM in CMIP3 Project used these emission scenarios to estimate the future climate of the World.

In 2008, twenty modeling groups around the world decided to generate new coordinated climate model experiments. CMIP5 is organized for this purpose and the previous deficiencies of the models are enhanced like clouds, carbon cycle, etc. The outputs of this project are used in the Fifth Assessment Report (AR5) of IPCC.

Representative Concentration Pathway (RCP) is substituted for the previous emission scenarios of CMIP3. RCP demonstrates the future radiative forcing of the World. The most optimistic one is RCP 2.6. The GHG concentrations will start to

decline after 2050s in this scenario. The most pessimistic one is RCP 8.5. The GHG concentrations always increase with respect to this scenario. RCP 4.5 is neither pessimistic nor optimistic one and predicts a middle way for radiative forcing (Figure 2.1) [1]. After obtaining the accurate climatological variables, future projections under different RCP options are simulated by GCMs in CMIP5 Project. The main drawback of using GCM for climate projections is its low resolution. The distance between two grid point on which climate variables are produced is in hundreds kilometers because simulating higher resolution needs huge computational power.

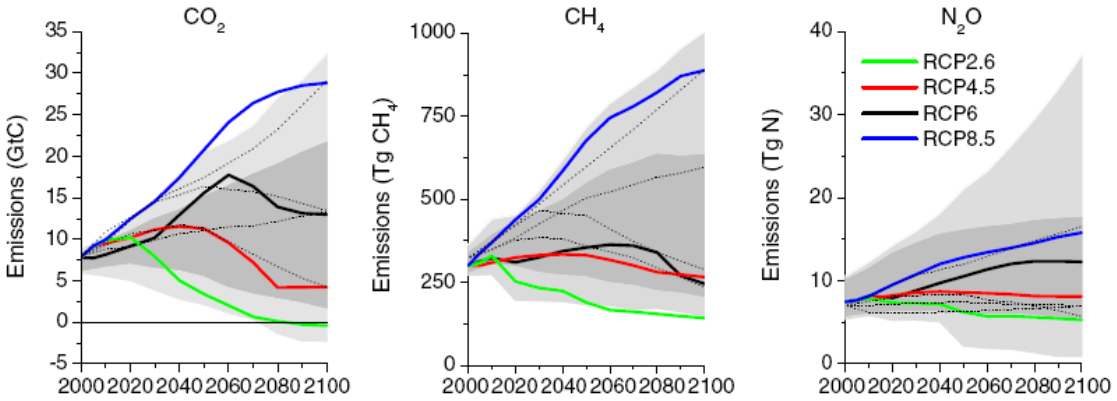

Figure 2.1. The GHG Emissions with respect to RCP 2.6, RCP 4.5 and RCP 8.5

There are two main roads to increase the resolution. These are statistical downscaling and dynamical downscaling. RCMs are the most common tools to carry out dynamical downscaling. The temperature, specific humidity, pressure, eastward and northward wind velocity outputs of GCMs are used as Initial Condition (IC) / Boundary Condition (BC) by RCMs and various climatic variables are produced in higher resolution over a limited region.

Prediction of Regional scenarios and Uncertainties for Defining EuropeaN Climate change risks and Effects (PRUDENCE) is the first comprehensive project started in 2001 and ended in 2004. In this project, several RCMs driven by GCM outputs are used to estimate the future climate of Europe. The resolution of these models outputs is 50 kilometers.

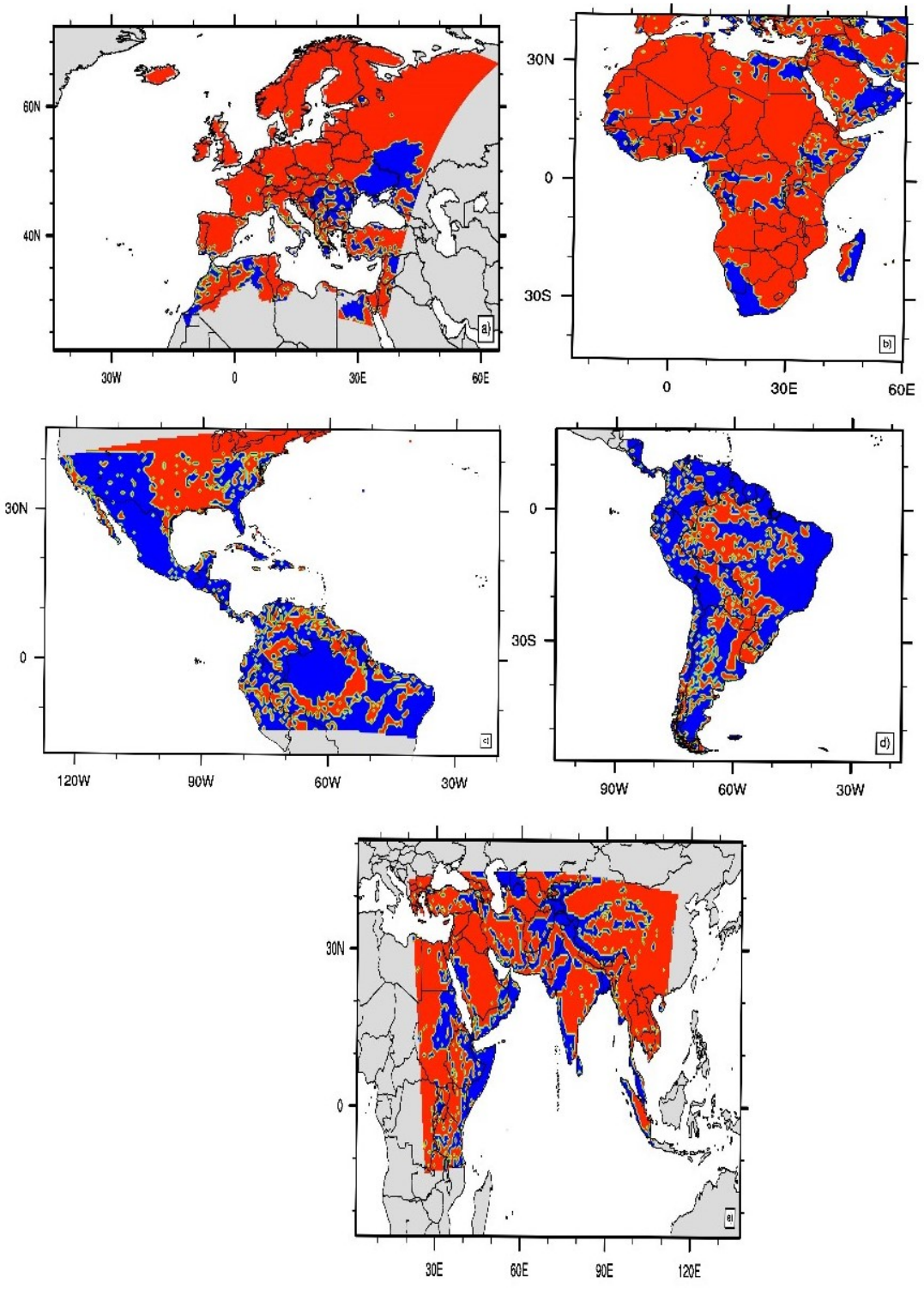

Figure 2.2. The Observed CORDEX Regions in this Thesis

The ENSEMBLES is the second comprehensive project, including more RCM simulations over Europe and West Africa. The resolution options are 25 and 50 kilometers. It is supported by European Comission's 6th Framework Programme and covers the period between the years 2004 and 2009. It was established under the "Global Change and Ecosystems" theme and focus on the impacts of models to scenarios of climate change and tried to increase the forecasting skills of climate models.

CORDEX is the last and most comprehensive project, regionally focusing on not only Europe but also whole Earth. It also includes higher now than before amount of RCM simulation driven by various GCM outputs. It was started to share the outcomes of this project with users after 2013 and the amount of shared data set are still enlarging. There are fifteen regions in which several GCM-RCM model combinations are used to perform climate simulations. In this thesis, five main regions, defined in CORDEX Project, are observed. These are Europe, Africa, Central America, South America and West Asia domains (Figure 2.2).

In the continuing part of this section, the detailed information about the climate modelling studies in the literature. In the first part, the researches including various statistical methodologies in the literature are briefly presented. In addition, information about some of the studies using monthly data set of CORDEX as climatic variables over various regions is given. In the second part, information and definitions of heat waves and some of their applications over different regions are illustrated. At last part, the definition of thermal comfort is given. Then significant information about thermal comfort standards and governing equations and most of the thermal comfort researches are presented. Finally, some of the studies including labor productivity estimations as a result of climate change are exemplified.

2.1. Monthly Climate Variables

There are several researches in the literature focusing on the selection of the representative climate models. Various statistical tools are used for this purpose. For example, Bayesian/relative-likelihood approach was used to calibrate double-counting

and certify at the same time in climate-model studies [2, 3]. In another study, Fars province of Iran was the focused area and the maximum and minimum temperature records of 27 weather stations covering the focused area were the observation data set. The researchers used three GCM outputs (HADCM3, CCCMA and ECHOG with respect to A2 and B2 emission scenario projections) as model results. Linear, second order, third order and multiple linear regression was applied to these data set to find a convenient model and they concluded that CCCMA/ECHOG is the most convenient one for the representation of minimum/maximum temperature. They also found that multiple regressions is the most appropriate method to find the suitable model. They also asserted that the performances of models are dependent to selected areas. In the future, the temperature increased was estimated as 5.12°C over the Fars province [4].

21 GCM temperature and precipitation data sets were used to compare the performances of models and Multi-model Ensemble approach over United States of America in January, February and March. Several indices, including El Nino/Southern Oscillation and Pacific Decadal Oscillation, are used for comparison. It was found that the difference of the projected temperatures of the multi model ensemble and any single model is apparent after especially 2080s and multi model ensemble results estimated warmer future over United States of America than any single model [5]. Another methodology to select the most convenient GCM to represent the climatology is discussed theoretically in another research. Correlation of model and observation results and distance measure are the main indicators [6].

Lee and Kim, apart from other research, firstly formed a cluster and then select five GCM among the cluster as best scenarios. Average and standard deviation and autocorrelation are used as statistical tools and K-means is applied to form a cluster. After forming cluster, Probability Density Function (PDF)s were formed and Skill Scores were acquired from these PDFs. MPI-M-ECHAM5, MIUB-ECHO-G, CSIRO-Mk30, MRI-CGCM2 and GISS-AOM are selected as the best representative ones for the climate projections over South Korea [7].

RMSE was one of the indicators used in climate studies [8–12]. The correlation between model and observation results were also carried out and defined as indicator in multi climate model studies [13, 14]. Bias was another tool to select the representative models [9].

In another research, selection of best representative models among 51 model simulations of 20 GCM of CMIP3 project with respect to A1B emission scenario was carried out for trend analysis. They found important differences between observation and some of the model results [15]. Another effort to leads impact researchers to gather the reliable GCM information was performed by Vano *et al.* An ensemble of accurate GCMs among 142 simulations of CMIP5 Project was constituted by using isolines and ranking tools [16].

The evaluation of RCMs to represent the temperature and precipitation patterns over Mediterranean region was practiced. The observation data set was selected as E-OBS and model outcomes were obtained from ENSEMBLES Project forcing by A1B emission scenario. They concluded that the performance of a model varied from region to region [17].

Lake Brullus was the selected domain and maximum, minimum and mean temperature records of meteorological stations and outcomes of RCM simulations from CORDEX Project were data set. One historical (1994-2005) and one future period (2006-2015) was the chosen period. RMSE, Absolute Average Error (AAE), Percent Bias [18], correlation coefficient, index of agreement [19] and coefficient of Efficiency [20] were the statistical tool to find the most convenient RCM to represent the temperature patterns over observed area (Detailed information will be given in the Section3.1) They found that MPI-M-MPI-ESM-LR - SMHI- RCA4 model combination is the most accurate one to simulate the temperature properties of Lake Brullus [21]. Correlation coefficient and coefficient of efficiency were also used to evaluate the performances of GCMs from SRES and TAR over the 55 regions from various parts of the World and USA with 70 station data set. They criticized the performances of GCMs to show the temperature and precipitation patterns over both smaller and larger areas [22].

Australia was focused area in the research of Evans *et al.* They proposed a methodology to eliminate the worse model combinations to simulate the temperature and precipitation properties of observed area [23].

CMIP3 data sets were the model projections and the observed domain was Arctic region in the research of Overland *et al.* [24]. The capability of the GCM outcomes to represent the previous patterns of temperature over observed region was the main selection criteria. They did not chose a unique model because each model have uncertainties [25] combined the reliable model projections and forms a subset of the successful ones. They indicated that the future projections should be carried out by using these successful ones [24].

Model performances of ERA40-driven ENSEMBLES and CORDEX Project outcomes in sense of temperature and precipitation by comparing E-OBS observation data set was carried out in the period between 1989 and 2008 by researchers. It was found that the models generally capture the pattern and the intensity of both the temperature and the precipitation and improvements could be achieved in CORDEX Project [26]. The performances of the temperature and precipitation variables of E-OBS were studied in the sense of seasonal distribution, intra-seasonal variability and extreme events [27]. E-OBS precipitation data set is used for various purposes in climate studies. For example, it was used to analyze the very long dry spell over Mediterranean Basin [28]. The heat waves, cold spells over Europe were also tested using E-OBS observation data set and reliable results were found [29].

The outcomes of this thesis also reveal that reliable improvements are attained in each situation over each domain, similar to [30]. The added value of RCMs is tried to be found with different forcing data and climatic variables. It is found that the added value is strongly dependent to forcing data, the variable and the observed region [31]. It also depends on the accuracy of the selection of physical scheme. The researchers discussed the performance of two main model types using convection-permitting and large-scale parametrization. They found that there is an important difference and improvement to use convection-permitting models [32].

Changing climate affects several sectors. One of them is the agriculture. Temperature, precipitation, moisture, wind velocity and direction, solar irradiance and other several climatic variables have patterns and magnitudes that change in time and region to region.. This directly affects the agricultural production. RCM outputs were used to estimate the future alteration in crop yield in Turkey [33–35]. In another study, multi-segment Statistical Bias correction method is applied to the climate model data acquired from CMIP5 Project GCM simulations and and this data is used as the input for the SALTMED model in order to estimate the crop yields in Mediterranean region [36]. Three GCM/RCM model combinations with respect to Representative Concentration Pathways (RCP 4.5 and RCP 8.5) are projected over Ghana and they found that changing climate adversely affects the agricultural production and naturally economic and social life [37]. MIT Regional Climate Model is used to understand the possible dangers for the irrigation system in West Africa and especially in Niger River basin and the calculated precipitation and runoff changes combined with social factors like population growth indicated that changing climate treats the agricultural production in the observed area [38].

The temperature and precipitation over sub-regions of Europe and Mediterranean are deeply analyzed by using the ENSEMBLES and PRUDENCE Projects. Station data sets are also used to analyze the changing climate in sub –regions of Europe and Mediterranean and several statistical tools such as skewness, probability density functions are used for this approach. The heat waves over these regions are also studied in the period between 2070-2100 [39–41].

The temperature and precipitation over MENA region is also observed by simulating COSMO-CLM in the years between 1979 and 2100 with respect to RCP 4.5. An important augmentation in temperature and a decline in precipitation are estimated [42]. The alteration in temperature and precipitation patterns over MENA region in three different future periods (2010-2040, 2040-2070 and 2070-2100) according to reference period (1970-2000) is also investigated by using RegCM4.4 as RCM and outputs of HadGEM2-ES and MPI-ESM-MR GCM outputs as forcing data [43]. The intensity, frequency and duration of heat waves over Eastern Mediterranean basin

in the future are analyzed with the help of RegCM4.0 driven by ECHOM5. It is found that the amount and duration of the heat waves will increase in the future [33, 44, 45].

In another study, seven RCM simulations, forced by the ERA-Interim reanalysis dataset in the period between 1990–2008 are performed over South America and it is concluded that the performance of RCM ensemble is reliable hence the bias in temperature is 2°C and precipitation is 20 % [46]. Amazon basin is essential for the climate studies because land use changes over this area affects the ecosystems an climate in local and global sense [47–49]. On the other hand, there are very limited researches dealing with climate change over this area. Simulation covering South America, defined in CORDEX Project, shows that an alteration up to 10 % (increase in northwestern part and decrease in southeastern part) in land use and land cover change happened in Amazon basin [50]. The future behaviour of the climatic variables over SAM are analyzed by using several GCM data set forcing RCMs with respect to RCP 8.5. Equally weighted ensemble of these results were found and Koppen-Trewartha (K-T) classification is carried out in [51].

CRCM5 RCM, driven by CanESM2 and MPIESM-LR GCM outcomes, was simulated over North America between years 1950 and 2100 and portrayed the temperature and precipitation patterns well. The maximum biases occurred in winter season [52]. Average annual minimum temperature of winter season over United States of America was analyzed by forming statistically ensembles in the period between 2041 and 2070. Daily output was used for the cultivation of agricultural crops [53]. GCM data set of CMIP5 Project is used for multi-model ensemble studies over New Jersey to find the change in the temperature and the precipitation in future. It was found that temperature will increase up to 7.6°C with respect to RCP 8.5 [54]. In another study, RegCM4 was forced by two different GCMs over Central America in the years between 1970-2100 and it was found that RegCM produces more accurate precipitation patters than GCMs [55]. Trend analysis of the soil moisture, the ground water level, the precipitation and the streamflow over American Midwest were also carried out by clustering several regional climate models [56]. temperature, precipitation and snowpack output of one very high resolution (0.125°), one regional (0.11°) and one global (1°) climate

model's over Rocky Mountains were compared with the observation data set and it was asserted that RCM and high resolution climate model produced better results [57].

Monthly precipitation, temperature, maximum temperature and minimum temperature of Africa were investigated by using the outputs of RCMs and it was asserted that the general performance of RCMs are similar but there were significant biases which also occured between not only models but also sub regions of the observed domain [58]. Equally weighted averages of CMIP5 precipitation, pressure and moisture data set over Congo Basin were used to analyze the cross correlations and strong correlations were found [59]. The ensemble average of four RCMs' precipitation outputs over Mbarali River catchment in Rufiji Basin was calculated in the period between 1979 and 2005. The performance of ensemble average gave better results than one RCM to represent the precipitation patters of the observed area [60]. Future projections of rainfall patterns via CMIP5 and ensemble mean of the biases of these GCMs were calculated by using three different statistical methods over Lake Victoria basin. Over this area, it was estimated that 10 year precipitation quantile values increase in the future [61]. Precipitation patterns of Southern Africa were analyzed by using the outputs of RCMs of CORDEX Projects. The powerful accords between the majority of the model and observation data set were obtained over the 20th South Latitude [62]. RCA4 RCM of CORDEX project with eight different GCMs over Kenyan Coast was used as a tool to investigate the climate change [63]. By taking ensemble of five GCM and RCM experiment over West Africa forced by reanalysis dataset, they found that the performance of models on various cases and the selection of methodologies are essential to give accurate outcomes to the decision makers [64]. The future precipitation, soil moisture and evapotranspiration outputs of RegCM forced by four different GCMs over West Africa were analyzed and they found that RCM improves the model biases [65]. Another research focused on the precipitation of Africa was carried out by using RegCM as RCM driven by four different GCMs and it was concluded that the uncertainties stemmed from the difference between the physical schemes of RCM and GCMs [66]. The future discharge over the West Africa was also investigated by giving the outputs of 15 different RCM outputs as input to the water balance model [67]. The performance of the seven GCMs over Africa and Europe to produce humidity and

temperature was investigated and it was found that the capability of representation depends on the selection of data set and alters region to region [68].

Multi model ensemble of climate model simulations was used to calculate the drought risk in Europe [69]. The precipitation and the rainfall extremes were studied by using RCMs at higher (12km) and lower (50km) resolutions over Europe. Ensemble average of models was applied as statistical tool and it was estimated that the probability of droughts over especially Southern Europe in summer and extremely heavy precipitation over the majority of Europe was high [70]. The frequency and intensity of snowfall were analyzed as climatic variables by forming an ensemble of KNMI-RACMO2 RCM model simulations taking EC-EARTH GCM model outputs as IC/BC with respect to RCP 4.5 and RCP 8.5 over Europe [71].

In another research over Europe, Belgium was the focused area and precipitation was the observed parameter to run COSMO-CLM with different physical schemes. The purpose was to find the differences between the results, coming from different simulations with different physical schemes. Meaningful differences between the daily precipitation extremes are obtained in summer, but there is not a significant difference in winter [72]. Heat stress is also studied in high resolution climate model over Belgium [73].

Outputs of LDMz and MM5 regional climate models driven by IPSL GCM were analyzed and IPSL produced generally produce consistent patterns of the precipitation and temperature over France [74]. The outputs of regional climate models of CORDEX Project over Mountainous range of the Northern French Alps were given to snowpack models and the snow conditions were studied in the second half of the 20th and 21th century. It was alleged that there is a strong correlation between the temperature alteration and snow conditions. 1.5°C elevation in Global temperature from pre-industrial levels induced 25 % decrease in winter snow depth [75]. COSMO-CLM, driven by ERA40data set between 1971 and 2000 over Germany and eastern France, was used as RCM to investigate the humidity, global radiation, precipitation and temperature and outcomes were compared with very high resolution (7 km) observation data set. It was

asserted that simulation outcomes produce reliable results [76]. Climate model ensemble technique was used to find the most accurate temperature, precipitation, global radiation and various climatic indices over Germany for two future periods [77]. The main reason behind using this technique was because single model could not portray the accurate information [78–81].

Poland was another observed area in the ensemble study of the RCM outputs of CORDEX with respect to RCP 4.5 and 8.5 in two future periods (2021-2050 and 2071-2100). It was determined that at least 1°C temperature increase will be taken place over the observed area in near future (2021-2050) and will reach to 3.8°C in the far future (2071-2100). The increase in winter season will be more than the other seasons [82]. The recorded temperature over Austria was 40.5°C in the summer of 2013. The intensity and frequency of heat waves over Europe have been increasing in the 21th century. [83–85] and they are hazardous [29,86,87]. The performance of climate models to produce rainfall patterns was studied with the help of four RCM simulations of ENSEMBLES Project over Italy by using two different statistical methods [88].

Various climatic outputs like sensible, latent and surface fluxes, maximum, minimum and mean temperatures produced by COSMO-CLM Regional Climate Model to the Community Land Model (CLM4.0) were compared with the ones of CORDEX Project and the previous version of COSMO-CLM Regional Climate Model over Europe. It was concluded that the performance of COSMO-CLM is improved in the new version [89]. COSMO-CLM was used to analyze the precipitation and temperature patterns over complex topographies like region of Alps in the period between 1971 and 2000 forcing via ERA-40 Reanalysis with very high resolution. It was asserted that the temperature and precipitation are well simulated [90]. The added value of RCM was investigated by using Precipitation data set of CORDEX Project over Alpine Region with lower and higher resolution [91].

RegCM3 was forced by CCSM over China for the period 1990-1999 and 2046-2055 and it was found that RegCM produces more accurate precipitation and temperature results than GCM over observed area with respect to observation data set [92]. RegCM4

was also used to simulate Indonesia in the period 1982 and 2000 and CRU was used as observation data set of rainfall for comparison. It was found that RegCM4 is capable of illustrating the rainfall patterns and characteristics during ENSO and captures the important cycles in the region but overestimates the rainfall amounts [93]. Another study in which RegCM was used covers East Asia. The precipitation of the East Asia was analyzed by giving CSIRO-Mk3.6.0's output as IC/BC to RegCM4.4. Moreover, inconsistency between precipitation outputs of RegCM3 and RegCM4.4 was determined over the majority of the eastern China [94]. The statistical and dynamical approaches were tested by using the precipitation and temperature outputs of WRF model forcing by ECHAM5 and IPSL-CM5A-LR over China. It was found that there is a significant difference between precipitation patterns [95]. The importance of dust aerosol for the RCM simulations over East Asia was analyzed via RegCM3 running in the period between 1991 and 2000 for reference period and 2091 and 2100 for future period [96].

CORDEX is another data source for climate studies over Asia. Better performing GCMs of CMIP5 and RCMs of CORDEX Project were collected together and ensemble mean of better performing CMIP5 GCMs and CORDEX RCMs were calculated over India and it was found that CORDEX-RCMs occasionally exhibited slightly superior skills compared to BEST-GCMs [97]. Indian monsoon summer rainfall was investigated by analyzing the CMIP5 outputs and it was inferred that the performance of the GCM models in producing precipitation data set is not well enough since they produce too little (too much) rainfall totals over the observed area [98]. The uncertainty in temperature and precipitation over South Asia in winter (JFMA) and monsoon season (JJAS) was analyzed via CORDEX data set and it was found that the bias is changing between 1°C and 3.6°C in temperature and 18 % and 60 % in precipitation. Moreover, the uncertainty in high elevations in both temperature and precipitation was higher than the one in low elevations [99]. Temperature of Himalayan Mountains was focused area and RCM was the data source for researchers. Estimation of the temperature of the high mountains was difficult and required further improvements and studies [100]. The temperature alteration in the 21th century over Himalayan region was studied via CORDEX data set with respect to different RCPs [101]. The outputs of CORDEX Project were used as inputs in other studies. Ganga river basin was the focused area

and SWAT is the model to estimate the runoff variable in the period between 2021 and 2100. It was found that the extremes of runoff will increase in non-monsoon months as a consequence of snowmelt runoff augmentation [102]. The temperature data sets of CORDEX and other climate model projects are used in various studies. In addition, several statistical tools were applied to estimate the most convenient model combiations but these studies were performed for only limited areas. Hence, it is essential to perform a comprehensive study, dealing with the various regions of earth and applying the same statistical tool. In this thesis, it is tried to fill this gap bu using same statistical tools for five different domains, defined in CORDEX Project.

2.2. Heat Waves

Heat wave is the occurrence of the everlasting extremely hot days and extremely hot day means that the day has the temperature being deviant from and bigger than the normal (average) value There are several researches about the heat waves over Europe, discussed in the following. One of them focused on whole Europe and Mediterranean [39, 103–105]. In this research, the daily maximum temperature at two meters had been gathered from the CORDEX Project outputs [104]. These are the final results of several Regional Climate Model (RCM) simulations driven by various Global Climate Models. (GCM) The distance between two grids in longitude and latitude is approximately 50 km (spatial resolution of $0.44^\circ \times 0.44^\circ$) in the observed dataset. It is good enough to represent climatic properties and capture the idiosyncratic properties of the special regions. All of the RCMs produce results in the years between 1950 and 2100. In the ENSEMBLES Project, whole GCM projections have been carried out via A1B emission scenario boxing out intermediateness of greenhouse gas emissions. More detailed information can be found in [106]. Analyses in this research [104], have been performed in one reference and two future periods in the research. The reference period was chosen between 1971 and 2000. Future periods are chosen as 2041-2070 and 2071-2100. The alteration of the investigated parameter was evaluated by exhibiting its difference between future periods and reference period. The present data involved Europe, some regions of Western Asia and a remote part of Northern Africa. The

observed region covering most of the Mediterranean region (-5° - 42° longitude and 28° - 45° latitude) encompassed Europe domain but did not include the Africa-Eurasia subduction zone under the 28th latitude. Although ENSEMBLES Project involves very high-resolution data set, it dealt with the impacts and results of climate variability and uncertainty on Europe. Hence, regional climate model simulations had been performed by zooming over Europe [106]. The spatial distribution and the amount of extremely hot day totals in spring and autumn season were similar to each other in the future. It was estimated that extremely hot day totals over sea in the period between 2071 and 2100 is approximately 60 days more than the calculated amounts in the reference period (1971-2000) in summer season. It is also concluded that temperature increases over the sea will be higher than land in eastern Mediterranean region. The difference of extremely hot day totals over sea and land was nearly 30 days. In addition, it was estimated that in the Southern Italy, the observed quantities will reach to maximum [104].

The Mediterranean region was separated into various parts in the previous studies. The observed region in this study mainly covered the Northern Mediterranean (41–48 N, 9.5W–38.5 E), and Central Mediterranean (28–46 N, 10.5–20.5 E) [107] Starting from Italy in the west, investigated domain extended to Central Anatolia (inland lying along in the western-eastern line in Turkey) in the east. Northern boundary passed through Black Sea and ends in the upper inlands of Romania. Hence, it consists of several climate types, determinant air movements and various topography and elevation. Heat and cold wave alteration and precipitation changes were observed over whole Mediterranean Region via climate model results with respect to A2 emission scenario [104]. The future period was taken as 2070-2100 and 1960-1990 was the reference one in this research. It was observed that Warming over East Mediterranean Africa in all season will be keener than the temperature climbing in other Mediterranean regions. After 2070, nearly 33 % of days will have maximum temperature being over 30 C in summer over continentals. The increase in the extremely hot day amount will be high under the 42th latitude in the observed region in the first observed period (2041 and 2070). In the years between 2071 and 2100, it will enlarge to northern and encompass whole continentals and coastal. The number of extremely hot days will reach up to

half of the season in Central Anatolia in that period. The changes in observed indices in the future will be higher in autumn compared to spring. The difference will be ocular and apparent after 2070. The adverse effects of heat waves will be seen over especially Cyprus, Greece and western Turkey. In the future, more than half of the summer season will be risky for human health in the aforementioned countries. This risk stems from not only the excess of hot days in the future but also the abrupt and keen change in their intensity and frequency. The consecutive six hot days will be occurred at least two times in a year in the years between 2071 and 2100. In addition to these, the longest duration of the consecutive hot days over land in that period will be more than 40 days. The alteration of the observed quantities in eastern Mediterranean will be seen obviously after 2070. A similar research has been performed by using the same quantities with the ENSEMBLES Project model results over a narrower part of the eastern Mediterranean. The future period was chosen between the years 2021 and 2050. The increases and shifts in the amount, frequency and intensity of the heat waves are not as much as the ones in the second period (2071 and 2100) [104]. The frequency of heat wave emerging in summer is more apparent and sharper than other season [108].

In another study, ERA-interim was another forcing data set in the study performing the heat wave analysis over Europe with the help of ensemble of RCM results of EURO-CORDEX Project. The 90th percentile of maximum temperature and heat waves are compared with the ones obtaining from the E-OBS observation data set. Hot days and heatwaves of summer season in Southern Europe was again well simulated by the models [74]. Specific regions by means of their climatological properties in a specific future and control period intervals are also studied in a detailed way [40, 41, 109–116]. The climate projections of Cyprus in 2026-2050 were one of them. Equally weighted averages (EWA) of six ENSEMBLES Project RCMs' give the best estimation results. Hence EWA of the differences between the future and reference period averages of these models were also calculated during this research. The minimum increase in the temperature is 1.5°C [117].

Some of the extreme event studies involve the entire world. Hence, GCM outputs were used and an ensemble, having different restrictions, was formed. The fraction of the hot days to the total days in the selected period was calculated. The fractions of Mediterranean basin were not as big as northern pole fractions, but they were bigger than most of the regions in the world [118]. Impacts of changing climate over the Eastern Mediterranean region were studied from five centuries ago to the end of the 21th century. It was estimated that the Northern Mediterranean, especially Turkey and Balkans, will be more adversely affected than the southern part. The hotspots were quantified by the aggregation of latest GCM data set (CMIP5) in the World. Mediterranean is one of the observed regions in which hotspot patterns can be seen more apparently [119].

In another study, the heat wave duration index (HWDI) was studied via 92 station data set from ten countries in the eastern Mediterranean region in 1958-2000. Decadal behaviors of observed quantities, including HWDI, were analyzed and general trends were figured out [120]. Three RCMs, forced by two different GCMs in the ENSEMBLES project, had been used to calculate 90th percentile of maximum temperature over Mediterranean Basin [121]. In this study, 500 hPa geopotential heights data and large scale circulation at the upper level atmosphere were also studied.

The capability of ENSEMBLES Project to represent the climate of European area is preceding climate project(PRUDENCE Project). The adverse effects of climate change can be perceived by focusing deeply on the interannual summer temperature variability in the range 1970-1999 [122]. These model demonstrations are more consistent to observed climatic conditions. The future estimations based on regional climate model results strongly depend on the robustness of model's success on testifying to show past climatic patterns. Consequently, newer model results are more appropriate for this kind of researches. Ensemble mean of six regional climate model results forcing the same GCM results are also studied for Europe, previously [123]. The reference period was chosen as 1961-1990 and the alteration of maximum temperature in the future period (2071-2100) with respect to reference period was calculated. It was estimated that the southern part of the Europe and North Africa coastals have the highest

temperature changes.

Climate Model data sets are not used only for a single purpose. In addition to being the cognizant of possible outcomes of changing climate directly, various social and natural subjects can be lightened with the help of these climate data sets. In accordance with this purpose, ENSEMBLES Project data set was taken into account for several topics involving agricultural yield estimation [33–35], labor productivity losses in the Mediterranean region [124–135]. A variety of indices including forest fire weather index [136], WBGTs were also computed through the instruments of these data sets.

Heat waves studies were carried out by using limited number of model combination results and the selection of reliable model combinations to represent the daily maximum temperature of the observed region was rarely performed. In this thesis, a new definition of heat wave is carried out. In addition, a new methodology to select the trustable model combinations which represent the daily maximum temperature patterns of observed domain is applied.

2.3. Thermal Comfort

Temperature, relative humidity, solar radiation and wind velocity are the climate variables which affect the health, security and comfort of workers. Thermal comfort is the pleasure of especially wokers with the thermal conditions while they are performing their jobs.

2.3.1. Thermal Comfort Methods

The Legislation about Protection of Workers from the Risks of Noise [137], the Legislation about Protection of Workers from the Risks of Vibration [138] and Struggle with Dust Legislation [139] determines the TLVs for workers which are the maximum allowable exposure values to protect health and safety of them in working environments. However, there is not any convenient legislation in Turkish law deciding the

tolerable values. After the Legislation about the Authorization of Laboratories which are performing Occupational Hygiene Measurement, Test and Analysis inured to the benefit in 20th February 2014 [140] inured in 20th February 2014, three main international standards were accepted as the base ones for thermal comfort measurements. The man standard is ISO 7730 (Ergonomics of the thermal environment – Analytical determination and interpretation of thermal comfort using calculation of the Predicted Mean Vote (PMV) indices and local thermal comfort criteria) which determines the thermal comfort conditions of working environment and the continuing parts and TLVs of this standard is applied for moderate environments. ISO7243 standard (Hot environments – Estimation of the heat stress on working man, based on the WBGT-index (wet bulb globe temperature) and it's suggested TLV's are valid for hot environments. ISO 11079 (Ergonomics of the thermal environment – Determination and interpretation of cold stress when using required clothing insulation (IREQ) and local cooling effects) is used for cold environments.

2.3.2. The Relation between Thermal Comfort and Labor Productivity

The employees working in humid and extremely hot environments fell more concentration losses, physical strain and discomfort than the ones working in moderate environments [141]. Therefore, labors working in risky environments in the sense of thermal discomfort have to have a rest while performing their jobs. Rest durations are defined in Annex-B of ISO 7243 graphically. The corresponding values according to heaviness of works and WBGT results are determined by NIOSH numerically as shown in Table 2.1 [142]. The proposed rest durations is to continue work in safely and healthily. If workers do not have a rest, they will be in risk, directly proportional to the highness of suggested duration and can not work in full capacity. In other words, calculated labor productivity loses is directly proportional to dangers for workers which adverse thermal comfort environments host.

Table 2.1. Determined rest durations of NIOSH with respect to the metabolic rate and WBGT for light clothing

MET / REST %	LIGHT	MEDIUM	HEAVY	VERY HEAVY
0%	31	28	27	25,5
25%	31,5	29	27,5	26,5
50%	32	30,5	29,5	28
75%	32,5	32	31,5	31
100%	39	37	36	34

2.3.3. Thermal Comfort Standards

There are three main Iso standards in the literature for thermal comfort studies. In the following part of this section, a brief information about this standards will be given.

2.3.3.1. ISO 7730 Standard. ISO 7730 standard comprises of two main parts. In the first part, personal discomfort is determined via PMV which is used in thesis. In the second part, zonal discomfort indices are introduced. PMV is calculated by using meteorological parameters (air temperature, relative humidity, mean radiant temperature, air velocity), clothing coefficient and metabolic rate. It is defined between the range -3 and +3. This index is used for moderate environment and can not be used for extremely hot and cold work places. Besides, there are six conditions which are necessary to use PMV as an index in thermal comfort measurements. These are;

- Metabolic rate has to be between 46 W/m^2 (0,8 met) and 232 W/m^2 (4 met)
- Clothing coefficient rate has to be between 0 $m^2 \cdot$ K/W(0 clo) and 0,310 $m^2 \cdot$ K/W (2 clo)
- Air temperature has to be between 10 °C and 30 °C
- Mean radiant temperature has to be between 10 °C and 40 °C
- Air velocity has to be 0 m/s and 1 m/s

- Pressure has to be between 0 Pa and 2 700 Pa

Mean Radiant Temperature is a temperature which scatters from a heat source. When sun rises in the snowy and cold weathers, the burning sensation in the face is because of mean radiant temperature. Similarly, when one opens the door of a refrigerator, the cooling sensation is also the result of mean radiant temperature. This temperature does not form burning sensation in cold weathers or cooling sensation in hot weathers. For example, workers, working in melting operations, feel more thermal discomfort than the others.

Metabolic rate is a coefficient which determines the total energy exhaust while labors are working. Its unit is either W/m^2 or met. It is collected under four titles according to ISO 7243 standard. These are light, medium, heavy and very heavy and are determined with respect to their physical activities like walking, running, moving their arms and legs, etc. For example, the works, employees are performing their jobs on the desk in offices are example of light works. Using CNC machines and controlling products on the production lines are accepted as moderate works. Hoeing in the farms is relatively harder work and it needs more energy, hence these sorts of jobs are defied as heavy works. Sledging is the hardest one among the aforementioned ones and it is an example very heavy works. More basic definitions for metabolic rates are determined in ISO 7730 standard. Metabolic rate is directly used to calculate PMV index, but it is a parameter to decide the TLV of WBGT.

Clothing coefficient is another important parameter for thermal comfort measurements. It identifies the effects of the clothes of workers. The magnitude of this index increases in direct proportion to the amounts of clothes which workers wear in workplaces. Heat stress increases when this coefficient increases. Unit of clothing coefficient is clo and the final value is attained by the summation of the clo values of each clothes. These values are indicated in the Annex-E of ISO 7730. Various combinations of clothes are also shown in this standard. On the other hand, this standard is appropriate for the moderate environment in the means of climate. If PMV is bigger than 2, this environment is defined as hot and it is necessary to use WBGT index, defined

in ISO 7243 standard. Similarly, if PMV is smaller than -2, the environment is defined as cold and ISO 11079 is the convenient standart to measure the thermal comfort.

2.3.3.2. ISO 11079 Standard. If the measured PMV is smaller than -2, then this environment is defined as cold. The primary remediation for these environments is augmenting temperature. In addition, relative humidity can be increased and air velocity can be decreased. If the working conditions and specialties of jobs don' let to do these improvements, than the unique solution is providing sufficient clothes for workers after determining the IREQ coefficient. This coefficient is used to calculate the minimum required clothing coefficient value. There are very limited working environments in which workers complain about the coldness of the working environment.

2.3.3.3. ISO 7243 Standard. WBGT index was developed by Oglou and Minard in 1957 to measure the heat stress in various activities in the USA army [143]. It mainly comprises of air temperature, natural wet bulb temperature and globe temperature and various forms and versions of this index have been produced. Air temperature, relative humidity, pressure, air velocity and these sorts of climatic variables can be easily obtained from meteorology stations, satellite data set and climate model results, but it is difficult to acquire globe temperature records and natural wet bulb temperature. Hence, it is not possible to calculate regional or large scale studies with these parameters. WBGT can be obtained without using globe temperature. One of them was developed by Australia Meteorology Bureau and it consists of only relative humidity and temperature and is used in several studies [144,145]. In addition to WBGT index, various thermal comfort index is used in literature and produce similar results. For example, ESI index which is a combination of relative humidity, temperature, sun radiation gives consistent results with WBGT [146,147]. Another index PSI is generally used for military purposes and used core temperature and hearth rate as input [148].

WBGT has different formulas based on the existence of radiation. The effect of air temperature, wet bulb temperature and globe temperature is included in Formula 2.1. The effect of the globe temperature is more dominant for the environments which

see the sun and air temperature is excluded from Formula 2.2.

$$WBGT_{\mathrm{IN}} = 0.7 \times T_{\mathrm{NW}} + 0.2 \times T_G + 0.1 \times T_A \tag{2.1}$$

$$WBGT_{\mathrm{OUT}} = 0.7 \times T_{\mathrm{NW}} + 0.3 \times T_G \tag{2.2}$$

where $\mathrm{WBGT_{IN}}$ is Indoor Wet Bulb Globe Temperature; $\mathrm{WBGT_{OUT}}$ is Outdoor Wet Bulb Globe Temperature; $\mathrm{T_{NW}}$ is Natural Wet Bulb Temperature; $\mathrm{T_G}$ is Globe Temperature and $\mathrm{T_A}$ is Air Temperature.

TLVs are given in the Annex-A of ISO 7243 standard Table 2.1. These values alter with respect to metabolic rate and the existence of air movement. For example, 25°C is the upper limit to continue to work comfort and safety for very heavy works when there is an air movement. If there is not any air movement in the workplaces, than TLV is 23°C. Similarly, TLV for heavy works when there is not any air movement is 25°C. It escalates to 26°C for the same work type if there is an air movement. Air movement is not significant for moderate and light works to determine TLV values. TLV of WBGT is 28°C for moderate works and 30°C for light ones. After WBGT is over 33°C, it is necessary to not continue to be in the work place even if they have a rest.

In USA, like in Turkey, there are not any comprehensive and regulatory standards which protect workers from extremely hot environments. Temperature has been increasing by changing climate in recent years and high temperatures harm workers. Therefore, it is important to protect workers from the hazardous effects of increasing temperature [149]. In another study in which it is concluded that various threshold limit values should be determined according to work types and climatic seasons, the intensity and frequency of heat stress in different sectors and time intervals were analyzed. According to the findings of this study, it was found that in Japan, there had

been at least 100 heat strain events, most of them in mines, in one year in 1955s. After some improvements made and some mines closed, heat strain events started to decrease in 1965s. Today, heat strain events rarely occur in Japan. Most of these happened in the outside work environments [150]. It is difficult to identify the heat strains. Therefore, a survey, directly contacting the 124 foresters, was made and it is found that one of three workers faced with heat strain while they are carrying out their jobs. Heat strain was more frequently seen at the alcohol abuser and perspiring workers in early afternoon at 14:00 o'clock. Hence, it was declared that loosing minerals and not taking new ones in to the body triggered heat strain [151]. It was understood that most of the heat strain events; directly dependent on the sexuality, age, climatic seasons and conditions and work types; in the years between 1991 and 1995 were more frequently seen on the agricultural laborer under the age of 60 in the August and September in Japan [150]. In Japan, thermal comfort limit values were determined with respect to the work types. In addition to the personal exposure limit values, they also constituted threshold limit values for working environments. These values, including climatic parameters like temperature, relative humidity, air velocity, chemical factors lie carbon dioxide, carbon monoxide dust concentrations in the air, the volume of air and the volume of air has to be ventilated per worker were determined for summer and winter season and for standing and sedentary works [42].

The adverse effects of heat on male and female workers varied. In USA, an investigation made with the combination of three metabolic rates and five clothing coefficients types and it was found that women are more than affected men by heat. In this research, it was also determined that the hearth rate of women were 15 beats more than the rate of men in a minute while they were performing their jobs [152].

The temperature and relative humidity, causing heat stress and heat strain, was observed in detail and it was understood that heat strain was more frequently seen in a working environment having 27°C and 100 % than the one having 40°C and 10 %. According to this study, it can be concluded that relative humidity is more dominant than the air temperature in the sense of adverse effects on workers. In WBGT index formula, the contribution of the wet bulb temperature, representing the effect of relative

humidity, is seven times the allotment of air temperature.

The surplus of temperature in the workplaces located in the industrialized and crowded cities is more than the ones found in uninhabited places and this escalated the thermal comfort problem. In the future, it is forecasted that the temperature increases in the industrialized regions will be more than the temperature augmentation in villages [153]. For example, the temperature in the crowded and construction intensive parts of the San Francisco is 11°C higher than the remaining part. Temperature increases also affected the life of people and also work life of workers in Australia. For example, the percentage of death increased in the range of 15 % and 17 % when the temperature exceeded 30°C in the years between 1979 and 2001. Likewise, the death amount accreted in the range of 19 % and 21 % when the minimum air temperature reached up to 24°C [154]. In a research performed in India,when the average WBGT is $29,7$°C and the clothing coefficient is 0.96 , it was found that core temperature reaches to 38°C ; very close to 39°C in which heat strain events might occur and $40,6$°C [155–157] in which the death risk is very high; in 64 minutes. This time might be shorter in the changing climate [158]. Moreover, the regions being suitable to work comfortably today might be uncomfortable to work in the future without making improvements in the workplaces. Due to these reasons, the temperature increases as a consequence of climate change has to be taken in consideration. For example, 2-4°C temperature increase will raise the risk level of some countries, like South Africa, from light level to medium, even high level [159].

Temperature increases as a result of climate change affect seriously workers who are working outside like agricultural laborers, building workers and mine workers and athletes. Outside workers are more frequently and adversely affected by the inconvenient air temperature, relative humidity and radiant temperature than the inside workers [160]. As an example to outside workers, splinters run and compete in the outside and frequently under the sun. Environmental air temperature, relative humidity and radiant temperature were main outside risk factors calculating via WBGT [161]. One of the basic and necessary solution to increase water and liquid consumption of workers practicing in hot environments, like athletes, workers dealing with heavy and

very heavy works take more water in comparison to the ones performing light and moderate works. For example, athletes lost approximately 3.7 liters of liquid via sweating during the marathon race in Los Angles run in a humid and hot environment [162].

In Turkey, agricultural workers are the leading ones who will be affected hazardously from climate change [144], because one of every four workers in Turkey are the agricultural workers. There were limited studies dealing with the effects of thermal comfort on workers' health, comfort and safety in the literature. One of them was focused on 124 corn producers in India and labor's health problems, discomforts and productivities with respect to WBGT were investigated. Hereunder, workers working in the hot environments felt pain and fatigue. Besides, returning of the heart rate to normal values took too long for these workers [163].

It is usually impossible to enhance the meteorological factors for especially outside workers. In such cases, it is reasonable for workers to change their clothes and wear lighter ones. For example, productivity of a labor having 1.15 clothing coefficient and working at 18.7°C is similar to one having 0.6 clothing coefficient and working at 23.2°C [164]. Improvements in the air velocities are essential to establish thermally comfortable environments for indoor workers. These sorts of improvements also augment the quality of air in the workplaces [165].

Covering with clothes, temperature and relative humidity, labors working in hot environments have to drink between 8 and 16 liters liquid to gain their liquid losses via perspiration. This amount reduced to 2 and 4 liters for the ones working in cold environments [166]. Besides, human body does not solely lose water while performing in hot environments. For example, exercising and doing sports in hot environments cause the augmentation of protein consumption [167]. Workers also lose sodium via sweating [168]. It is certain that supplying liquid for workers when WBGT reaches to 28°C [161]. This fact coincides with the outcomes of the study performed in India investigating the thermal conditions of corn producers. According to this study, serious discomforts can be seen when WBGT reaches to 28°C and productivity begins to decrease approximately % 5 for every 1°C increase after that value. Moreover, tem-

perature measurements were taken from 22 agricultural laborers working in sugar cane producing throughout 15 days and the amount of sugar canes that they cut were also recorded. It was found that the laborers drinking at least 7-8 liters water in a day were more productive than the others who were drinking less water [169]. In another research, field studies about thermal comfort conditions were done on 105 workers sowing sugar cane in Costa Rica and Nicaragua in 2010. These countries were humid and hot in almost whole year because of their locations. In the morning, at 7:30 o'clock, the critical temperature value of 26°C was generally recorded and temperature records reached up to the values at 9:15 A.M. which workers have to rest at least 25 % of their normal working hours [170].

Liquid loading of workers, cooling workers, and accustoming workers to heat before start to work is essential to reduce the physiological and physiochemical stress [171]. Nevertheless, it is difficult to adapt to working environments for laborers working in (very) heavy and (extremely) hot jobs. Another research was done in China to understand the alterations in the bodies of workers while they are accustoming to the heavy jobs. In accordance with this purpose, young university students were asked for climbing the stairs orderly at the same speed where air temperature was 37°C, the globe temperature was 41°C and relative humidity altered between 20 % and 40 %. It was seen that their heart rates, core temperatures increased and serious increases in the blood pressures were observed [172]. This job represented the heavy one and researchers tried to immobilize the environmental conditions. In work life, it is not easy to find workplaces in which climatological parameters are constant. The temperature interval of 32 and 35°C is critical, because workers are affected seriously from hot environments beyond these temperatures. Besides, it should not be dropped below 19°C to protect workers from unfavorable cold environments [173].

When temperature records were 10°C higher than the seasonal normal in Orissa state of India in 1998, 2042 deaths were occurred as a result of heat wave. This amount was totally 1625 in four states; including Orissa; in the years between 1978 and 1997 [174]. Another study, done in the same country, focused on 8 fabrics and 100 thermal comfort measurements via WBGT index were taken in four years. It

was investigated whether workers were exposed to adverse thermal comfort working conditions and they have health problems related to hot environments. As for those results, it was understood that nearly 28 % of workers were faced with the risk of heat related illness [175]. Declared heat related 20 cases were seen in United States of America in the years between 2012 and 2013. Among them, 13 cases were fatal as a result of heat stroke and most of the workplaces where the deaths were seen were medium or heavy works in outside. 4 of the workers died in their first day of work and 5 of them died within three days of the work. After observations were made in these workplaces, it was seen that workers were not accustomed to their new jobs and employers did not take any precautions to reduce the heat stress [176]. 49 heat related cases, causing discomfort, unsafety and illness, were detected in the period between 1988 and 1998 in USA with respect to OSHA statistics. 46 of these cases resulted with death [177]. In Japan, on an average 13.8 workers died in a year in the period between the years 1991 and 2001 because of heat related illness. In 2001, 194 workers, whom heat waves triggered illness, were in the hospital more than four days in 2001. Most of these illness occurred in summer and were seen among employees working outside. 47 workers died as a result of heat stroke in the extremely hot summer of 2010 [178].

Insured employees who had an accident which are collected under the topic of "extreme heat, radiation and lightening effects" were investigated by using data set of 2014 Yearly Statistics of Turkish Social Security Institution. 125 male and 14 female workers had an accident. None of these accidents were fatal and 77 workers returned to work the day after, but 32 of them were in hospital more than five days.

Most of the heat stroke events are seen in heavy work conditions but they are rarely reported and recorded. For example, a survey research was made with 91 open mine workers and 56 closed mine workers from three different mines. It was found that 79 % of the closed mine workers have risk to become ill as a consequence of heat strain. The same ratio reached up to 87 % for the open mine workers. More than half of three diseases were not fatal and did not induce serious health problems [179]. The main factors, including heat stroke in workplaces are the need of physical labor force, existence of hot and humid workplace conditions, long working and short rest durations

and not using Personal Protective Equipment. Hearth is one of the most affected organ, because heat stroke triggers disorder in heartbeat which can be fatal [180]. In other words, the increase in core temperature after heat stroke occurs is not unique reason causing the fatal and irreversible damages in human body because after-effects which heat stroke triggers also damaged human body [181]. For example, sodium losses as a result of sweating induced transient hypernatremia. The core temperature ad hearth rate of 160 university students performing different jobs with various metabolic rates were measured to understand the adverse effects of insufficient thermal comfort conditions on human health. It was found that the core temperature increases until the air temperature reaches to 34°C. After that temperature, core temperature does not increase. The augmentations in the relative humidity induce the increase of core temperature more rapidly. The effects of relative humidity and temperature are more easily understood than the effects of air movement. There has been an increasing temperature tendency in the amount of patients who were in hospital less than one day in summer and the last months of spring in Canada [182]. The heart rate of the workers performing heavy jobs alters between 140 and 160, and this amount is not affected by the augmentation in core temperature. This rate is directly proportional to temperature increase and hence is increases with an elevation of core temperature [183].

In another study, the rest durations, the maximum working hours and WBGT index are taken in consideration to determine the governing equations for light, moderate and heavy jobs [184]. Working without rest adversely affects the human health. 28 % of the labors, working in construction sector in Hong Kong, have heat-related health problems [185].

The critical core temperature, recommended by WHO to stop working, is 37.7°C. Sickness, giddiness, weakness, headache, blurred vision, black out, spasm, prickling and deliquium are the possible illness if one continues to work after these determined temperature. The heart disorders as a consequence of thermal stress can also happen when workers pass form hot environment to cold one to have a rest. Therefore, employees working in hot environments have to go to cool ones step by step and they have to be accustomed to new ones.

The classification of the work types causing death as a result of heat stress was done in Japan. Working in front of furnaces, metal sector, gardening, automotive industry and construction sector are the most risky ones as these work types are also gathered in the risky group in this study. Risks on workers depending on thermal comfort conditions in India were observed and it was found that increasing temperatures affected adversely not only production but also heath of workers. The researchers foresee that temperature will increase in the future as a result of climate change. They found that agriculture, ceramics, automotive, steel-iron and textile industries, which are also risky ones in Turkey according to the findings in this book, are the most risky ones in the sense of heat stress. They also commented that it is very difficult to find the health statistics, which show the direct effects of heat stress on occupational health, in India, likewise in Turkey [186]. In another study, temperature, relative humidity and WBGT measurements were taken from 21 employees working in ceramics industry, power plant production, construction sector, knife industry and agriculture sector and the highest WBGT is obtained in agriculture sector. Ceramics industry and agriculture sector were investigated in our study and they are also declared as risky ones. It has to be pay attention to these sectors because fatigues and heat cramps can be seen [187]. Heart rate, sharp increases in heart rate, walking speed and productivity of 120 employees, working in brick production in India were analyzed. Serious augmentations in heart rates and fluctuation in heart rates were seen when WGBT was between the range of 26.9°C and 30.4°C. The workers, dealing with the transportation of bricks were less affected because they were adapted to temperature increases by decreasing their walking speeds. On the other hand, their production extremely decreased when air temperature was higher than 34.9°C. 96 heat related illness were reported in the years between 1991 and 1994 from the United Kingdom Military Forces located in Cyprus. It was understood that most of these cases happened when WBGT was in the range of 26°C and 29°C [188].

One of the main consequences of adverse thermal comfort conditions is the losses in labor productivities. For example, performance test was applied to two different groups, containing 7 workers, when WGBT was 17.7°C and 30.2°C. These jobs are light one like writing documents in the desk and heavy one like lifting heavy objects. Workers

at both group felt tired and productivity losses were seen [189]. In another study, six healthy university students who sit without performing any job were chosen and heart rates, core temperatures, sweating, running a temperature event and face rashness in first thirty minutes and after thirty minutes were analyzed when temperature was 21°C and 35°C. Increases were found in both parameters [190].

Productivity studies are generally done for the office workers instead of rest studies. Hence, PMV index which is more suitable than WBGT index in the moderate environments is used for the office jobs. Working on the hot environments adversely affects the health of the workers; on the other hand, firms primarily have to take precautions to diminish the conditions of working environment. It is estimated that the total cost to increase the productivity of workers by 5 % is approximately 125 billion dollars in United States of America. Although this amount seems extremely high, it also mentioned that investment amortizes itself in a very short period. The productivity of the office workers is also analyzed in another research by using a different methodology. The environment temperature was adjusted to 17°C, 21°C and 28°C and 21 workers were subjected to neurobehavioral tests to investigate their productivities. According to findings, it was understood that the thermal discomfort as a result of hot and cold working environments induces reduction in the productivities of workers [191]. In another study, a more specific office environment; call center; was chosen to observe the decrease in productivities of workers by increasing temperature in Finland. In an environment which has a temperature altering between 21.9°C and 28.5°C; 1°C augmentation in temperature causes 1.8 % productivity losses and losses can reach up to 7 % depending on the increase in temperature [192].

In a construction area, the effects of metabolic rate and rest duration on productivity of the workers in a hot and humid environment are indirectly observed by looking the percentage of finished works in Hong Kong. It was found that nearly 58 % of putting up a wall finished in the first 5 minutes and 94 % of the job finished in the first 40 minutes [193]. The same data set was used in another study and it was suggested to employees to work 120 minutes and have a rest of 15 minutes in an environment in which WBGT was $28,9°C \pm 1,9°C$. When WBGT in the environment

increases to $32,1°C \pm 2,1°C$, the proposed work period decreases to 115 minutes and suggested rest duration increases to 20 minutes. At the end of the work, the heart rate, blood pressure and core temperature of workers increase nearly 10 %. Another interesting remark in that study was that excessive use of alcohol usage increases the health risks. The workers drinking alcohol has higher heart rates than the other ones. Therefore, it is advised workers to not drink alcohol especially lunch.

It also affects the Occupational Safety if employers do not obey the recommended rest durations. Hence, the losses in the productivities of workers can not be considered as the economic losses of the firms. It is more frequent to see occupational accidents in a workplace where employers do not give permission to workers to have a rest. The productivity losses and corresponding occurrence of occupational accidents of workers are directly related to the working period without having a rest.

In a specific research, iron and steel industry is found as one of the dangerous sectors in which hazardous heat strain is more frequently seen by researchers. Extremely hot environments cause health problems in the steel workplaces and this fact was revealed in previous studies. For instance, a survey was performed with approximately 60.000 workers and it was found that nonmalignant digestive system diseases occurred and the death risk increase three and a half fold in the environments where the WBGT is bigger than 26.1°C. In another study, WBGT measurements were taken from 54 workers who were melting electric spring and casting in China. Hereunder, the measurements taken in consecutive two days showed that WBGT is between the range 25.4°C and 28.7°C in casting and 30°C and 33.2°C in the melting electric spring jobs. Moreover, signs of fatigue increased and abnormalities were seen in blood pressure and heart rate in concurrence with the increase in temperature [194]. In another study, dealing with melting and casting jobs in Iran, WBGT measurements were taken and it altered between 22°C and 40.8°C and the average of these measurements was 30.7°C. The measurements were also classified according to the metabolic rates as light, moderate, heavy and very heavy and it was found that 69 % of them were over the limit values [195]. WBGT measurements were also taken in a work place in The United Arab Emirates where various types of works were done. Two of them are taken in the

furnace area; casting were operating; and they are calculated as 32.5°C and 32°C [196]. In India, the thermal comfort measurements were taken from 350 employees who were working in casting sector. WBGT changed between 33.47°C and 38.03°C in the areas where forging operations were performing and between 32.17°C and 37.31°C in the ones where melting jobs were performing [197]. Heat strain was felt in most of the departments of steel and iron production sector, and hence they are the ones in which integrative precautions and regulations have to be done. The furnaces; heat treatment is densely done; are the places where extra precautions have to be taken and special importance has to be given. In addition to furnaces, dyhouses, cutting, coiling and slitting are the other work types in this sector which it is necessary to improve the thermal conditions and decrease temperature and relative humidity in those jobs.

Specialization of workers at least in two jobs; including light and heavy one; is required in the tractor production factory which involves various work types. By this way, heat strain on the workers can be reduced to the level being riskless via rotation in the jobs. Labor productivities of workers in automotive sector in which most of the jobs are similar, depending on temperature and relative humidity records in the environment were observed. Statistically significant results were found and it was calculated that productivity decreases as relative humidity and/or WBGT increases [198]. According to a specific study, focusing on various sectors, extreme temperature and high relative humidity were more frequently observed in the jobs of iron-steel industry, glass industry and some of the military and aircraft facilities. Heat strain was determined as one of the main risk factor in one of the outstanding Air Force Station in India with respect to taken WBGT measurements. The average temperatures changed between 24.2°C and 30.2°C and the maximum temperatures reached up to 35°C in the constructing asphalt road and the minimum records were obtained in the radar laboratories [199]. In this study, similar WBGT results and outcomes were acquired. Workers, especially dealing with chemical operations, have to be rest.

The temperature and humidity of the environment has to be kept constant during the process of obtaining cotton yarn. Therefore, it is not possible to intervene the operation of the established system. There are some arrangements to reform the work-

ing conditions. One of them is improving the design of the machines to decrease the heat stress on workers. Others are to supply convenient air conditioning systems in the workplaces and decreasing the clothing coefficients of the workers. It is observed that another important physical risk for the workers in textile sector is dust. Hence, in addition to improvements in the thermal conditions, reduction in the dust concentration is also attained if the adequate ventilation is activated in these sorts of workplaces. Although firms have sufficient equipment and source for the air conditioning, they sometimes do not activate them to not spend more money for energy consumption.

Corrugated board production is a process which is made at high precision and at a certain pressure, temperature and relative humidity to prevent deterioration and contortion. Huge amount of water is used at a high pressure to provide necessary moisturizing conditions in an attempt to attain convenient wimpling and prepare a mixture for epoxying. Temperature has to be in the range between 120°C and 180°C to dry the mixture. Huge amount of energy is necessary to ensure these conditions. According to the 2012 statistics, 91 firms at 114 fabrics produce more than 1.3 million tons of corrugated board production in Turkey. In this ector, thermal conditions show an alteration with respect to season, the location of the workplaces, mode of production and work types. By all accounts, the machines, producing corrugated boards spread heat in especially summer season and the workers, using these machines have risk in the sense of thermal comfort. The results come together in two edge of heaps because of the differences of the workplaces' thermal comfort conditions. From these results, it is understood that the heat stress risk can be eliminated by improving the working conditions.

Several thermal comfort measurements were taken from various parts of workplaces of different firms which produce plastic equipment by using black granule. It was observed that only one of the firms have high WBGT values. Hence, thermal comfort measurements were taken from two more firms to understand and observe the heat stress risk in the workplaces. Plastic crate and small plastic equipment for electric systems are produced in these two firms by using black granule. None of the WBGT was over the critical values in these workplaces because they are well-organized and

wide having suitable ventilation systems. The success in the arrangement of machines and workplaces prevent the possible heat stress. It can be concluded that arranging the working conditions and workplaces is effective and of top priority solution to annihilate the heat stress in plastic sector.

Furnace temperatures have to be over 1000°C for porcelain production and this induces naturally a hot environment. In these workplaces, losses in production of workers, especially working close to furnaces, can be seen. Maximum WBGT records in this sector in Turkey were measured in the factories, located in Kutahya city on November, although seasonal and annual air temperature records of İzmir city is higher than Kütahya and some measurements were taken from the fabrics in İzmir city. According to these results, it can be concluded that thermal conditions in this sector were not affected by the location and outside temperature and relative humidity. There are some studies, dealing with the hazardous effects of thermal comfort on the health and safety of workers and labor productivity losses base on these effects. In one of the research, labor productivity losses of workers in construction and ceramic sectors depending on the WBGT measurements were calculated and it was envisaged that the losses change in the range of 10 % and 60 %. In an extensive study, carried out in India, WBGT measurements were taken from 587 metal workers, 426 ceramics workers and 934 quarry workers. Approximately 75 % of WBGT index was calculated between 30.1°C and 35.5°C and 10 % of them was in the range 38.6°C and 41.2°C [200]. These temperatures are high enough to give rest periods for workers. WBGT index was measured in Thailand from 23 ceramics workers and average WBGT was calculated as 33.3°C [201]. This amount indicates that these workers were under serious risk, stemming from adverse thermal comfort conditions.

Whole jobs around the furnaces of manufacturing of ceramics medical products involve high risk in the sense of thermal comfort. Improvements have to be made by taking into consideration of all workers in these parts of the fabrics. Establishment of ventilation systems or remediation in the air conditioning systems for reducing the heat stress is necessary to reduce the heat strain risks of workers. Water dispensers have to set up periodically because liquid necessity of workers is very high in these

departments. Burning the candle at both ends has to be precluded and workers have to be rest in certain periods. Besides, employees have to wear light clothes and the workplaces have to be arranged to prevent draught exposures in the passing ways of workers.

Aluminum sector was investigated in several researches because it is one of the most risky one in the sense of thermal comfort. Heat stress of workers was calculated via WBGT and a guide was published including adverse effects of thermal comfort on workers healthy in this sector [202]. Heart rate and core temperatures of workers in aluminum sector were recorded and by this means, heat stress on workers was investigated. The average WBGT index, measuring in 4 weeks in July and August, is analyzed and found as 24°C. Besides, hearth rates reached up to levels in which cause health problems [203].

There were not any studies about thermal comfort conditions in construction sites and worksites in Turkey, but there were several ones in which investigated the heat stress in these workplaces. For example, workplaces were classified to different groups in a study in which necessary precautions were tried to be determined to prevent the occupational accidents in constructions, stemming from personal and organizational stress. One of the main factor, triggering stress and occupational accidents is hot temperature and it is collected under the topic of insufficient physical environment [204]. Occupational injuries are more frequently seen in such adverse workplaces than in the ones, having suitable thermal environment. Reducing the environmental temperatures in these workplaces is one of the prime solutions to prevent occupational injuries, because hot environments in constructions and worksites induce occupational illness and accidents. In another research, it was found that 36 of 216 workers in 29 different worksites in China have serious heat related disorders [140]. Constructions have serious heat exposure risk because building workers, likewise farmers, are exposed to hot environment directly. Approximately, 64 % of heat related deaths happened in construction sector in Japan with respect to 2010 statistics. There are various studies in the literature in which WBGT is used to estimate the thermal comfort of the workers. Most of these studies used direct measurements in fabrics or small farms. There

were very limited researches, using the climatic variables of the climate model and estimate the alteration of WBGT in a large area. In this thesis, WBGT is calculated in continental scale by using climatic variables of model combinations. Moreover, it is the first time that the daily outputs of five different regions of CORDEX Project are used to project the current and further alteration of WBGT.

3. DATA

CORDEX is the newest initiative including climate projections over several domains. Europe Region (EUROPE) is one of these domains over which several RCMs simulate past and future climate. EUROPE-CORDEX takes advantage of daily and monthly temperature, maximum temperature time series, starting with 1950 and ending up 2100. Aforesaid RCMs are run by using several GCM outputs of three Representative Concentration Pathways (RCP2.6, RCP4.5 and RCP8.5) classified by possible radiative forces in 21th century corresponding with pre-industrial value, as IC/BC. All of them are taken into account as model results in this thesis. E-OBS dataset [205] from the EU-FP6 project ENSEMBLES [206] is chosen as the observation data set since it produces results over the same grids with RCM models used in CORDEX Project for one of the selected areas. For the others, WCRP [207] and CRU data sets [208] are used as observation data set for the other areas. There are very limited observation data set in the literature. Most of them have very low resolution. Majority of the ones having high resolutions do not cover the period between 1976 and 2005. CRU is the one having high resolution, covering the observed time scale and it is the most widely used and reliable observation data set. However, CRU does not have Daily observation data set. WCRP is the unique daily data set having high resolution over the whole World. Hence, the daily maximum temperature of WCRP is used as observation data set.

There are various types of huge data sets used in this thesis. In the following, the names and abbreviations of these data sets, applied in different sub-sections, will be presented.

3.1. Historical and Observed Monthly Temperature Data Set

The observed areas are the Europe, Africa, West Asia, Central and South America for which the coverage areas are defined in CORDEX Project. The monthly average temperature of RCM-GCM combinations acquiring from CORDEX Project is the an-

alyzed climatic variable in this section of the thesis. 26 RCM-GCM combinations over Europe, 27 combinations over Africa, 17 combinations over West Asia, 14 combinations over Central America and 9 combinations over South America are available in CORDEX Project and are used as data sets in this thesis. The names and abbreviations of the model combinations for each domain are shown in Tables 3.3 to 3.7.

For the CORDEX-Europe domain, E-OBS daily temperature data sets, having the same resolutions with model combinations (0.44 ° x 044 °), are monthly averaged and are used as observation data set for comparison. Monthly CRU temperature data sets with 0.5 ° x 0.5 ° resolutions are chosen as the observation data sets for the remaining areas. The model combinations, having 0.44 ° x 044 ° rotated resolutions, are bilinearly interpolated to the CRU grids.

Table 3.1. The Names and Abbreviations of GCMs

Model Name	**Institution Name**	**Regional Climate Model**
CCCma	Canadian Centre for Climate Modelling and Analysis, Canada	CanESM2
CNRM-CERFACS	Centre National de Recherches Météorologiques, France	CNRM-CM5
CSIRO-QCCCE	The Commonwealth Scientific and Industrial Research Organisation, Australia	CSIRO-Mk3-6-0
ICHEC-EC-EARTH	EC-Earth community, currently lead by Swedish Meteorological and Hydrological Institute	EC-EARTH
IPSL-INERIS	Institut Pierre Simon Laplace, France	IPSL-CM5A
MIROC	International Centre for Earth Simulation, Model for Interdisciplinary Research on Climate, Switzerland	MIROC5
MOHC	Met Office Hadley Centre,UK	HadGEM2
MPI-M	Max Planck Institute for Meteorology	MPI-ESM
NCC	Norwegian Climate Centre	NorESM
NOAA-GFDL	National Oceanic and Atmospheric Administration,Geophysical Fluid Dynamics Laboratory	GFDL

Table 3.2. The Names and Abbreviations of RCMs

Model Name	**Institution Name**	**Regional Climate Model**
CLMcom	Climate Limited-area Modelling Community (CLM-Community), Switzerland	CCLM4-8-17
CLMcom	Climate Limited-area Modelling Community (CLM-Community), Switzerland	CCLM5-0-6
CNRM	Météo-France / Centre National de Recherches Météorologiques, France	ALADIN52
CNRM	Météo-France / Centre National de Recherches Météorologiques, France	ALADIN53
DMI	Danish Meteorological Institute, Denmark	HIRHAM5
HMS	Hungarian Meteorological Service, Hungaria	ALADIN52
ICTP	Abdus Salam International Centre for Theoretical Physics, Italy	RegCM4-3
IPSL-INERIS	Institut Pierre-Simon Laplace, France	WRF331F
KNMI	Royal Netherlands Meteorological Institute, De Bilt, The Netherlands,Netherlands	RACMO22E
KNMI	Royal Netherlands Meteorological Institute, De Bilt, The Netherlands,Netherlands	RACMO22T
MPI-CSC	Helmholtz-Zentrum Geesthacht, Climate Service Center, Max Planck Institute for Meteorology, Germany	REMO2009
RMIB-Ugent	Royal Meteorological Institute of Belgium and Ghent University, Belgium	ALARO-0
RCA4	Swedish Meteorological and Hydrological Institute, Rossby Centre, Sweden	RCA4
UCAN	University of Cantabria, Spain	WRF341I
UQAM	Universite du Quebec a Montreal, Canada	CRCM5

The meaning of the abbrevations of the GCMs and RCMs is listed in Table 3.1 and Table 3.2. For example, in MPI–M–MPI–ESM–LR-CLM–CCLM4–8–17–v1; MPI-M indicates Max Planck Institute for Meteorology, MPI-ESM indicates the name of GCM, -LR indicates low resolution, CLM indicates the Climate Limited-area Modelling Community (CLM-Community) leading by Switzerland, CCLM4–8–17 is the name of their RCM. In other words, Climate Limited-area Modelling Community (CLM)'s CCLM4–8–17 Regional Climate Model is forced by the outputs of Max Planck Institute for Meteorology (MPI-M)'s Global Climate Model MPI-ESM.

Table 3.3. The Names and Abbreviations of RCM / GCM model combinations for the monthly temperature of Europe

EUROPE	**GCM–RCM**
CCCma–CanESM2–SMHI–RCA4–v1	CCCma–RCA4
CNRM–CERFACS–CNRM–CM5–CLMcom–CCLM5–0–6–v1	CNRM–CLM
CNRM–CERFACS–CNRM–CM5–CNRM–ALADIN53–v1	CNRM–CNRM
CNRM–CERFACS–CNRM–CM5–HMS–ALADIN52–v1	CNRM–HMS
CNRM–CERFACS–CNRM–CM5–RMIB–UGent–ALARO–0–v1	CHRM–RMIB
CNRM–CERFACS–CNRM–CM5–SMHI–RCA4–v1	CNRM–RCA4
CSIRO–QCCCE–CSIRO–Mk3–6–0–SMHI–RCA4–v1	CSIRO–RCA4
ICHEC–EC–EARTH–CLMcom–CCLM5–0–6–v1	ICHEC–CLM
ICHEC–EC–EARTH–KNMI–RACMO22E–v2	ICHEC–KNMI
ICHEC–EC–EARTH–SMHI–RCA4–v1	ICHEC–RCA4
ICHEC–EC–EARTH–KNMI–RACMO22E–v1	ICHEC–KNMI
ICHEC–EC–EARTH–DMI–HIRHAM5–v1	ICHEC–DMI
IPSL–IPSL–CM5A–MR–IPSL–INERIS–WRF331F–v1	IPSL–IPSL
IPSL–IPSL–CM5A–MR–SMHI–RCA4–v1	IPSL–RCA4
MOHC–HadGEM2–ES–KNMI–RACMO22E–v2	MOHC–KNMI
MOHC–HadGEM2–ES–SMHI–RCA4–v1	MOHC–RCA4
MIROC–MIROC5–CLMcom–CCLM5–0–6–v1	MIROC–CLM
MIROC–MIROC5–SMHI–RCA4–v1	MIROC–RCA4
MPI–M–MPI–ESM–LR–SMHI–RCA4–v1	MPI–RCA4
NCC–NorESM1–M–SMHI–RCA4–v1	NCC–RCA4
NOAA–GFDL–GFDL–ESM2M–SMHI–RCA4–v1	NOAA–RCA4
MOHC–HadGEM2–ES-CLM–CCLM5–0–6–v1	MOHC–CLM
MPI–M–MPI–ESM–LR-CLM–CCLM4–8–17–v1	MPI–CLM1
MPI–M–MPI–ESM–LR-CLM–CCLM5–0–6–v1	MPI–CLM2
MPI–M–MPI–ESM–LR–MPI–CSC–REMO2009–v1	MPI–REMO1
MPI–M–MPI–ESM–LR–MPI–CSC–REMO2009–v2	MPI–REMO2

Table 3.4. The Names and Abbreviations of RCM / GCM model combinations for the monthly temperature of Africa

AFRICA	**GCM – RCM**
CCCma-CanESM2 – UQAM-CRCM5–v1	CCCma-UQAM
CSIRO-QCCCE-CSIRO-Mk3-6-0 – SMHI-RCA4–v1	CSIRO-RCA4
MIROC-MIROC5 – SMHI-RCA4–v1	MIROC-RCA4
MOHC-HadGEM2-ES – SMHI-RCA4–v1	MOHC-RCA4
MPI-M-MPI-ESM-LR – SMHI-RCA4–v1	MPI-RCA4
CCCma-CanESM2 – SMHI-RCA4–v1	CCCma – RCA4
CNRM-CERFACS-CNRM-CM5 – CLMcom-CCLM4-8-17–v1	CNRM- CLM
CNRM-CERFACS-CNRM-CM5 – SMHI-RCA4–v1	CNRM-RCA4
ICHEC-EC-EARTH – CLMcom-CCLM4-8-17–v1	ICHEC-CLM
ICHEC-EC-EARTH – KNMI-RACMO22T–v1	ICHEC-KNMI
ICHEC-EC-EARTH – MPI-CSC-REMO2009–v1	ICHEC-MPI
ICHEC-EC-EARTH – SMHI-RCA4–v1	ICHEC-RCA4
ICHEC-EC-EARTH – KNMI-RACMO22T–v2	ICHEC-KNMI2
ICHEC-EC-EARTH – DMI-HIRHAM5–v2	ICHEC-DMI
IPSL-IPSL-CM5A-LR – GERICS-REMO2009–v1	IPSL- REMO
IPSL-IPSL-CM5A-MR – SMHI-RCA4–v1	IPSL-RCA4
MIROC-MIROC5 – GERICS-REMO2009–v1	MIROC-REMO
MOHC-HadGEM2-ES – CLMcom-CCLM4-8-17–v1	MOHC-CLM
MOHC-HadGEM2-ES – GERICS-REMO2009–v1	MOHC-REMO
MOHC-HadGEM2-ES – KNMI-RACMO22T–v2	MOHC-KNMI
MPI-M-MPI-ESM-LR – CLMcom-CCLM4-8-17–v1	MPI-CLM
MPI-M-MPI-ESM-LR – MPI-CSC-REMO2009–v1	MPI-REMO
MPI-M-MPI-ESM-LR – UQAM-CRCM5–v1	MPI-UQAM
NCC-NorESM1-M – DMI-HIRHAM5–v1	NCC-DMI
NCC-NorESM1-M – SMHI-RCA4–v1	NCC-RCA4
NOAA-GFDL-GFDL-ESM2G – GERICS-REMO2009–v1	NOAA-REMO
NOAA-GFDL-GFDL-ESM2M – SMHI-RCA4–v1	NOAA-RCA4

Table 3.5. The Names and Abbreviations of RCM / GCM model combinations for the monthly temperature of Central America

CENTRAL AMERICA	**GCM – RCM**
MOHC-HadGEM2-ES–ICTP-RegCM4-3–v4	MOHC-RegCM
MPI-M-MPI-ESM-LR–SMHI-RCA4–v1	MPI-RCA4
CNRM-CERFACS-CNRM-CM5–SMHI-RCA4–v1	CNRM-RCA4
CCCma-CanESM2–SMHI-RCA4–v1	CCCma-RCA4
CSIRO-QCCCE-CSIRO-Mk3-6-0–SMHI-RCA4–v1	CSIRO-RCA4
ICHEC-EC-EARTH–SMHI-RCA4–v1	ICHEC-RCA4
IPSL-IPSL-CM5A-MR–SMHI-RCA4–v1	IPSL-RCA4
MIROC-MIROC5–SMHI-RCA4–v1	MIROC-RCA4
MOHC-HadGEM2-ES–ICTP-RegCM4-3–v2	MOHC-RegCM
MOHC-HadGEM2-ES–SMHI-RCA4–v1	MOHC-RCA4
MPI-M-MPI-ESM-MR–ICTP-RegCM4-3–v4	MPI-RegCM
MPI-M-MPI-ESM-MR–ICTP-RegCM4-3–v4	MPI-RegCM2
NCC-NorESM1-M–SMHI-RCA4–v1	NCC-RCA4
NOAA-GFDL-GFDL-ESM2M–SMHI-RCA4–v1	NOAA-RCA4

Table 3.6. The Names and Abbreviations of RCM / GCM model combinations for the monthly temperature of South America

SOUTH AMERICA	**GCM – RCM**
CCCma-CanESM2–SMHI-RCA4–v3	CCCma-RCA4
CSIRO-QCCCE-CSIRO-Mk3-6-0–SMHI-RCA4–v3	CSIRO-RCA4
IPSL-IPSL-CM5A-MR–SMHI-RCA4–v3	IPSL-RCA4
ICHEC-EC-EARTH–SMHI-RCA4–v3	ICHEC-RCA4
MIROC-MIROC5–SMHI-RCA4–v3	MIROC-RCA4
MOHC-HadGEM2-ES–SMHI-RCA4–v3	MOHC-RCA4
MPI-M-MPI-ESM-LR–SMHI-RCA4–v3	MPI-RCA4
NCC-NorESM1-M–SMHI-RCA4–v3	NCC-RCA4
NOAA-GFDL-GFDL-ESM2M–SMHI-RCA4–v3	NOAA-RCA4

Table 3.7. The Names and Abbreviations of RCM / GCM model combinations for the monthly temperature of West Asia

WEST ASIA	**GCM – RCM**
CSIRO-QCCCE-CSIRO-Mk3-6-0–SMHI-RCA4–v2	CSIRO-RCA4
IPSL-IPSL-CM5A-MR–SMHI-RCA4–v2	IPSL-RCA4
CCCma-CanESM2–SMHI-RCA4–v2	CCCma-RCA4
CCCma-CanESM2–IITM-RegCM4-4–v5	CCCma-RegCM
CNRM-CERFACS-CNRM-CM5–IITM-RegCM4-4–v5	CNRM-RegCM
CNRM-CERFACS-CNRM-CM5–SMHI-RCA4–v2	CNRM-RCA4
CSIRO-QCCCE-CSIRO-Mk3-6-0–IITM-RegCM4-4–v5	CSIRO-RegCM
ICHEC-EC-EARTH–SMHI-RCA4–v2	ICHEC-RCA4
IPSL-IPSL-CM5A-LR–IITM-RegCM4-4–v5	IPSL-RegCM
MIROC-MIROC5–SMHI-RCA4–v2	MIROC-RCA4
MOHC-HadGEM2-ES–SMHI-RCA4–v2	MOHC-RCA4
MPI-M-MPI-ESM-LR–MPI-CSC-REMO2009–v1	MPI-REMO
MPI-M-MPI-ESM-LR–SMHI-RCA4–v2	MPI-RCA4
MPI-M-MPI-ESM-MR–IITM-RegCM4-4–v5	MPI-RegCM
NCC-NorESM1-M–SMHI-RCA4–v2	NCC-RCA4
NOAA-GFDL-GFDL-ESM2M–IITM-RegCM4-4–v5	NOAA-RegCM
NOAA-GFDL-GFDL-ESM2M–SMHI-RCA4–v2	NOAA-RCA4

3.2. Future Monthly Temperature Data Set

The observed areas are Europe, Africa, West Asia, Central and South America for which the coverage areas are defined in CORDEX Project. The RCM-GCM combinations are obtained from CORDEX Project and monthly average temperature is climatic variable that is analyzed. RCM-GCM combinations for RCP 2.6, RCP 4.5 and RCP 8.5 over these domains are used for the future estimation of aforementioned variables in this thesis.

3.3. Historical, Observed and Future Daily Maximum Temperature Data Set

The observed areas are the same in 3.1 Section. The RCM-GCM combinations are obtained from CORDEX Project and daily maximum temperature is the climatic variable, that is analyzed. 22 RCM-GCM combinations over Europe, 26 combinations over Africa, 11 combinations over West Asia, 14 combinations over Central America and 9 combinations over South America are available in CORDEX Project and are used as data sets in this thesis. The names and abbreviations of the model combinations for each domain are shown in Tables 3.8 to 3.12.

For the CORDEX-Europe domain, E-OBS daily maximum temperature data sets, having the same resolution with model combinations (0.44 ° x 0.44 °), are monthly averaged and are used as observation data set for comparison. Daily WCRP maximum temperature data sets with 0.5 ° x 0.5 ° resolutions are chosen as the observation data sets for the other areas. They bilinear interpolated to the grids of model combinations, having 0.44 ° x 0.44 ° rotated resolutions.

Table 3.8. The Names and Abbreviations of RCM / GCM model combinations for the daily maximum temperature of Europe

EUROPE	**GCM – RCM**
MIROC-MIROC5-SMHI-RCA4-v1	MIROC-RCA4
MOHC-HadGEM2-ES-KNMI-RACMO22E-v2	MOHC-KNMI
MOHC-HadGEM2-ES-SMHI-RCA4-v1	MOHC-RCA4
MPI-M-MPI-ESM-LR-SMHI-RCA4-v1	MPI-RCA4
CCCma-CanESM2-SMHI-RCA4-v1	CCCma-RCA4
CCCma-CanESM2-UCAN-WRF341I-v2	CCCma-UCAN
CNRM-CERFACS-CNRM-CM5-CLMcom-CCLM5-0-6-v1	CNRM-CLM
CNRM-CERFACS-CNRM-CM5-SMHI-RCA4-v1	CNRM-RCA4
CSIRO-QCCCE-CSIRO-Mk3-6-0-SMHI-RCA4-v1	CSIRO-RCA4
ICHEC-EC-EARTH-CLMcom-CCLM5-0-6-v1	ICHEC-CLM
ICHEC-EC-EARTH-DMI-HIRHAM5-v1	ICHEC-DMI
ICHEC-EC-EARTH-KNMI-RACMO22E-v1	ICHEC-KNMI
ICHEC-EC-EARTH-KNMI-RACMO22E-v2	ICHEC-KNMI2
ICHEC-EC-EARTH-SMHI-RCA4-v1	ICHEC-RCA4
IPSL-IPSL-CM5A-MR-SMHI-RCA4-v1	IPSL-RCA4
MIROC-MIROC5-CLMcom-CCLM5-0-6-v1	MIROC-CLM
MOHC-HadGEM2-ES-CLMcom-CCLM5-0-6-v1	MOHC-CLM
MPI-M-MPI-ESM-LR-CLMcom-CCLM4-8-17-v1	MPI-CLM
MPI-M-MPI-ESM-LR-CLMcom-CCLM5-0-6-v1	MPI-CLM2
MPI-M-MPI-ESM-LR-MPI-CSC-REMO2009-v1	MPI-REMO
MPI-M-MPI-ESM-LR-MPI-CSC-REMO2009-v2	MPI-REMO2
NCC-NorESM1-M-SMHI-RCA4-v1	NCC-RCA4
NOAA-GFDL-GFDL-ESM2M-SMHI-RCA4-v1	NOAA-RCA4

Table 3.9. The Names and Abbreviations of RCM / GCM model combinations for the daily maximum temperature of Africa

AFRICA	**GCM – RCM**
CSIRO-QCCCE-CSIRO-Mk3-6-0-SMHI-RCA4-v1	CSIRO-RCA4
IPSL-IPSL-CM5A-MR-SMHI-RCA4-v1	IPSL-RCA4
MIROC-MIROC5-SMHI-RCA4-v1	MIROC-RCA4
MOHC-HadGEM2-ES-SMHI-RCA4-v1	MOHC-RCA4
MPI-M-MPI-ESM-LR-SMHI-RCA4-v1	MPI-RCA4
CCCma-CanESM2-SMHI-RCA4-v1	CCCma-RCA4
CCCma-CanESM2-UQAM-CRCM5-v1	CCCma-UQAM
CNRM-CERFACS-CNRM-CM5-CLMcom-CCLM4-8-17-v1	CNRM-CLM
CNRM-CERFACS-CNRM-CM5-SMHI-RCA4-v1	CNRM-RCA4
ICHEC-EC-EARTH-DMI-HIRHAM5-v2	ICHEC-DMI
ICHEC-EC-EARTH-KNMI-RACMO22T-v1	ICHEC-KNMI
ICHEC-EC-EARTH-KNMI-RACMO22T-v2	ICHEC-KNMI2
ICHEC-EC-EARTH-MPI-CSC-REMO2009-v1	ICHEC-REMO
ICHEC-EC-EARTH-SMHI-RCA4-v1	ICHEC-RCA4
IPSL-IPSL-CM5A-LR-GERICS-REMO2009-v1	IPSL-REMO
MIROC-MIROC5-GERICS-REMO2009-v1	MIROC-REMO
MOHC-HadGEM2-ES-CLMcom-CCLM4-8-17-v1	MOHC-CLM
MOHC-HadGEM2-ES-GERICS-REMO2009-v1	MOHC-REMO
MOHC-HadGEM2-ES-KNMI-RACMO22T-v2	MOHC-KNMI
MPI-M-MPI-ESM-LR-CLMcom-CCLM4-8-17-v1	MPI-CLM
MPI-M-MPI-ESM-LR-MPI-CSC-REMO2009-v1	MPI-REMO
MPI-M-MPI-ESM-LR-UQAM-CRCM5-v1	MPI-UQAM
NCC-NorESM1-M-DMI-HIRHAM5-v1	NCC-DMI
NCC-NorESM1-M-SMHI-RCA4-v1	NCC-RCA4
NOAA-GFDL-GFDL-ESM2G-GERICS-REMO2009-v1	NOAA-REMO
NOAA-GFDL-GFDL-ESM2M-SMHI-RCA4-v1	NOAA-RCA4

Table 3.10. The Names and Abbreviations of RCM / GCM model combinations for the daily maximum temperature of Central America

CENTRAL AMERICA	**GCM – RCM**
MPI-M-MPI-ESM-MR-ICTP-RegCM4-3-v2	MPI-RegCM
MOHC-HadGEM2-ES-ICTP-RegCM4-3-v2	MOHC-RegCM
CCCma-CanESM2-SMHI-RCA4-v1	CCCma-RCA4
CNRM-CERFACS-CNRM-CM5-SMHI-RCA4-v1	CNRM-RCA4
CSIRO-QCCCE-CSIRO-Mk3-6-0-SMHI-RCA4-v1	CSIRO-RCA4
ICHEC-EC-EARTH-SMHI-RCA4-v1	ICHEC-RCA4
IPSL-IPSL-CM5A-MR-SMHI-RCA4-v1	IPSL-RCA4
MIROC-MIROC5-SMHI-RCA4-v1	MIROC-RCA4
MOHC-HadGEM2-ES-ICTP-RegCM4-3-v4	MOHC-RegCM
MOHC-HadGEM2-ES-SMHI-RCA4-v1	MOHC-RCA4
MPI-M-MPI-ESM-LR-SMHI-RCA4-v1	MPI-RCA4
MPI-M-MPI-ESM-MR-ICTP-RegCM4-3-v4	MPI-RegCM
NCC-NorESM1-M-SMHI-RCA4-v1	NCC-RCA4
NOAA-GFDL-GFDL-ESM2M-SMHI-RCA4-v1	NOAA-RCA4

Table 3.11. The Names and Abbreviations of RCM / GCM model combinations for the daily maximum temperature of South America

SOUTH AMERICA	**GCM – RCM**
MIROC-MIROC5-SMHI-RCA4-v3	MIROC-RCA4
CCCma-CanESM2-SMHI-RCA4-v3	CCCma-RCA4
CSIRO-QCCCE-CSIRO-Mk3-6-0-SMHI-RCA4-v3	CSIRO-RCA4
ICHEC-EC-EARTH-historical-r12i1p1-SMHI-RCA4-v3	ICHEC-RCA4
IPSL-IPSL-CM5A-MR-SMHI-RCA4-v3	IPSL-RCA4
MOHC-HadGEM2-ES-SMHI-RCA4-v3	MOHC-RCA4
MPI-M-MPI-ESM-LR-SMHI-RCA4-v3	MPI-RCA4
NCC-NorESM1-M-SMHI-RCA4-v3	NCC-RCA4
NOAA-GFDL-GFDL-ESM2M-SMHI-RCA4-v3	NOAA-RCA4

Table 3.12. The Names and Abbreviations of RCM / GCM model combinations for the daily maximum temperature of West Asia

WEST ASIA	**GCM – RCM**
CSIRO-QCCCE-CSIRO-Mk3-6-0-SMHI-RCA4-v2	CSIRO-RCA4
CCCma-CanESM2-SMHI-RCA4-v2	CCCma-RCA4
CNRM-CERFACS-CNRM-CM5-SMHI-RCA4-v2	CNRM-RCA4
ICHEC-EC-EARTH-SMHI-RCA4-v2	ICHEC-RCA4
IPSL-IPSL-CM5A-MR-SMHI-RCA4-v2	IPSL-RCA4
MIROC-MIROC5-SMHI-RCA4-v2	MIROC-RCA4
MOHC-HadGEM2-ES-SMHI-RCA4-v2	MMOHC-RCA4
MPI-M-MPI-ESM-LR-MPI-CSC-REMO2009-v1	MPI-REMO
MPI-M-MPI-ESM-LR-SMHI-RCA4-v2	MPI-RCA4
NCC-NorESM1-M-SMHI-RCA4-v2	NCC-RCA4
NOAA-GFDL-GFDL-ESM2M-SMHI-RCA4-v2	NOAA-RCA4

3.4. Historical and Future Daily Relative Humidity

Historical and future daily relative humidity data sets, used in this thesis, are RCM-GCM combinations for RCP 2.6, RCP 4.5 and RCP8.5 over aforementioned domains.

4. METHODOLOGY

4.1. Method 1: GCM-RCM Combination Selection with respect to Monthly Temperature Data Set

Three main statistical tools (AAE, RMSE, T-Test) are used as indicator and four main methods are used to select the most convenient GCM-RCM Combination in this thesis. In the following, these are explained in detail.

4.1.1. Statistical Method 1: AAE as Indicator and Monthly Average Temperature as Data Set

Step 1: The difference between the model and the observation values at each grid is computed and average errors (AE) are calculated for each season. Positive/Negative values reveal the overestimation/underestimation of model and hence desirable AE is "0". It follows from this that having AE close to "0" is one the significant indicator that portrays the reliability of the model.

The monthly temperature of MPI–M –MPI–ESM–LR-CLM–CCLM4–8–17–v1 in summer season in the years between 1976 and 2005 is taken as the model combation data set. Similarly, The monthly temperature of E-OBS in summer season in the years between 1976 and 2005 is taken as the observation data set. First of all the averages of 90 monthly temperature data set (3 months x 30 years) of both observation and model combination data set is calculated (Figure 4.1). As it is shown in the Figure 4.1, these averages are taken for each grid point (longitude, latitude).

Step 2: After this preliminary operation is carried out, absolute values of errors (AAE) are calculated for each grid point. Similar expectations in "Step 1" are also valid for AAE.

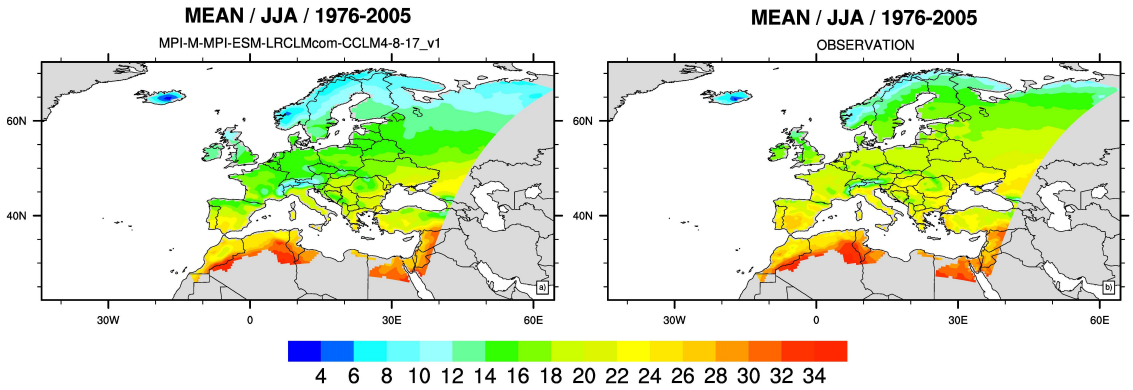

Figure 4.1. Mean of the model combination (MPI–M– MPI– ESM –LR- CLM–CCLM4–8–17–v1) and observation (E-OBS) data set in summer season in the period between the years 1976 and 2005

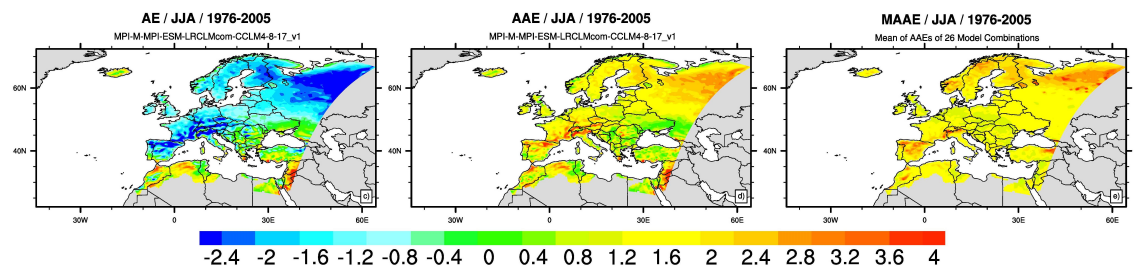

Figure 4.2. The difference between model combination and observation (AE), Absolute Value of The difference between model combination and observation (AAE), The Mean of 26 Models AAEs in each grid (MAAE)

Step 3: Then the mean value of these AAE values is calculated (MAEE) for each season and grid point. MAEE will be used as an indicator which separates the representative and unrepresentative models in the following steps.

The difference between the thirty years average of model combination (MPI–M–MPI–ESM–LR-CLM–CCLM4–8–17–v1) in the first column of Figure 4.1) and observation data set (E-OBS in the second row of Figure 4.1) is taken (first column of Figure 4.2) and AE is found in each grid point (AE). Then, the absolute value of the calculated difference is taken and AAE is found in each grid (second column of Figure 4.2). By this way, 26 AAE (for 26 model combinatios for Europe) is calculated for each grid point. At the last step, the averages of these 26 AAEs are calculated for each grid point and these average values of each grid point are assigned with MAAE (third column of Figure 4.2).

Step 4: Absolute values of errors (AAE) of every models in each season are compared with the mean value of absolute value of average errors (MAEE) at the corresponding season. If the AAE of a model at a given point grid point is smaller than MAAE at the same grid point, this value at that grid (DAEE) is assigned the value of "1". Otherwise DAEE is shown by "0". This operation is carried out for each grid at each season for all of the models. This is the first selection procedure. This is a simple but effective way to understand the success of a model by comparing the outcomes of all of its possible alternatives. All opportunities in this project are used to find the most suitable model/model combinations, representing the climatology patterns of observed region in the most correct way.

The AAE of model combination (MPI–M–MPI–ESM–LR-CLM–CCLM4–8–17–v1) in summer season (second row of Figure 4.2)in each grid is compared with the mean of all of the AAEs of all model combinations in each grid (third row of Figure 4.2) and the first row of first column of Figure 4.3 is obtained. If AAE of the model combination in a grid point is smaller than the mean of all of the AAEs of all model combinationsat the same grid point, then this grid point is assigned with 1. If it is bigger than MAAE, then it is assigned with 0. This operation is carried out for each

grid point in eah season (Figure 4.3).

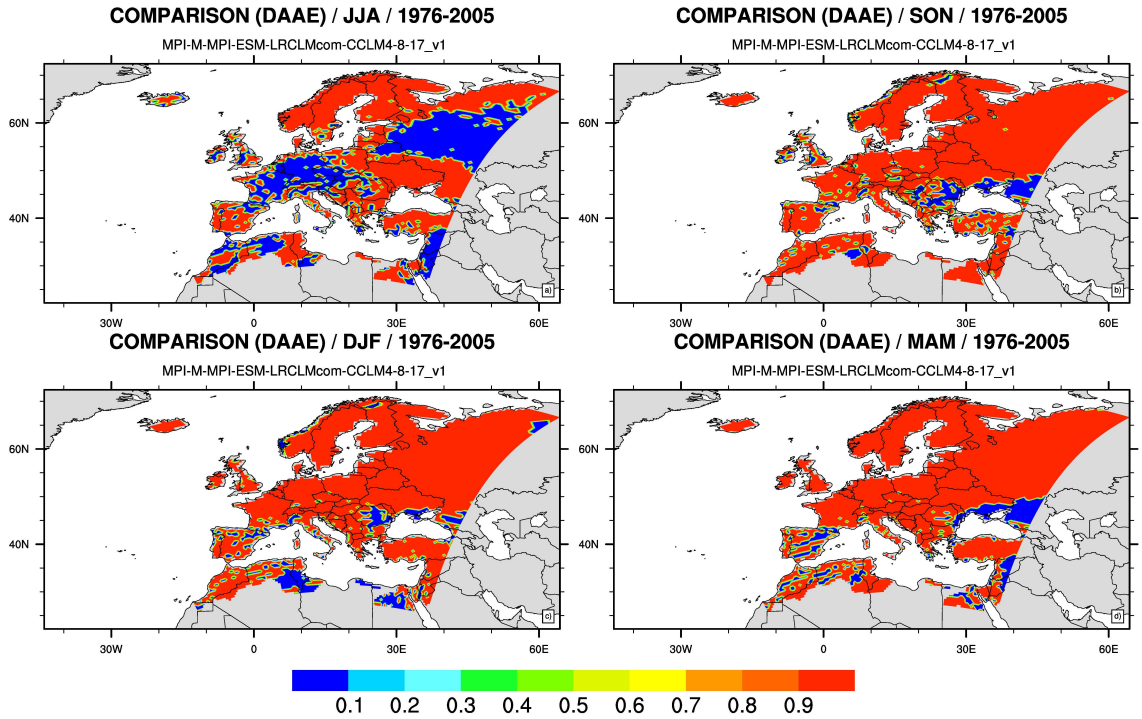

Figure 4.3. The comparison of model combination (MPI–M–MPI–ESM–LR-CLM–CCLM4–8–17–v1) with MAAE in each grid

It is problematic to exemplify the success of a model by a single value in every domain. It is one of the biggest drawbacks to assign a single value as a coefficient for a model over a huge area in multi-model ensemble studies. Hence, the advantage of this operation is to decide the accuracy of a model at specific areas in the studied domain by observing whole grid points.

Step 5: The previous step (Step 4) is fulfilled for each season. Thereby, the inter comparisons of models are carried out for each season. It is more comprehensive to measure the progress of a model in every season. In climate model studies, the success of a model is not determined season by season. Hereby, four obtained outcomes (comparison for four season / DAEE) for each model are summed up (SDAAE). Generated SDAAE values alter between 0 and 4. If SDAAE of a model at a grid point is close to 4, then it can be accepted that this model represents the climatology at that point

well in every season.

The comparison results (DAAEs, shown in Figure 4.3) of four seasons in each grid are added and sum of them, changing between 0 and 4 , is obtained for each grid (SDAAE, shown in the first row of Figure 4.4). 26 SDAAE (for 26 model combinatios for Europe) is calculated for each grid point. Then, the averages of these 26 SDAAEs are calculated for each grid point and these average values of each grid point are assigned with MSDAAE (second column of Figure 4.4).

Step 6: Operations made so for are carried out again to determine the model combinations which are representative in all/majority of the seasons. The average of SDAEE of all models at each seasons and every grid points is calculated (MSDAEE). Then, the representativeness of a model is testified by performing a comparison. Namely, if the SDAAE of a model at a unique grid is bigger than MSDAAE at the same grid, it is assigned the value of "1" (DSDAAE). This is the second selection procedure.

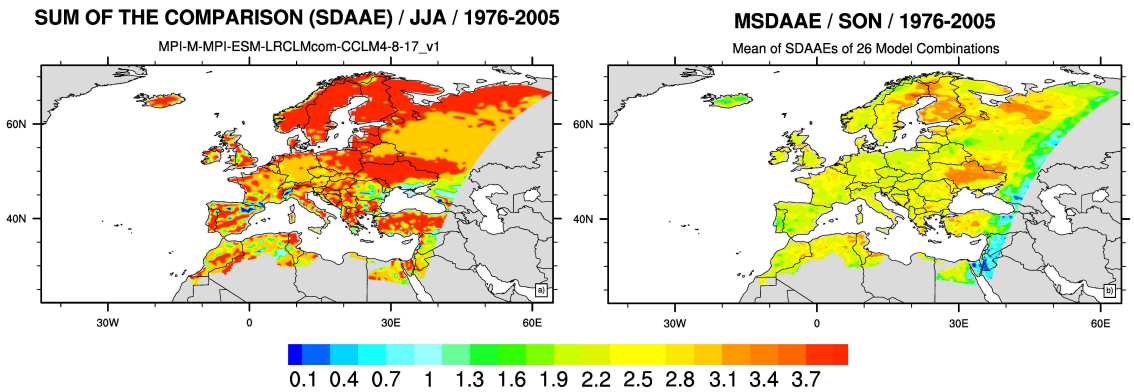

Figure 4.4. The comparison of the sum of comparisons of all seasons (SDAAE) of model combination (MPI–M–MPI–ESM–LR-CLM–CCLM4–8–17 –v1) with MSDAAE in each grid

The value in each grid point in the first column of Figure 4.4 is compared to the value in each grid point in the second column of Figure 4.4. If the value of a grid point in the first graph (first column) is bigger than the corresponding one in the second

graph, than it is assigned with 1. If it is smaller than the one in MSDAAE, than it is assigned wth 0. By this way, Figure 4.5, which represents the sucess of MPI–M –MPI–ESM–LR-CLM–CCLM4–8–17–v1 model combinations.

Step 7: The spatial averages of whole grid points covering an observed region are calculated (WDSDAAE) and a unique value is found for each model. There are 26 unique WDSDAAE values and the averages (AWDSDAAE) and standard deviation (VWDSDAAE) of these values are calculated. By summing AWDSDAAE and VWDSDAAE are added and a limit value (TWDSDAAE) is found to use in further comparison steps.

In Table 5.3, the spatial average of the sucess of all grid point is represented. It demonstrates that 85 % of MPI–M –MPI–ESM–LR-CLM–CCLM4–8–17–v1 is sucessful.The spatial averages and standard deviation of 26 model combinations' sucess ratio is calculated. The average value is found as 0.48 and standard deviation is calculated as 0.22. The sucess of each model is compared with the average value (0.48) and the sum of average value and standard deviation (0.48 + 0.22) = 0.70. If the model combination is bigger than 0.70, than it is defined as the most representative model combination. If the model combination is bigger than 0.48 but smaller than 0.70, than it is defined as better representative model combination. If it is smaller than 0.48, than it is defined as unrepresentative model combination. Hence, MPI–M –MPI–ESM–LR-CLM–CCLM4–8–17–v1, having coefficient as 0.85, is defined as the most representative model combination.

Step 8: There are two different methodologies from this point. If the unique WDSDAAE value of a model is bigger than AWDSDAAE, then it is collected in the set of "good representative models" (TEST5 - Model_n). In the other option, if the WDSDAAE value of a model is bigger than TWDSDAAE, then it is collected in the set of the "better representative models" (TEST1 - Model_n).

Step 9: The calculated unique values (hosting the whole domain) of the "good/ better representative models" are appointed as the coefficients of these models. The

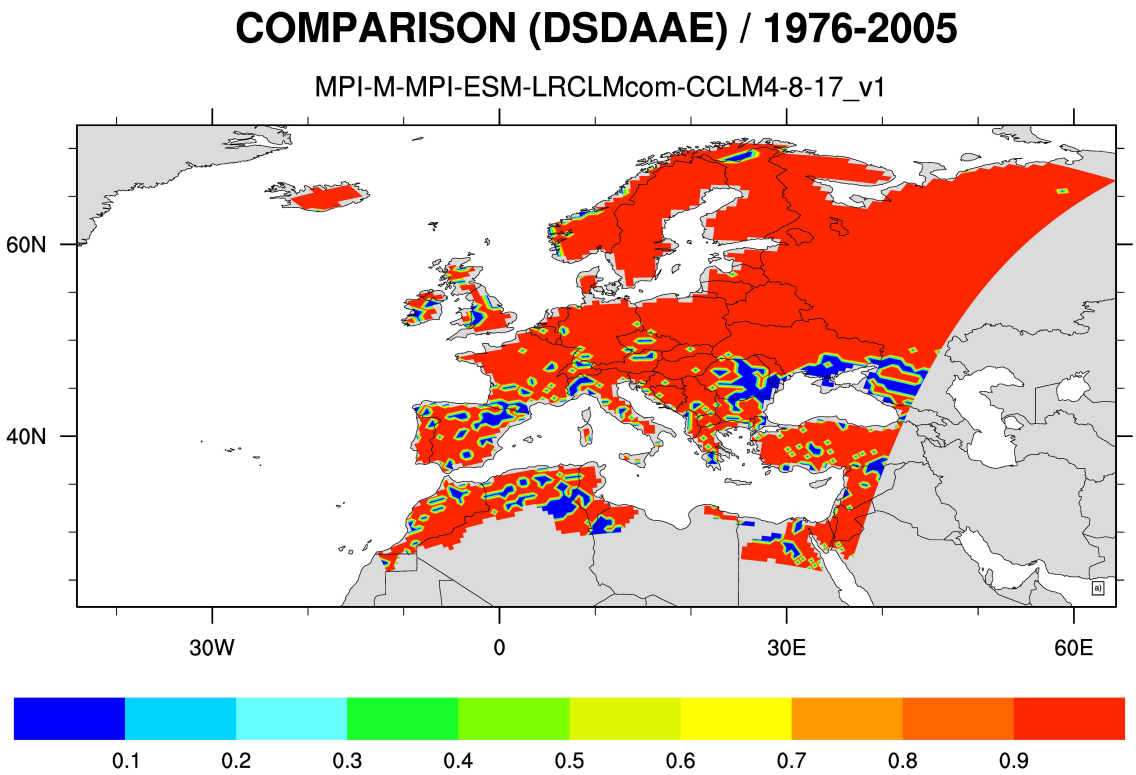

Figure 4.5. The map of all second comparison (DSDAAE) of model combination (MPI–M–MPI–ESM–LR-CLM–CCLM4–8–17–v1) with MSDAAE in each grid

models outside of these groups (unrepresentative models) are excluded from further operations.

Step 10: Up until now, the selection procedure of models are mentioned. After that point, 8 different test types, taking the "good/better representative models" for estimation, will be clarified. There are four main strategies to define the eight different test types. The tests from Test1 to Test4 are applied to the "better representative models". The tests from Test5 to Test8 are applied to "good representative models".

Test 1: In Step 9, the spatial averages of the "better representative models" are attained as their weighting coefficients in our multi- model approach. For example, if "n" different "better representative models" are procured in Step 9; the following formula is applied to find the most appropriate model ensemble to picture the climatology of the observed region in a chosen period.

Similar methodology was used to classify house prices of the various countries in the World [209].

$$TEST1 = \frac{\sum_{n=1}^{N}(\mathbf{C}_n \times \mathbf{M}_{i,j\ ,n})}{\sum_{n=1}^{N}\mathbf{C}_n} \tag{4.1}$$

where C_n) symbolizes the coefficient of the nth "better representative model" and $M_{i,j,n}$) is defined to be the value of observed variable (temperature) of nth "better representative model" at i^{th} longitude and j^{th} latitude.

Test 2: The only difference between Test1 and Test2 stems from the weighting coefficients of "better representative models". In this test, the models are equally weighted to form an ensemble.

For example, C_n s for Europe are 0.85, 0,78, 0.86, 0,78 and 0.79. These values are multiplied with all of the AAE values on all of the grids of corresonding

model combinations ($M_{i,j,n}$). For example, 0.85 is C_n of MPI–M –MPI–ESM–LR-CLM–CCLM4–8–17–v1 model combination and the second column of Figure 4.2 is multiplied with this value. This operation is carried out for the most representative / better representative model combinations in each season and the ones named Test1 and Test5 of Figure 5.33, 5.34, 5.35, 5.36 and 5.37 are found. Equally weighted averages of the most representative / better representative model combinations in each season are calculated and the ones named Test2 and Test6 of Figure 5.33, 5.34, 5.35, 5.36 and 5.37.

$$TEST2 = \frac{\sum_{n=1}^{N} \mathbf{M}_{i,j\ ,n}}{N} \tag{4.2}$$

Test 3: Spatial averages of "better representative models", namely SDAAE (see Step 6) are calculated and a unique value is obtained and assigned to each model as its weighting coefficient in multi-model approach. A formula similar to the Test1 is applied to obtain the ensemble.

$$TEST3 = \frac{\sum_{n=1}^{N} (\mathbf{D}_n \times \mathbf{M}_{i,j\ ,n}\ )}{\sum_{n=1}^{N} \mathbf{D}_n} \tag{4.3}$$

where D_n symbolizes the coefficient of the nth "better representative model" and $M_{i,j,n}$ defines the value of observed variable (temperature or precipitation) of nth "better representative model" at the ith longitude and the jth latitude.

For example, D_n is the spatial average of MPI–M–MPI–ESM–LR-CLM–CCLM4 –8–17–v1 (the spatial average of the Figure in the first column of 4.4). The second column of Figure 4.2 is multiplied with this value. This operation is carried out for the most representative / better representative model combinations in each season and the ones named Test3 and Test7 of the Figure 5.33, 5.34, 5.35, 5.36 and 5.37 are found. Test 4: The spatial average of the AAEs (in Step 2) of the "better representative models" are calculated and then normalized between "0" and "1" (NAEE). It can be

asserted that "the less absolute error a model has, the more it can exemplify". Hence, the necessary weighting coefficients of the "better representative models" are obtained by subtracting NAEE from "1".

$$TEST4 = \frac{\sum_{n=1}^{N}(\mathbf{1} - \mathbf{NAAE}_n) \times (\mathbf{M}_{i,j\ ,n})}{\sum_{n=1}^{N} \mathbf{1} - \mathbf{NAAE}_n} \tag{4.4}$$

where 1-$NAAE_n$ symbolizes the coefficient of the nth "better representative model" (subtracting normalized absolute average error from "1") and $M_{i,j,n}$ defines the value of observed variable (temperature or precipitation) of the nth "better representative model" at the ith longitude and the jth latitude.

"Test 5 - Test 8" are same as "Test 1- Test 4" respectively; the only difference between them is that "Test 5-Test 8" use the "better representative models" for the ensemble approach, while "Test 1-Test 4" use the "the most representative models".

EWA: Equally weighted average of all available models is calculated as it is one of the most common tools used in the multi-model studies. The success of model combinations and proposed ensemble methods are testified by comparing the outcomes of EWE and aforementioned Tests.

4.1.2. Statistical Method 2: RMSE as Indicator and Monthly Average Temperature as Data Set

Step 1 & Step 2: The Root Mean Square Error (RMSE) of each grid is calculated in each season. The RMSE, having value close to "0", is one of the significant indicators which portrays the reliability of the model.

After that point, same steps (from Step 3 to Step 10) and same tests (from Test 1 to Test 8) are applied in this statistical method. The only difference is that RMSE

substitutes for AAE in the calculations and the governing equations.

4.1.3. Statistical Method 3: T-Test as Indicator and Monthly Average Temperature as Data Set

Step 1 – 5: In this methodology, there are significant differences from the previous statistical methods. In the previous ones, the main indicators are RMSE and AAE. If a model combination has small values of these indicators, it can be well enough to represent the climatological variable patterns. In Statistical Method 3, the student t-test is applied to the monthly temperature results of the model combinations and the observation data set at 95 % confidence interval for each grid points in each season. If the temperature value at a grid point passes the test, then we assign the value "1", otherwise "0" is assigned for this grid point (TT). For each model, we sum up the TT values of all seasons at each grid. Then the STT values alter between 0 and 4. If the STT of a model at a grid point is close to 4, then we accept that this model represents the climatology well at that point in every season.

Step 6: Operations made so for are carried out again. The average of the STT of all models at each season and every grid point is calculated (MSTT). Then, the representativeness of a model is testified by performing the comparison. If the STT of a model at a given grid is bigger than MSTT at the same grid, we assign the value "1" (DSTT). This is the second selection procedure.

Step 7: The spatial averages of all grid points covering observed region are calculated (WDSTT) and a unique value is found for each model. The average (AWDSTT) and standard deviation (VWDSTT) of these values are calculated. Average (AWDSTT) and one standard deviation (VWDSTT) are added and limit value (TWDSTT) is found to use in further comparison steps.

Step 8: From this point on, we follow two separate methodologies. If the unique WDSTT value of a model is bigger than AWDSTT, then it is collected in the set of "good representative models" (TEST5- Model_n). In the other option, if the WDSTT

value of a model is bigger than TWDSTT, then it is collected in the set of the "better representative models" (TEST1- Model_n).

Step 9: The calculated unique values (hosting the whole domain) of the "better/ the most representative models" are appointed as the coefficients of these models. The models outside of these groups (unrepresentative models) are excluded from further operations.

Step 10: Up until now, selection procedure of models are mentioned. After that point, 8 different test types, taking the "good/the best representative models" for estimation, will be clarified. There are four main strategies to define the eight different test types. The tests from Test1 to Test4 are applied to the "best representative models". The tests from Test5 to Test8 are applied to "better representative models".

4.1.4. Statistical Method 4: T-Test as Indicator and Annual Average Temperature as Data Set

Step 1 – 5: The only difference of this method from Statistical Method III stems from the data set. The main indicator is again the Student T-Test, but this time it is applied to the yearly averages. In the previous methodology, there are 90 monthly data sets for each grid point in the period between 1976 and 2005 (30 years) in each season and the T-test is applied to these data sets. In this method the, T-test is applied to 30 annual data sets for each grid points in each season. After that point, same steps (from Step 6 to Step 10) in Statistical Method III and same tests (from Test 1 to Test 8) are applied for this statistical method.

4.2. Method 3: Future Projections of Temperature

The most convenient model combinations, methods, and tests, obtained by the previous methods, are used to find the future alterations of the inspected climatological variables. The future periods are selected as the 2050s (between the years 2036 and 2065) and 2080s (between the years 2066 and 2095). The period between the years

1976 and 2005 is chosen as the reference period. Both reference and future periods are split into climatic seasons. The alteration is found by subtracting the average of observed variables in future period from the one of reference period in each season.

4.3. Method 4: GCM-RCM Combination Selection with respect to Daily Maximum Temperature Data Set and Application to Heat Waves

The robustness and accuracy of the data sets, used in extreme event studies in climate science, are constructed over unique values. For heat wave analysis, the convenience of the results of a model is determined by comparing the outcomes of 95 % (99 % or 90 %) of the observed variable of the model and observation data set. The remaining percentages or the distribution of the data set drop beneath the radar. It is possible that both distributions and percentage values of the model and observation data set are close to each other. However, the whole range has to be counted on to claim that these two data sets show same patterns. Hence, the following calculations are applied for this purpose.

$$EM_{n,k} = \frac{\sum_{m}^{n} |(\mathbf{PM}_{i,j\ ,k\ ,m}) - \mathbf{OM}_{i,j\ ,k\ ,m}|}{15} \tag{4.5}$$

where m stands for the percentiles and takes the values 1, 5, 10, 25, 32, 45, 50, 55, 68, 75, 90, 95 and 99 percentiles and min/max refers to the minimum/maximum values.

k stands for the seasons and i is the longitude and j is the latitude.

PM is the percentile of the model and OM is the percentile of the observation data set.

For example, $\mathrm{PM_{i,j,m,k}}$ is the "m^{th}" percentile of the model at the "i^{th}" longitude and the "j^{th}" latitude in the "k^{th}" season. We also define

$$\mathbf{AEM_k} = \frac{\sum_{i=1}^{s}(\mathbf{EM}_{i,k})}{s} \tag{4.6}$$

$$\mathbf{STDAEM_k} = \sum_{i=1}^{s}(\sigma(\mathbf{EM_{i,k}}) \tag{4.7}$$

$$\mathbf{AEM2_k} = \mathbf{AEM_k} + \mathbf{STDAEM_k} \tag{4.8}$$

where "s" is the number of model combinations $\mathrm{STDAEM_{n,k}}$ is the standard deviation. We also define

$$\mathbf{SEM}_{n,k} = 1 \quad if \quad \mathbf{EM}_{n,k} < \mathbf{AEM}_{n,k} \tag{4.9}$$

$$\mathbf{SEM}_{n,k} = 1 \quad if \quad \mathbf{EM}_{n,k} >= \mathbf{AEM}_{n,k} \tag{4.10}$$

$$\mathbf{TSEM}_n = \sum_{k=1}^{4} \mathbf{SEM}_{n,k} \tag{4.11}$$

$$\mathbf{M}_n = \text{"}representative\text{"} \quad if \quad \mathbf{TSEM}_n = 4 \tag{4.12}$$

$$\mathbf{M}_n = \text{"}unrepresentative\text{"} \quad if \quad \mathbf{TSEM}_n < 4 \tag{4.13}$$

$$\mathbf{SEM2}_{n,k} = 1 \quad if \quad \mathbf{EM}_{n,k} < \mathbf{AEM2}_{n,k} \tag{4.14}$$

$$\mathbf{SEM2}_{n,k} = 0 \quad if \quad \mathbf{EM}_{n,k} >= \mathbf{AEM2}_{n,k} \tag{4.15}$$

$$\mathbf{TSEM2}_n = \sum_{k=1}^{4} \mathbf{SEM2}_{n,k} \tag{4.16}$$

$$\mathbf{M}_n = \text{"}representative\text{"} \quad if \quad \mathbf{TSEM2}_n = 4 \tag{4.17}$$

$$\mathbf{M}_n = \text{"}unrepresentative\text{"} \quad if \quad \mathbf{TSEM2}_n < 4 \tag{4.18}$$

In the literature, there are various "heat wave" and "extremely hot day" definitions. One of the "extremely hot day" definitions is the day having the daily maximum temperature above the 90th (95th) percentile of maximum temperature value in a calendar day in 1976–2005 (calculate for each day over a centered 5-day window at each grid point). The definition of "Consecutive period of hot days" depends on "extremely hot day". If there are at least six "consecutive extremely hot days", this period is accepted as the "consecutive period of hot days"; and the longest duration of consecutive hot days is also used to show the duration of heat wave.

In the literature, another definition of "extremely hot day" takes the 30°C (35°C or 40°C) as the threshold value and if maximum temperature in a day is bigger than this temperature, then it is accepted as an "extremely hot day". "Consecutive period of hot days" and "the longest duration of Consecutive period of hot days" definition is similar to the previous one.

In this thesis, the maximum temperature in the 20th century and the beginning of 21th century (till 2017 for Europe) is accepted as an "extremely hot day" (EHD) and hence there is no "Consecutive period of hot days" and "the longest duration of Consecutive period of hot days" in the reference period. The future periods are selected as the 2050s (between years 2036 and 2065) and 2080s (between years 2066 and 2095). The number of "Extremely hot day", "Consecutive period of hot days" and "the longest duration of Consecutive period of hot days" (frequency, intensity and duration of heat waves) in the future period is calculated with respect to the EHD value for each grid point and season. "The best representative models", defined in this section, are used for this operation.

4.4. Method 5: Application to WBGT and Labor Productivity

In this thesis, an analysis of thermal comfort is performed by applying a host of definitions [210]. Heat Stress Index, PMV, Discomfort Index and WBGT are indices examples which can be used to achieve this purpose. Daily WBGT, which is most commonly applied among these indices, is calculated for each climatic season in the

period between 1970 and 2100. Different calculations are carried out by using different formulas [211]. Outdoor WBGT is calculated by the simplified governing equation of Australian Bureau of Meteorology. Relative humidity and maximum air temperature are the two climatic variables in this equation, as shown in 4.19 and 4.20 [212]. The year between 1971 and 1999 is selected as the reference period that represents today's temperature and labor productivity conditions (1976-2005 for Europe) More meaningful and accurate conclusions as to changes in the future can be drawn via an analysis of the reference period. The periods 2036–2065 (2050s) and 2066–2095 (2080s) are future ones in which the same analysis is carried out.

$$WBGT = 0.567 \times T_{\mathrm{a}} + 3.94 + 0.393 \times e_{\mathrm{s}} \tag{4.19}$$

$$e_{\mathrm{s}} = \frac{RH \times 6.105 \times \exp \frac{17.27 \times T_{\mathrm{a}}}{237.7 + T_{\mathrm{a}}}}{100} \tag{4.20}$$

where e_s is wator vapor pressure, RH is relative humidity and T_a is air temperature.

Further calculations are carried out in each season. First of all, daily WBGT is calculated with respect to Equation 4.19 and 4.20 and they are separated to seasons. Secondly, WBGT is classified to the sub groups TLVs being in accordance with the definition of [213] and [214]. Maximum permitted hours in a day are determined with respect to these values. Workers have to have a rest in 25, 50, 75 percentage of their working hours if WBGT reaches the corresponding TLV values. As shown in Table 2.1, the lowest WBGT, being suitable to continue to work, is 27.5°C. Workers have to rest fifteen minutes in a hour if WBGT is bigger than this value. Similarly, workers have to rest thirty (forty-five) minutes in a hour if WBGT is bigger than 29.5(31.5)°C. It is suggested to workers to not continue to work if WBGT is bigger than 36°C. The total amounts of the days in these aforementioned intervals are calculated and formula 4.21

is used to obtain the total losses in labor productivity in each season over observed regions.

$$DLP = \frac{D1 \times 25 + D2 \times 50 + D3 \times 75 + D4 \times 100}{100} \tag{4.21}$$

DLP represents the total losses of labor productivity (in terms of percentage).

D1 indicates the total amount of the days in which WBGT is between 27.5°C and 29.5°C.

D2 indicates the total amount of the days in which WBGT is between 29.5°C and 31.5°C.

D3 indicates the total amount of the days in which WBGT is between 31.5°C and 36°C.

D4 indicates the total amount of the days in which WBGT is bigger than 36°C .

TDA symbolizes the total amount of the days in the analyzed season in the observed period.

5. RESULTS

5.1. Application of Statistical Methodologies to the Monthly Temperature Data

5.1.1. Application of Statistical Methodology 1 to the Monthly Temperature Data: The Case of Europe

In this part, the Statistical Methodology I, described in Section 4, is applied to the monthly temperature of Europe.

Step 1: Average Errors of 26 Models

The model combinations and observation data set are separated to the climatic seasons. Average Errors of 26 Models are acquired by calculating the difference of average values of model combinations and observation results, obtained from E-OBS, between the years 1976 and 2005. This operation is carried out for each season and annually (not shown). The attained AEs are used in the following steps.

Step 2: The Absolute Value of Average Temperature Error Values of 26 Models

In this part, the second step of the statistical methodology is carried out. The spatial representations of each GCM-RCM combinations are figured out. The demonstrations are performed in each season and also annually. At the end of this process, the representative and unrepresentative models are decided. Hence, the models are separated to the most representative and unrepresentative ones from the beginning and the figures are plotted with respect to this appropriation. The representative and unrepresentative model projections of temperature over Europe are shown in Table 1 and 2. It is found that MOHC-CLM, MPI-CLM1, MPI-CLM2, MPI-REMO1 and MPI-REMO2 model combinations are the best representative model combinations to simulate the temperature of Europe. The remaining ones are less representative for the

same variable over the same region. It turns out that the models in Table 5.2 are more successful than the ones in Table 5.1 to represent the temperature patterns of Europe.

Table 5.1. The Names and Abbreviations of unrepresentative RCM / GCM model combinations

UNREPRESENTATIVE MODEL COMBINATIONS	**ABBREVIATION**
Global Climate Model -Regional Climate Model	**GCM - RCM**
CCCma-CanESM2 - SMHI-RCA4-v1	CCCma - RCA4
CNRM-CERFACS-CNRM-CM5 - CLMcom-CCLM5-0-6-v1	CNRM - CLM
CNRM-CERFACS-CNRM-CM5 - CNRM-ALADIN53-v1	CNRM - CNRM
CNRM-CERFACS-CNRM-CM5 - HMS-ALADIN52-v1	CNRM – HMS
CNRM-CERFACS-CNRM-CM5 - RMIB-UGent-ALARO-0-v1	CHRM – RMIB
CNRM-CERFACS-CNRM-CM5 - SMHI-RCA4-v1	CNRM – RCA4
CSIRO-QCCCE-CSIRO-Mk3-6-0 - SMHI-RCA4-v1	CSIRO – RCA4
ICHEC-EC-EARTH - CLMcom-CCLM5-0-6-v1	ICHEC – CLM
ICHEC-EC-EARTH - KNMI-RACMO22E-v2	ICHEC – KNMI
ICHEC-EC-EARTH - SMHI-RCA4-v1	ICHEC – RCA4
ICHEC-EC-EARTH - KNMI-RACMO22E-v1	ICHEC – KNMI
ICHEC-EC-EARTH - DMI-HIRHAM5-v1	ICHEC – DMI
IPSL-IPSL-CM5A-MR - IPSL-INERIS-WRF331F-v1	IPSL – IPSL
IPSL-IPSL-CM5A-MR - SMHI-RCA4-v1	IPSL – RCA4
MOHC-HadGEM2-ES - KNMI-RACMO22E-v2	MOHC – KNMI
MOHC-HadGEM2-ES - SMHI-RCA4-v1	MOHC – RCA4
MIROC-MIROC5 - CLMcom-CCLM5-0-6-v1	MIROC – CLM
MIROC-MIROC5 - SMHI-RCA4-v1	MIROC – RCA4
MPI-M-MPI-ESM-LR - SMHI-RCA4-v1	MPI – RCA4
NCC-NorESM1-M - SMHI-RCA4-v1	NCC – RCA4
NOAA-GFDL-GFDL-ESM2M - SMHI-RCA4-v1	NOAA - RCA4

The absolute values of the Average Errors (AE) are calculated for each model in each season and annually. The spatial distributions of these absolute values are shown in Figures 5.1- 5.10. The five representative models produce trustable results annually, excluding the north-eastern part of the observed region, Northern Africa and Spain. In winter season, AAE is smaller than 1.3 for most of the regions in all combinations. Northern Black Sea coastal and western Russia domains have more absolute errors than the remaining part of the observed region. It seems that MPI-CLM have the smallest errors and is good to show temperature patterns of Europe in the period between 1976 and 2005. However, ICHEC-KNMI, ICHEC-RCA4 and ICHEC-CLM are also

Table 5.2. The Names and Abbreviations of representative RCM / GCM model combinations

REPRESENTATIVE MODEL COMBINATIONS	**ABBREVIATION**
Global Climate Model -Regional Climate Model	**GCM - RCM**
MOHC-HadGEM2-ESCLMcom-CCLM5-0-6-v1	MOHC – CLM
MPI-M-MPI-ESM-LRCLMcom-CCLM4-8-17-v1	MPI – CLM1
MPI-M-MPI-ESM-LRCLMcom-CCLM5-0-6-v1	MPI – CLM2
MPI-M-MPI-ESM-LRMPI-CSC-REMO2009-v1	MPI – REMO1
MPI-M-MPI-ESM-LRMPI-CSC-REMO2009-v2	MPI – REMO2

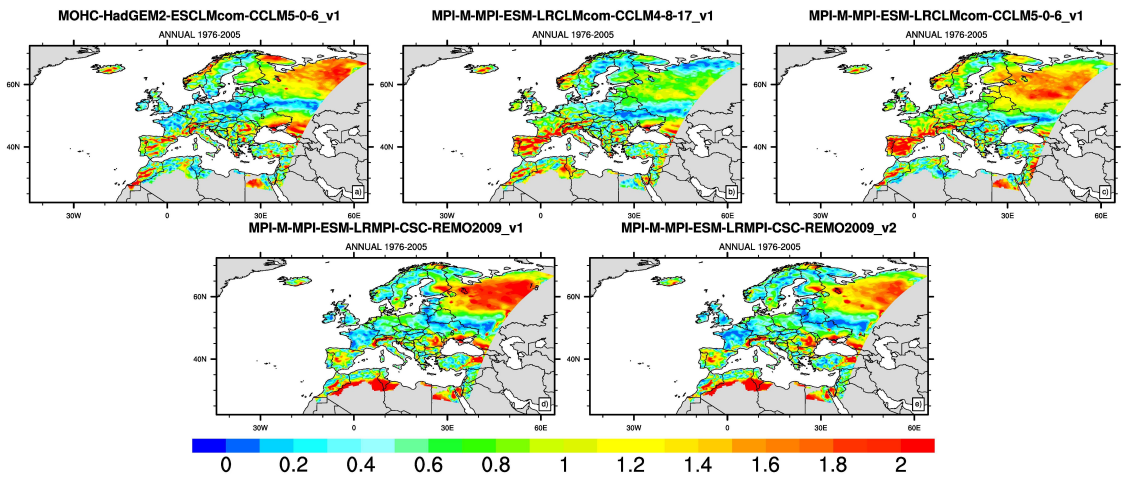

Figure 5.1. The Annual Absolute Value of The Average Temperature Errors of The Representative Models in The Statistical Methodology 1 in the period between the years 1976 and 2005

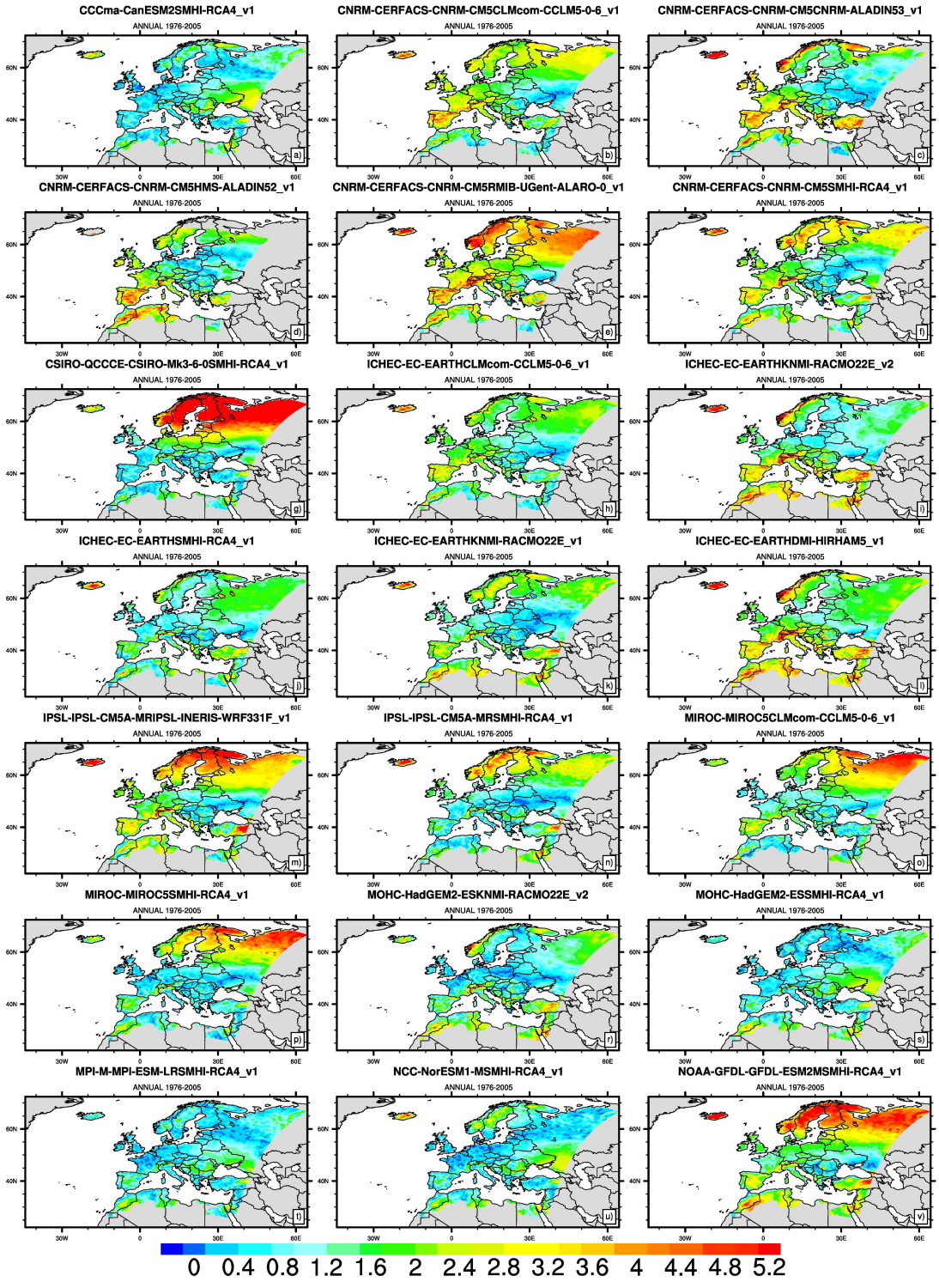

Figure 5.2. The Annual Absolute Value of The Average Temperature Errors of The Unrepresentative Models in The Statistical Methodology 1 in the period between the years 1976 and 2005

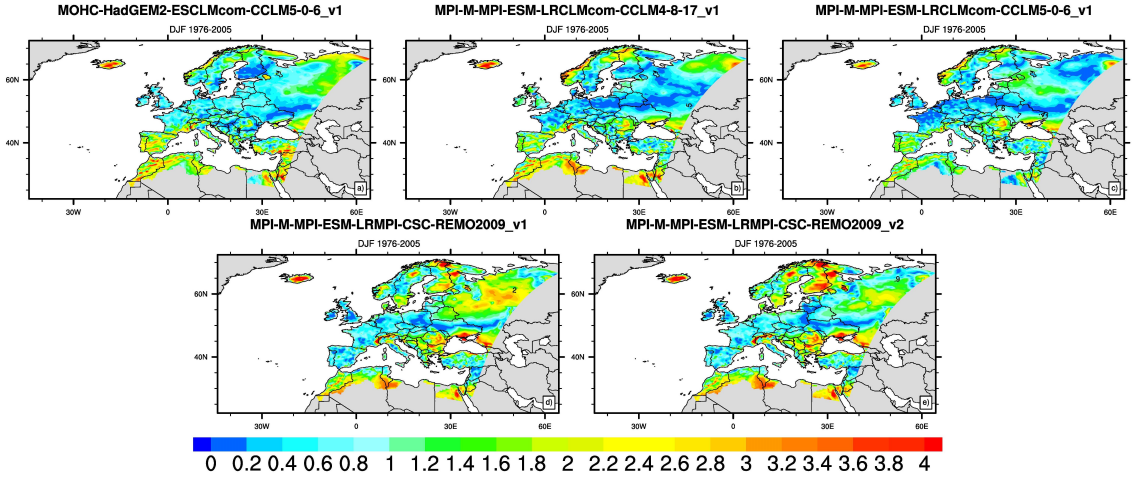

Figure 5.3. The Absolute Value of The Average Temperature Errors of The Representative Models in Statistical Methodology 1 in the period between the years 1976 and 2005 in Winter Season

well enough to represent the temperature over the same region in winter season by having small absolute error values. The capability of these models in other seasons pushed them to the cluster of less representative models. For example, it is shown that the AAEs of these three models in spring season are dramatically bigger than the most representative models although the AAEs are similar in winter season for these three unrepresentative and representative models. Our purpose is to select the successful model combinations which provide a good representation in each season on an individual basis. Northern Black Sea coastal and western Russia domains are also problematic regions in representing temperature for GCM-RCM combinations in spring season. MPI-RECMO1 and MPI-RECMO2 combinations produce more valid results than the remaining model combinations but other three best representative model combinations estimation aren't as good as these two ones in summer season. Northern Black Sea coastal are precisely projected by most of these five models but the problem over western Russia domain still exists in summer season. In autumn season, all of the representative and unrepresentative models have similar results.

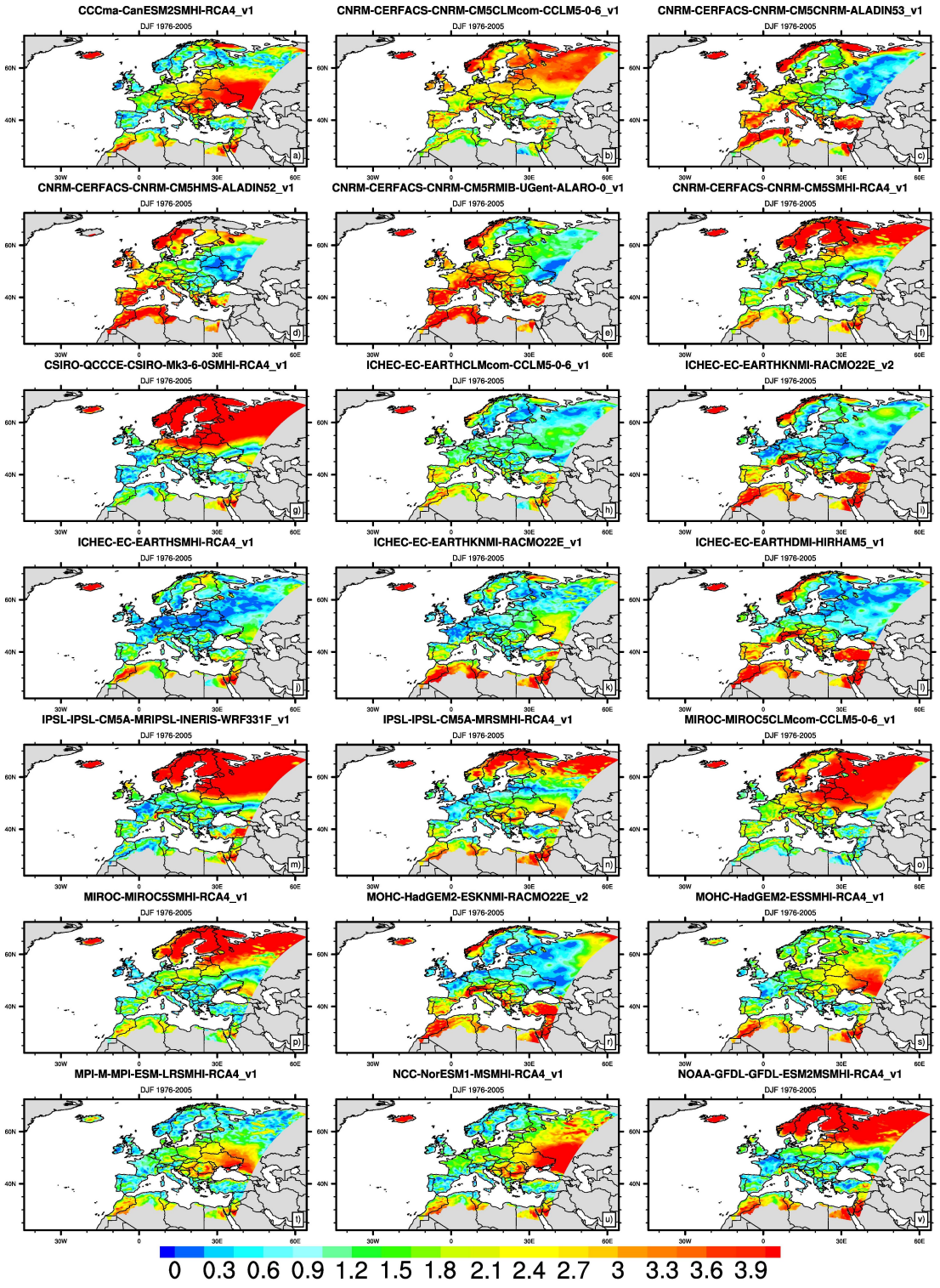

Figure 5.4. The Absolute Value of The Average Temperature Errors of The Unrepresentative Models in Statistical Methodology 1 in the period between the years 1976 and 2005 in Winter Season

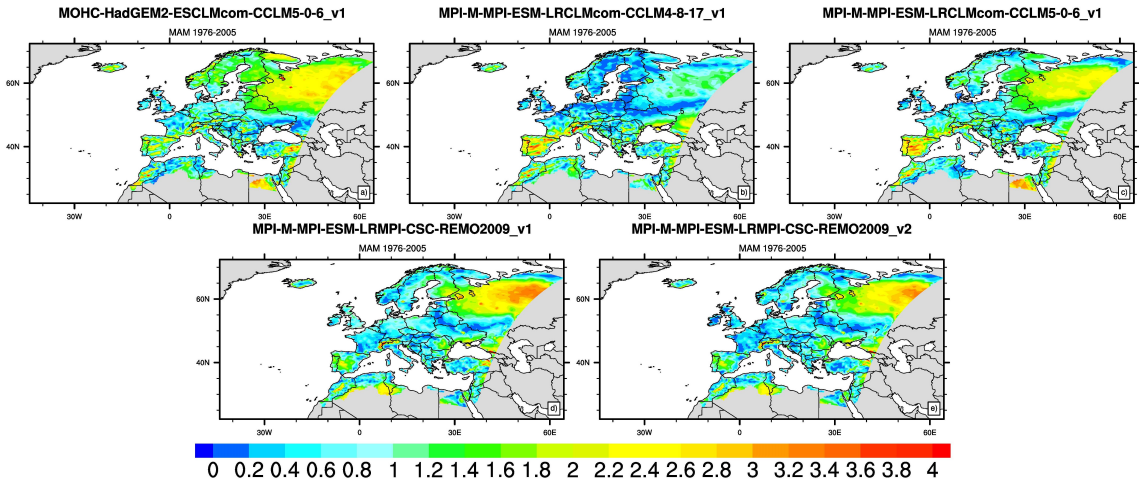

Figure 5.5. The Absolute Value of The Average Temperature Errors of The Representative Models in Statistical Methodology 1 in the period between the years 1976 and 2005 in Spring Season

In Figure 5.11, the spatial averages of the model combinations are shown. If these spatial averages of model combinations are solely taken in consideration, the problematic regions would be missed. If the spatial distributions of the AAEs of each model combinations are investigated season by season, reaching a comprehensive outcome would be very difficult. Hence, the following methodology is applied to find the most suitable and accurate model combinations for the representation of Europe's temperature pattern as a whole.

Step 3: The Mean of the Absolute Value of Average Errors of 26 Models (MAEE) in each season and annually

The procedure in Step 3 is applied and averages of the AAEs of all of the model combinations in each season are calculated as shown in Figure 5.11. It also contains the distribution of the temperature over Europe when all of the model combinations are equally weighted. The spring season has the maximum AAEs and northern Africa and western Russia are the regions containing the maximum errors. This spatially distributed map will be used as the limit value to select the most/ more representative

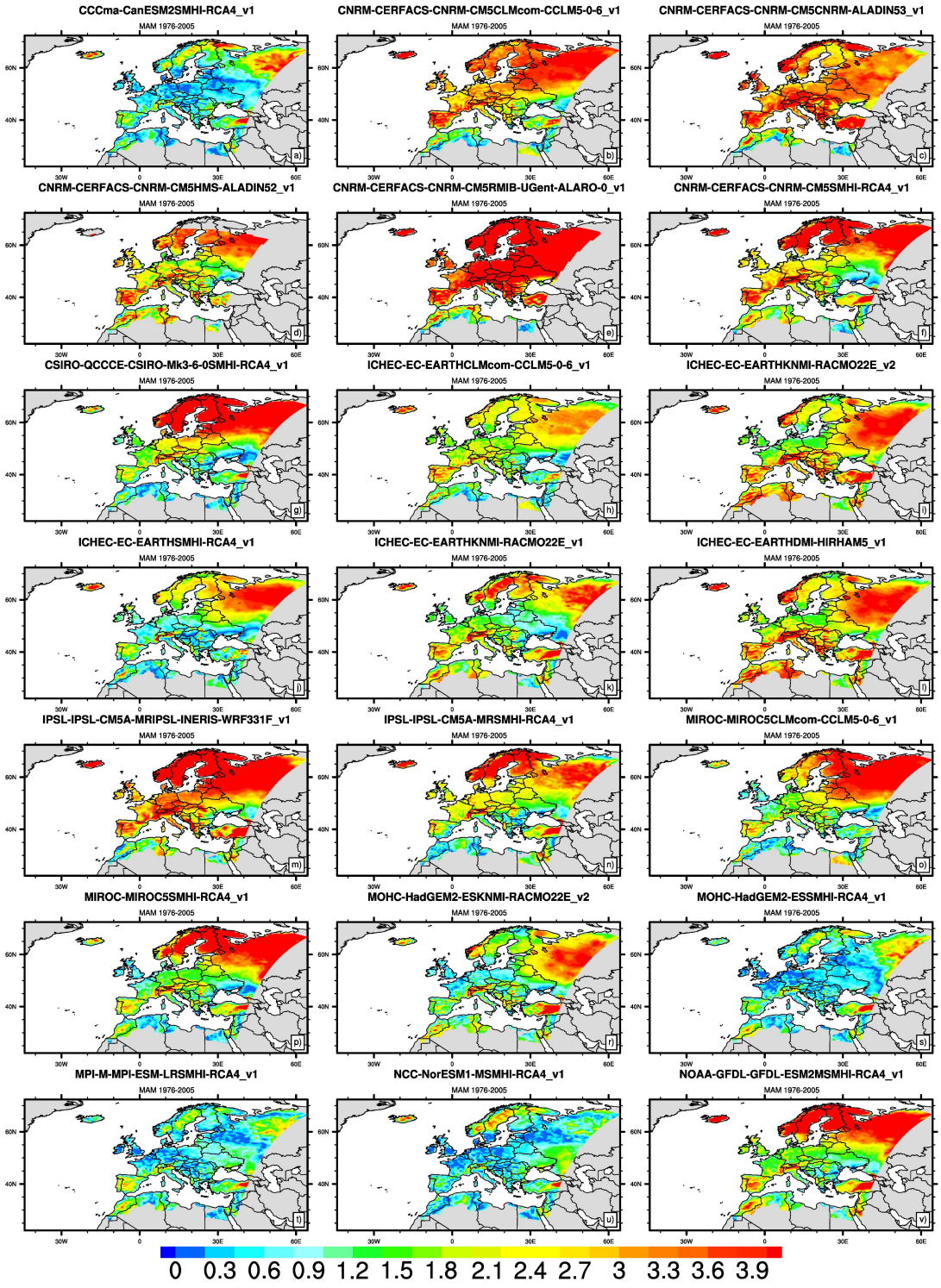

Figure 5.6. The Absolute Value of The Average Temperature Errors of The Unrepresentative Models in Statistical Methodology 1 in the period between the years 1976 and 2005 in Spring Season

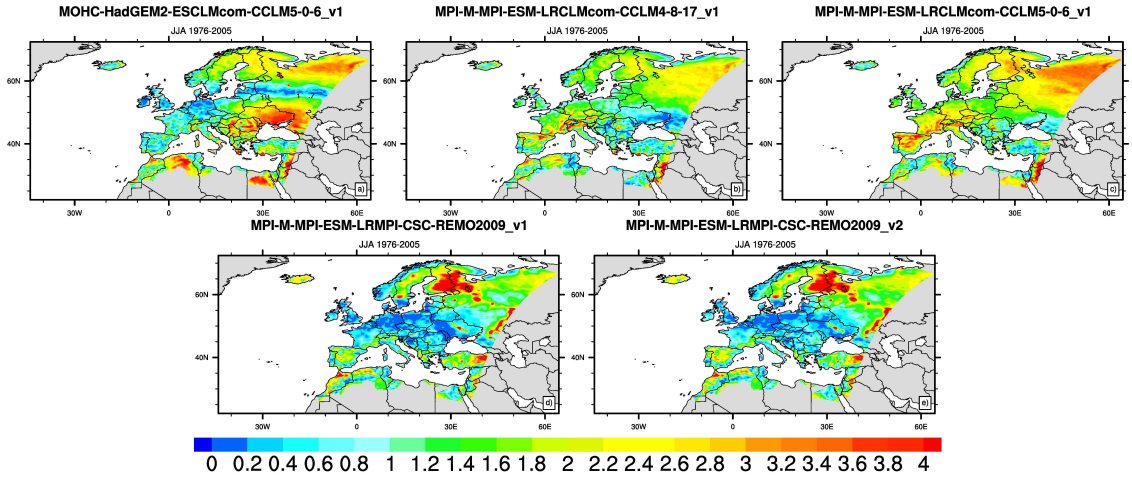

Figure 5.7. The Absolute Value of The Average Temperature Errors of The Representative Models in Statistical Methodology 1 in the period between the years 1976 and 2005 in Summer Season

models.

Step 4: Comparison of Models' "Absolute Value of Average Error Values (AAE)" with "Mean of the Absolute Value of Average Error Values of 26 Model (MAEE)"

The amount of model combinations and their capacities are limited. Hence, the following procedure is based on inter comparison of model combinations. If a model combination has smaller AAE than the other model, it is denoted as successful according to compared one. Averaging the AAEs of whole model combinations includes the AAEs of all models and "successful" model can be found indirectly by comparing the AAEs of this model with the average of AAEs of the entire model (MAEE). If AAE of a model combination at a grid point in a season is smaller than the MAEE at the same grid point in the same season, it is symbolized with "1" and it is denoted as "0" at the exact opposite situation. (DAEE) This operation is done for entire grid points in the observed area in each season for each model combinations.

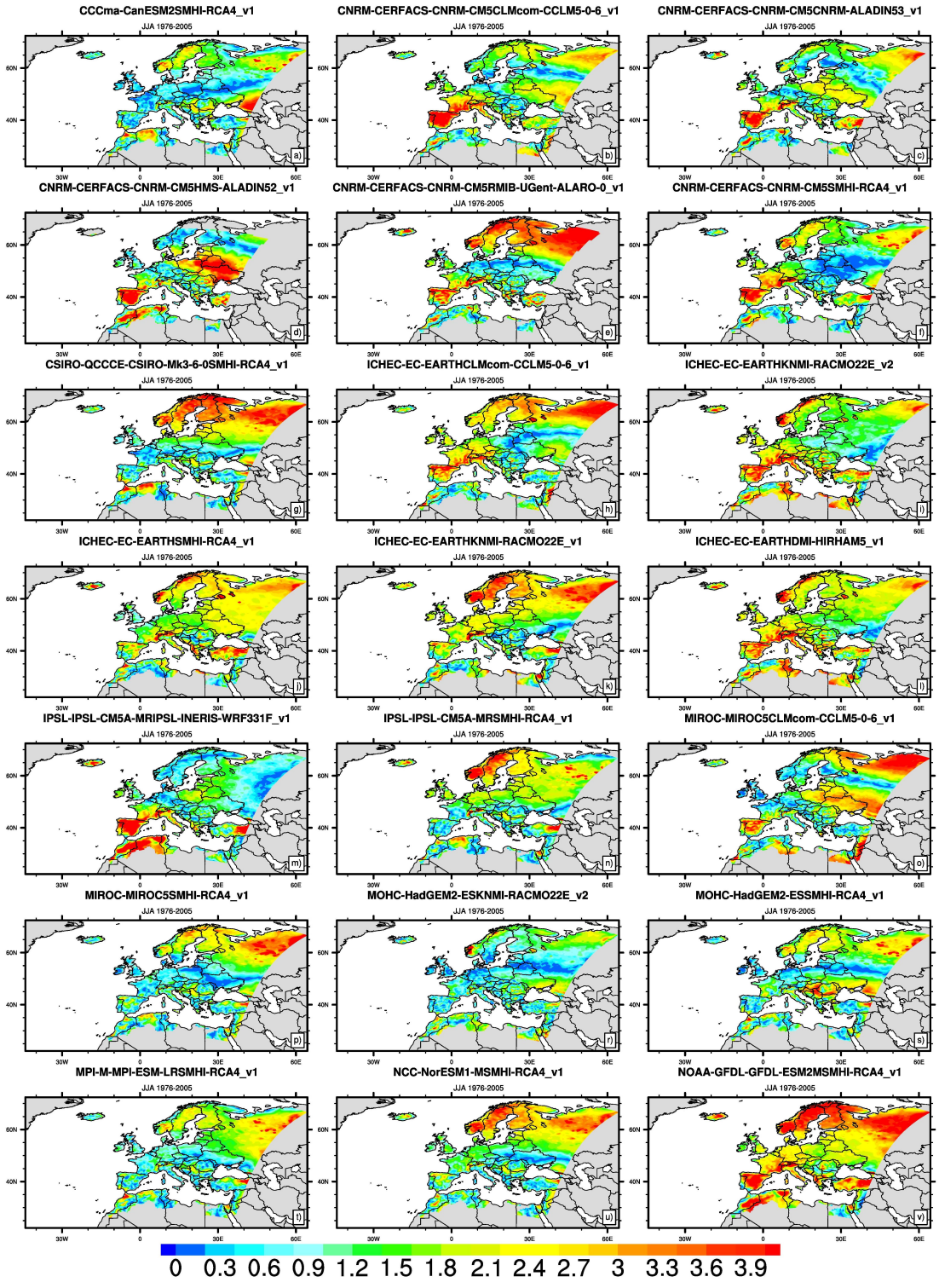

Figure 5.8. The Absolute Value of The Average Temperature Errors of The Unrepresentative Models in Statistical Methodology 1 in the period between the years 1976 and 2005 in Summer Season

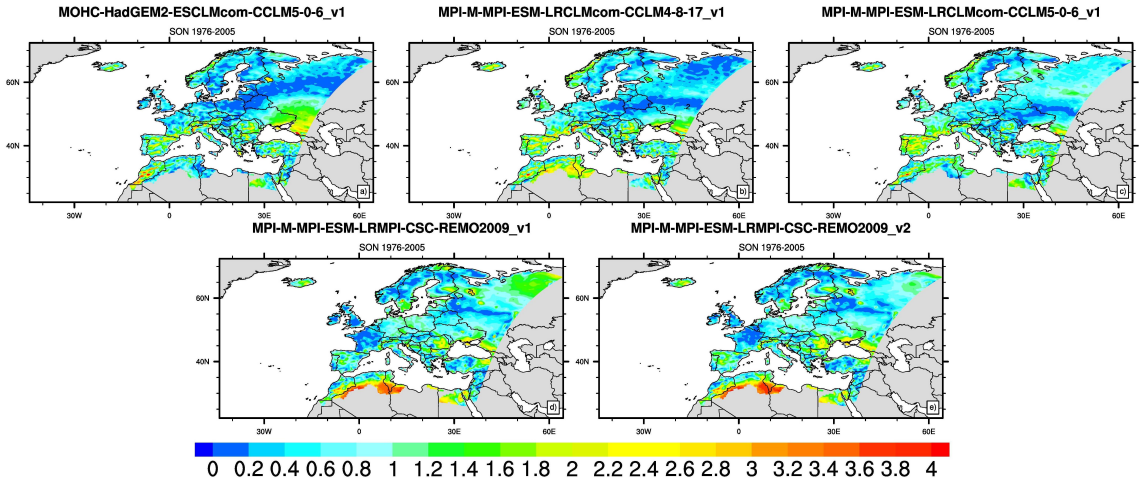

Figure 5.9. The Absolute Value of The Average Temperature Errors of The Representative Models in Statistical Methodology 1 in the period between the years 1976 and 2005 in Autumn Season

In annual base, MOHC-CLM and MPI-CLM1 have bigger errors than MAEE over only Northern Black sea Coastal. MPI-CLM2 produces good results over Northern Black sea Coastal but it is worse than the average over some parts of Spain and western Russia. Both MPI-REMO1 and MPI-REMO2 have bigger errors than MAEE over Northern Black sea Coastal and the lands close to Sahara. In addition to these areas, MPI-REMO1 also doesn't simulate some parts of western Russia (Figure 5.12 and Figure 5.13).

In winter season, MOHC-CLM combination produces bad results over only Spain, Portugal, Syria, western coastal of Italia, Greece and Turkey and some parts of North Africa. MPI-CLM1 and MPI-CLM2 combinations have bigger errors than the other models over Romania and Crimea.MPI-REMO1 and MPI-REMO2 projections have larger errors over Central western Russia, Finland, Bulgaria, Romania and Northern Greece. In the remaining parts, these models have smaller AAE's than the MAAE. They also represent the temperature patterns over problematic regions (western Russia, North Africa and Black Seas coastal well enough (Figure 5.14 and Figure 5.15).

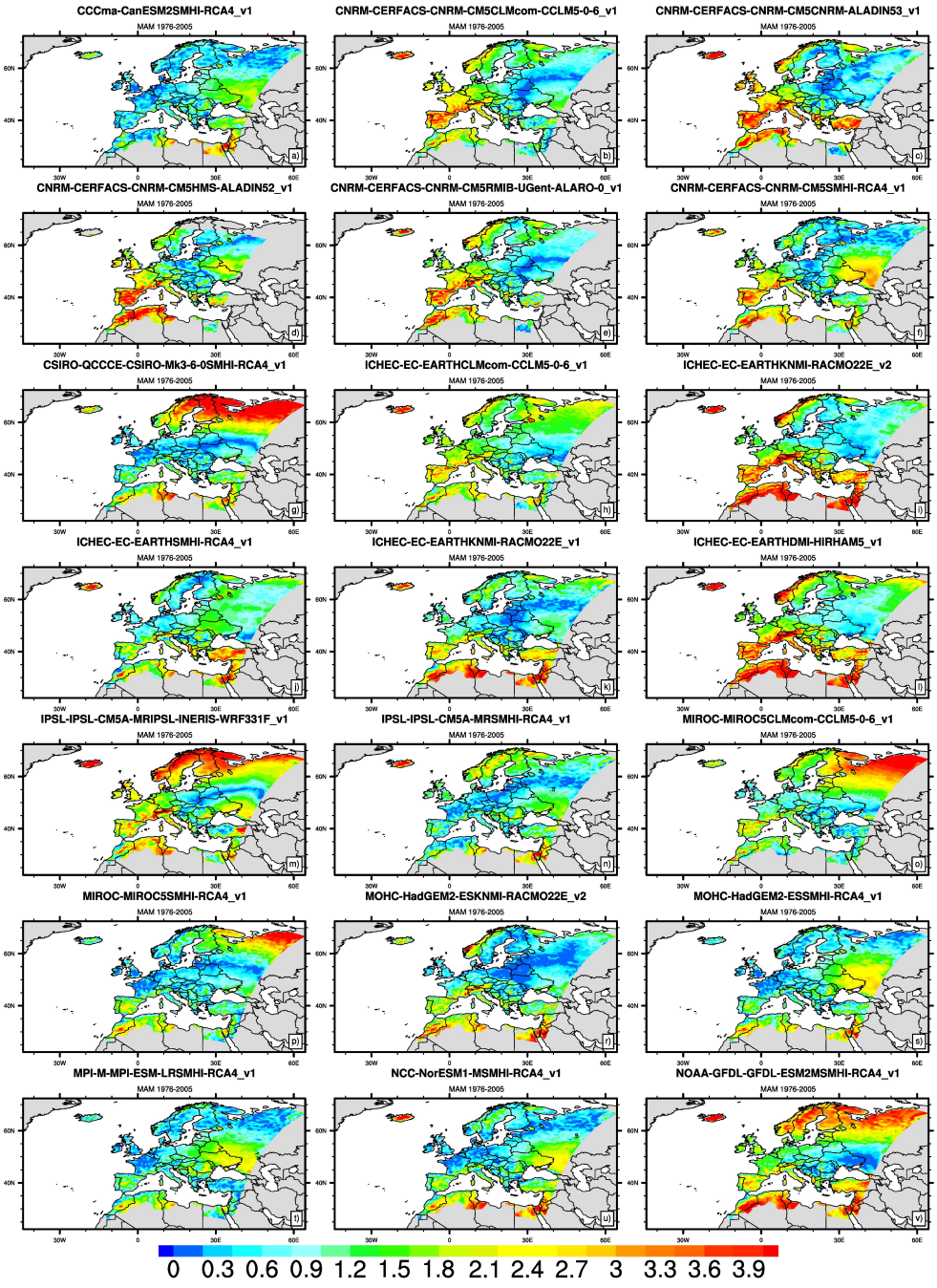

Figure 5.10. The Absolute Value of The Average Temperature Errors of The Unrepresentative Models in Statistical Methodology 1 in the period between the years 1976 and 2005 in Autumn Season

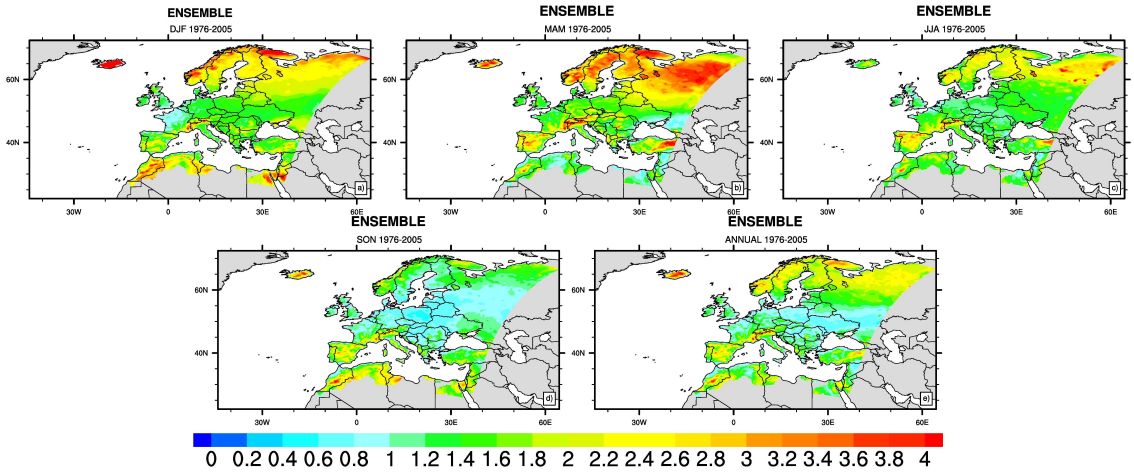

Figure 5.11. Mean of the Absolute Value of Average Error Values of 26 Model (MAEE) in each season and annually over Europe in the period between 1976 and 2005

In spring season, MOHC-CLM combination doesn't generate good results over only observed part of Egypt, interior parts of Syria and a small portion of observed part of Algeria. MPI-CLM1 and MPI-CLM2 combinations have bigger errors than the other models over Northern Black Sea coastal, interior Syria and western Spain.MPI-REMO1 and MPI-REMO2 projections have larger errors over Northern Black Sea coastal, the lands close to Sahara and interior Syria. In the remaining parts, these models have smaller AAE's than the MAAE. They also represent the temperature patterns over problematic western Russia well enough (Figure 5.16 and Figure 5.17).

In summer season, MOHC-CLM combination is well enough only over Western Europe, Norway, Sweden, Finland and Central western Russia. It has bigger AAE values than MAEE over the remaining part of the observed domain. Norway, Turkey, Northern Black Sea coastal, Northern Africa and Greece are the regions which MPI-CLM2 combination made best estimations. MPI-CLM1 produces small errors than MAEE over Central Europe, Turkey, Northern Black Sea coastal, Spain and Tunisia. MPI-REMO1 and MPI-REMO2 projections have larger errors over only Northern Africa, southern Turkey and Finland (Figure 5.18 and Figure 5.19).

In autumn season, MOHC-CLM, MPI-CLM1 and MPI-CLM2 combinations have smaller errors than the MAEE over entire region eluding some parts of Greece, Bulgaria and Russia. MPI-REMO1 and MPI-REMO2 projections have bad results over Central Europe and the lands close to Sahara (Figure 5.20 and Figure 5.21).

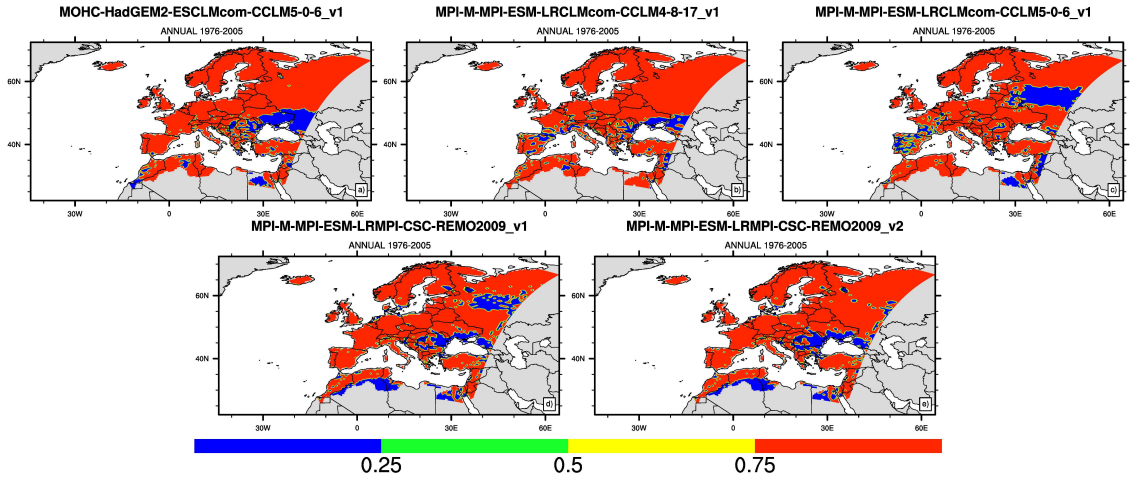

Figure 5.12. Annual DAEE of the Representative Models in the Statistical Methodology 1 in the period between 1976 and 2005

Step 5: The Sum of the DAEEs of all seasons of 26 Models

In the previous step, the AEE of a model at a grid in a season is compared with the MAEE at the corresponding grid and season and the value "0" (model has bigger AEE than MAEE) and the value "1" ((model has smaller AEE than MAEE) are assigned as the outcome of the comparison (DAEE). This operation is carried out for each season. However, in climate studies, it is very rare to deal with a unique season. The climatology of observed region is generally analyzed altogether. Hence, the model combination selection criteria should not depend on the success of models in a unique season. Due to this reason, the effects of each season have to be regarded and the success of a model can be determined by analyzing the success of this model in each season. The spatial summations of each DAEE of grid points in each season are carried out to look the overall representation of a model of the temperature of Europe by looking deeply one graph (SDAEE). SDAEE at a grid point has to be close

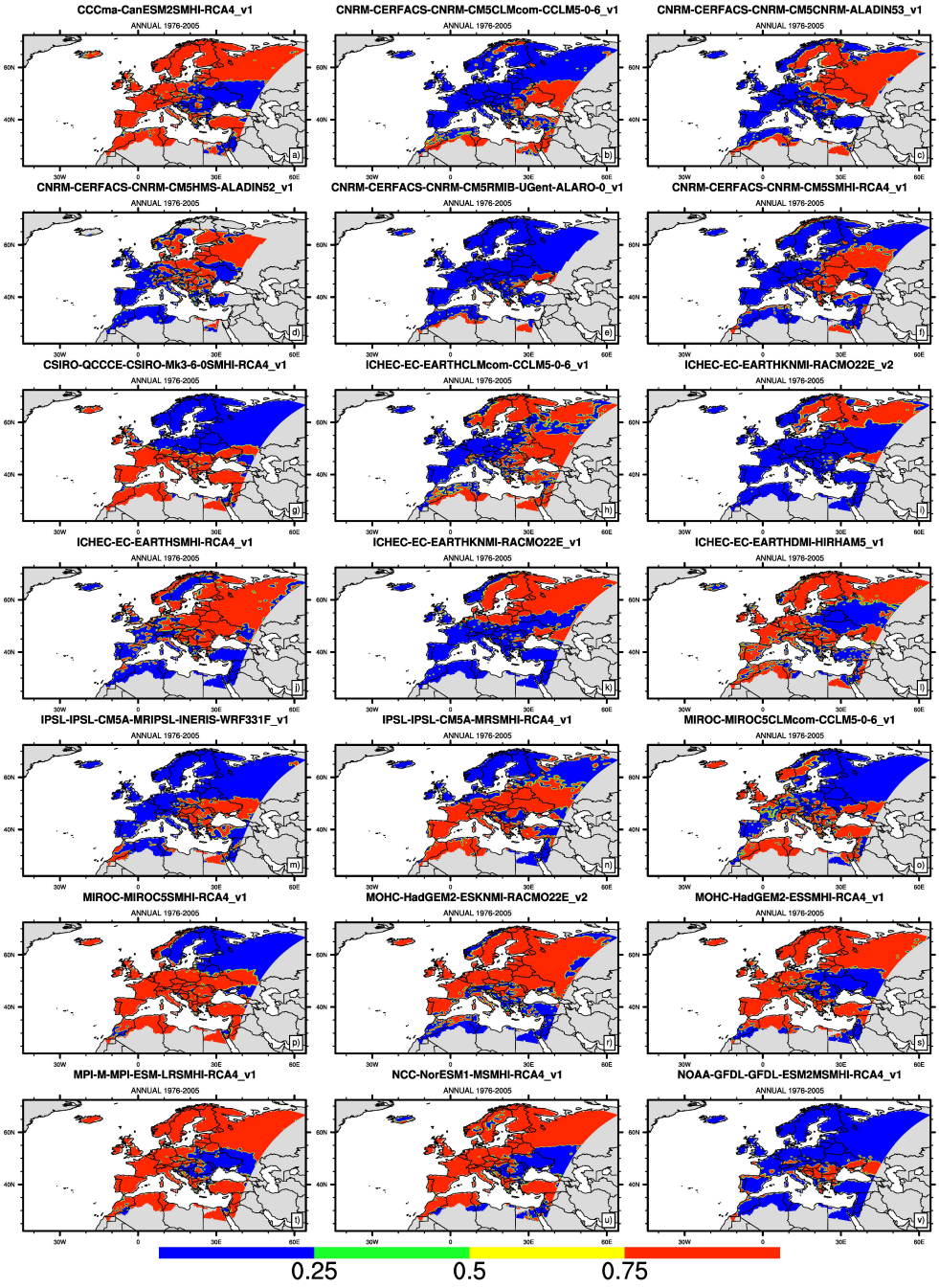

Figure 5.13. Annual DAEE of the Unrepresentative Models in the Statistical Methodology 1 in the period between 1976 and 2005

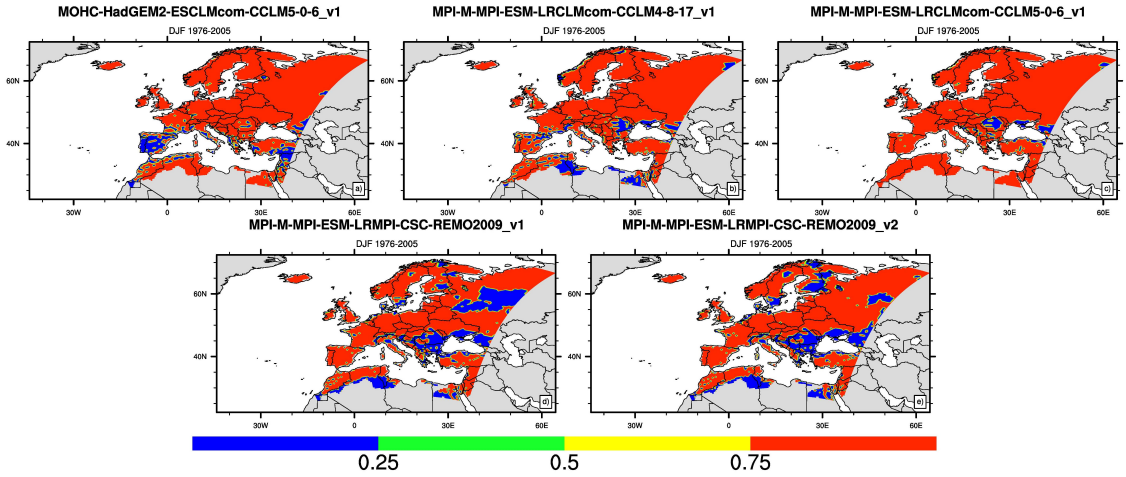

Figure 5.14. DAEE of the Representative Models in the Statistical Methodology 1 in the period between the years 1976 and 2005 in Winter Season

to "4" if it is considered as a representative model. Otherwise, it can' produce good results in some seasons. For example, SDAEE of a model combination has to be 3 for a grid point if model combination has smaller absolute errors (AEE) than the average absolute errors (MAEE) in three seasons.

The collections of the DAEEs in all of the seasons of model combinations are portrayed in Figure 5.22 and Figure 5.23. MOH-CLM has smaller AEEs than MAEEs in all of the seasons over France, Finland, Norway, Sweden, Central Europe, Northern Turkey and Central Western Russia. It is unsuccessful in at least one season over Spain and Northern Russia. MPI-CLM1 is well enough to represent the temperature over Fınland, Norway, Sweden, some parts of Turkey and Russia. In three seasons, It is successfully represents the temperature over West Europe and Central western Russia. Finland, Turkey and Northern Africa are the regions for which MPI-CLM2 generates good results with having SDAEE value of "4". However, it is unrepresentative of at least one season over the remaining part of the observed region. MPI-REMO1 and MPI-REMO2 are two of the best models to present the temperature over Spain, Portugal, France, Norway, Sweden and most of the Central Europe. However they aren't good enough to project the temperature over Northern Black Sea Coastal.

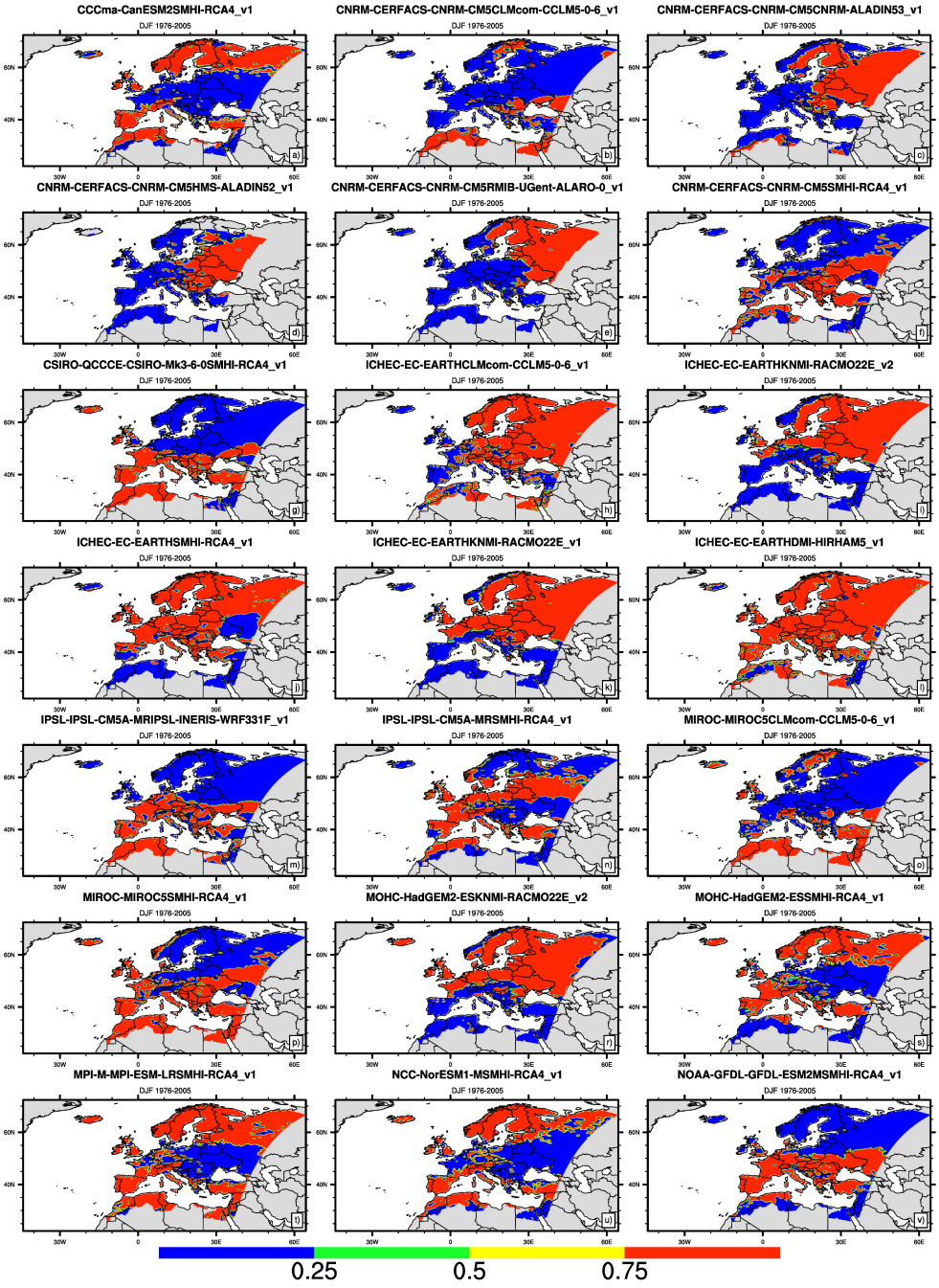

Figure 5.15. DAEE of the Unrepresentative Models in the Statistical Methodology 1 in the period between the years 1976 and 2005 in Winter Season

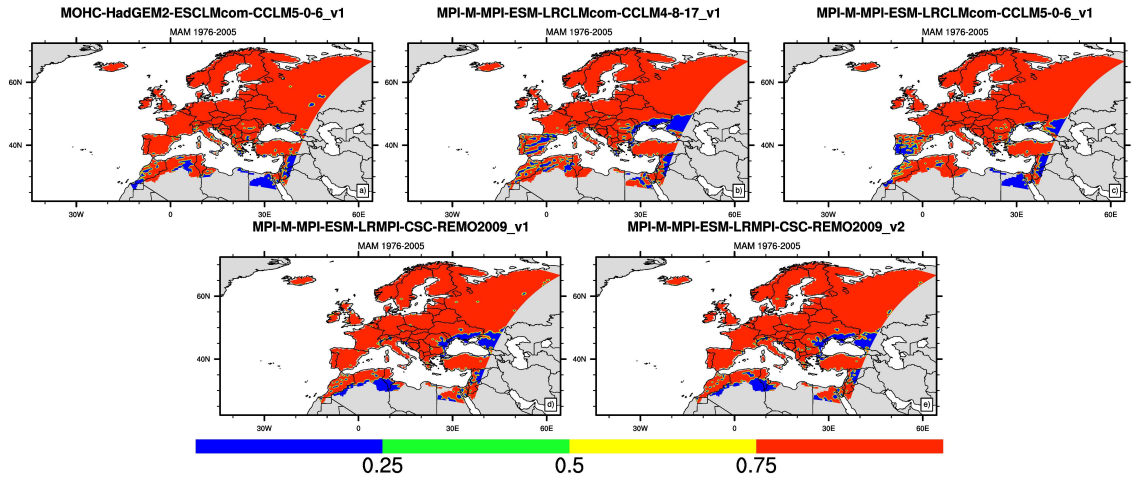

Figure 5.16. DAEE of the Representative Models in the Statistical Methodology 1 in the period between the years 1976 and 2005 in Spring Season

One of the most important outcomes of this methodology emerges at that point because it gives scientists a chance to continue their research with the most convenient model combinations. For example, if Spain is the focused area in a climate study, CCCma-RCA4, CSIRO-RCA4, MPI-RCA4, MPI-REMO1 and MPI-REMO2 will be the most appropriate model combinations. Besides, the reliability of the research should be questioned if one of the CNRM-CNRM, CHRM-HMS, CNRM-RMIB, ICHEC-KNMI1 or ICHEC-KNMI2 model combinations is chosen. Moreover, it can be alleged that Global Climate Model of MPI is better than the other GCMs to simulate the temperature of Spain because four of the five model combinations which include MPI as GCM is better than the average, having SDAEE of "4" or "3". It can also be asserted that Regional Climate Model REMO is good to represent the temperature over Europe because there are two model combinations using REMO as RCM and both of them are very successful in each season over almost each grid. Finally, it can be claimed that the model combination of MPI- REMO is one of the most convenient options to simulate the temperature patterns over Spain.

On the other hand, it can be claimed if a researcher chooses Absolute Average of Error (AAE) as an indicator. There are several indicators which will be introduced in

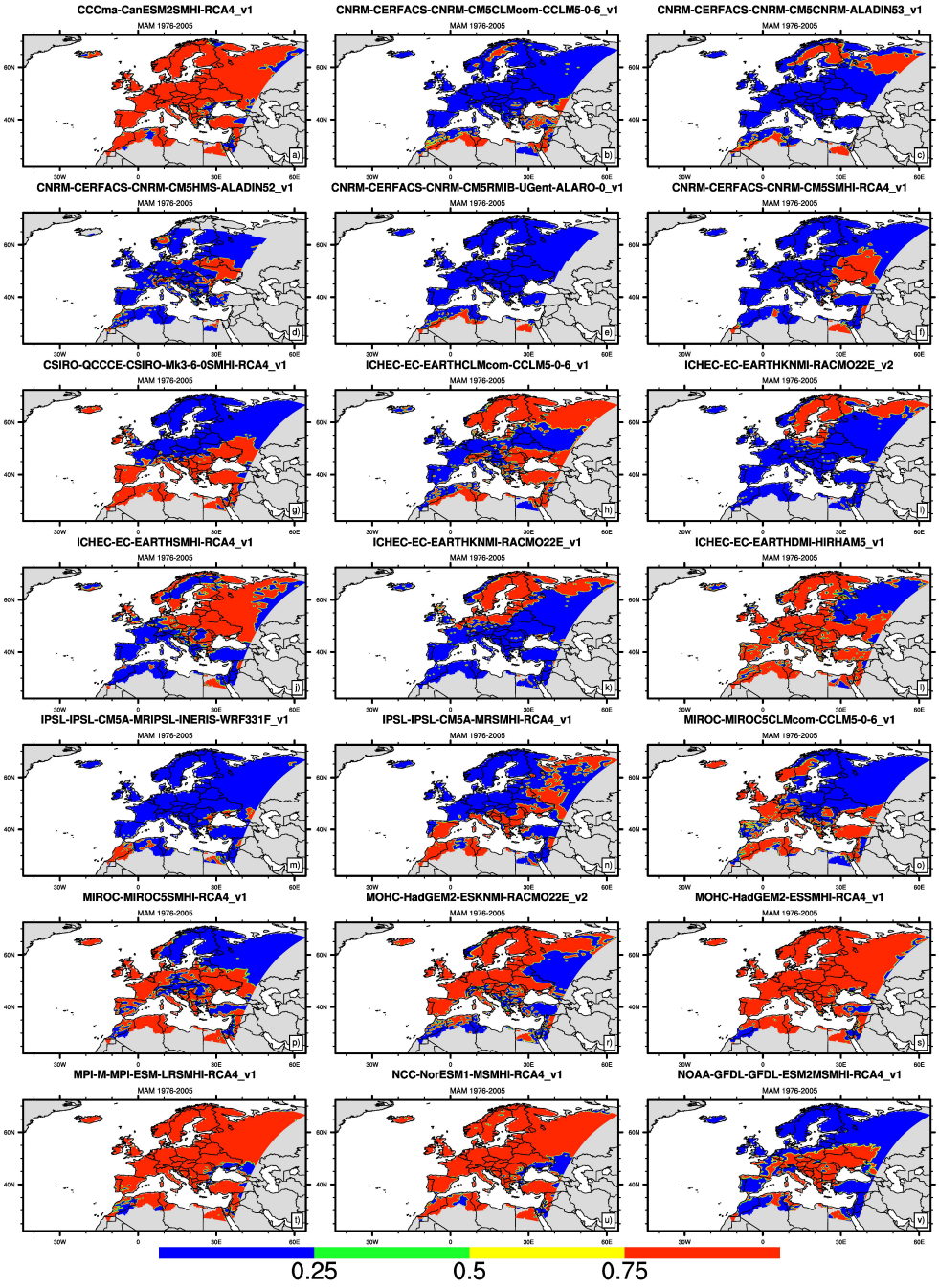

Figure 5.17. DAEE of the Unrepresentative Models in the Statistical Methodology 1 in the period between the years 1976 and 2005 in Spring Season

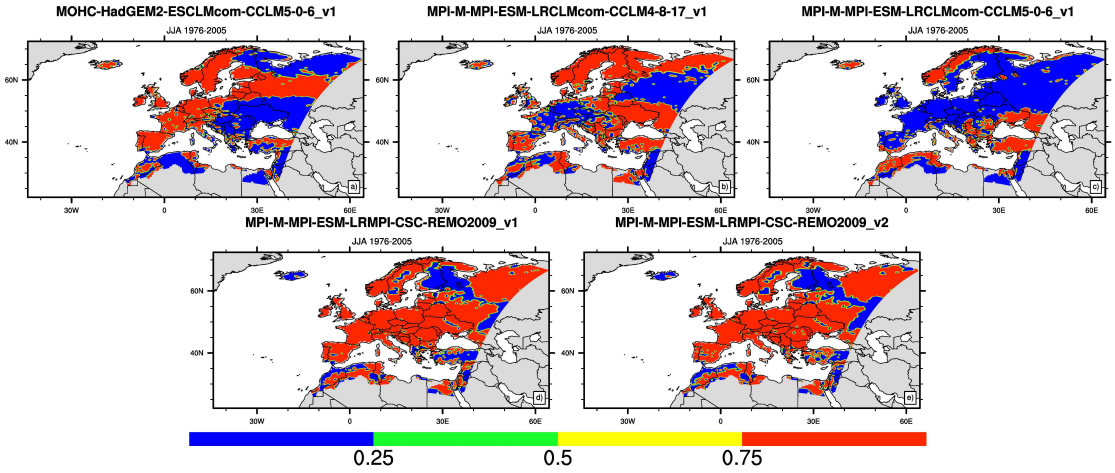

Figure 5.18. DAEE of the Representative Models in the Statistical Methodology 1 in the period between the years 1976 and 2005 in Summer Season

this thesis to separate successful and unsuccessful model combinations from each other like Root Mean Error Square (RMSE), the Student T-test and correlation coefficient. It will be more trustable if these aforementioned model combinations are in the "representative" set at every turn after the necessary operations and calculations are fulfilled according to all of these indicators mentioned above.

Step 6: The Average of "SDAEE"s of 26 Models

In this step, the average of the SDAEE values of each model is calculated (MSDAEE). It is expected that it alters between "0" and "4". In the next step, similar methods are applied for the model combination comparison. The SDAEE value of a model combination has to be bigger than MSDAEE. Higher SDAEE value a model combination has, more successful this model is. Hence, "1" is assigned to the gird point If SDAEE value of a model combination at that grid point is bigger than MSDAEE value at that corresponding grid point. In the opposite case, it is assigned to value "0".

It is expected that MSDAEE value can be around "2" if the AEEs of models are normally distributed and close to each other. However, it is seen that MSDAEE values

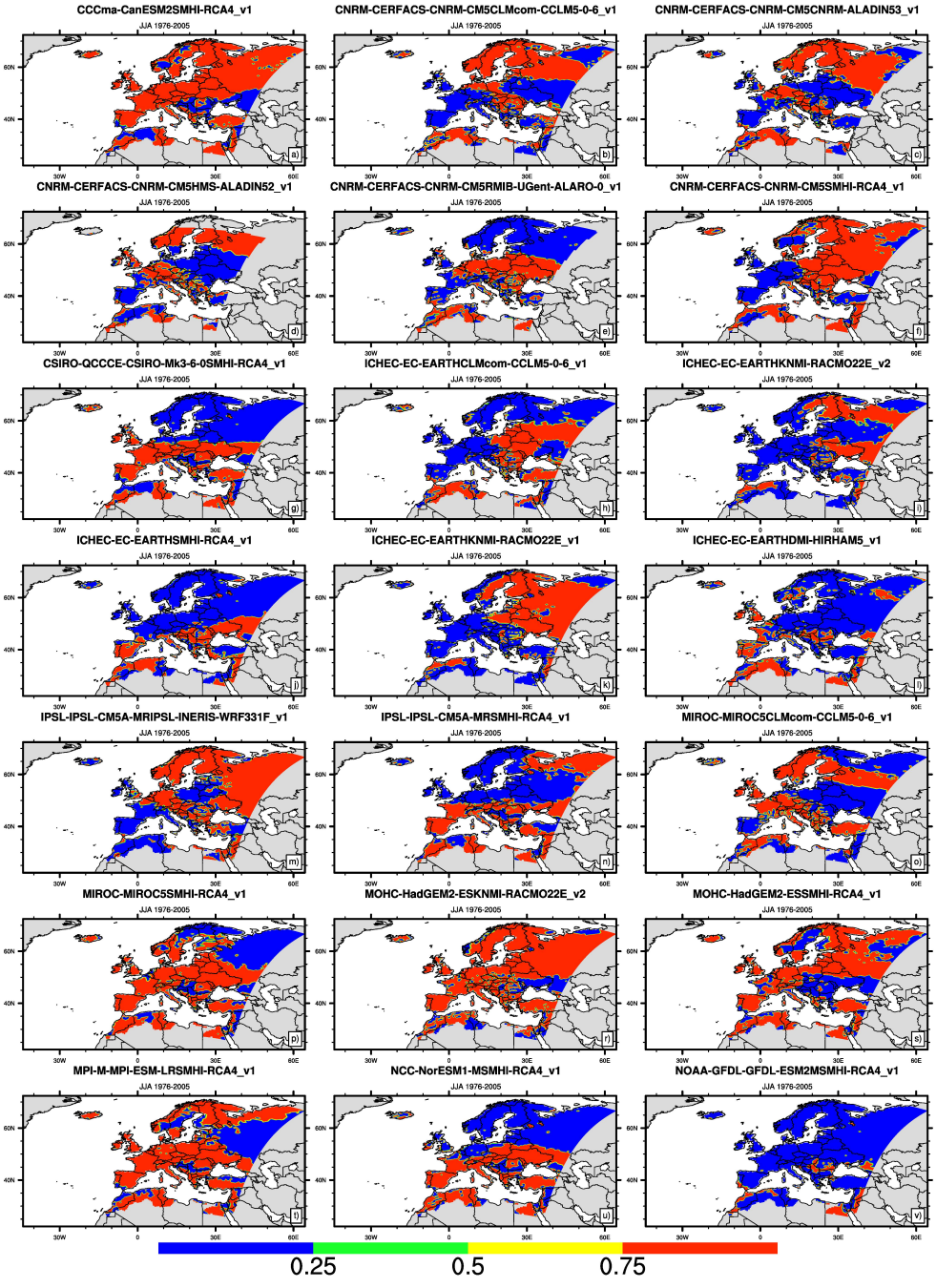

Figure 5.19. DAEE of the Unrepresentative Models in the Statistical Methodology 1 in the period between the years 1976 and 2005 in Summer Season

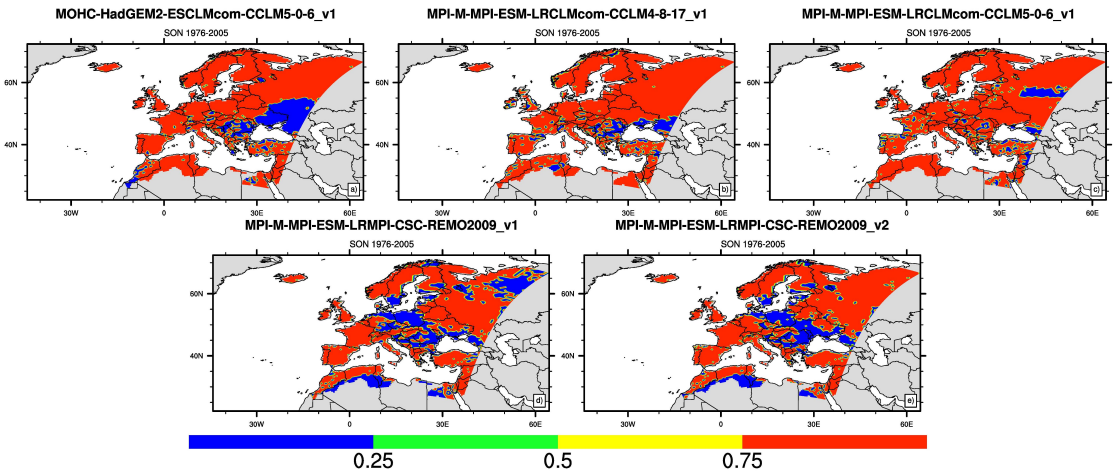

Figure 5.20. DAEE of the Representative Models in the Statistical Methodology 1 in the period between the years 1976 and 2005 in Autumn Season

at eastern boundaries of the observed regions are smaller than 2 and even they decline till 1.3. The reason behind this outcome should be that some models have very high AAEs and hence the distributions of AAEs of the model combinations at those points are left skewed. As a result of this, the amount of model combinations passing the MAEE value is smaller than expected under normal conditions. If this distribution is right skewed, than the amount of successful model combinations will be greater than expected as it happens over some parts of Russia, Finland, in the majority of Ukraine and some grid points of Central Turkey.

All of the Model Combinations produce the most unreliable outcomes over the Northern Black Sea coastal and Romania because all of the "representative" model combinations aren't successful to pass the test over this region. In other words, DS-DAEE value of each representative model combination at the grid points covering this region is lower than the MSDAEE (Figure 5.24 and Figure 5.25). Hence, the projection of temperature over this region by using these proposed model combinations should be unreliable but these model combinations are the best ones if the whole region is taken into consideration. In the rest of the observed area, these "representative" model combinations perform better than the most of the other model combinations (Figure 5.26

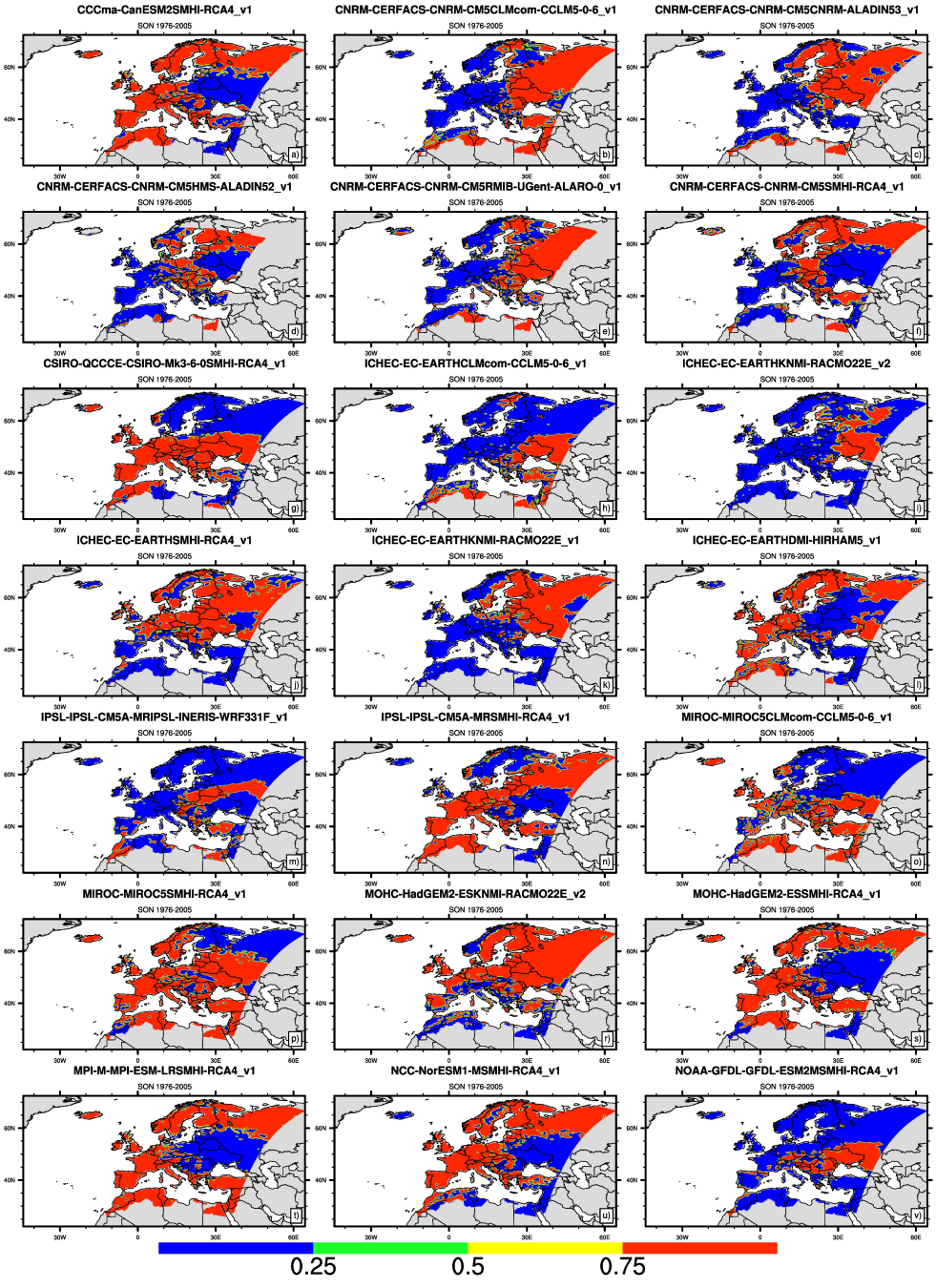

Figure 5.21. DAEE of the Unrepresentative Models in the Statistical Methodology 1 in the period between the years 1976 and 2005 in Autumn Season

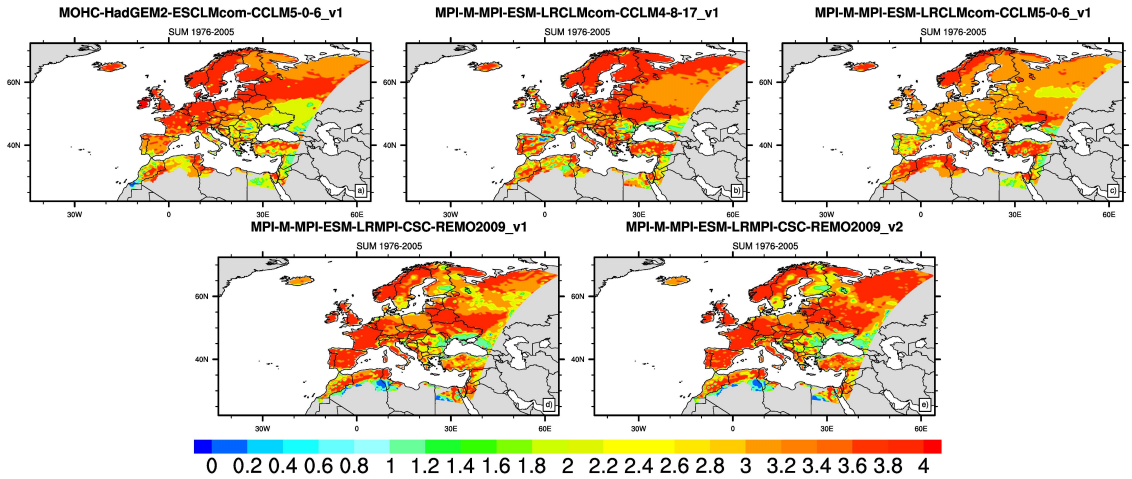

Figure 5.22. The "SDAEE"s of the Representatıve Models in the Statistical Methodology 1 in the perıod between the years 1976 and 2005

and Figure 5.27).

Step 7: The Average of "WDSDAEE"s of 26 Models

In this step, the final limit values are obtained to define the representative and unrepresentative model combinations. The spatial averages of DSDAAE values covering the observed region are calculated and single values are obtained for each model combination (WDSDAAE). It is estimated that WDSDAAE of a model combination has to be close to "1" if it is good enough to represent the temperature over the observed region because it passes the test in Step 6 and can produce better results than the average (Figure 5.28).

Step 8: The Separation of Models as Representative and Unrepresentative

At this step, the average and standard deviation of WDSDAAE values of 26 model combinations are calculated (SAWSDAAE and AWSDAAE). The standard deviation and average of these values are added and another limit value is obtained (TWSDAAE). Then the WSDAAE value of each model is compared with AWSDAAE and if it is bigger

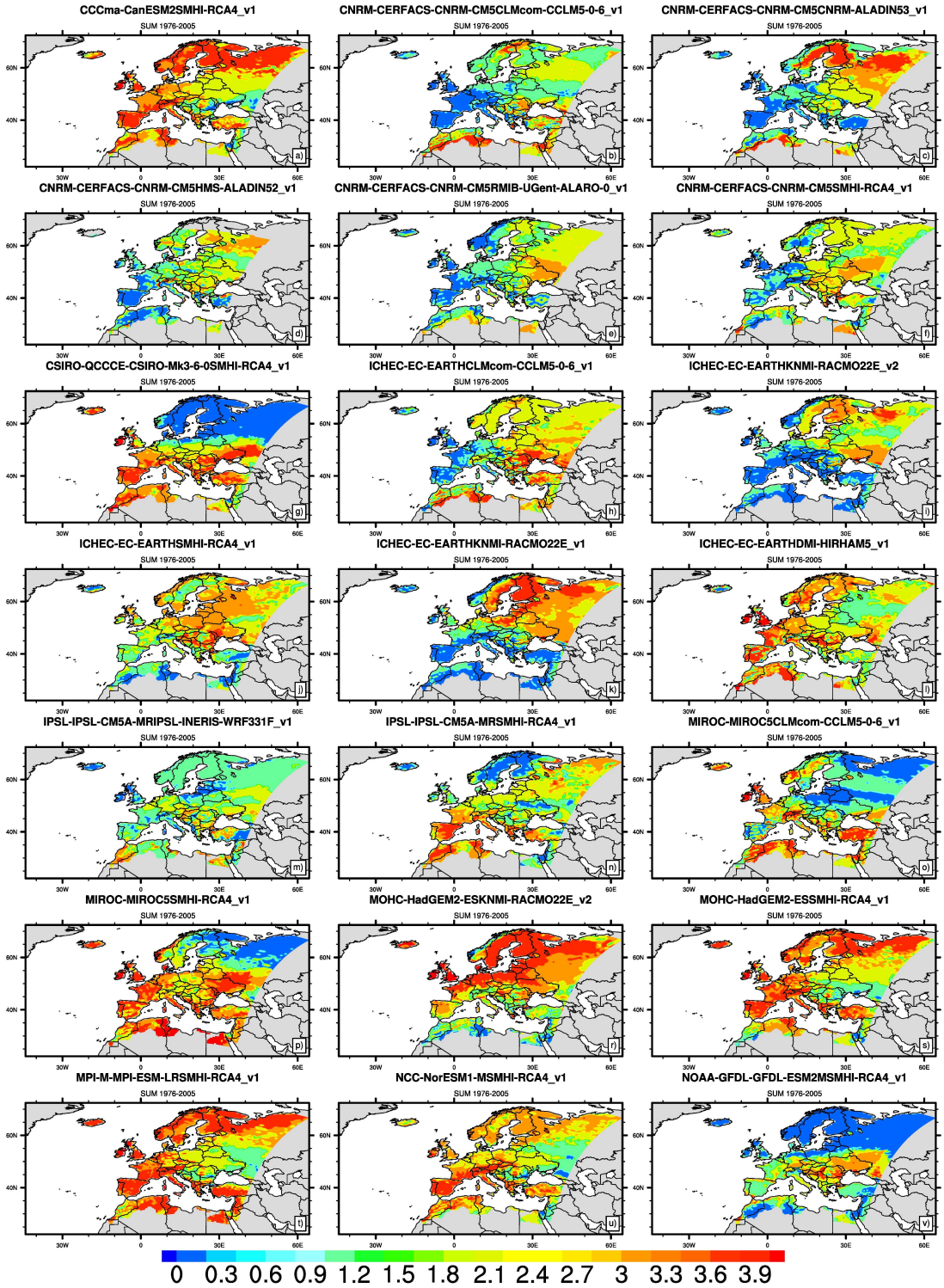

Figure 5.23. The "SDAEE"s of the Unrepresentative Models in the Statistical Methodology 1 in the period between the years 1976 and 2005

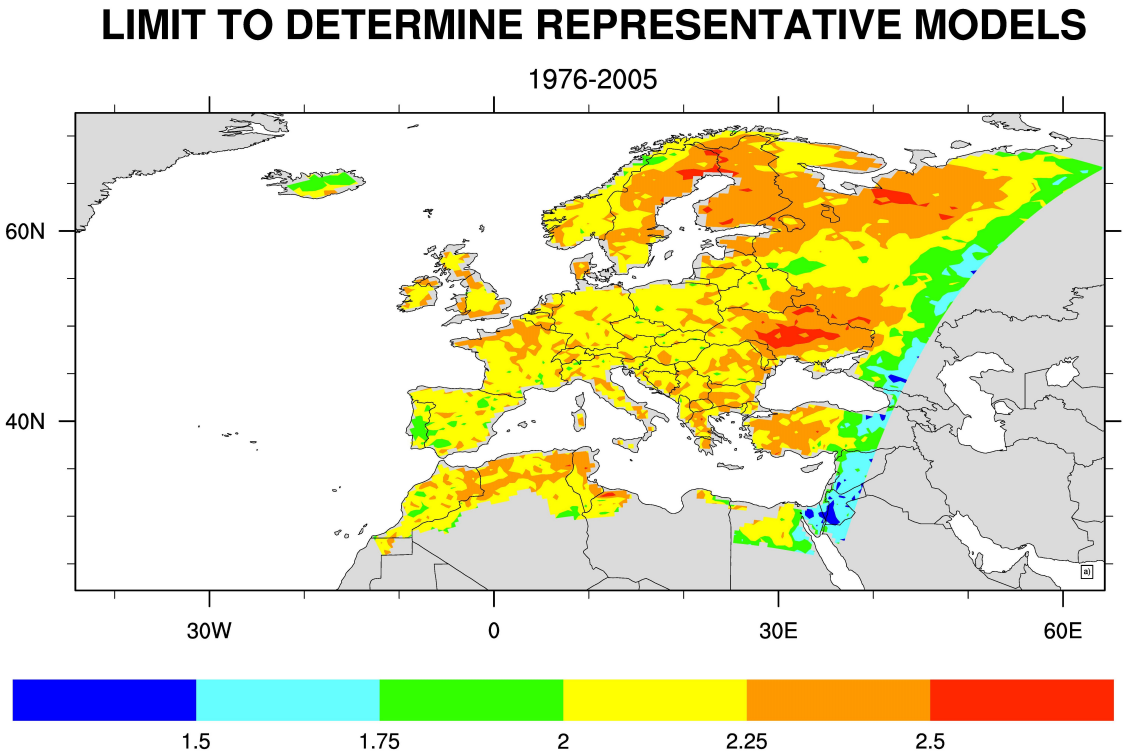

Figure 5.24. The "MSDAEE of the Model Combinations in the Statistical Methodology 1 in the period between the years 1976 and 2005

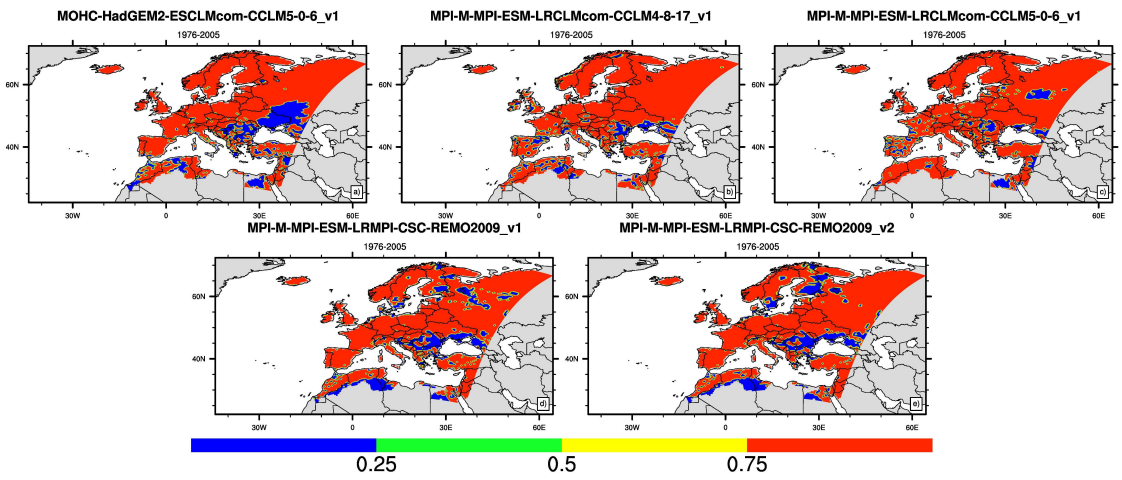

Figure 5.25. The "DSDAEE of the Representative Model Combinations in the Statistical Methodology 1 in the period between the years 1976 and 2005

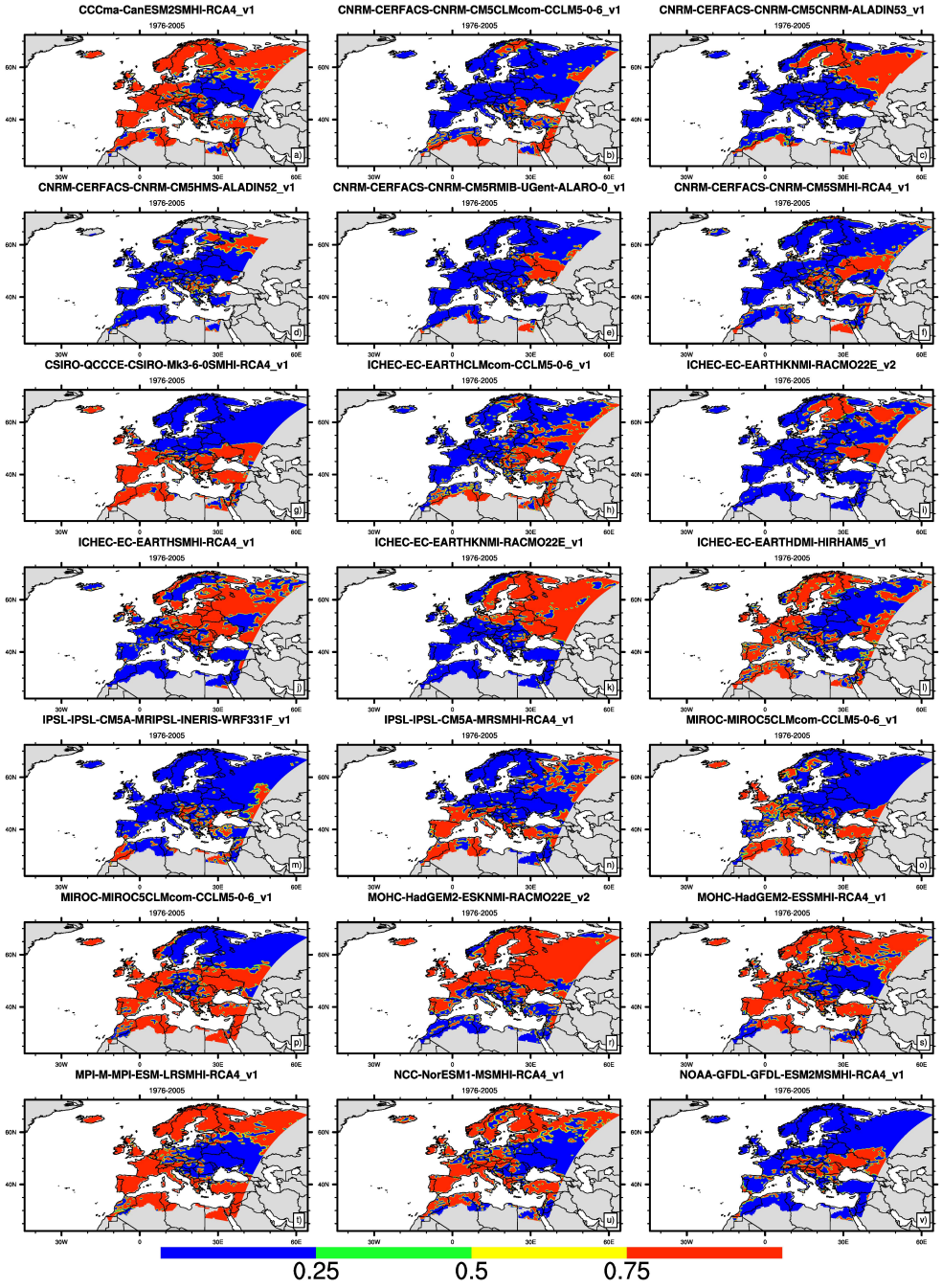

Figure 5.26. The "DSDAEE of the Unrepresentative Model Combinations in the Statistical Methodology 1 in the period between the years 1976 and 2005

Table 5.3. The coefficients of The Most Representative Models

GCM - RCM Model Combination	**Coefficient**
MOHC-HadGEM2-ES - CLMcom-CCLM5-0-6-v1	0.78415
MPI-M-MPI-ESM-LR - CLMcom-CCLM4-8-17-v1	0.85187
MPI-M-MPI-ESM-LR - CLMcom-CCLM5-0-6-v1	0.86438
MPI-M-MPI-ESM-LR - MPI-CSC-REMO2009-v1	0.78276
MPI-M-MPI-ESM-LR - MPI-CSC-REMO2009-v2	0.78535

Table 5.4. The coefficients of The Unrepresentative Models

GCM - RCM Model Combination	**Coefficient**
CCCma-CanESM2 - SMHI-RCA4-v1	0.65687
CNRM-CERFACS-CNRM-CM5 - CLMcom-CCLM5-0-6-v1	0.25874
CNRM-CERFACS-CNRM-CM5 - CNRM-ALADIN53-v1	0.34572
CNRM-CERFACS-CNRM-CM5 - HMS-ALADIN52-v1	0.17717
CNRM-CERFACS-CNRM-CM5 - RMIB-UGent-ALARO-0-v1	0.17590
CNRM-CERFACS-CNRM-CM5 - SMHI-RCA4-v1	0.26033
CSIRO-QCCCE-CSIRO-Mk3-6-0 - SMHI-RCA4-v1	0.48133
ICHEC-EC-EARTH - CLMcom-CCLM5-0-6-v1	0.40111
ICHEC-EC-EARTH - KNMI-RACMO22E-v2	0.21624
ICHEC-EC-EARTH - SMHI-RCA4-v1	0.45353
ICHEC-EC-EARTH - KNMI-RACMO22E-v1	0.41978
ICHEC-EC-EARTH - DMI-HIRHAM5-v1	0.53157
IPSL-IPSL-CM5A-MR - IPSL-INERIS-WRF331F-v1	0.18467
IPSL-IPSL-CM5A-MR - SMHI-RCA4-v1	0.39297
MIROC-MIROC5 - CLMcom-CCLM5-0-6-v1	0.36458
MIROC-MIROC5 - SMHI-RCA4-v1	0.61001
MOHC-HadGEM2-ES - KNMI-RACMO22E-v2	0.64337
MOHC-HadGEM2-ES - SMHI-RCA4-v1	0.62728
MPI-M-MPI-ESM-LR - SMHI-RCA4-v1	0.68864
NCC-NorESM1-M - SMHI-RCA4-v1	0.56612
NOAA-GFDL-GFDL-ESM2M - SMHI-RCA4-v1	0.19936

than AWSDAAE, this model is collected under the set of “more representative” model combinations. More determiner limit value (TWSDAAE) is used to find the most accurate model combinations. If WDSDAAE is bigger than TWSDAAE, this model is collected under the set of “most representative” model combinations (Table 5.3 and Table 5.4).

Finally, it is concluded that MOHC-CLM, MPI-CLM1, MPI-CLM2, MPI-REMO1 and MPI-REMO2 are the most representative model combinations for the temperature projection over Europe “according to statistical methodology 1 (AAE is the indicator)”. As shown in Table 5.3, WDSDAAE values of 78 % of the grid points in MOHC-CLM model combination, 85 % of the grid points in MPI-CLM1 model combination, 86 % of the grid points in MPI-CLM2 model combination, 78 % of the grid points in MPI-REMO1 model combination and 78 % of the grid points in MPI-REMO2 model combination, are higher than WSDAAE. These percentages also show the strength of the success of the model combinations. There is a discernible line between the most representative model combinations and unrepresentative model combinations. MPI-RCA4, defining in unrepresentative model combinations, has the maximum percentage with 68 % which is at least 10 % smaller than the model combinations, defined in the most representative ones.

All of the successful models produce accurate results over the majority of the domain. The exceptions are interior lands of Libya and Algeria, small land sections of northern Spain some coastal region of the Northern Black Sea for MPI-CLM1 model combination. As it was discussed before, interior lands of Northern Africa and Northern Black Sea Coastal are the parts where majority of model combinations produce unsuccessful results. MPI-CLM1 and MPI-CLM2 produce better results than the remaining combinations. The performance of MPI-CLM2 is inefficient over the same underrepresented regions of MPI-CLM1 model combinations, excluding interior lands of Libya and Algeria. In addition to these regions, a small part of central western part of Russia is also classified as underrepresented regions. MPI-REMO1 is also unsuccessful over the same regions. Underrepresented regions, simulated by MPI-REMO1 and MPI-REMO2 expand through the interior lands of north-western Russia and eastern

Finland. Using CNRM-CLM, CNRM-RMIB, CNRM-RCA4, CNRM-HMS, NOAA-RCA4 and IPSL-IPSL combination for projection of European temperature pattern may produce unreliable outcomes with respect to this methodology.

It is misguidedness to generalize the success of the model combinations for whole Europe. These model combinations may be accepted as the best representative ones when the overall assessment for Europe is carried out. The performances of the Model combinations to demonstrate the temperature over different regions/ countries alter. For example, if the principal groomed region is Turkey, then MIROC-CLM1, MIROC-CLM2, MOHC-RCA4, MPI-RCA4 and NCC-RCA4 may also be predicated on.

After that point, the main purpose is to find the most convenient coefficients for these most representative model combinations to form a suitable ensemble. After that point, all of the figures are drawn and tables are prepared according to Test5, Test6, Test7 and Test8 through this thesis. These tests, described in Methodology, are valid for the most representative model combinations. "More representative" and the "most unrepresentative" model combinations are obtained by comparing WSDAAE with AWSDAAE instead of TWSDAAE. If the comparison is directly performed with the average value, "More representative" model combinations are found. If the comparison is performed with the addition of average value and one standard deviation, "the most representative" model combinations are obtained.

5.1.2. Application of Statistical Methodology 2 to the Monthly Temperature Data: The Case of Europe

In this part, the Statistical Methodology II is applied to the monthly temperature of Europe and the procedure is almost the same as in Statistical Methodology I. The unique difference stems from the error indicator. Root Mean Square Error (RMSE) is used as indicator, instead of Absolute Value of Average Error (AAE) and the remaining steps are the same in Statistical Methodology 1.

MPI-CLM1, MPI-CLM2, MPI-REMO1 and MPI-REMO2 are the most representative model combinations for the temperature projection over Europe "according to statistical methodology 2 (RMSE being the indicator)" and MOHC-CLM, is excluded due to the outcomes of the. As shown in Table 5.5 and 5.6, WDSDAAE values of 87 % of the grid points in MPI-CLM1 model combination, 83 % of the grid points in MPI-CLM2 model combination, 82 % of the grid points in MPI-REMO1 model combination and 80 % of the grid points in MPI-REMO2 model combination, are higher than WSDAAE. CCCma-RCA4, MOHC-CLM defined to be in unrepresentative model combinations, has the maximum percentage with 74 % which is at least 6 % smaller than the model combinations, defined to be in the most representative ones and they are also good to simulate the temperature patterns of Europe.

All of the successful models produce accurate results over the majority of the domain. For MPI-CLM1 model combination, the exceptions are interior lands of Libya and Algeria, small sections of eastern Spain some coastal region of Northern Black Sea. As it was discussed before, interior lands of Northern Africa and Northern Black Sea Coastal are the parts where majority of model combinations produce unsuccessful results. MPI-CLM2 generates more unrepresentative results than MPI-CLM1 combination. The performance of MPI-CLM2 is inefficient over the same underrepresented regions of MPI-CLM1 model combinations. In addition to these regions, the central western part of Russia and western Spain are also qualified as underrepresented regions. MPI-REMO1 is also unsuccessful over the same regions. However, it is better than MPI-CLM2 to represent the temperature of central western Russia. Underrepresented regions, simulated by MPI-REMO2 expanded through the interior lands in Romania. On the other hand, they are good at representing the temperature patterns of Spain. Using CNRM-RMIB and IPSL-IPSL model combinations for projection of European temperature pattern may lead to produce unreliable results.

It is misguidedness to generalize the success of the model combinations for whole Europe. These model combinations may be accepted as the best representative ones when overall assessment for Europe is carried out. The performances of the Model combinations to demonstrate the temperature over different regions/ countries alter. For

example, if the principal groomed region is Spain, then CCCma-RCA4, CSIRO-RCA4, ICHEC-DMI, IPSL-RCA4, MIROC-RCA4, MOHC-CLM, MOHC-KNMI, MOHC - RCA4, MPI-RCA4 and NCC-RCA4 may be relied on and MPI-CLM2 has to be excluded for further calculations over Spain (Figure 5.27 and Figure 5.28).

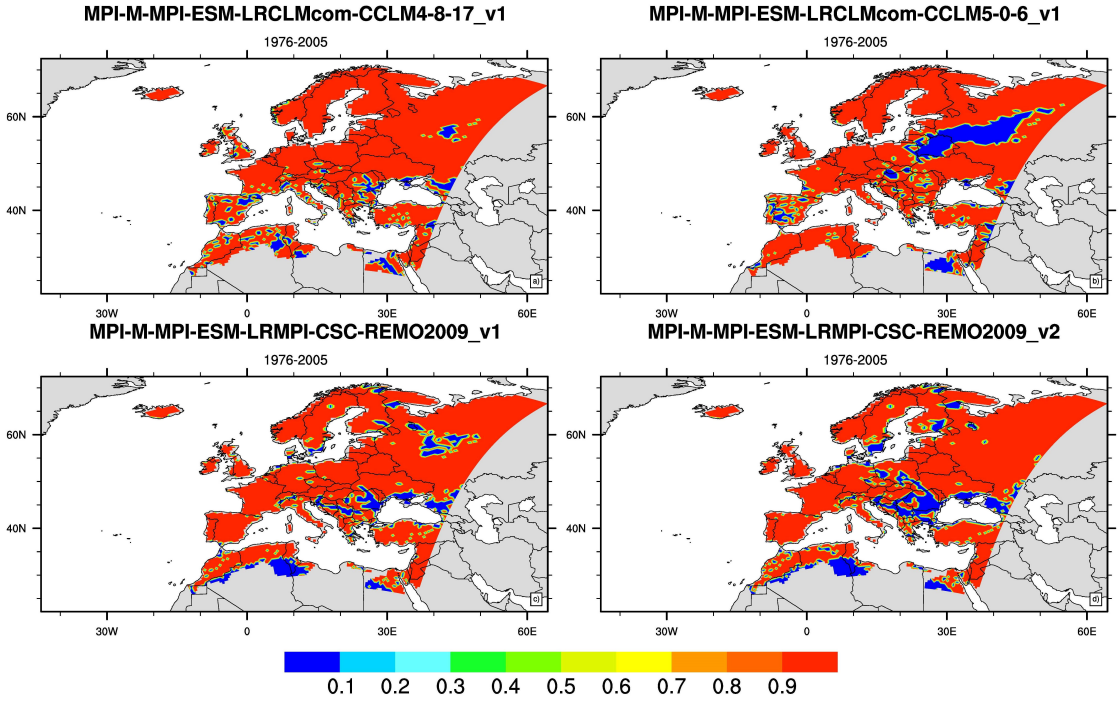

Figure 5.27. The "DSDAEE of the Representative Model Combinations in the Statistical Methodology 2 in the period between the years 1976 and 2005

5.1.3. Application of Statistical Methodology 3 to the Monthly Temperature Data: The Case of Europe

In this part, the Statistical Methodology III is applied to the monthly temperature of Europe where T-Test is used as indicator. The blue parts in the maps indicate the grid points that either don't pass student T-Test or pass the test but are less successful to represent the temperature compared to other models. Hence, we conclude that the red points not only represent the areas where the model combinations are successful but they are also confidential.

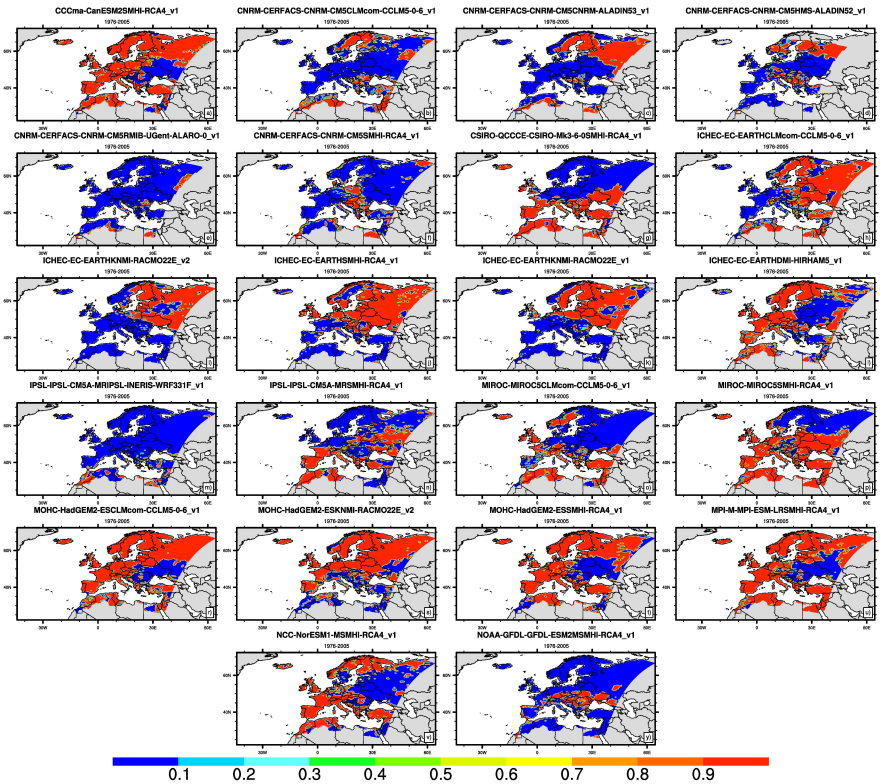

Figure 5.28. The "DSDAEE of the Unrepresentative Model Combinations in the Statistical Methodology 2 in the period between the years 1976 and 2005

Table 5.5. The coefficients of The Most Representative Models

GCM - RCM Model Combination	**Coefficient**
MPI-M-MPI-ESM-LR-CLMcom-CCLM4-8-17-v1	0.86736
MPI-M-MPI-ESM-LR-CLMcom-CCLM5-0-6-v1	0.83201
MPI-M-MPI-ESM-LR-MPI-CSC-REMO2009-v1	0.82685
MPI-M-MPI-ESM-LR-MPI-CSC-REMO2009-v2	0.80302

Table 5.6. The coefficients of The Unrepresentative Models

GCM - RCM Model Combination	**Coefficient**
CCCma-CanESM2-SMHI-RCA4-v1	0.74444
CNRM-CERFACS-CNRM-CM5-CLMcom-CCLM5-0-6-v1	0.28793
CNRM-CERFACS-CNRM-CM5-CNRM-ALADIN53-v1	0.35358
CNRM-CERFACS-CNRM-CM5-HMS-ALADIN52-v1	0.27374
CNRM-CERFACS-CNRM-CM5-RMIB-UGent-ALARO-0-v1	0.10826
CNRM-CERFACS-CNRM-CM5-SMHI-RCA4-v1	0.24027
CSIRO-QCCCE-CSIRO-Mk3-6-0-SMHI-RCA4-v1	0.48213
ICHEC-EC-EARTH-CLMcom-CCLM5-0-6-v1	0.60087
ICHEC-EC-EARTH-KNMI-RACMO22E-v2	0.35385
ICHEC-EC-EARTH-SMHI-RCA4-v1	0.54686
ICHEC-EC-EARTH-KNMI-RACMO22E-v1	0.42077
ICHEC-EC-EARTH-DMI-HIRHAM5-v1	0.58479
IPSL-IPSL-CM5A-MR-IPSL-INERIS-WRF331F-v1	0.11200
IPSL-IPSL-CM5A-MR-SMHI-RCA4-v1	0.44301
MIROC-MIROC5-CLMcom-CCLM5-0-6-v1	0.39337
MIROC-MIROC5-SMHI-RCA4-v1	0.67832
MOHC-HadGEM2-ES-CLMcom-CCLM5-0-6-v1	0.73193
MOHC-HadGEM2-ES-KNMI-RACMO22E-v2	0.62887
MOHC-HadGEM2-ES-SMHI-RCA4-v1	0.66759
MPI-M-MPI-ESM-LR-SMHI-RCA4-v1	0.74027
NCC-NorESM1-M-SMHI-RCA4-v1	0.50913
NOAA-GFDL-GFDL-ESM2M-SMHI-RCA4-v1	0.17633

The outcomes of this methodology are very different than the previous ones. First of all, the distributions of the successful grid points vary a lot. Second, successful domains of the model combinations over Europe don't overlap. CCCma-RCA4, MOHC-CLM1, MPI-CLM1, MPI-CLM2 and MPI-REMO2 are the most representative model combinations for the temperature projection over Europe "according to statistical methodology 3 (T-Test being the indicator)". As shown in Table 5.7 and Table 5.8, WDSDAAE values of 66 % of the grid points in MOHC-CLM model combination, 65 % of the grid points in MPI-CLM1 model combination, 63 % of the grid points in MPI-CLM2 model combination, 59 % of the grid points in MPI-REMO2 model combination and 59 % of the grid points in CCCma-RCA4 model combination are higher than WSDAAE. MPI-MPI, NCC-RCA4 defined to be in unrepresentative model combinations, has the maximum percentage with 55 % which is at least 4 % smaller than the model combinations, defined to be in the most representative ones and they are second in order to simulate the temperature patterns of Europe.

CCCma-RCA4 passes the T-test and more successful than majority of the model combinations over Scandinavian countries, the Western Europe, the Northern Russia and Northern Africa. MOHC-CLM is good at representing the temperature over almost whole region, except Ukraine and Ukraine border of Russia. MPI-CLM generates unreliable results over Northern Black Sea Coastal, Belarus, and Eastern Baltic Sea Coastal. MPI-CLM1 and MPI-CLM2 aren't good at projecting the temperature over especially Wester Europe and Northern coastal of Black Sea. MPI-REMO2 also produces similar results to MPI-CLM2 but it is representative over France unlike MPI-CLM2 (Figure 5.29 and Figure 5.30).

5.1.4. Application of Statistical Methodology 4 to the Monthly Temperature Data: The Case of Europe

In this part, the Statistical Methodology IV is applied to the annual temperature of Europe where T-Test is used as indicator.

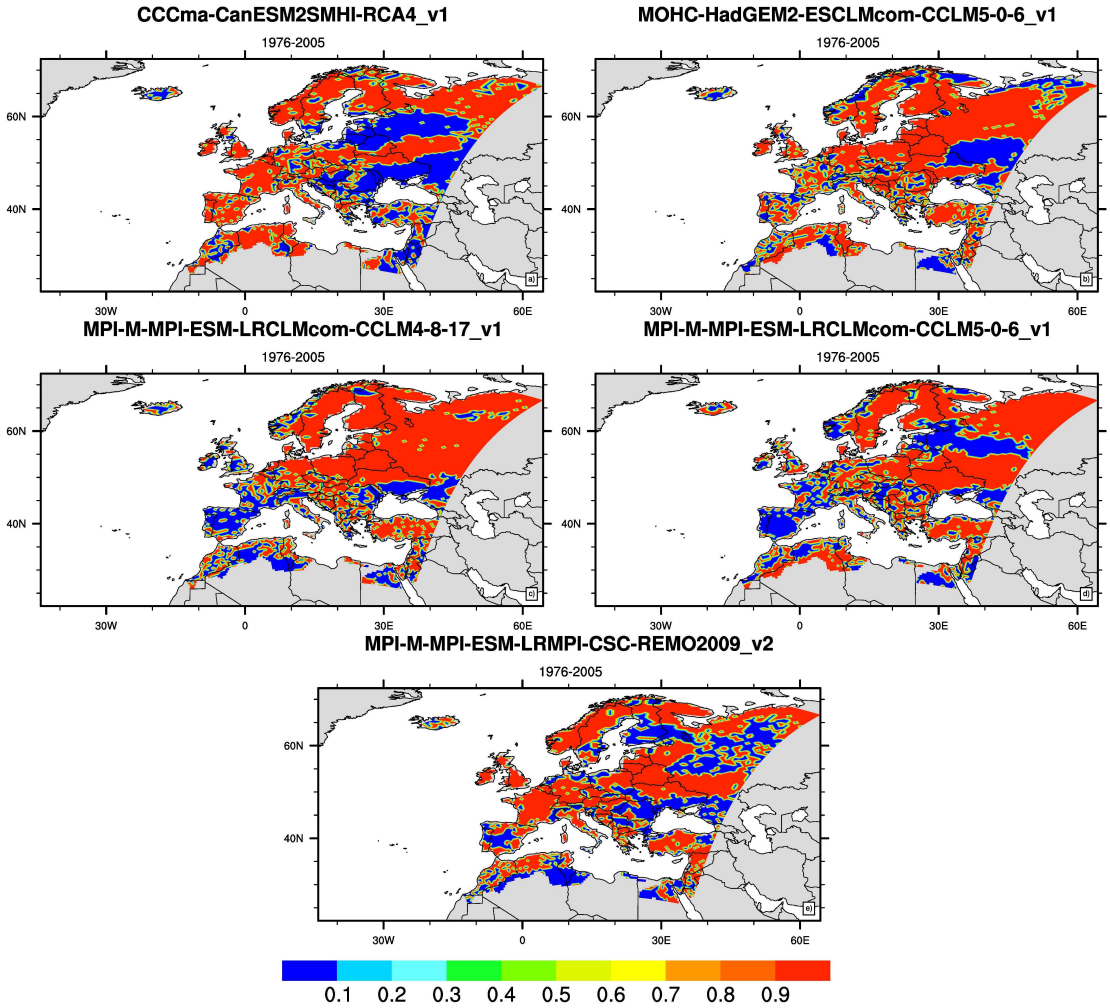

Figure 5.29. The "DSDAEE of the Representative Model Combinations in the Statistical Methodology 3 in the period between the years 1976 and 2005

Table 5.7. The coefficients of The Most Representative Models

GCM - RCM Model Combination	**Coefficient**
MPI-M-MPI-ESM-LR-MPI-CSC-REMO2009-v2	0.59750
CCCma-CanESM2-SMHI-RCA4-v1	0.58896
MOHC-HadGEM2-ES-CLMcom-CCLM5-0-6-v1	0.66362
MPI-M-MPI-ESM-LR-CLMcom-CCLM4-8-17-v1	0.65886
MPI-M-MPI-ESM-LR-CLMcom-CCLM5-0-6-v1	0.63364

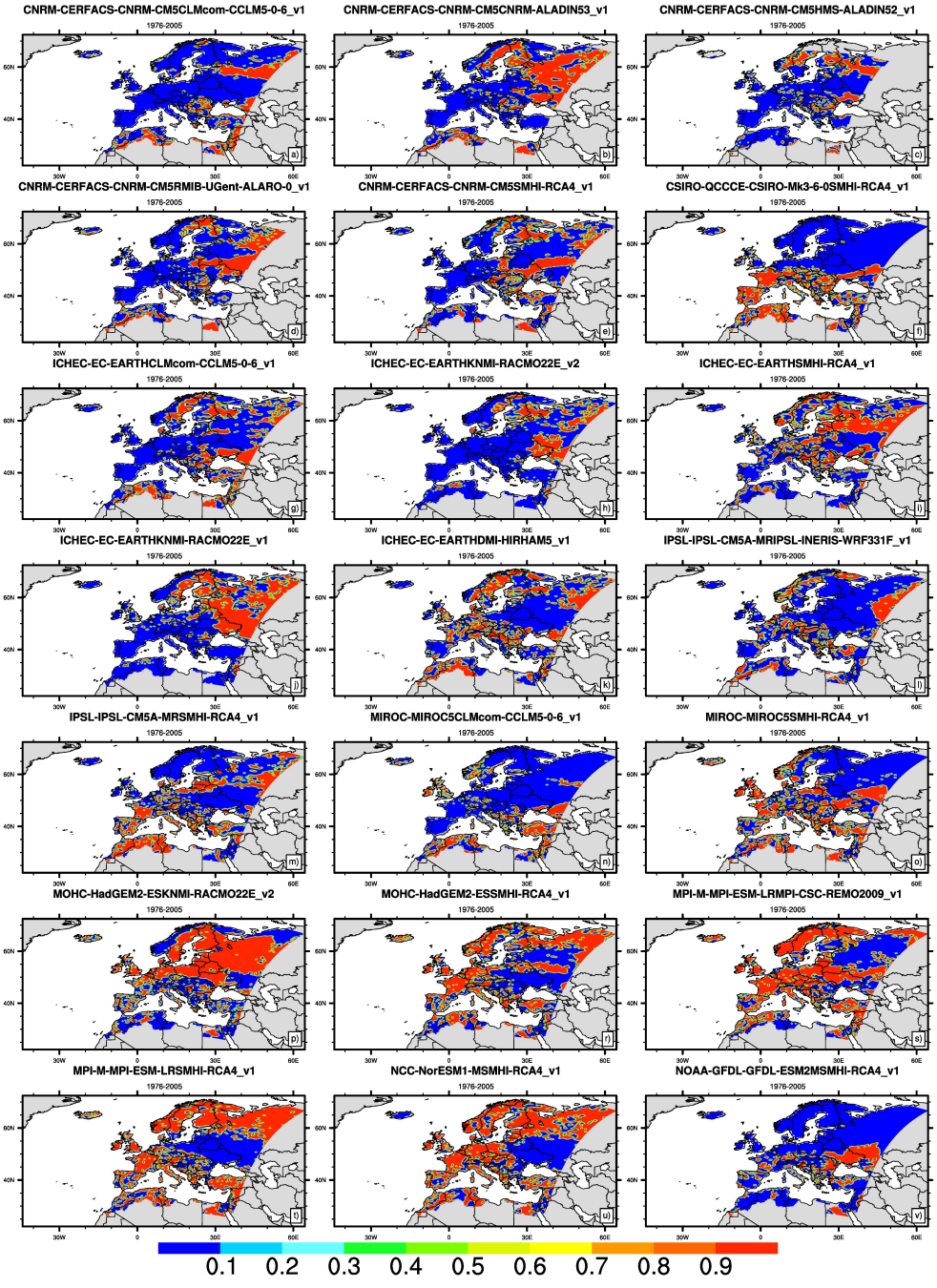

Figure 5.30. The "DSDAEE of the Unrepresentative Model Combinations in the Statistical Methodology 3 in the period between the years 1976 and 2005

Table 5.8. The coefficients of The Unrepresentative Models

GCM - RCM Model Combination	**Coefficient**
CNRM-CERFACS-CNRM-CM5-CLMcom-CCLM5-0-6-v1	0.24841
CNRM-CERFACS-CNRM-CM5-CNRM-ALADIN53-v1	0.36526
CNRM-CERFACS-CNRM-CM5-HMS-ALADIN52-v1	0.22134
CNRM-CERFACS-CNRM-CM5-RMIB-UGent-ALARO-0-v1	0.31810
CNRM-CERFACS-CNRM-CM5-SMHI-RCA4-v1	0.31454
CSIRO-QCCCE-CSIRO-Mk3-6-0-SMHI-RCA4-v1	0.35485
ICHEC-EC-EARTH-CLMcom-CCLM5-0-6-v1	0.31513
ICHEC-EC-EARTH-KNMI-RACMO22E-v2	0.19678
ICHEC-EC-EARTH-SMHI-RCA4-v1	0.37967
ICHEC-EC-EARTH-KNMI-RACMO22E-v1	0.32168
ICHEC-EC-EARTH-historical-r3i1p1-DMI-HIRHAM5-v1	0.38781
IPSL-IPSL-CM5A-MR-IPSL-INERIS-WRF331F-v1	0.25933
IPSL-IPSL-CM5A-MR-SMHI-RCA4-v1	0.37867
MIROC-MIROC5-CLMcom-CCLM5-0-6-v1	0.25318
MIROC-MIROC5-SMHI-RCA4-v1	0.42117
MOHC-HadGEM2-ES-KNMI-RACMO22E-v2	0.52621
MOHC-HadGEM2-ES-SMHI-RCA4-v1	0.48689
MPI-M-MPI-ESM-LR-MPI-CSC-REMO2009-v1	0.55361
MPI-M-MPI-ESM-LR-SMHI-RCA4-v1	0.53773
NCC-NorESM1-M-SMHI-RCA4-v1	0.55421
NOAA-GFDL-GFDL-ESM2M-SMHI-RCA4-v1	0.21902

The outcomes of this methodology are very different than the first two methodologies but are nearly tantamount to the previous ones (outcomes of Statistical Methodology III). CCCma-RCA4, MOHC-CLM1, MPI-CLM1, MPI-CLM2 and MPI-REMO2 are again the most representative model combinations for the temperature projection over Europe according to statistical methodology VI (T-Test is the indicator and applied to yearly averages). As shown in Table 5.9 and Table 5.10, WDSDAAE values of 66 % of the grid points in MOHC-CLM model combination, 68 % of the grid points in MPI-CLM1 model combination, 66 % of the grid points in MPI-CLM2 model combination, 61 % of the grid points in MPI-REMO2 model combination and in CCCma-RCA4 model combination are higher than WSDAAE. MPI-RCA4, NCC-RCA4 defined to be in unrepresentative model combinations, has the maximum percentage with 55 % which is at least 4 % smaller than the model combinations, defined to be in the most representative ones and they are second in order to simulate the temperature patterns of Europe (Figure 5.31 and Figure 5.32).

The performances of model combinations over sub-regions are very similar to the ones obtained by applying Statistical Methodology III.

Table 5.9. The coefficients of The Most Representative Models

GCM - RCM Model Combination	**Coefficient**
CCCma-CanESM2-SMHI-RCA4-v1	0.60683
MOHC-HadGEM2-ES-CLMcom-CCLM5-0-6-v1	0.66243
MPI-M-MPI-ESM-LR-MPI-CSC-REMO2009-v2	0.60862
MPI-M-MPI-ESM-LR-CLMcom-CCLM4-8-17-v1	0.68546
MPI-M-MPI-ESM-LR-CLMcom-CCLM5-0-6-v1	0.65945

5.1.5. Evaluation of Statistical Methodologies over Europe Temperature

In winter season, there is an observable difference between the proposed ensembles (PES) and EWA (equally weighted averages) almost all of the observed area. The interior lands of the North Africa and the Northern Black Sea coastal are the exceptions where EWA generates better results. The AAE of proposed ensembles including

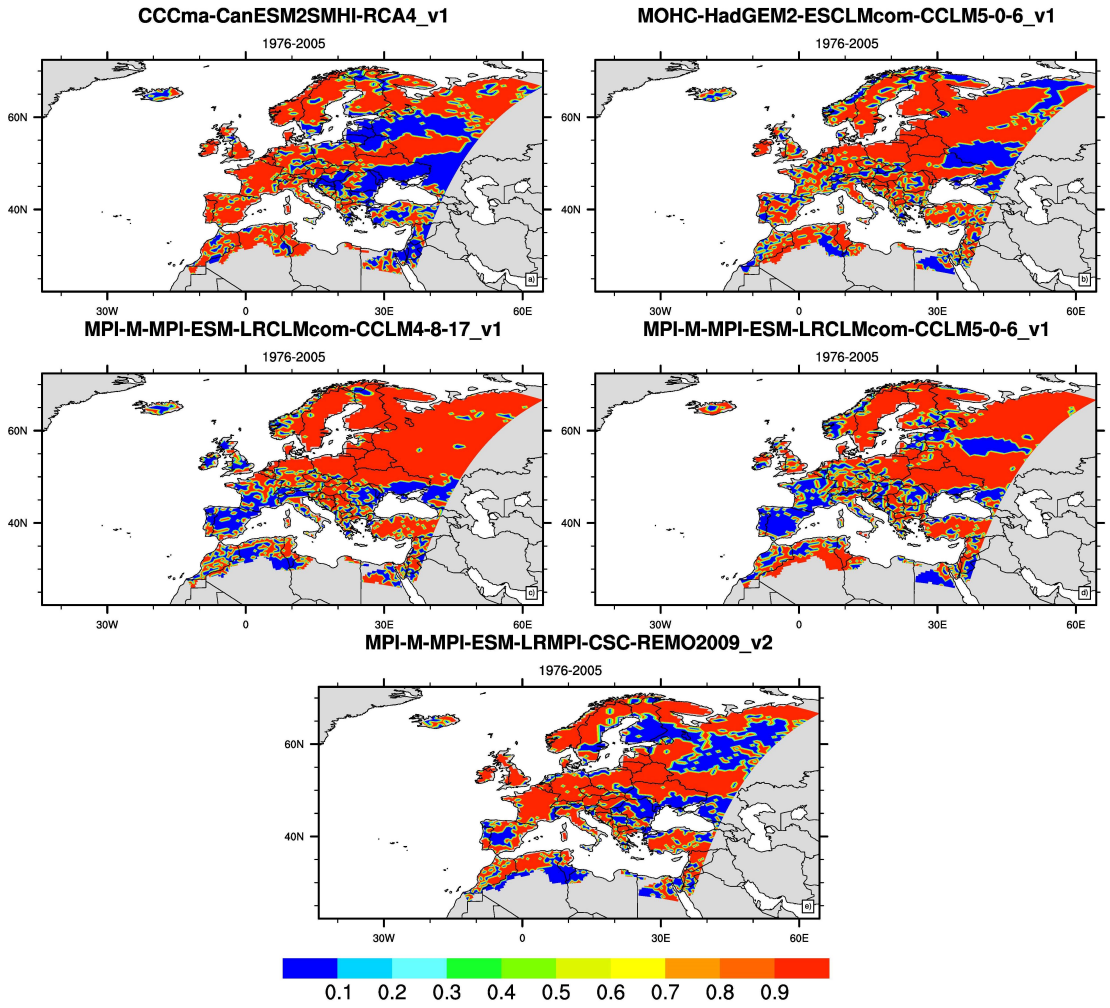

Figure 5.31. The "DSDAEE of the Representative Model Combinations in the Statistical Methodology 4 in the period between the years 1976 and 2005

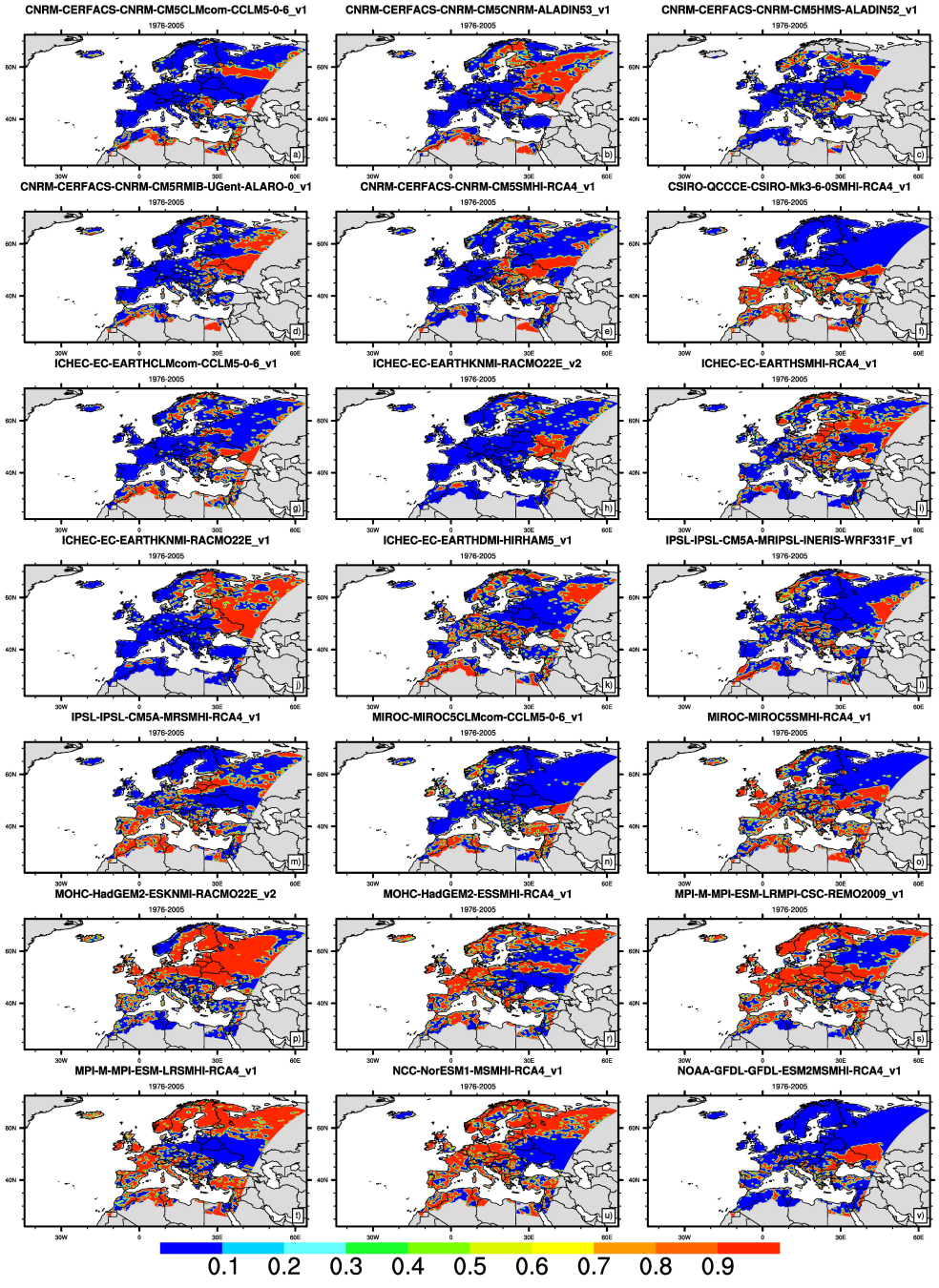

Figure 5.32. The "DSDAEE of the Unrepresentative Model Combinations in the Statistical Methodology 4 in the period between the years 1976 and 2005

Table 5.10. The coefficients of The Unrepresentative Models

GCM - RCM Model Combination	**Coefficient**
CNRM-CERFACS-CNRM-CM5-CLMcom-CCLM5-0-6-v1	0.25258
CNRM-CERFACS-CNRM-CM5-CNRM-ALADIN53-v1	0.36653
CNRM-CERFACS-CNRM-CM5-HMS-ALADIN52-v1	0.20059
CNRM-CERFACS-CNRM-CM5-RMIB-UGent-ALARO-0-v1	0.31510
CNRM-CERFACS-CNRM-CM5-SMHI-RCA4-v1	0.29051
CSIRO-QCCCE-CSIRO-Mk3-6-0-SMHI-RCA4-v1	0.37927
ICHEC-EC-EARTH-CLMcom-CCLM5-0-6-v1	0.28773
ICHEC-EC-EARTH-KNMI-RACMO22E-v2	0.15945
ICHEC-EC-EARTH-SMHI-RCA4-v1	0.35107
ICHEC-EC-EARTH-KNMI-RACMO22E-v1	0.31632
ICHEC-EC-EARTH-historical-r3i1p1-DMI-HIRHAM5-v1	0.38066
IPSL-IPSL-CM5A-MR-IPSL-INERIS-WRF331F-v1	0.25155
IPSL-IPSL-CM5A-MR-SMHI-RCA4-v1	0.38483
MIROC-MIROC5-CLMcom-CCLM5-0-6-v1	0.25318
MIROC-MIROC5-SMHI-RCA4-v1	0.44400
MOHC-HadGEM2-ES-KNMI-RACMO22E-v2	0.53912
MOHC-HadGEM2-ES-SMHI-RCA4-v1	0.49424
MPI-M-MPI-ESM-LR-MPI-CSC-REMO2009-v1	0.56434
MPI-M-MPI-ESM-LR-SMHI-RCA4-v1	0.55302
NCC-NorESM1-M-SMHI-RCA4-v1	0.55977
NOAA-GFDL-GFDL-ESM2M-SMHI-RCA4-v1	0.20532

representative model combinations is smaller than EWA in the remaining part of the observed area. Proposed ensembles estimate the temperature of the domain approximately 1°C better than EWA (Figure 5.33).

In spring season, EWA has smaller AAE values than PES only over Northern Black Sea coastal. In the north-eastern part of the observed domain, there isn't a significant difference between EWA and PES. PES estimates the temperature of the rest of the domain anew nearly 1°C better than EWA (Figure 5.34).

In summer season, EWA has smaller AAE values than the PES only over interior lands of Finland. In the central part of the observed domain, there isn't a significant difference between EWA and PES. PES estimates the temperature of the rest of the domain again almost 1°C better than EWA. Even, the difference between EWA and PES reaches up to 2°C over northern Spain and northern Italy (Figure 5.35).

In autumn season, EWA has smaller AAE values than the PES only over Northern Black Sea coastal. In the central part of the observed domain, there isn't a significant difference between EWA and PES. PES estimates better results over Italy, Turkey and United Kingdom (Figure 5.36).

Table 5.11. The Amount of Total and successful GCM – RCMs

GCM	**TOTAL**	**successful**	**RCM**	**TOTAL**	**successful**
CCCma	4	2 (50 %)	CLM	24	11 (45.8 %)
CNRM	20	0	REMO	8	6 (75 %)
CSIRO	4	0	RCA4	44	2 (4.6 %)
ICHEC	20	0	CNRM	4	0
IPSL	8	0	HMS	4	0
MOHC	12	3 (25 %)	RMIB	4	0
MIROC	8	0	DMI	4	0
MPI	20	14 (70 %)	KNMI	12	0
NCC	4	0	IPSL	4	0
NOAA	4	0			

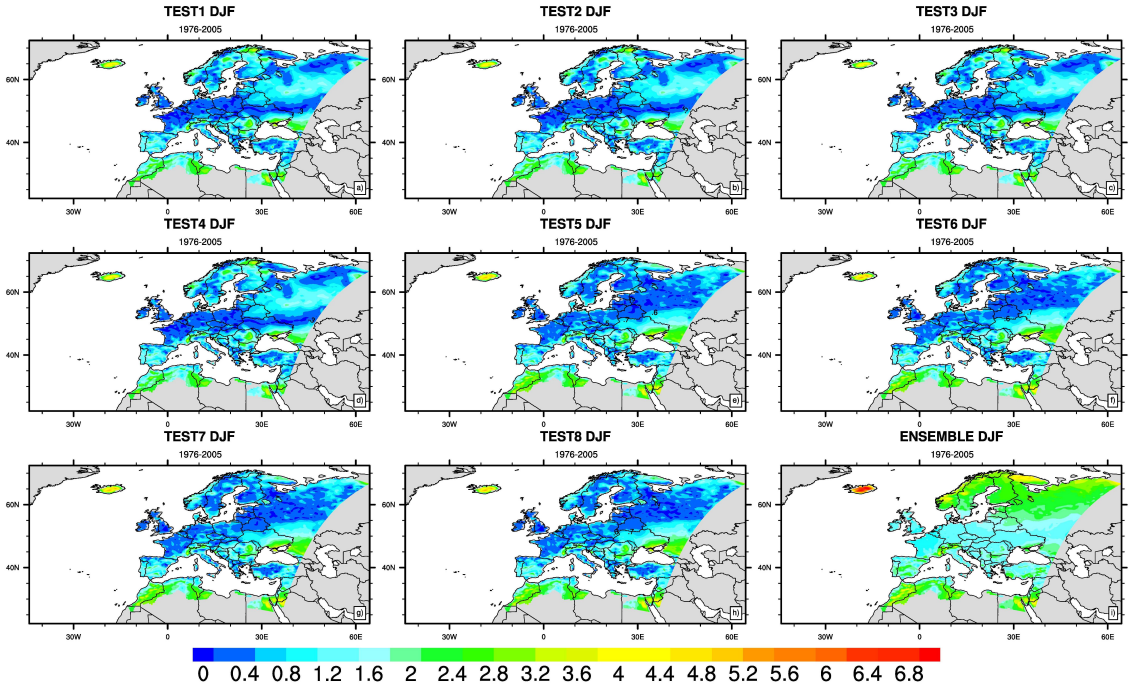

Figure 5.33. AAE of various Test Types and EWA (Equally Weighted Ensemble) over Europe in the period between the years 1976 and 2005 in winter season.

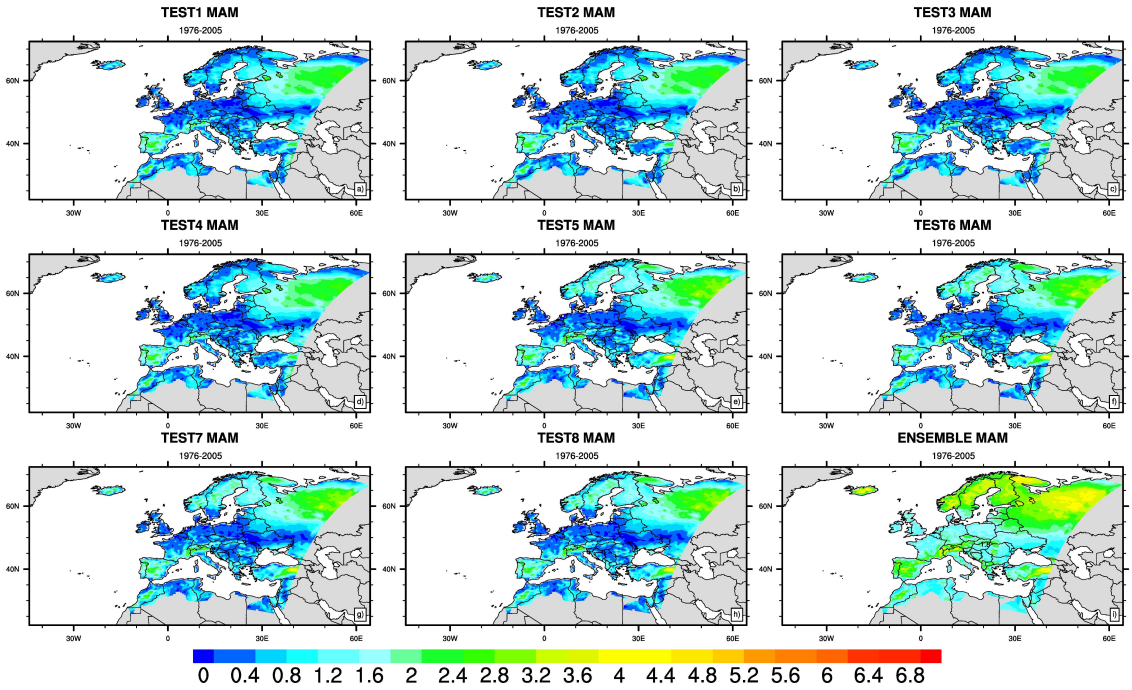

Figure 5.34. AAE of various Test Types and EWA (Equally Weighted Ensemble) over Europe in the period between the years 1976 and 2005 in spring season.

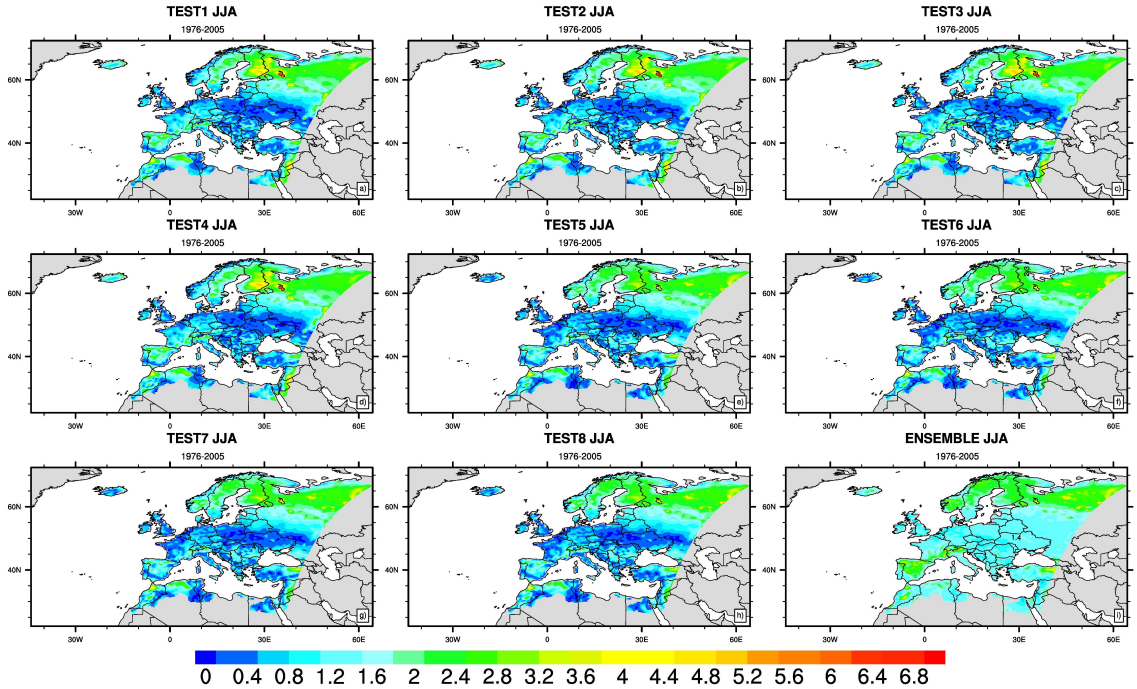

Figure 5.35. AAE of various Test Types and EWA (Equally Weighted Ensemble) over Europe in the period between the years 1976 and 2005 in summer season.

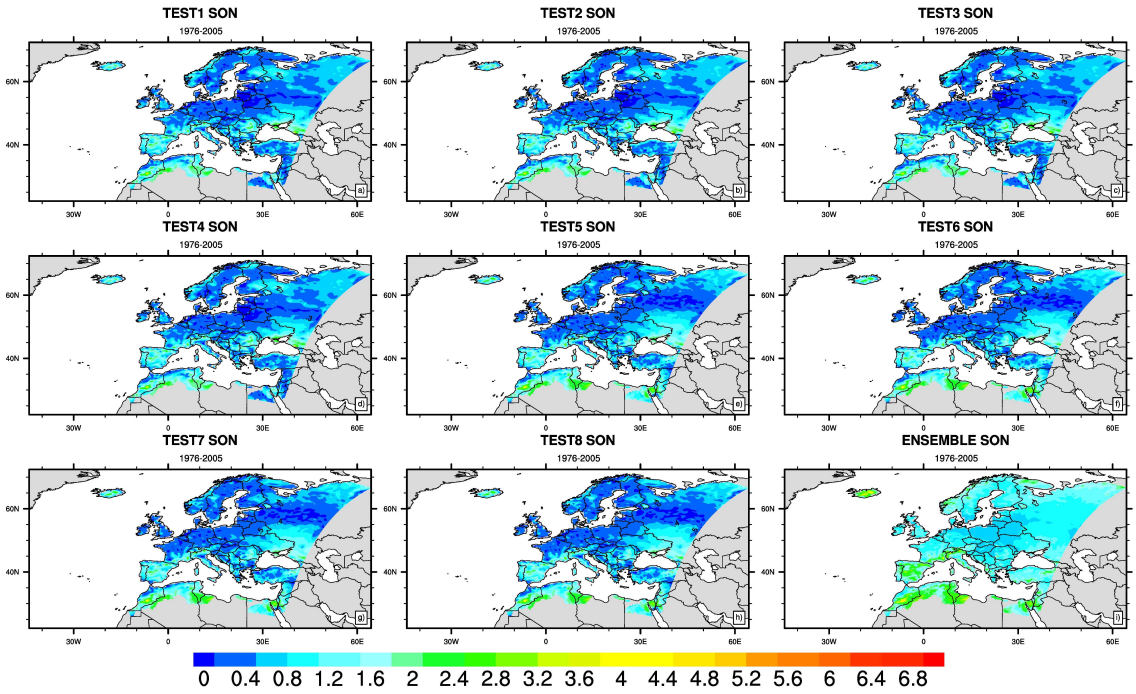

Figure 5.36. AAE of various Test Types and EWA (Equally Weighted Ensemble) over Europe in the period between the years 1976 and 2005 in autumn season.

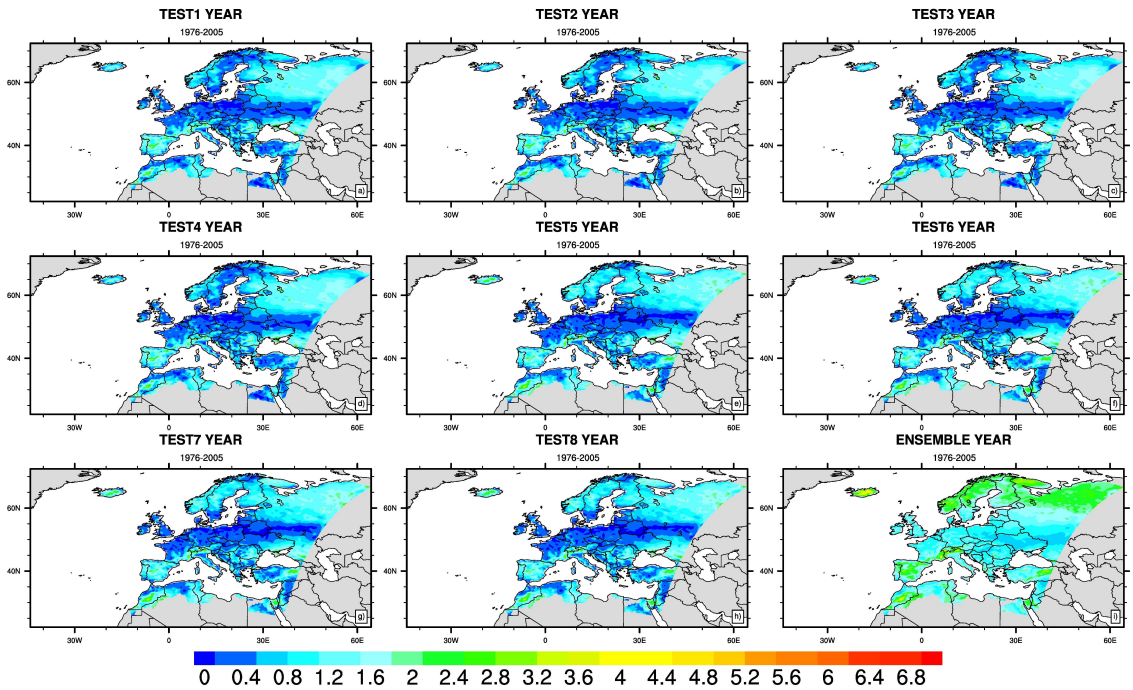

Figure 5.37. AAE of various Test Types and EWE (Equally Weighted Ensemble) over Europe in the period between the years 1976 and 2005 annually

ICHEC, MPI and CNRM are the most applied GCMs over Europe in the CORDEX Project and MPI is the most successful one when overall Europe is taken consideration. RCA4 is the most used RCM in the GCM-RCM model combinations in simulations over Europe and REMO is the most successful one with a very high percentage. Hence, simulating MPI as GCM and using it's outcomes as initial conditions- boundary conditions in the REMO is the most convenient choice in order to project overall European temperature (Table 5.11).

There isn't significant difference between suggested PES. The difference between absolute average errors is 0.13°C in winter, 0.23°C in spring, 0.3°C in summer and 0.17°C in autumn. On the other hand, the difference between the maximum one of the absolute average errors of PES is severely smaller than EWA. The difference is 0.9°C in winter, 0.3°C in spring, 0.8°C in summer and 0.5°C in autumn. It is difficult to estimate the most convenient methodology and test via these results. Hence, the following part of this section is carried out for two main reasons. One of them is to find the most appropriate methodology and test. The second one is to decide through which Representative Concentration Pathways, the temperature is changing. There are three main Representative Concentration Pathways, demonstrating the greenhouse gas emissions in the future of the World as they are described in the previous parts. These are RCP2.6, RCP4.5 and RCP8.5. In the following part, the temperatures over the observed region in the period between 2006 and 2017 are calculated with respect to PES subject to each of these Representative Concentration Pathways.

5.1.6. Application of Statistical Methodology 1 to the Monthly Temperature Data: The Case of Africa

As shown in Table 5.12 and 5.13, CCCma-UQAM, CSIRO-RCA4, MIROC-RCA4, MOHC-RCA4 and MPI-RCA4 combinations are the hotshot ones for Africa. 79 % of the grid points in CSIRO-RCA4 model combination, 78 % of the grid points in MPI-RCA4 model combination, 82 % of the grid points in MIROC-RCA4 model combination and 75 % of the grid points in CCCma-UQAM and MOHC-RCA4 model combination, are higher than WSDAAE. MPI- REMO and ICHEC-DMI defining in unrepresentative

model combinations, has the maximum percentage with 69 % which is at least 6 % smaller than the model combinations, defined in the most representative ones and they are second in order to simulate the temperature patterns of Africa.

CCCma-UQAM is well enough to figure out the temperature properties of the observed area. Temperature patterns are portrayed efficiently over Africa continental except Ethiopia, Somali, Djibouti, southern coastal of South Africa Republic, Madagascar, Northern Egypt and North-eastern Libya. Temperature patterns of Arabian Peninsula except Oman and Yemen is also well portrayed. Turkey and Gulf Sea coastal of Iran aren't projected truly. CSIRO-RCA4 generates the temperature accurately over Africa excluding Southern Namibia, South-western coastal of South Africa Republic, eastern Madagascar, Northern Egypt and Libya. It doesn't properly present the temperature of Oman and Iraq. MIROC-RCA4 doesn't procreate good results over Madagascar, South Africa Republic, southern Botswana, Namibia, Mozambique, Morocco, Northern Egypt, North-eastern Libya and Central Africa- Democratic Republic of Congo border. North-eastern Libya, Northern Egypt, Morocco, same parts of South Africa Republic, Namibia, Africa Horn, Mali-Niger border, Saudi Arabia and Iran are the regions over where MOHC-RCA4 produces unreliable temperature patterns. MPI-RCA4 is good at representing the temperature of Sub-Saharan Africa and Northern Africa with some minor exceptions. Madagascar, Mozambique, interior South Africa Republic and interior lands of Saudi Arabia are unrepresentative domains of this model combination. CCCma-RCA4 and NCC-RCA4 model combinations are clustered in the unrepresentative model set, however they also produce meaningful temperature results. MPI-UQAM model combination is good in simulating Northern Africa's temperature. On the other hand, taking ICHEC-CLM, ICHEC-KNMI, ICHEC-KNMI2 and ICHEC-RCA4 model combinations in consideration may lead to an inaccurate portrait of the temperature of Africa (Figure 5.38 and 5.39).

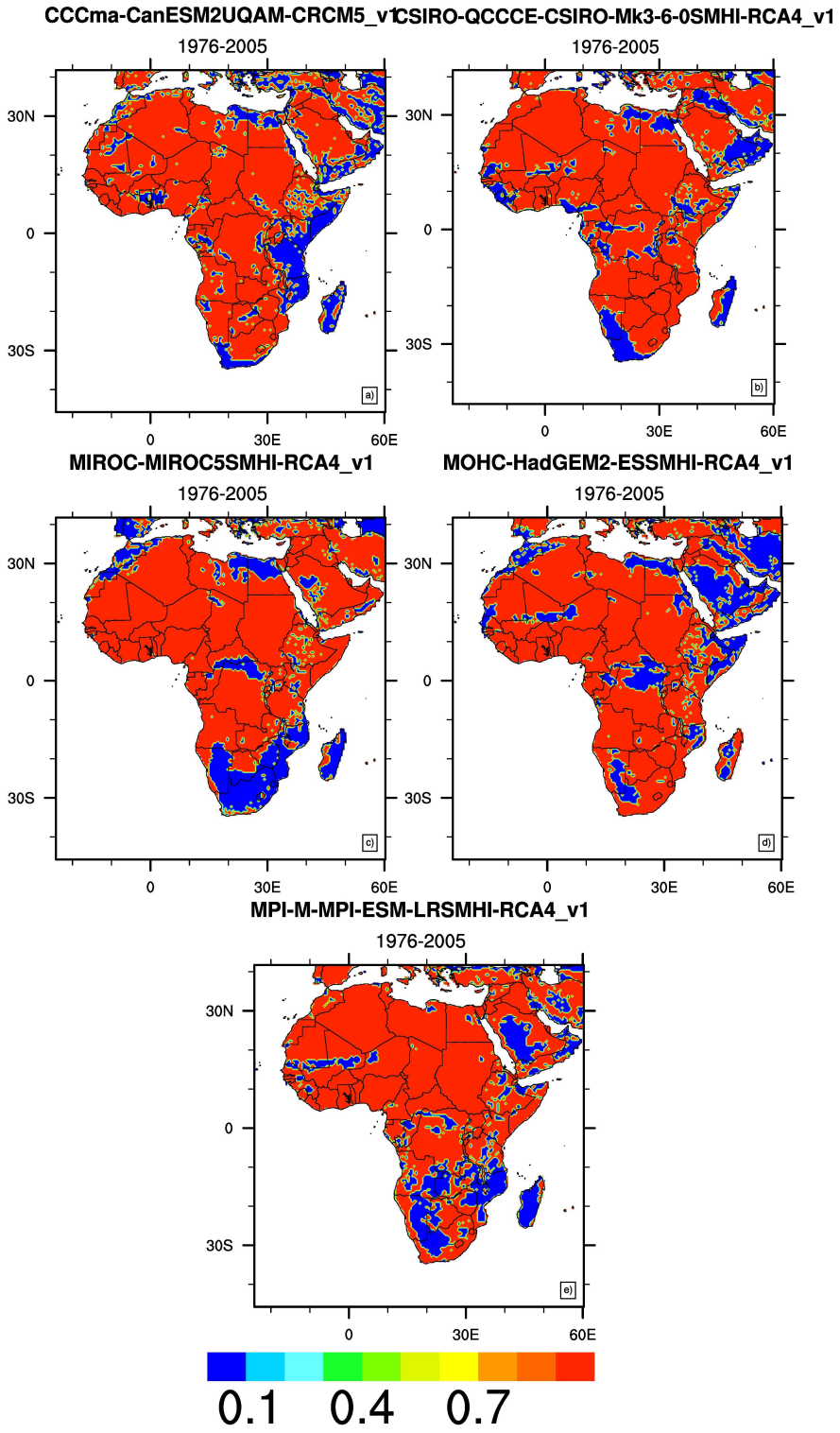

Figure 5.38. The "DSDAEE of the Most Representative Model Combinations in Statistical Methodology 1 in the period between the years 1976 and 2005

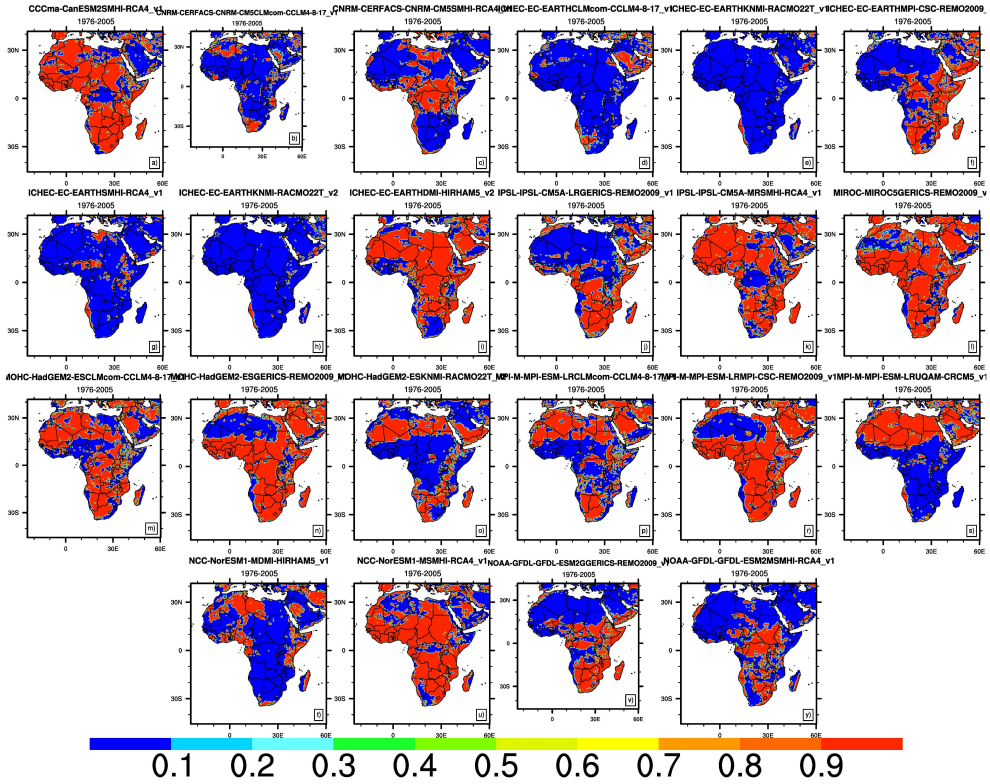

Figure 5.39. The "DSDAEE of the Unrepresentative Model Combinations in Statistical Methodology 1 in the period between the years 1976 and 2005

Table 5.12. The coefficients of The Most Representative Models

GCM - RCM Model Combination	**Coefficient**
CCCma-CanESM2-UQAM-CRCM5-v1	0.75351
CSIRO-QCCCE-CSIRO-Mk3-6-0-SMHI-RCA4-v1	0.79917
MIROC-MIROC5-SMHI-RCA4-v1	0.77725
MOHC-HadGEM2-ES-SMHI-RCA4-v1	0.75833
MPI-M-MPI-ESM-LR-SMHI-RCA4-v1	0.78171

Table 5.13. The coefficients of The Unrepresentative Models

GCM - RCM Model Combination	**Coefficient**
CCCma-CanESM2-SMHI-RCA4-v1	0.67636
CNRM-CERFACS-CNRM-CM5-CLMcom-CCLM4-8-17-v1	0.20580
CNRM-CERFACS-CNRM-CM5-SMHI-RCA4-v1	0.30903
ICHEC-EC-EARTH-CLMcom-CCLM4-8-17-v1	0.14757
ICHEC-EC-EARTH-KNMI-RACMO22T-v1	0.052966
ICHEC-EC-EARTH-MPI-CSC-REMO2009-v1	0.39100
ICHEC-EC-EARTH-SMHI-RCA4-v1	0.10031
ICHEC-EC-EARTH-KNMI-RACMO22T-v2	0.050847
ICHEC-EC-EARTH-DMI-HIRHAM5-v2	0.69616
IPSL-IPSL-CM5A-LR-GERICS-REMO2009-v1	0.41036
IPSL-IPSL-CM5A-MR-SMHI-RCA4-v1	0.69258
MIROC-MIROC5-GERICS-REMO2009-v1	0.72896
MOHC-HadGEM2-ES-CLMcom-CCLM4-8-17-v1	0.60732
MOHC-HadGEM2-ES-GERICS-REMO2009-v1	0.68016
MOHC-HadGEM2-ES-KNMI-RACMO22T-v2	0.40123
MPI-M-MPI-ESM-LR-CLMcom-CCLM4-8-17-v1	0.52309
MPI-M-MPI-ESM-LR-MPI-CSC-REMO2009-v1	0.69236
MPI-M-MPI-ESM-LR-UQAM-CRCM5-v1	0.43366
NCC-NorESM1-M-DMI-HIRHAM5-v1	0.27776
NCC-NorESM1-M-SMHI-RCA4-v1	0.67190
NOAA-GFDL-GFDL-ESM2G-GERICS-REMO2009-v1	0.39706
NOAA-GFDL-GFDL-ESM2M-SMHI-RCA4-v1	0.28054

5.1.7. Application of Statistical Methodology 2 to the Monthly Temperature Data: The Case of Africa

As shown in Table 5.14 and 5.15, Same model combinations in the previous sectionturned out to be the hotshot ones over Africa. 82 % of the grid points in CSIRO-RCA4 model combination, 81 % of the grid points in MPI-RCA4 model combination, 79 % of the grid points in MIROC-RCA4 model combination and 77 % of the grid points in CCCma-UQAM and 77 % of the grid points in MOHC-RCA4 model combination, are higher than WSDAAE. MIROC- REMO and ICHEC-DMI listing in unrepresentative model combinations, has the maximum percentage with 65 % which is at least 2 % smaller than the model combinations, defined in the most representative ones and they are second in order to simulate the temperature patterns of Africa.

Problematic regions with regards to typify the temperature patterns over the observed region are similar. CCCma-UQAM represents the temperature of the Africa and Arabian Peninsula very well, except Oman, Yemen, Morocco, Madagascar, Mozambique Ethiopia, Somali, Djibouti, southern coastal of South Africa, Northern Egypt and North-eastern Libya. CSIRO-RCA4 also bodies forth temperature of overall Africa very well. Exceptions are eastern Madagascar, southern South Africa Republic, Northern Egypt and North-eastern Libya in Africa continental and Oman in Arabia Peninsula. Namibia, South Africa Republic, Central Africa- Democratic Congo Republic border, Madagascar, Morocco, Northern Egypt and North-eastern Libya are the regions where MIROC-RCA4 doesn't produce trustful results. Africa Horn, Central Africa- Democratic Congo Republic border, Morocco, Northern Egypt and North-eastern Libya are the ones where MOHC-RCA4 doesn't achieve to represent the temperature very well. MPI-RCA4 can't exemplify temperature patterns over Madagascar, minor parts of Mozambique and Tanzania and Namibia- South Africa Republic border. ICHEC-CLM, ICHEC-KNMI, ICHEC-KNMI2 and ICHEC-RCA4 model combinations are again in the cluster of unrepresentative set and almost nowhere they manage to determine the temperaure profile. CCCma-RCA4 and NCC-RCA4 model combinations are clustered in the unrepresentative model set, however they also produce meaningful temperature results. MPI-UQAM model combination is good in simulating Northern Africa's tem-

perature. On the other hand, taking ICHEC-CLM, ICHEC-KNMI, ICHEC-KNMI2 and ICHEC-RCA4 model combinations in calculations to portray African temperature can lead to produce inaccurate results. Again, CCCma-RCA4 and NCC-RCA4 model combinations, classifyied in the unsuccessful model set, are the most accurate model combinations after the successful ones (Figure 5.40 and 5.41).

Table 5.14. The coefficients of The Most Representative Models

GCM - RCM Model Combination	**Coefficient**
CCCma-CanESM2-UQAM-CRCM5-v1	0.77688
CSIRO-QCCCE-CSIRO-Mk3-6-0-SMHI-RCA4-v1	0.82065
MIROC-MIROC5-SMHI-RCA4-v1	0.79661
MOHC-HadGEM2-ES-SMHI-RCA4-v1	0.78821
MPI-M-MPI-ESM-LR-SMHI-RCA4-v1	0.81933

5.1.8. Application of Statistical Methodology 3 to the Monthly Temperature Data: The Case of Africa

The achievement of model combinations to perform temperature of Africa alters region by region with respect to Statistical Methodology III. T-test is an important indicator to formulate distinguishes the regions over which model combinations are succeeded.

As shown in Table 5.16 and 5.17, only two of the model combinations in the previous section are gathered in the set of successful models subject to this methodology. These are CSIRO-RCA4 and MIROC-RCA4. None of the model combinations are prospering to describe the temperature patterns of Africa with a percentage higher than 50 %. In other words, at least half of the grid points in each model can't pass T-test. Hence, it is difficult to assert a model combination, riding high for representation of Africa Continental's temperature. 42 % of the grid points in CSIRO-RCA4, MIROC-RCA4 AND MOHC-CLM model combination, 41 % of the grid points in MIROC-REMO and CCCma-RCA4 model combination and 40 % of the grid points in IPSL-RCA4 model combination, are higher than WSDAAE. MOHC- REMO, clus-

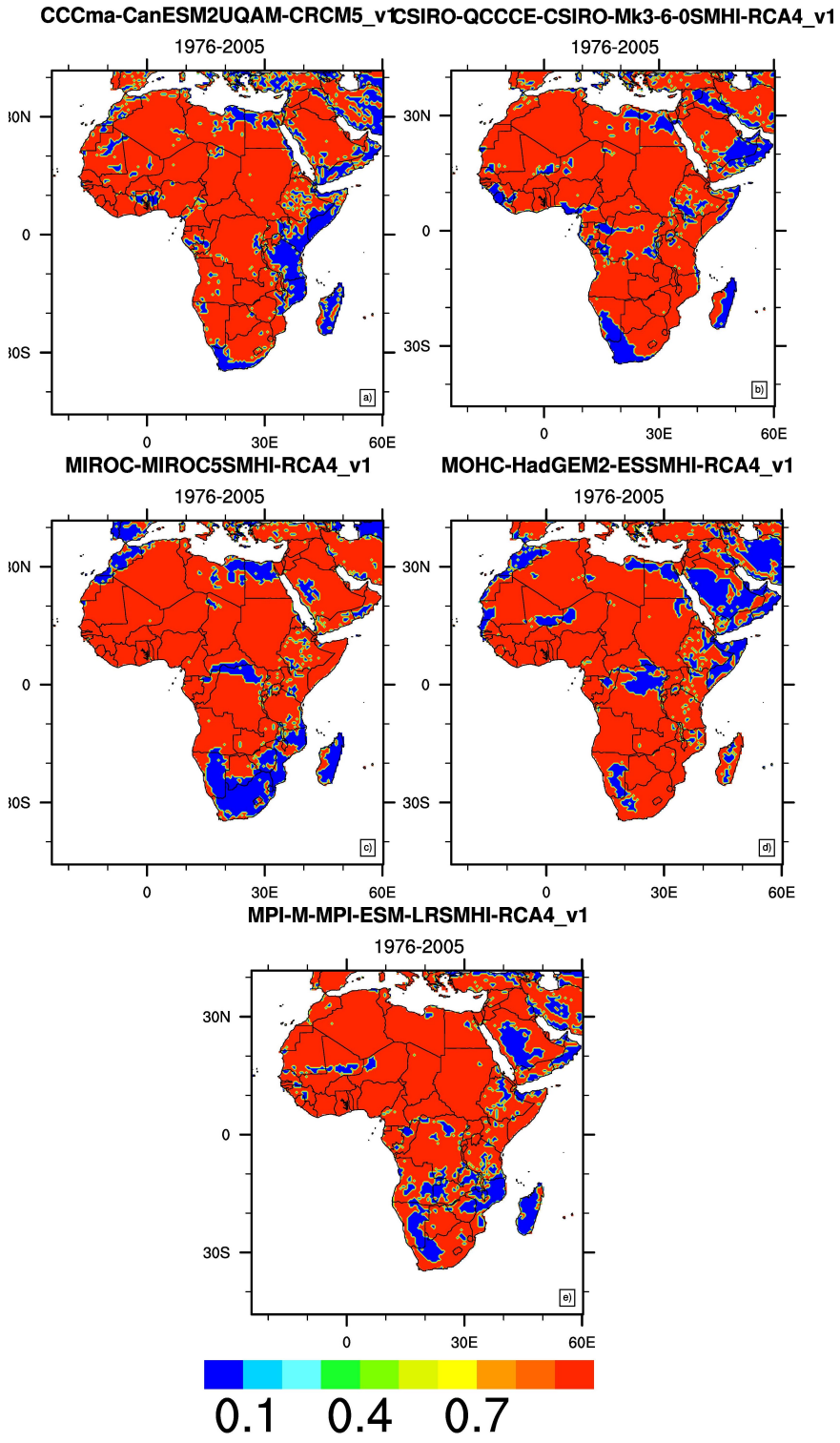

Figure 5.40. The "DSDAEE of the Most Representative Model Combinations in Statistical Methodology 2 in the period between the years 1976 and 2005

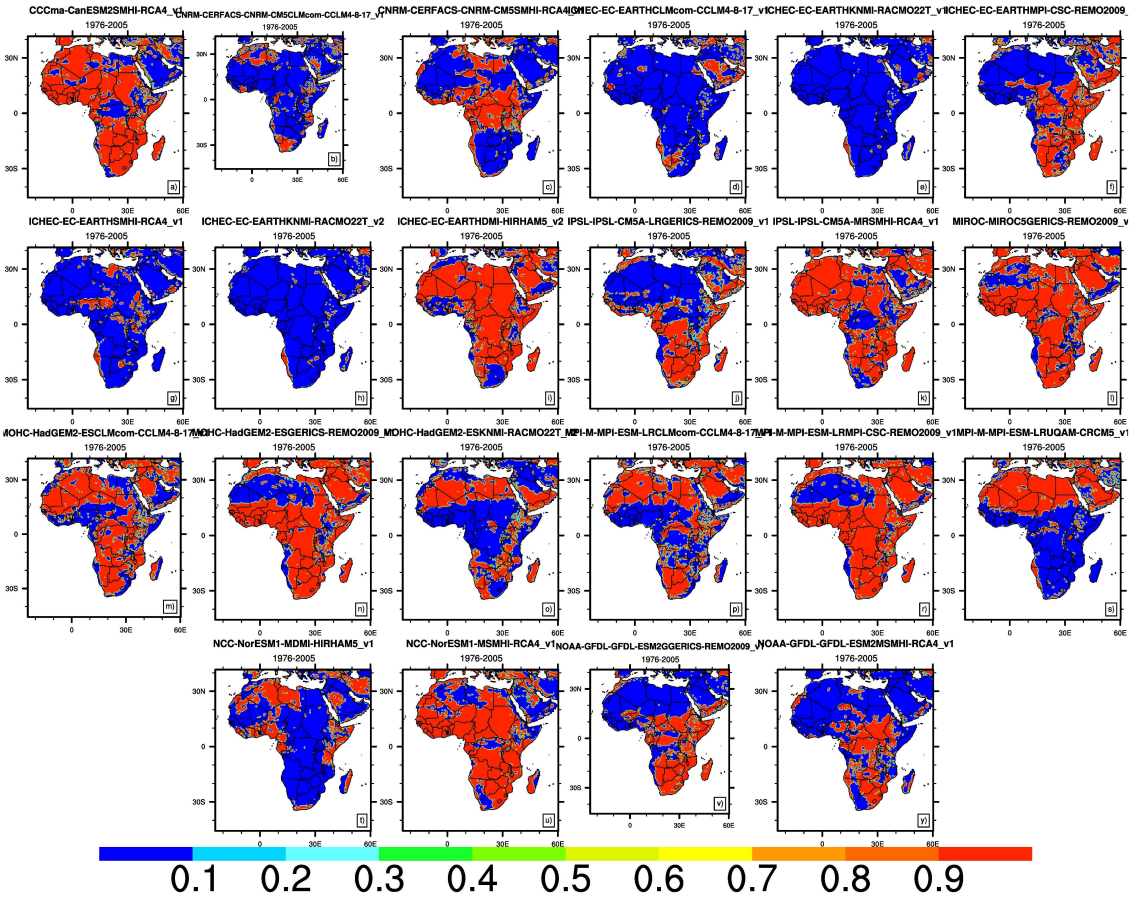

Figure 5.41. The "DSDAEE of the Unrepresentative Model Combinations in Statistical Methodology 2 in the period between the years 1976 and 2005

Table 5.15. The coefficients of The Unrepresentative Models

GCM - RCM Model Combination	**Coefficient**
CCCma-CanESM2-SMHI-RCA4-v1	0.70032
CNRM-CERFACS-CNRM-CM5-CLMcom-CCLM4-8-17-v1	0.21011
CNRM-CERFACS-CNRM-CM5-SMHI-RCA4-v1	0.35864
ICHEC-EC-EARTH-CLMcom-CCLM4-8-17-v1	0.14794
ICHEC-EC-EARTH-KNMI-RACMO22T-v1	0.054646
ICHEC-EC-EARTH-MPI-CSC-REMO2009-v1	0.43922
ICHEC-EC-EARTH-SMHI-RCA4-v1	0.12734
ICHEC-EC-EARTH-KNMI-RACMO22T-v2	0.054135
ICHEC-EC-EARTH-DMI-HIRHAM5-v2	0.74372
IPSL-IPSL-CM5A-LR-GERICS-REMO2009-v1	0.42212
IPSL-IPSL-CM5A-MR-SMHI-RCA4-v1	0.71333
MIROC-MIROC5-GERICS-REMO2009-v1	0.75431
MOHC-HadGEM2-ES-CLMcom-CCLM4-8-17-v1	0.62412
MOHC-HadGEM2-ES-GERICS-REMO2009-v1	0.70251
MOHC-HadGEM2-ES-KNMI-RACMO22T-v2	0.41876
MPI-M-MPI-ESM-LR-CLMcom-CCLM4-8-17-v1	0.54654
MPI-M-MPI-ESM-LR-MPI-CSC-REMO2009-v1	0.71895
MPI-M-MPI-ESM-LR-UQAM-CRCM5-v1	0.45142
NCC-NorESM1-M-DMI-HIRHAM5-v1	0.28149
NCC-NorESM1-M-SMHI-RCA4-v1	0.69309
NOAA-GFDL-GFDL-ESM2G-GERICS-REMO2009-v1	0.41065
NOAA-GFDL-GFDL-ESM2M-SMHI-RCA4-v1	0.30823

terining in unrepresentative model combinations, has the maximum percentage with 40 % which is nearly the same with the model combinations, defined to be in the most representative ones and they are the second in order to simulate the temperature patterns of Africa.

In contrast to the previous methodologies, the problematic and triumphant regionsin terms of the representation of their temperature profiles vary model to model. For example, Mediterranean coastal of Africa is well simulated by IPSL-RCA4 and MOHC-CLM. Hence these two model combinations can be used for further studies focusing on North Africa. Temperature over Egypt and Libya is also exhibited accomplishedly by MIROC-RCA4 model combination. MOHC-CLM brings temperature simulation of North-Western Africa to a successful conclusion. CCCma-RCA4 and CSIRO-RCA4 are the most representative model combinations over South Africa, except coastal domains. The temperature profice of Central Africa is successfully portrayed by MIROC-REMO and MIROC-RCA4. These two model combinations are also the best ones to project the temperature of Sub-Saharan Africa. ICHEC-KNMI1 and ICHEC-KNMI2 are the worst ones to estimate the temperature of the Africa because almost all of their grid points can't pass T-test or be better than the majority of model combinations (Figure 5.42 and 5.43)

Table 5.16. The coefficients of The Most Representative Models

GCM - RCM Model Combination	**Coefficient**
CCCma-CanESM2-SMHI-RCA4-v1	0.41935
CSIRO-QCCCE-CSIRO-Mk3-6-0-SMHI-RCA4-v1	0.42271
IPSL-IPSL-CM5A-LR- SMHI-RCA4-v1	0.40861
MIROC-MIROC5-GERICS-REMO2009-v1	0.41438
MIROC-MIROC5-SMHI-RCA4-v1	0.42504
MOHC-HadGEM2-ES-CLMcom-CCLM4-8-17-v1	0.42110

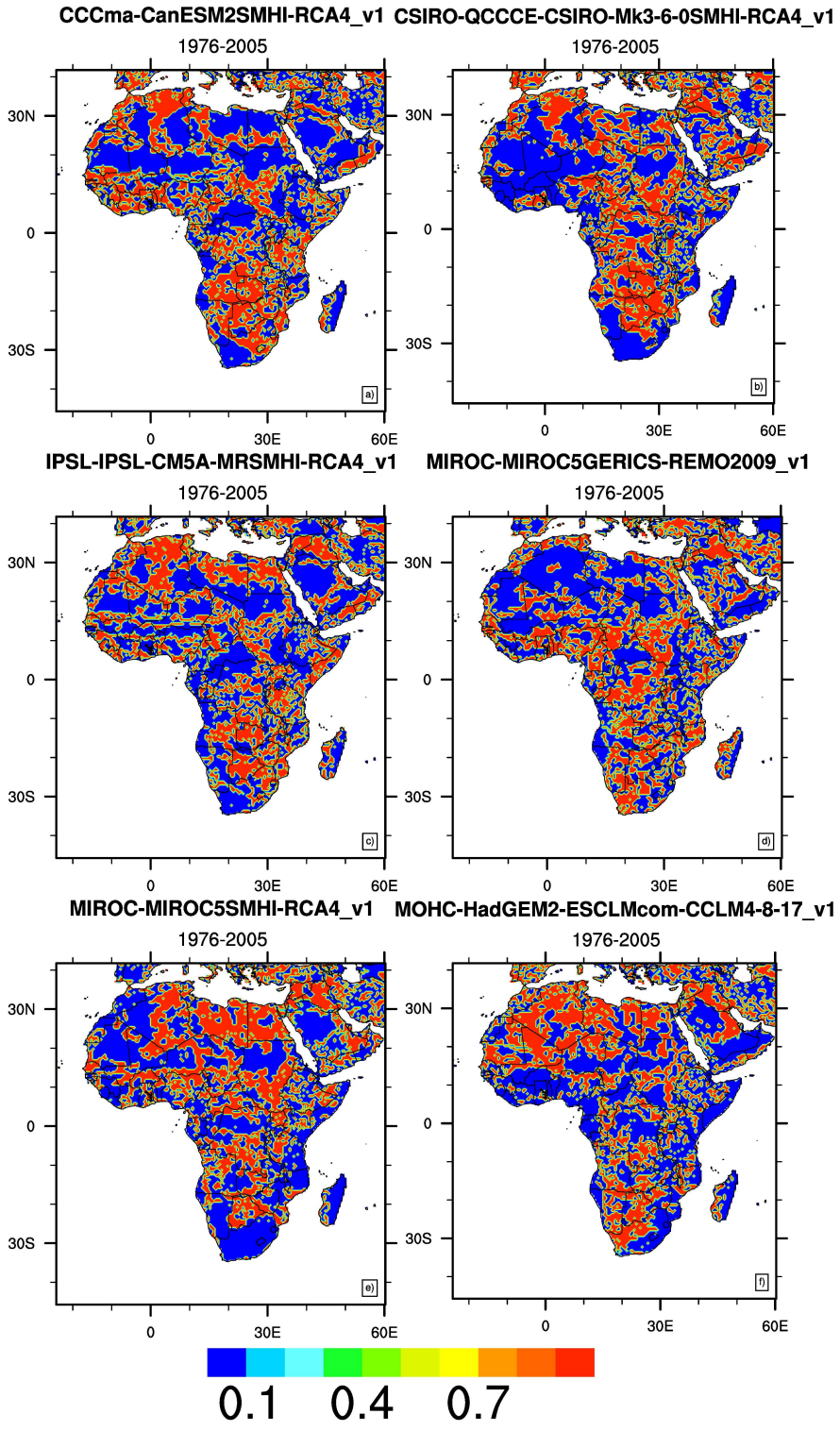

Figure 5.42. The "DSDAEE of the Most Representative Model Combinations in Statistical Methodology 3 in the period between the years 1976 and 2005

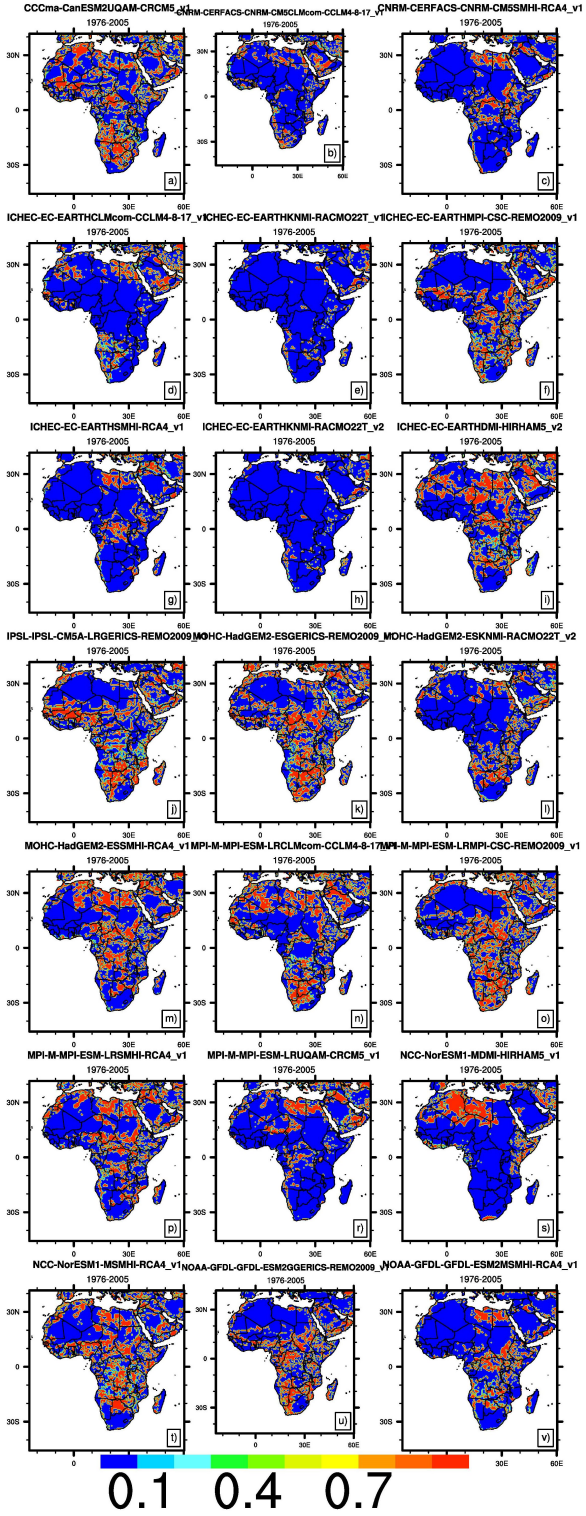

Figure 5.43. The "DSDAEE of the Unrepresentative Model Combinations in Statistical Methodology 3 in the period between the years 1976 and 2005

Table 5.17. The coefficients of The Unrepresentative Models

GCM - RCM Model Combination	**Coefficient**
CCCma-CanESM2-UQAM-CRCM5-v1	0.38413
CNRM-CERFACS-CNRM-CM5-CLMcom-CCLM4-8-17-v1	0.18242
CNRM-CERFACS-CNRM-CM5-SMHI-RCA4-v1	0.16898
ICHEC-EC-EARTH-CLMcom-CCLM4-8-17-v1	0.17548
ICHEC-EC-EARTH-KNMI-RACMO22T-v1	0.072034
ICHEC-EC-EARTH-MPI-CSC-REMO2009-v1	0.25066
ICHEC-EC-EARTH-SMHI-RCA4-v1	0.14779
ICHEC-EC-EARTH-KNMI-RACMO22T-v2	0.065240
ICHEC-EC-EARTH-DMI-HIRHAM5-v2	0.32415
IPSL-IPSL-CM5A-MR- GERICS-REMO2009-v1	0.33270
MOHC-HadGEM2-ES-GERICS-REMO2009-v1	0.40335
MOHC-HadGEM2-ES-KNMI-RACMO22T-v2	0.21384
MOHC-HadGEM2-ES-SMHI-RCA4-v1	0.34899
MPI-M-MPI-ESM-LR-CLMcom-CCLM4-8-17-v1	0.33657
MPI-M-MPI-ESM-LR-MPI-CSC-REMO2009-v1	0.37821
MPI-M-MPI-ESM-LR-SMHI-RCA4-v1	0.31750
MPI-M-MPI-ESM-LR-UQAM-CRCM5-v1	0.18929
NCC-NorESM1-M-DMI-HIRHAM5-v1	0.20164
NCC-NorESM1-M-SMHI-RCA4-v1	0.36967
NOAA-GFDL-GFDL-ESM2G-GERICS-REMO2009-v1	0.29098
NOAA-GFDL-GFDL-ESM2M-SMHI-RCA4-v1	0.19747

5.1.9. Application of Statistical Methodology 4 to the Monthly Temperature Data: The Case of Africa

Five of the model combinations in the previous section are also found as representative ones in this section (Table 5.18 and 5.19). These are CCCma-RCA4, CSIRO-RCA4, MIROC-REMO, MIROC-RCA4 and MOHC-CLM. The unique exemption is IPSL-RCA4. It is excluded from the representative set, however it is the first order in the rank for simulating the temperature over Africa among the unrepresentative model combination set. MOHC-CLM is the new model combination found itself among the representative one. It is the best one among the unrepresentative ones given in the previous section.

43 % of the grid points in CSIRO-RCA4 and CCCma-RCA4, 44 % of the grid points in MIROC-REMO and MOHC-CLM model combination, 41 % of the grid points in MIROC-RCA4 and 42 % of the grid points in MOHC-CLM model combination, are higher than WSDAAE. IPSL-RCA4 clustering in the unrepresentative model combinations, has the maximum percentage with 41 % which is nearly same with the model combinations, defined in the most representative ones and it is second in order to simulate the temperature patterns of Africa.

Similar to the previous section, the problematic and triumphant regions in which temperature designs are not shown or well-performed vary model to model. On the other hand, the successes of the model combinations over various regions are also similar to previous ones. For example, Mediterranean coastal of Africa is well simulated by MOHC-CLM. Hence these two model combinations can be used for further studies focusing on North Africa. Temperature over Egypt and Libya is also shown accomplishedly by MIROC-RCA4 model combination. MOHC-CLM brings temperature simulation of North-Western Africa to a successful conclusion. CCCma-RCA4 and CSIRO-RCA4 are the most representative model combinations over South Africa, except coastal domains. Temperature of Central Africa is successfully portrayed by MIROC-REMO and MIROC-RCA4. These two model combinations are the best ones to project the temperature of Sub-Saharan Africa. ICHEC-KNMI1 and ICHEC-

KNMI2 are again the worst ones to estimate the temperature of the Africa because almost all of their grid points can't pass T-test, applying the annual averages, or be better than majority of model combinations (Figure 5.44 and 5.45).

Table 5.18. The coefficients of The Most Representative Models

GCM - RCM Model Combination	**Coefficient**
CCCma-CanESM2-SMHI-RCA4-v1	0.43301
CSIRO-QCCCE-CSIRO-Mk3-6-0-SMHI-RCA4-v1	0.43958
MIROC-MIROC5-GERICS-REMO2009-v1	0.44272
MIROC-MIROC5-SMHI-RCA4-v1	0.45339
MOHC-HadGEM2-ES-CLMcom-CCLM4-8-17-v1	0.44397
MOHC-HadGEM2-ES-GERICS-REMO2009-v1	0.42811

5.1.10. Evaluation Of Statistical Methodologies Over Africa Temperature

ICHEC, MPI and MOHC are the most applied GCMs over Africa in CORDEX Project but CSIRO is the most successful one when overall Africa is considered. RCA4 is the most used RCM in the GCM-RCM model combinations in simulations over Africa and it is the most successful one with a very high percentage. Hence, simulating CSIRO as GCM and using its outcomes as initial conditions- boundary conditions in the RCA4 is the most convenient choice to project overall African temperature (Table 5.20).

5.1.11. Application of Statistical Methodology 1 to the Monthly Temperature Data: The Case of Central America

As shown in Table 5.21 and 5.22, MOHC-RegCM1 and MPI-RCA4 combinations are the successful ones over Central America. 70 % of the grid points in MPI-RCA4 model combination and 66 % of the grid points in MOHC-RegCM1 model combination are higher than WSDAAE. NCC-RCA4, defining in unrepresentative model combinations, has the maximum percentage with 62 % which is at least 4 % smaller than the model combinations, defined in the most representative ones and it is second in order

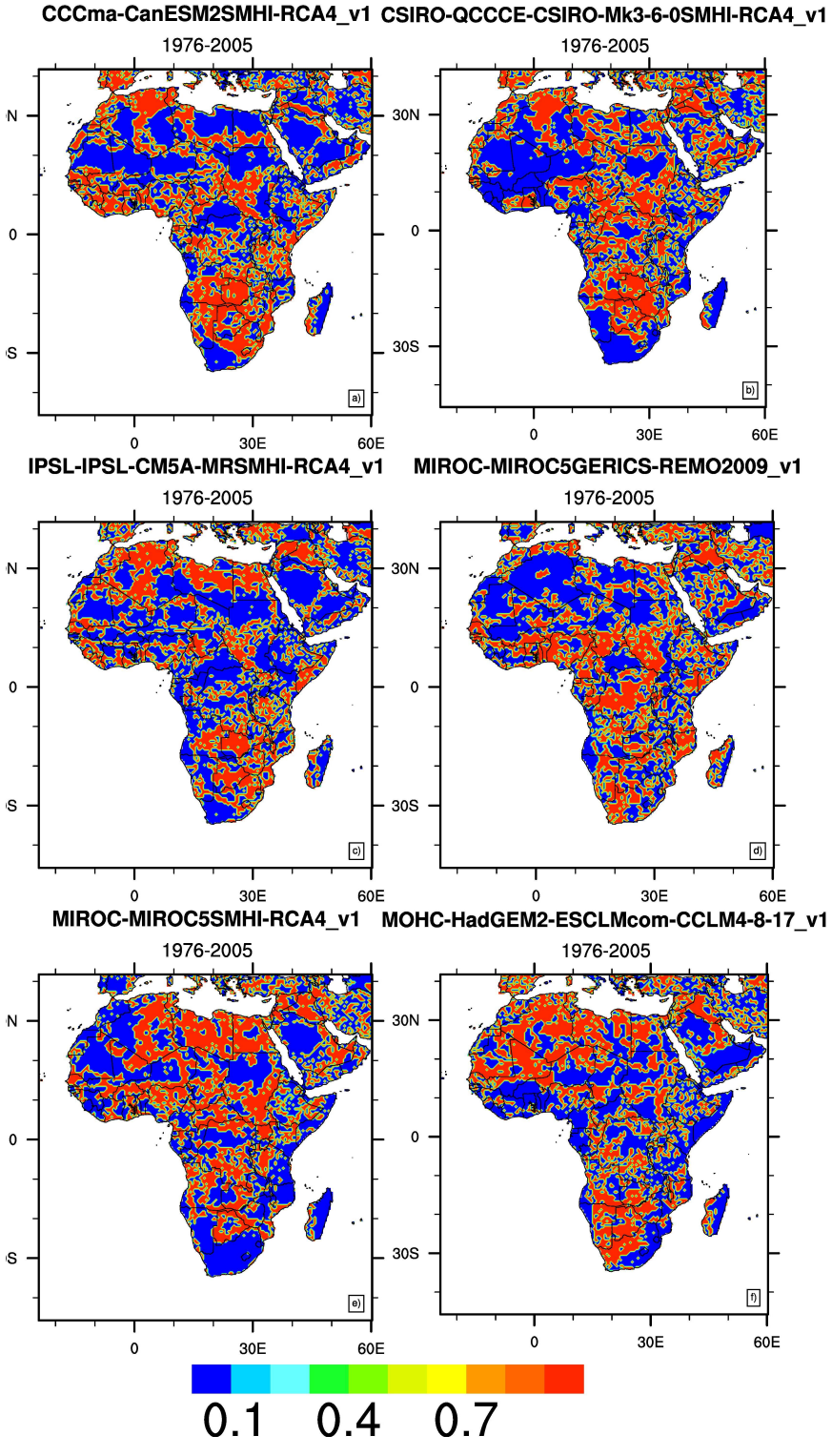

Figure 5.44. The "DSDAEE of the Most Representative Model Combinations in Statistical Methodology 4 in the period between the years 1976 and 2005

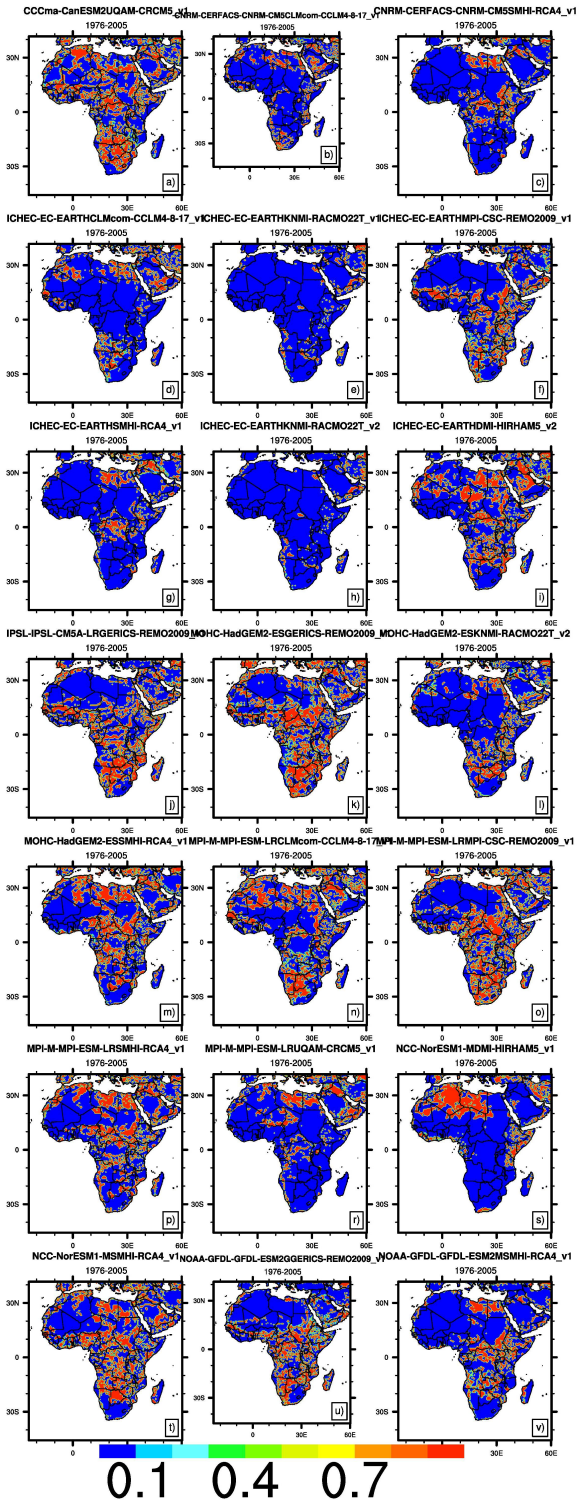

Figure 5.45. The "DSDAEE of the Unrepresentative Model Combinations in Statistical Methodology 4 in the period between the years 1976 and 2005

Table 5.19. The coefficients of The Unrepresentative Models

GCM - RCM Model Combination	**Coefficient**
CCCma-CanESM2-UQAM-CRCM5-v1	0.38947
CNRM-CERFACS-CNRM-CM5-CLMcom-CCLM4-8-17-v1	0.18513
CNRM-CERFACS-CNRM-CM5-SMHI-RCA4-v1	0.16898
ICHEC-EC-EARTH-CLMcom-CCLM4-8-17-v1	0.18447
ICHEC-EC-EARTH-KNMI-RACMO22T-v1	0.074445
ICHEC-EC-EARTH-MPI-CSC-REMO2009-v1	0.25453
ICHEC-EC-EARTH-SMHI-RCA4-v1	0.14684
ICHEC-EC-EARTH-KNMI-RACMO22T-v2	0.065532
ICHEC-EC-EARTH-DMI-HIRHAM5-v2	0.33818
IPSL-IPSL-CM5A-LR-GERICS-REMO2009-v1	0.31560
IPSL-IPSL-CM5A-MR-SMHI-RCA4-v1	0.41379
MOHC-HadGEM2-ES-KNMI-RACMO22T-v2	0.22903
MOHC-HadGEM2-ES-SMHI-RCA4-v1	0.35922
MPI-M-MPI-ESM-LR-CLMcom-CCLM4-8-17-v1	0.34454
MPI-M-MPI-ESM-LR-MPI-CSC-REMO2009-v1	0.39348
MPI-M-MPI-ESM-LR-SMHI-RCA4-v1	0.32554
MPI-M-MPI-ESM-LR-UQAM-CRCM5-v1	0.18951
NCC-NorESM1-M-DMI-HIRHAM5-v1	0.21676
NCC-NorESM1-M-SMHI-RCA4-v1	0.38128
NOAA-GFDL-GFDL-ESM2G-GERICS-REMO2009-v1	0.30435
NOAA-GFDL-GFDL-ESM2M-SMHI-RCA4-v1	0.21062

Table 5.20. The Amount of Total and successful GCM – RCMs

GCM	**TOTAL**	**successful**	**RCM**	**TOTAL**	**successful**
CCCma	8	4 (50 %)	CLM	16	2 (12.5 %)
CNRM	8	0	REMO	24	3 (12.5 %)
CSIRO	4	4 (100 %)	RCA4	40	15 (37.5 %)
ICHEC	24	0	DMI	8	0
IPSL	8	1 (12.5 %)	KNMI	12	0
MOHC	16	5 (37.5 %)	UQAM	8	2 (25 %)
MIROC	8	6 (75 %)			
MPI	16	2 (12.5 %)			
NCC	8	0			
NOAA	8	0			

to simulate the temperature patterns of Central America.

MOHC-RegCM1 is well enough to figure out the temperature properties of the observed area. Temperature patterns are portrayed efficiently over Central America except Pacific coastal of Mexico, Colombia, Ecuador and Peru, Southern Bolivia, Brazil-Guyana-Suriname borders, minor part of central Venezuela and central part of interior lands of United States of America (Oklahoma, Kansas, Missouri and Arkansas). MPI-RCA4 simulates the majority of the observed area very wel, excluding Guatemala, minor Pacific coastal of Mexico, Colombia, Ecuador and Peru, Southern Bolivia, Brazil-Guyana-Suriname borders, minor part of central Venezuela , Nevada, Oregon, Atlantic coastal of eastern Brazil. NCC-RCA4, collecting in the unrepresentative model set, is also good at representing the temperature of the domain except Mexico, Gulf of Mexico coastal and Atlantic coastal of Brazil, Suriname, Guyana. CNRM-RCA4 and CSIRO-RCA4 don't simulate the temperature of the observed very well. They are successful over limited minor areas of the Central America and it isn't useful to apply these model combinations to project the temperature of Central America (Figure 5.46 and 5.47).

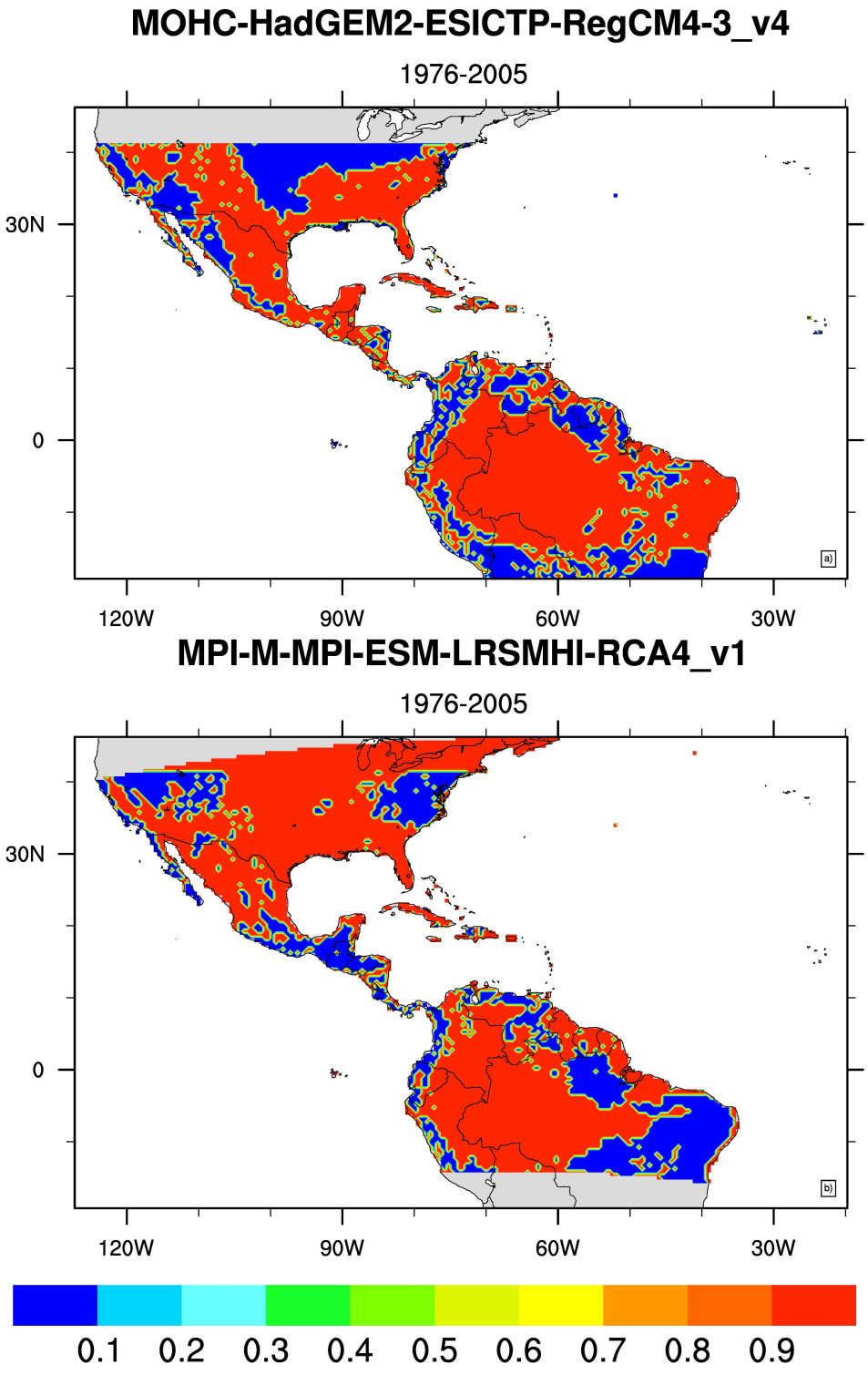

Figure 5.46. The "DSDAEE of the Most Representative Model Combinations in Statistical Methodology 1 in the period between the years 1976 and 2005

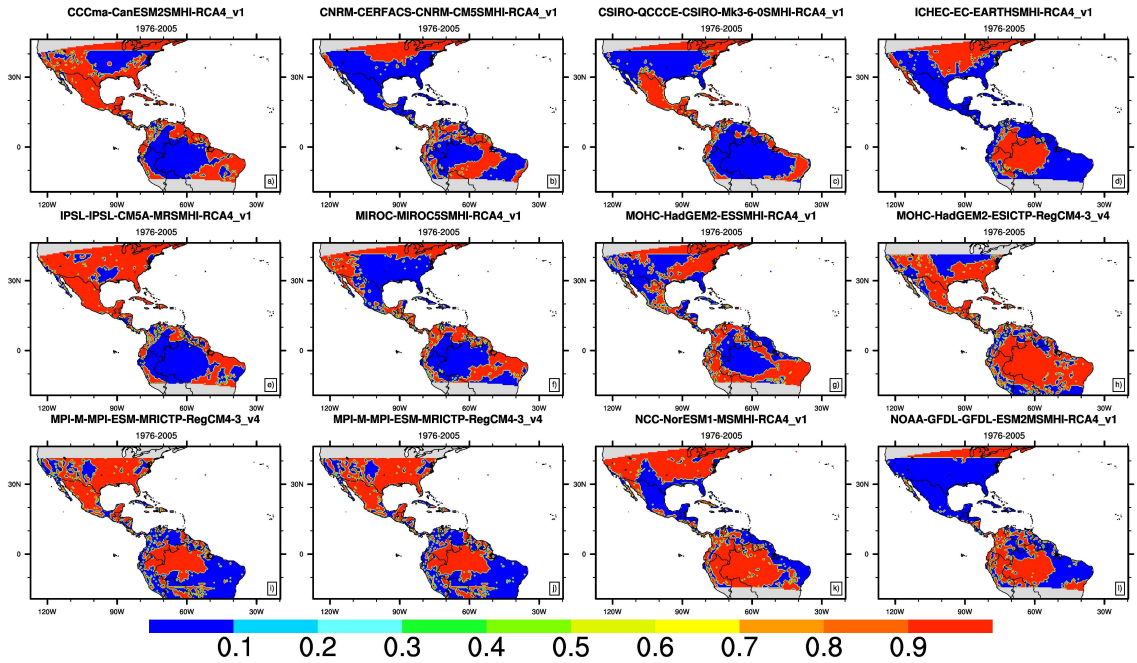

Figure 5.47. The "DSDAEE of the Unrepresentative Model Combinations in Statistical Methodology 1 in the period between the years 1976 and 2005

Table 5.21. The coefficients of The Most Representative Models

GCM - RCM Model Combination	**Coefficient**
MOHC-HadGEM2-ES-ICTP-RegCM4-3-v4	0.66951
MPI-M-MPI-ESM-LR-SMHI-RCA4-v1	0.70632

Table 5.22. The coefficients of The Unrepresentative Models

GCM - RCM Model Combination	Coefficient
CCCma-CanESM2-SMHI-RCA4-v1	0.57244
CNRM-CERFACS-CNRM-CM5-SMHI-RCA4-v1	0.37512
CSIRO-QCCCE-CSIRO-Mk3-6-0-SMHI-RCA4-v1	0.37619
ICHEC-EC-EARTH-SMHI-RCA4-v1	0.40642
IPSL-IPSL-CM5A-MR-SMHI-RCA4-v1	0.60693
MIROC-MIROC5-SMHI-RCA4-v1	0.43973
MOHC-HadGEM2-ES-ICTP-RegCM4-3-v2	0.51726
MOHC-HadGEM2-ES-SMHI-RCA4-v1	0.53097
MPI-M-MPI-ESM-MR-ICTP-RegCM4-3-v4	0.61232
MPI-M-MPI-ESM-MR-ICTP-RegCM4-3-v4	0.51793
NCC-NorESM1-M-SMHI-RCA4-v1	0.62781
NOAA-GFDL-GFDL-ESM2M-SMHI-RCA4-v1	0.36942

5.1.12. Application of Statistical Methodology 2 to the Monthly Temperature Data: The Case of Central America

As shown in Table 5.23 and 5.24, IPSL-RCA4, MOHC-RegCM1 and MPI-RCA4 combinations are the successful ones over Central America. 63 % of the grid points in MPI-RCA4 ad IPSL-RCA4 model combination and 66 % of the grid points in MOHC-RegCM1 model combination are higher than WSDAAE. NCC-RCA4, defining in unrepresentative model combinations, has the maximum percentage with 62 % which is at least 1 % smaller than the model combinations, defined in the most representative ones and it is second in order to simulate the temperature patterns of Central America.

MOHC-RegCM1 is well enough to figure out the temperature properties of the observed area. Temperature patterns are portrayed efficiently over Central America except southern Central America, some pacific coastal of Mexico, Colombia, Ecuador, Brazil-Guyana-Suriname borders, minor part of central Venezuela, Arizona and California and central part of observed interior lands of United States of America (Oklahoma, Kansas, Missouri and Arkansas). MPI-RCA4 simulates the majority of the observed

area very well, excluding Guatemala, El-Salvador, minor Pacific coastal of Mexico, Colombia, Ecuador and Peru, Southern Bolivia, Brazil-Guyana-Suriname borders, minor part of central Venezuela, Georgia, South and North Carolina, Atlantic coastal of eastern Brazil. IPSL-CLM draws temperature accurately over the majority of the Central America, except interior land of Colombia, Peru and North-eastern Brazil, Georgia, minor part of Atlantic coastal of Brazil.

NCC-RCA4, collecting in the unrepresentative model set, is also good at representing the temperature of the domain except Mexico, Gulf of Mexico coastal and Atlantic coastal of Brazil, Suriname, Guyana. NOAA-RCA4 can't simulate the temperature over especially northern part of Central America and CSIRO-RCA4 don't simulate the temperature over more than half of the observed region. Hence, it will be risky to use these model combinations to project the temperature of that region (Figure 5.48 and 5.49).

Table 5.23. The coefficients of The Most Representative Models

GCM - RCM Model Combination	**Coefficient**
IPSL-IPSL-CM5A-MR-SMHI-RCA4-v1	0.63997
MPI-M-MPI-ESM-LR-SMHI-RCA4-v1	0.63666
MOHC-HadGEM2-ES-ICTP-RegCM4-3-v4	0.66671

5.1.13. Application of Statistical Methodology 3 to the Monthly Temperature Data: The Case of Central America

As shown in Table 5.25 and 5.26, MPI-RCA4, MPI-RegCM1 and NCC-RCA4 and IPSL-RCA4 combinations are the successful ones over Central America with respect to this methodology among model combinations, although their capability to present the temperature is very limited. 39 % of the grid points in MPI-RCA4 and MPI-RegCM1 model combinations and 38 % of the grid points in IPSL-RCA4 and NCC-RCA4 model combinations are higher than WSDAAE. MOHC-RegCM, defining in unrepresentative model combinations, has the maximum percentage with 36 % which is at least 2 %

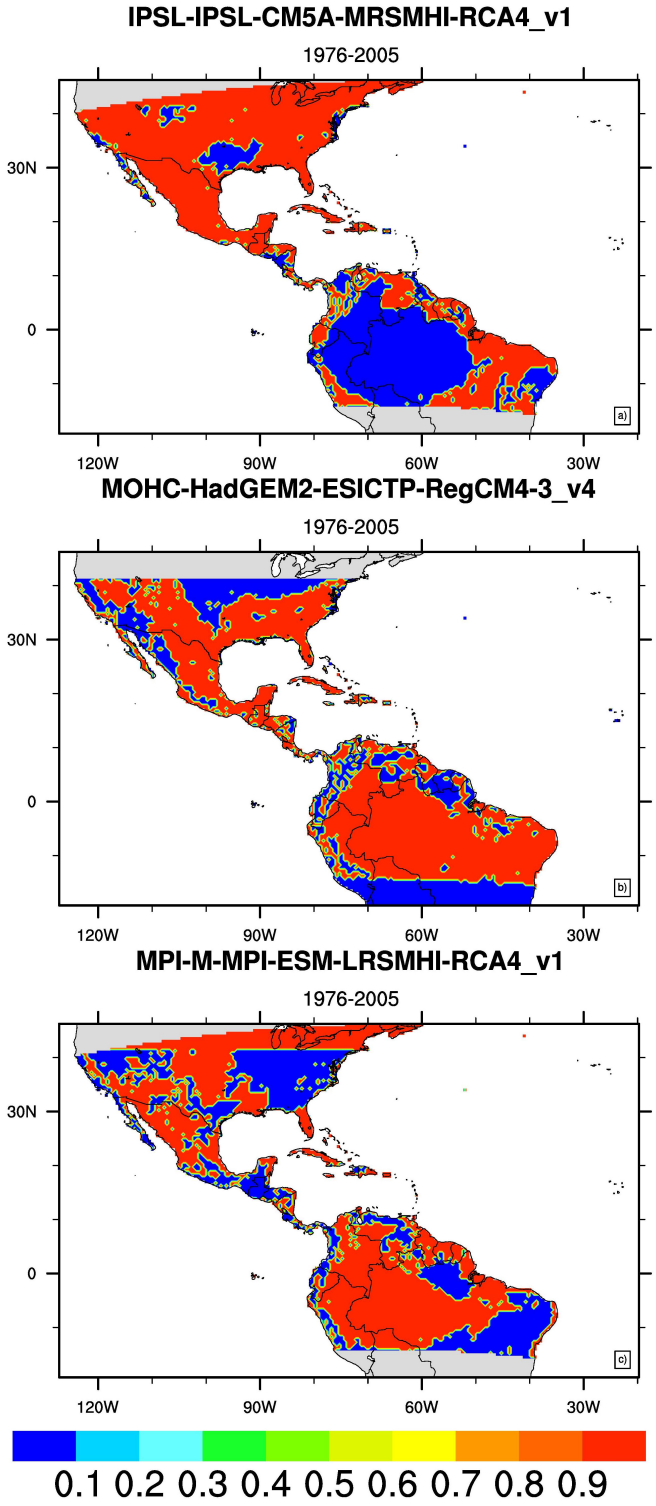

Figure 5.48. The "DSDAEE of the Most Representative Model Combinations in Statistical Methodology 2 in the period between the years 1976 and 2005

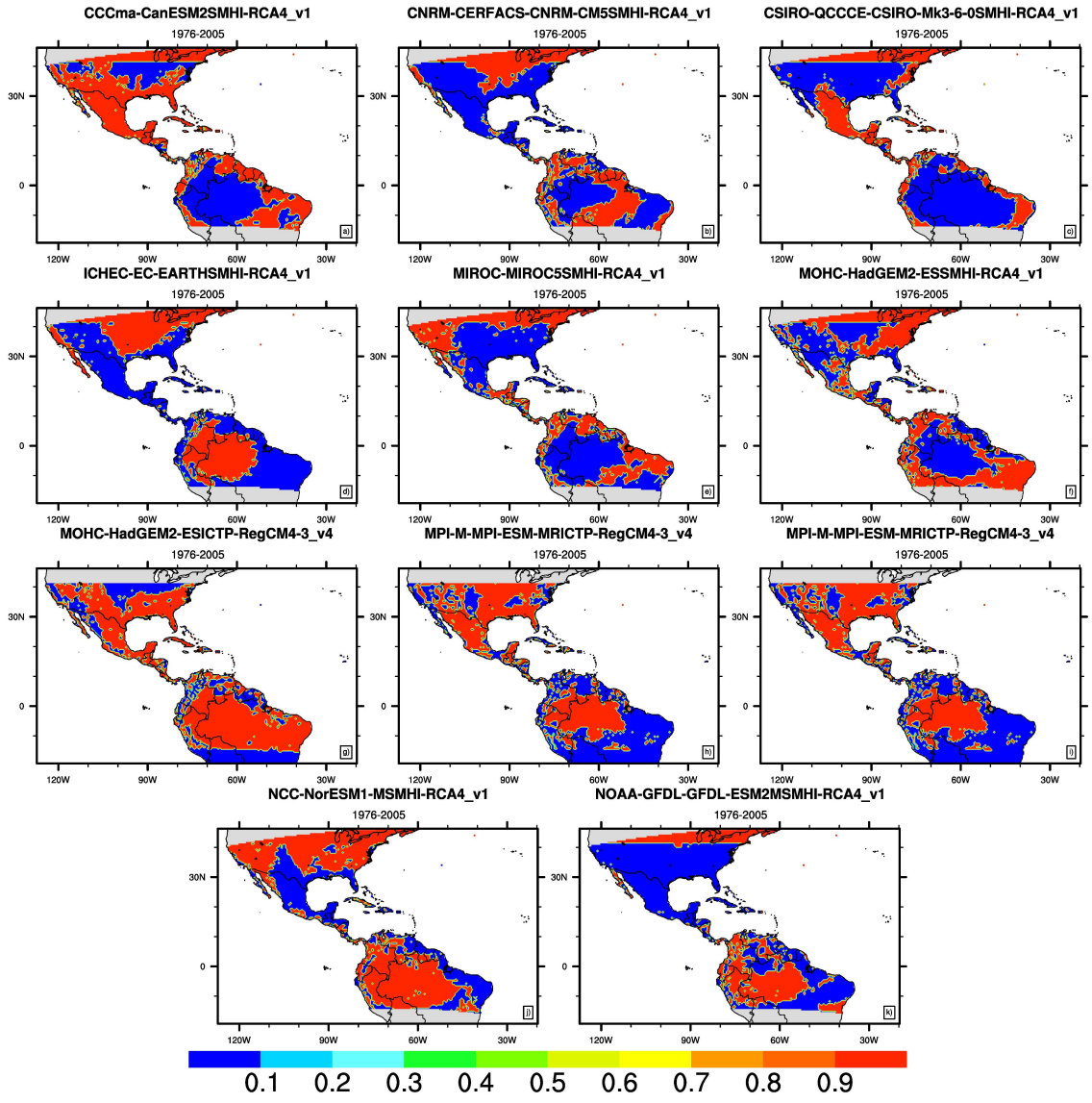

Figure 5.49. The "DSDAEE of the Unrepresentative Model Combinations in Statistical Methodology 2 in the period between the years 1976 and 2005

Table 5.24. The coefficients of The Unrepresentative Models

GCM - RCM Model Combination	**Coefficient**
CCCma-CanESM2-SMHI-RCA4-v1	0.59692
CNRM-CERFACS-CNRM-CM5-SMHI-RCA4-v1	0.41137
CSIRO-QCCCE-CSIRO-Mk3-6-0-SMHI-RCA4-v1	0.36629
ICHEC-EC-EARTH-historical-r12i1p1-SMHI-RCA4-v1	0.44161
MIROC-MIROC5-SMHI-RCA4-v1	0.42689
MOHC-HadGEM2-ES-SMHI-RCA4-v1	0.53057
MOHC-HadGEM2-ES-ICTP-RegCM4-3-v2	0.48847
MPI-M-MPI-ESM-MR-ICTP-RegCM4-3-v4	0.60525
MPI-M-MPI-ESM-MR-ICTP-RegCM4-3-v2	0.47620
NCC-NorESM1-M-SMHI-RCA4-v1	0.62239
NOAA-GFDL-GFDL-ESM2M-SMHI-RCA4-v1	0.34800

smaller than the model combinations, defined in the most representative ones and it is second in order to simulate the temperature patterns of Central America .

All of the model combinations are successful to show the temperature patterns over the eastern domain of the observed part of America. MPI-RCA4 and NCC-RCA4 are good at the neighbor of the Center of the observed part of the South America continental. MOHC- RegCM is representative over the center of the observed part of the South America continental. All of the model combinations aren't successful to project the temperature of Mexico, Guatemala, El-Salvador, Nicaragua, Costa Rica, Panama, Honduras and Belize. There isn't any model combinations in the unrepresentative set and hence it means that the temperature at the grid points of the whole model combinations in CORDEX Project over these countries aren't trustable. None of the model combinations pass T-test and hence the temperature outputs of them conform to the observed one. This region is one of the significant regions where researchers have to focus on and make necessary improvements to simulate temperature correctly.

CSIRO-RCA4 is ineffective to demonstrate the temperature over both sides (north and south) of Central America hence almost all grid points is inefficient to pass

T-Test. NOAA-RCA4 is unsuccessful over the southern part of Central America. It can be alleged that using these models for temperature projections over the aforementioned parts of Central America leads researchers to misinterpretation. Moreover, a general assessment for the temperature of Mexico, Guatemala, El-Salvador, Nicaragua, Costa Rica, Panama, Honduras and Belize isn't possible according to outcomes of this methodology (Figure 5.50 and 5.51).

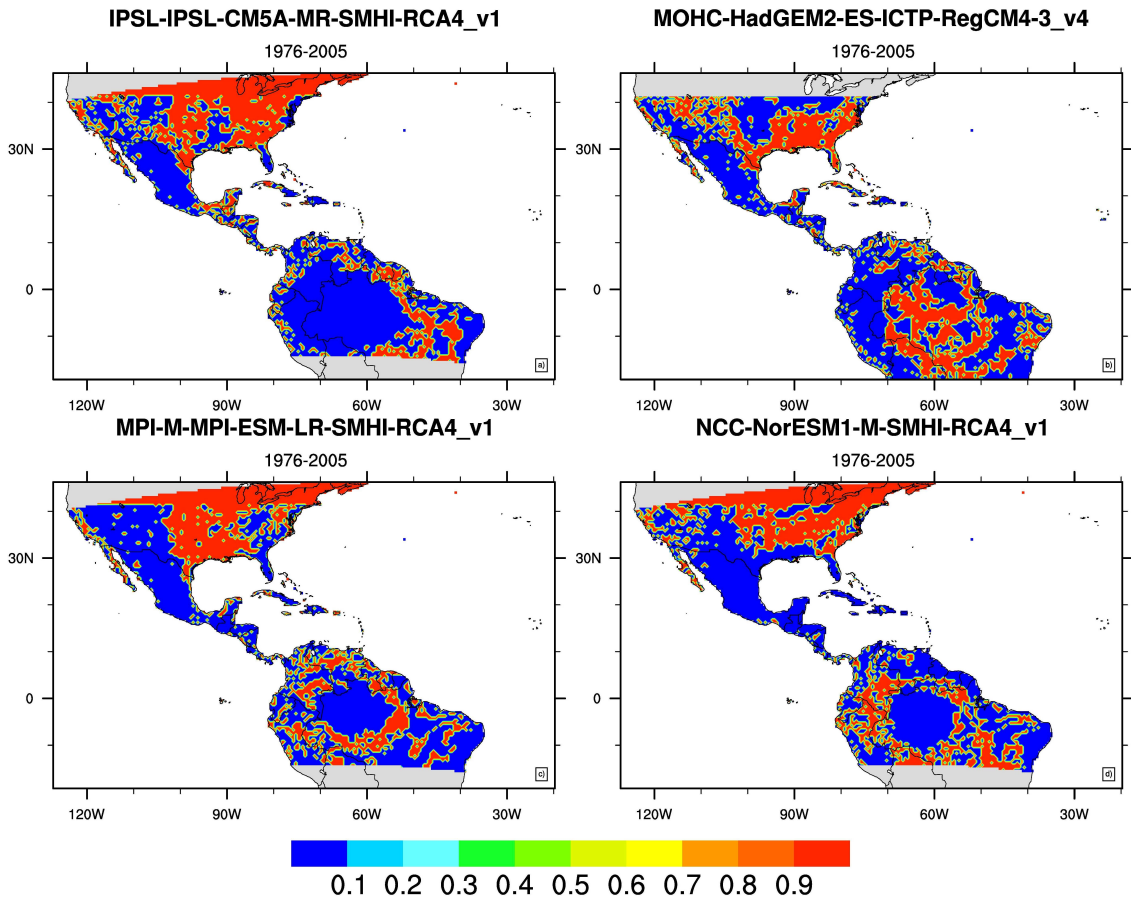

Figure 5.50. The "DSDAEE of the Most Representative Model Combinations in Statistical Methodology 3 in the period between the years 1976 and 2005

5.1.14. Application of Statistical Methodology 4 to the Monthly Temperature Data: The Case of Central America

As shown in Table 5.27 and 5.28, MPI-RCA4 and NCC-RCA4 combinations are the successful ones over Central America with respect to this methodology among model

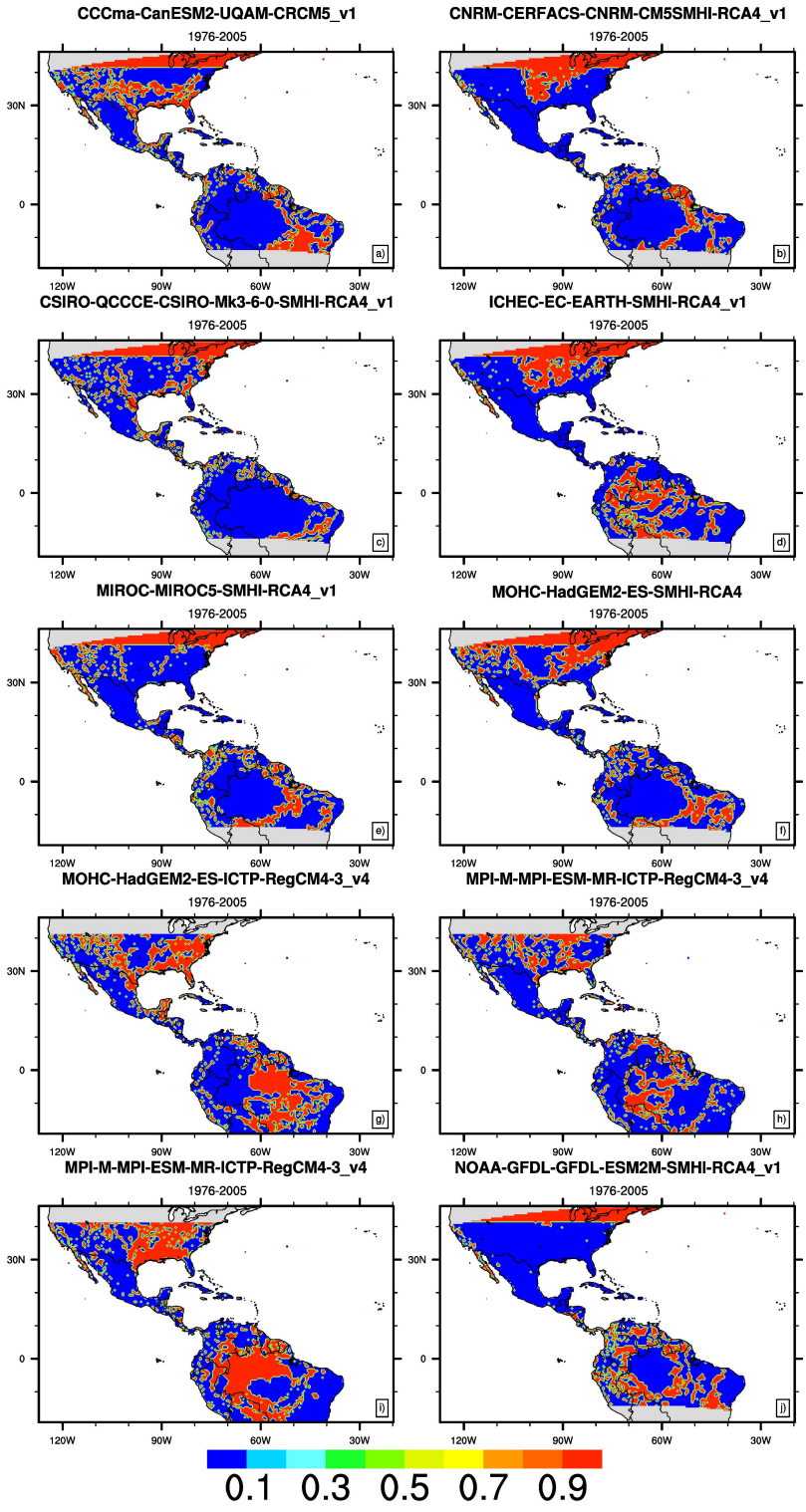

Figure 5.51. The "DSDAEE of the Unrepresentative Model Combinations in Statistical Methodology 3 in the period between the years 1976 and 2005

Table 5.25. The coefficients of The Most Representative Models

GCM - RCM Model Combination	**Coefficient**
MPI-M-MPI-ESM-LR-SMHI-RCA4-v1	0.39704
MPI-M-MPI-ESM-MR-ICTP-RegCM4-3-v2	0.39301
NCC-NorESM1-M-SMHI-RCA4-v1	0.38435
IPSL-IPSL-CM5A-MR-SMHI-RCA4-v1	0.38343

Table 5.26. The coefficients of The Unrepresentative Models

GCM - RCM Model Combination	**Coefficient**
CCCma-CanESM2-SMHI-RCA4-v1	0.34890
CNRM-CERFACS-CNRM-CM5-SMHI-RCA4-v1	0.26528
CSIRO-QCCCE-CSIRO-Mk3-6-0-SMHI-RCA4-v1	0.26662
ICHEC-EC-EARTH-SMHI-RCA4-v1	0.33645
MIROC-MIROC5-SMHI-RCA4-v1	0.28227
MOHC-HadGEM2-ES-ICTP-RegCM4-3-v4	0.36315
MOHC-HadGEM2-ES-SMHI-RCA4-v1	0.32803
MOHC-HadGEM2-ES-ICTP-RegCM4-3-v4	0.34889
MPI-M-MPI-ESM-MR-ICTP-RegCM4-3-v4	0.28143
NOAA-GFDL-GFDL-ESM2M-SMHI-RCA4-v1	0.27809

combinations, although their capability to present the temperature is very limited. 41 % of the grid points in MPI-RCA4 model combination and 39.9 % of the grid points in NCC-RCA4 model combination are higher than WSDAAE. MPI-RegCM, MOHC-RegCM and IPSL-RCA4, defining in unrepresentative model combinations, have the maximum percentage with 39 % which is nearly same with the model combinations, defined in the most representative ones and they are second in order to simulate the temperature patterns of Central America.

Both of the model combinations are successful to show the temperature patterns over the eastern domain of the observed part of America. MPI-RCA4 and NCC-RCA4 are good at the neighbor of the Center of the observed part of the South America continental. MPI-RegCM1 and MPI-RegCM2, defining in the unrepresentative models, are well enough to simulate the temperature of center of southern part of Central America. All of the model combinations aren't successful to project the temperature of Mexico, Guatemala, El-Salvador, Nicaragua, Costa Rica, Panama, Honduras and Belize. There aren't any model combinations among the unrepresentative set and hence it means that the temperature at the grid points of the whole model combinations in CORDEX Project over these countries aren't trustable. None of the model combinations pass T-test and hence the temperature outputs of them conform to the observed one. This region is one of the significant region where researchers have to focus on and make necessary improvements to simulate temperature correctly with respect to this methodology(Figure 5.52 and 5.53).

Table 5.27. The coefficients of The Most Representative Models

GCM - RCM Model Combination	**Coefficient**
MPI-M-MPI-ESM-LR-SMHI-RCA4-v1	0.41316
NCC-NorESM1-M-SMHI-RCA4-v1	0.39902

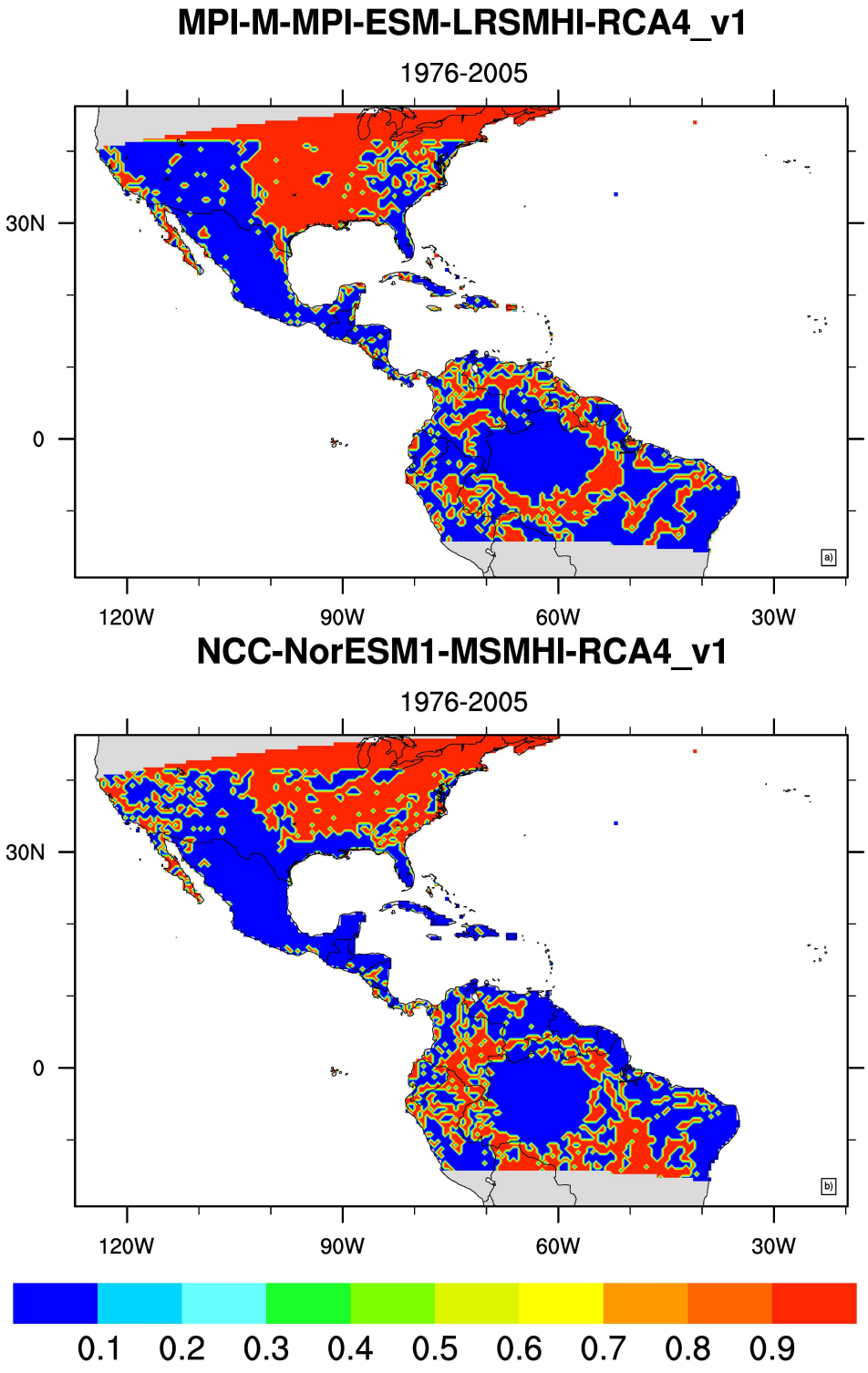

Figure 5.52. The "DSDAEE of the Most Representative Model Combinations in Statistical Methodology 4 in the period between the years 1976 and 2005

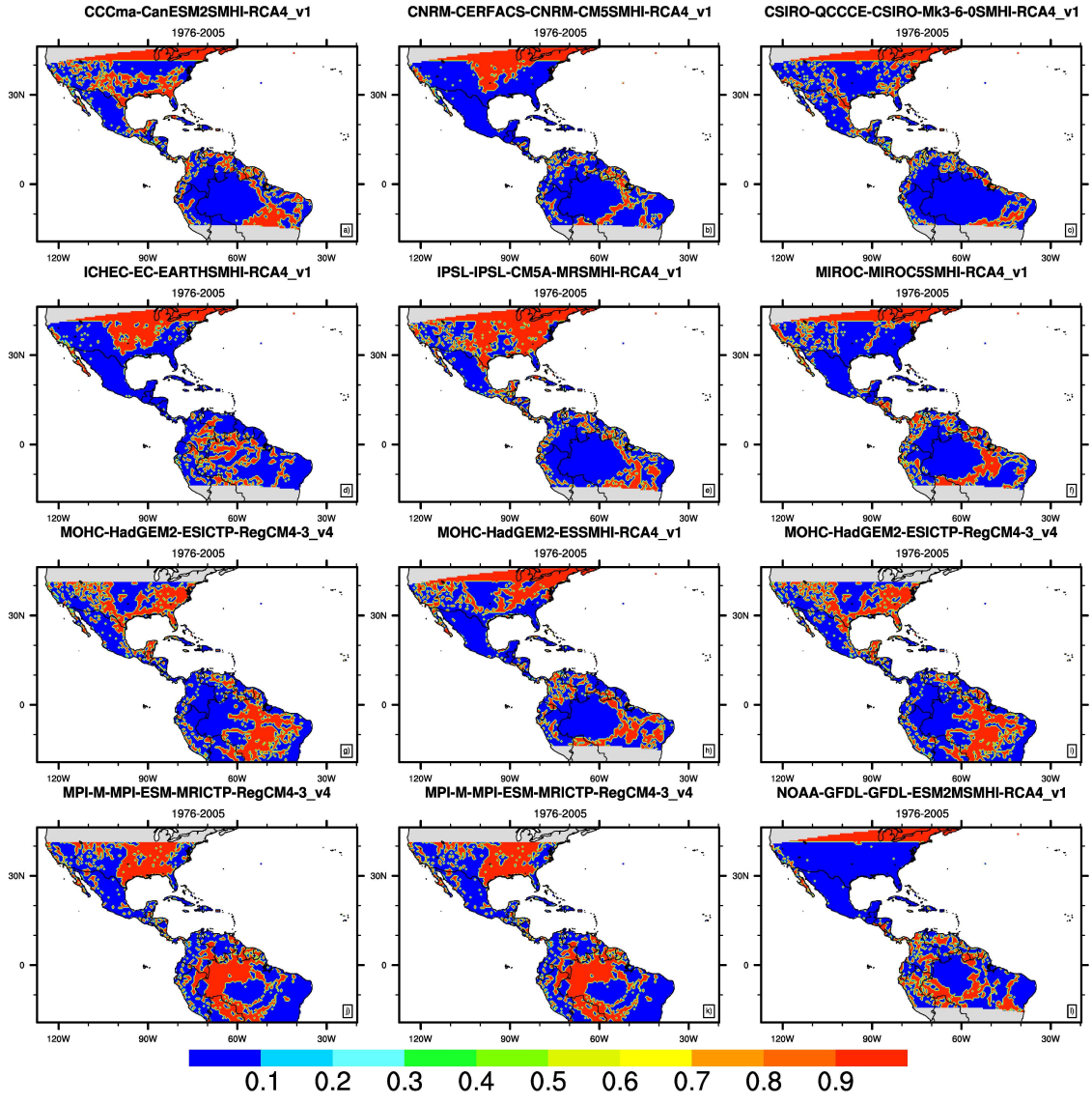

Figure 5.53. The "DSDAEE of the Unrepresentative Model Combinations in Statistical Methodology 4 in the period between the years 1976 and 2005

Table 5.28. The coefficients of The Unrepresentative Models

GCM - RCM Model Combination	**Coefficient**
CCCma-CanESM2-SMHI-RCA4-v1	0.36094
CNRM-CERFACS-CNRM-CM5-SMHI-RCA4-v1	0.26542
CSIRO-QCCCE-CSIRO-Mk3-6-0-SMHI-RCA4-v1	0.27973
ICHEC-EC-EARTH-SMHI-RCA4-v1	0.31813
IPSL-IPSL-CM5A-MR-SMHI-RCA4-v1	0.39347
MIROC-MIROC5-SMHI-RCA4-v1	0.31438
MOHC-HadGEM2-ES-ICTP-RegCM4-3-v4	0.39275
MOHC-HadGEM2-ES-SMHI-RCA4-v1	0.35331
MOHC-HadGEM2-ES-ICTP-RegCM4-3-v2	0.34529
MPI-M-MPI-ESM-MR-ICTP-RegCM4-3-v4	0.30183
MPI-M-MPI-ESM-MR-ICTP-RegCM4-3-v2	0.39208
NOAA-GFDL-GFDL-ESM2M-SMHI-RCA4-v1	0.29302

Table 5.29. The Amount of Total and successful GCM – RCMs

GCM	**TOTAL**	**successful**	**RCM**	**TOTAL**	**successful**
MOHC	12	2 (16.6 %)	RCA4	40	8(20 %)
NCC	4	2 (50 %)	REGCM	16	3 (18.75%)
CNRM	4	0			
CSİRO	4	0			
ICHEC	4	0			
IPSL	4	2 (50 %)			
MİROC	4	0			
MPI	12	5 (41.6 %)			
NOAA	4	0			

5.1.15. Evaluation Of Statistical Methodologies Over Central America Temperature

MPI and MOHC are the most applied GCMs over Central America in CORDEX Project but NCC and IPSL are the most successful one overall Central America is taken consideration. RCA4 is the most used RCM in the GCM-RCM model combinations in simulations over Central America and it is the most successful one with a very high percentage. Hence, simulating NCC or IPSL as GCM and using it's outcomes as initial conditions- boundary conditions in the RCA4 is the most convenient choice to project overall Central America temperature (Table 5.29).

5.1.16. Application of Statistical Methodology 1 to the Monthly Temperature Data: The Case of South America

As shown in Table 5.30 and 5.31, CCCma-RCA4 and CSIRO-RCA4 combinations are the successful ones over South America. 69 % of the grid points in CCCma-RCA4 model combination and 67 % of the grid points in CSIRO-RCA4 model combination are higher than WSDAAE. IPSL-RCA4, defining in unrepresentative model combinations, has the maximum percentage with 65 % which is at least 2 % smaller than the model combinations, defined in the most representative ones and it is second in order to simulate the temperature patterns of South America.

CCCma-RCA4 is well enough to figure out the temperature properties of the observed area, especially northern part of South America. Temperature patterns are portrayed efficiently over northern South minor Peru coastal and small interior land of Brazil. Uruguay, Paraguay, Chile, Argentina are the regions where CCCma-RCA4 can't produce trustable results. CSIRO-RCA4 generates reliable results over whole region except Northern Argentina, Paraguay, southern and minor part of Chile, Northern and Atlantic coastal of Brazil. IPSL-RCA4, falling into unrepresentative cluster, is good enough to simulate temperature over South America except southern Argentina, Chile and northern Brazil. ICHEC-RCA4 is the most unrepresentative model combination over South America since it doesn't procreate confidential outcomes over the majority

of the observed region (Figure 5.55 and 5.54).

Table 5.30. The coefficients of The Most Representative Models

GCM - RCM Model Combination	**Coefficient**
CCCma-CanESM2-SMHI-RCA4-v3	0.69636
CSIRO-QCCCE-CSIRO-Mk3-6-0-SMHI-RCA4-v3	0.67063

Table 5.31. The coefficients of The Unrepresentative Models

GCM - RCM Model Combination	**Coefficient**
ICHEC-EC-EARTH-SMHI-RCA4-v3	0.14069
IPSL-IPSL-CM5A-MR-SMHI-RCA4-v3	0.65588
MIROC-MIROC5-SMHI-RCA4-v3	0.56816
MOHC-HadGEM2-ES-SMHI-RCA4-v3	0.40776
MPI-M-MPI-ESM-LR-SMHI-RCA4-v3	0.46885
NCC-NorESM1-M-SMHI-RCA4-v3	0.43364
NOAA-GFDL-GFDL-ESM2M-SMHI-RCA4-v3	0.27942

5.1.17. Application of Statistical Methodology 2 to the Monthly Temperature Data: The Case of South America

As shown in Table 5.32 and 5.33, CCCma-RCA4 model combination is the unique successful one over South America. 71 % of the grid points in CCCma-RCA4 model combination is higher than WSDAAE. IPSL-RCA4 and CSIRO-RCA4, defining in unrepresentative model combinations, has the maximum percentage with 65 % and 66 % respectively which is at least 5 % smaller than the model combinations, defined in the most representative ones and it is second in order to simulate the temperature patterns of Southern America.

CCCma-RCA4 is well enough to figure out the temperature properties of the observed area, especially northern part of South America. Temperature patterns are portrayed efficiently over northern South minor Peru coastal and small interior land of Brazil. Uruguay, Paraguay, Chile, Argentina are the regions where CCCma-RCA4 can't

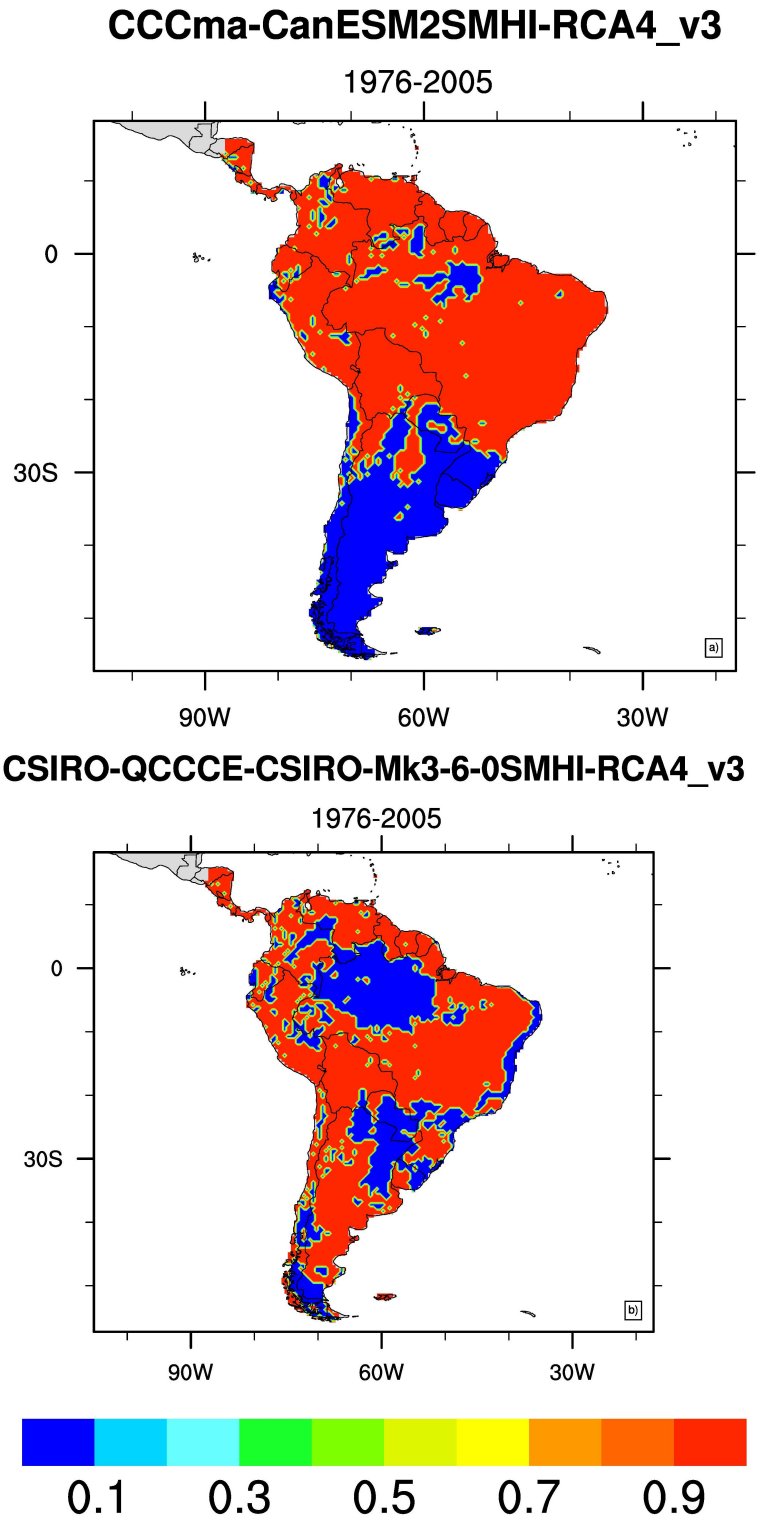

Figure 5.54. The "DSDAEE of the Most Representative Model Combinations in Statistical Methodology 1 in the period between the years 1976 and 2005

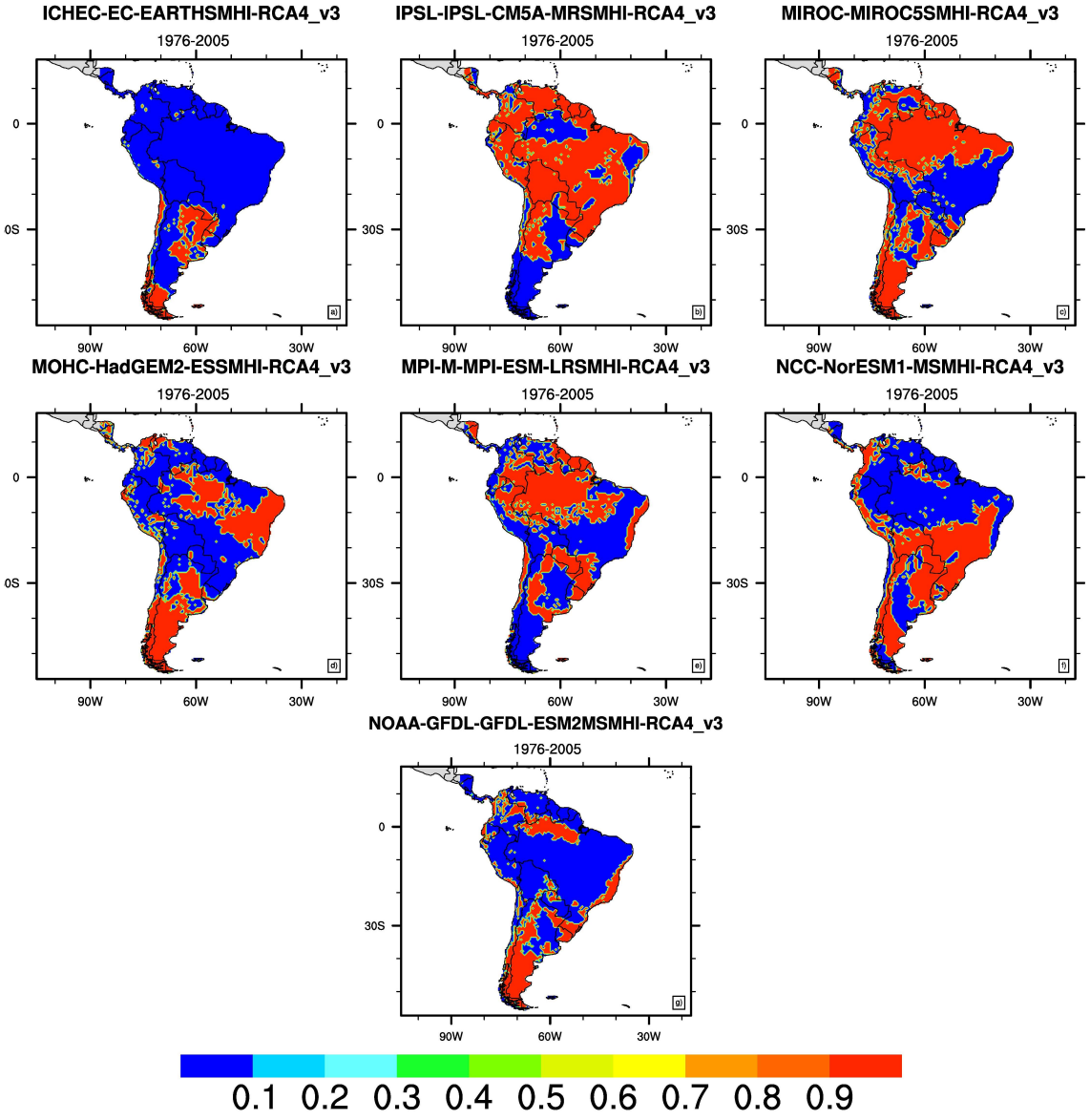

Figure 5.55. The "DSDAEE of the Unrepresentative Model Combinations in Statistical Methodology 1 in the period between the years 1976 and 2005

produce trustable results. IPSL-RCA4 and CSIRO-RCA4, falling into unrepresentative cluster, are good enough to simulate temperature over South America except southern Argentina, Chile and northern Brazil. ICHEC-RCA4 is the most unrepresentative model combination over South America since it doesn't procreate confidential outcomes over the majority of the observed region (Figure 5.56 and 5.57).

Table 5.32. The coefficients of The Most Representative Models

GCM - RCM Model Combination	**Coefficient**
CCCma-CanESM2-SMHI-RCA4-v3	0.71923

Table 5.33. The coefficients of The Unrepresentative Models

GCM - RCM Model Combination	**Coefficient**
CSIRO-QCCCE-CSIRO-Mk3-6-0-SMHI-RCA4-v3	0.66867
ICHEC-EC-EARTH-historical-r12i1p1-SMHI-RCA4-v3	0.10638
IPSL-IPSL-CM5A-MR-SMHI-RCA4-v3	0.65242
MIROC-MIROC5-SMHI-RCA4-v3	0.52994
MOHC-HadGEM2-ES-SMHI-RCA4-v3	0.42838
MPI-M-MPI-ESM-LR-SMHI-RCA4-v3	0.47231
NCC-NorESM1-M-SMHI-RCA4-v3	0.47517
NOAA-GFDL-GFDL-ESM2M-SMHI-RCA4-v3	0.24361

5.1.18. Application of Statistical Methodology 3 to the Monthly Temperature Data: The Case of South America

As shown in Table 5.34 and 5.35, CSIRO-RCA4 model combination is the unique successful one over South America. 33 % of the grid points in CSIRO-RCA4 model combination is higher than WSDAAE. MIROC-RCA4, defining in unrepresentative model combinations, has the maximum percentage with 30 % which is at least 3 % smaller than the model combinations, defined in the most representative ones and it is second in order to simulate the temperature patterns of Southern America.

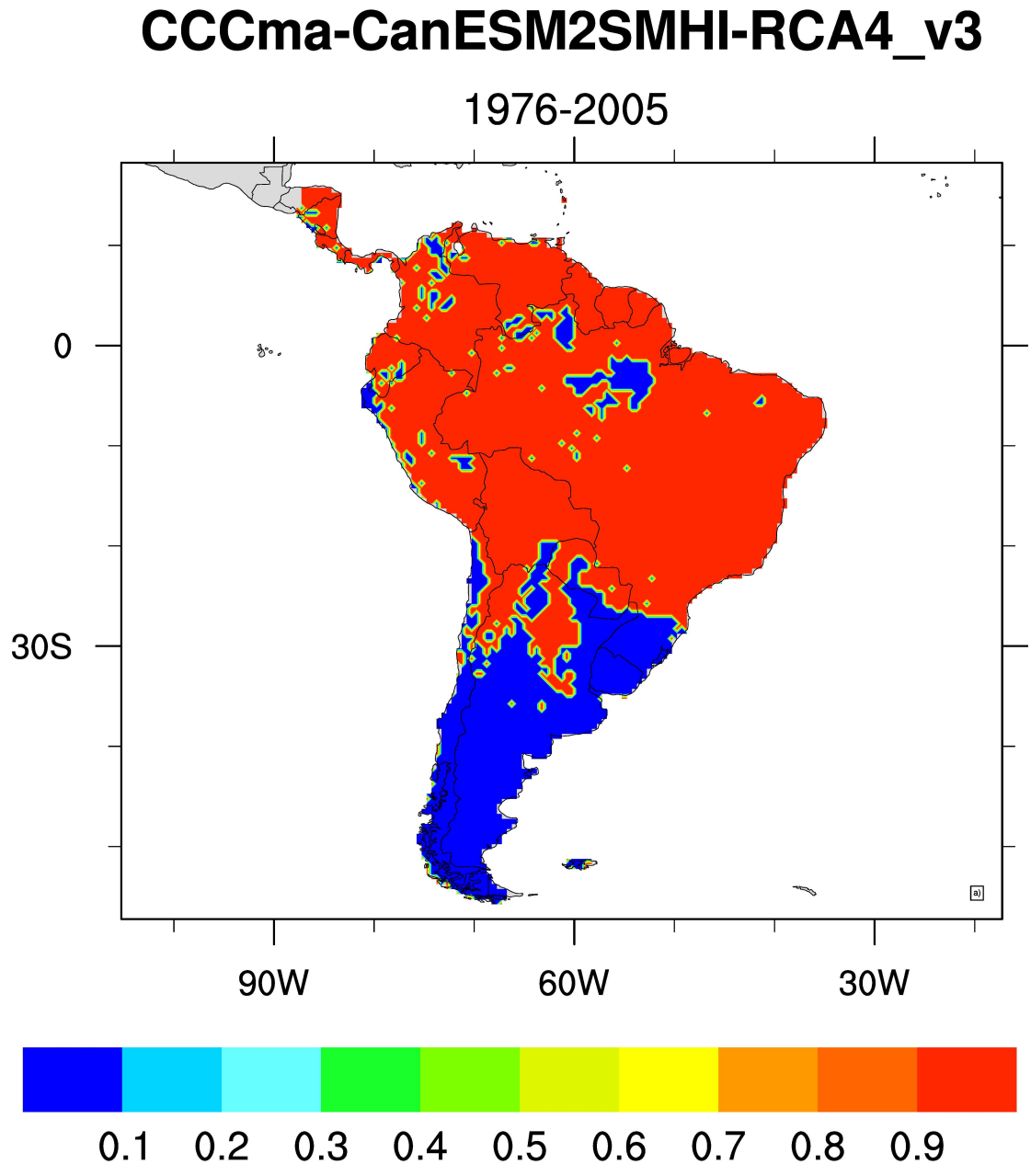

Figure 5.56. The "DSDAEE of the Most Representative Model Combinations in Statistical Methodology 2 in the period between the years 1976 and 2005

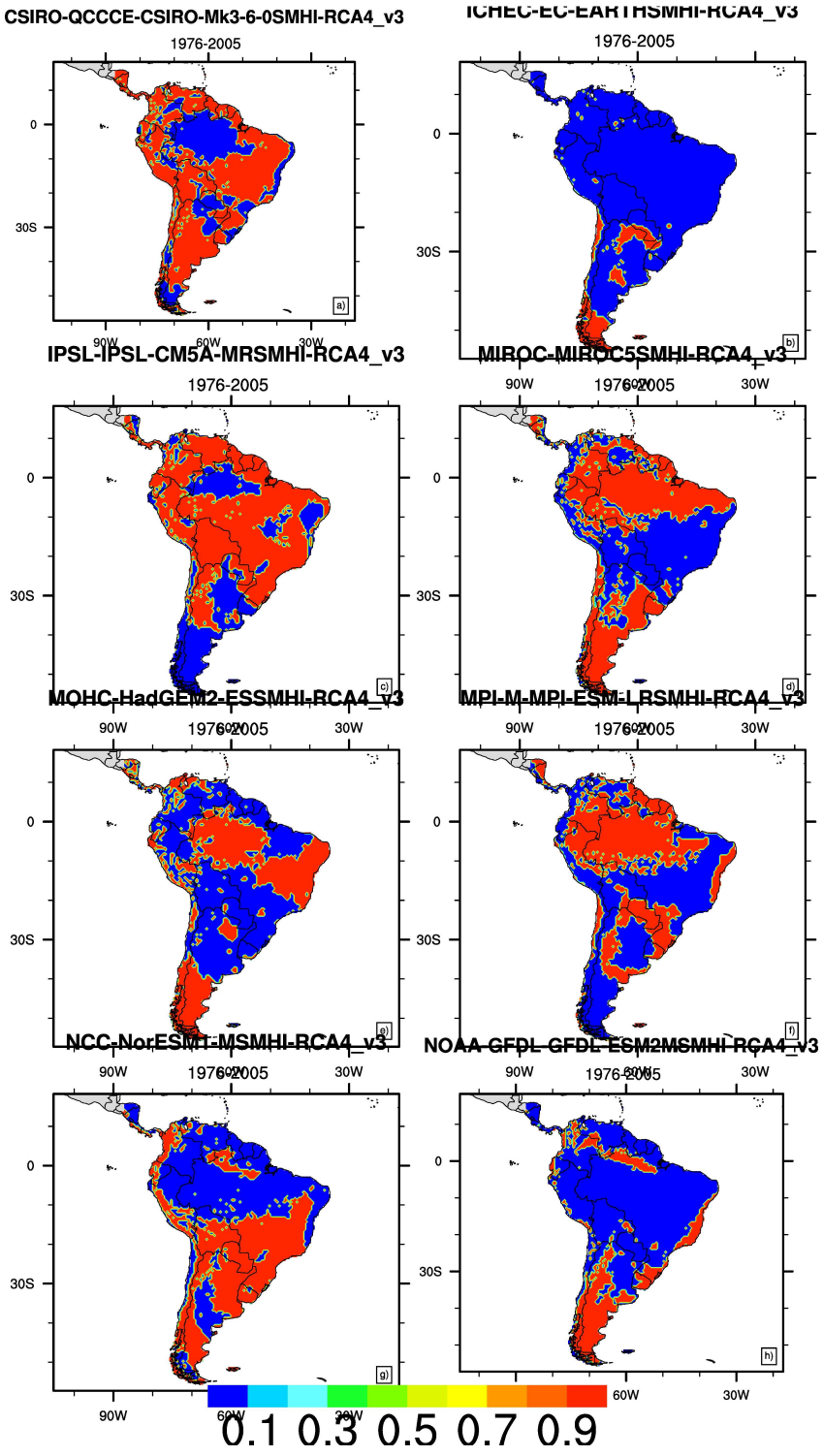

Figure 5.57. The "DSDAEE of the Unrepresentative Model Combinations in Statistical Methodology 2 in the period between the years 1976 and 2005

It is difficult to claim that there is trustworthy model combination, indicating the temperature properties of the whole South America continental perfectly. CSIRO-RCA4 is the most credible one, however it can't approximate the temperature of especially coastal. Interior lands are well projected by not only CSIRO-RCA4, but also MIROC-RCA4 which is in the cluster of unreliable model combinations. ICHEC-RCA4 is again the most unrepresentative model combination over South America since it doesn't procreate confidential outcomes over the majority of the observed region (Figure 5.58 and 5.59).

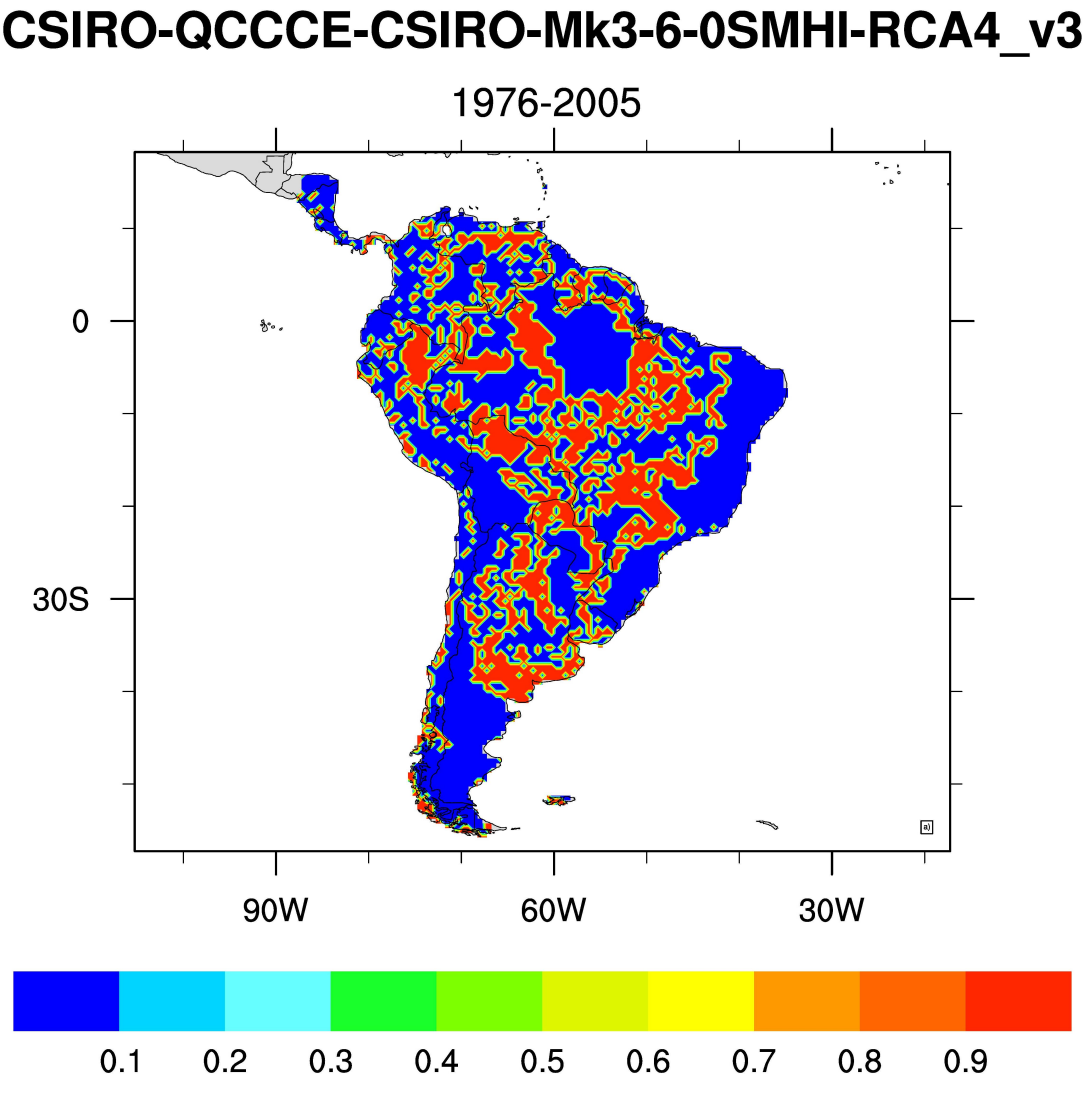

Figure 5.58. The "DSDAEE of the Most Representative Model Combinations in Statistical Methodology 3 in the period between the years 1976 and 2005

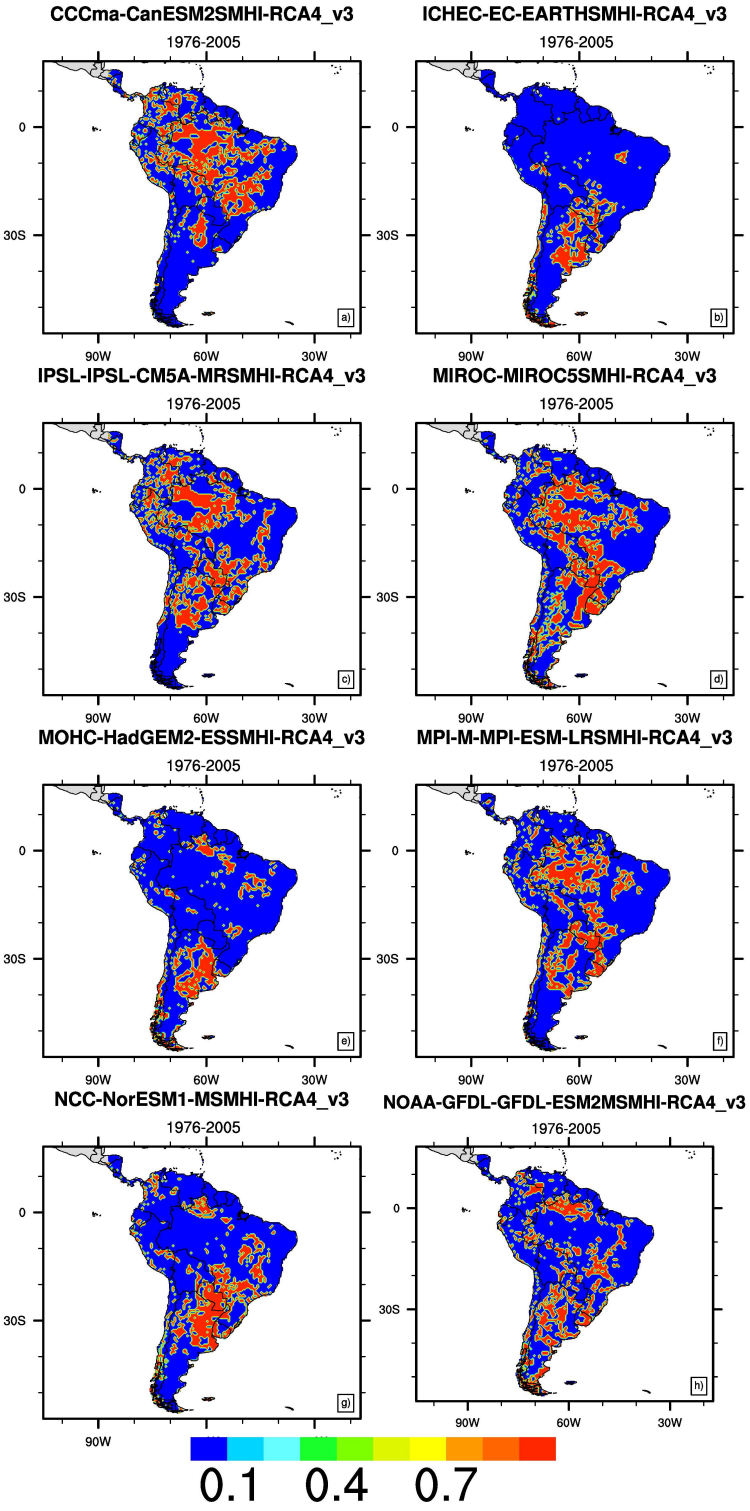

Figure 5.59. The "DSDAEE of the Unrepresentative Model Combinations in Statistical Methodology 3 in the period between the years 1976 and 2005

Table 5.34. The coefficients of The Most Representative Models

GCM - RCM Model Combination	Coefficient
CSIRO-QCCCE-CSIRO-Mk3-6-0-SMHI-RCA4-v3	0.33479

Table 5.35. The coefficients of The Unrepresentative Models

GCM - RCM Model Combination	Coefficient
CCCma-CanESM2-SMHI-RCA4-v3	0.28303
ICHEC-EC-EARTH-SMHI-RCA4-v3	0.12353
IPSL-IPSL-CM5A-MR-SMHI-RCA4-v3	0.28799
MIROC-MIROC5-SMHI-RCA4-v3	0.30906
MOHC-HadGEM2-ES-SMHI-RCA4-v3	0.15543
MPI-M-MPI-ESM-LR-SMHI-RCA4-v3	0.24872
NCC-NorESM1-M-SMHI-RCA4-v3	0.22224
NOAA-GFDL-GFDL-ESM2M-SMHI-RCA4-v3	0.23789

5.1.19. Application of Statistical Methodology 4 to the Monthly Temperature Data: The Case of South America

As shown in Table 5.36 and 5.37, CSIRO-RCA4 and MIROC-RCA4 model combinations are evaluated as the unique successful ones over South America. 36 % of the grid points in CSIRO-RCA4 model combination and 34 % of the grid points in MIROC-RCA4 model combination are higher than WSDAAE. CCCma-RCA4, defining in unrepresentative model combinations, has the maximum percentage with 29 % which is at least 4 % smaller than the model combinations, defined in the most representative ones and it is second in order to simulate the temperature patterns of Southern America.

It is again difficult to claim that there is straight model combination, indicating the temperature properties of the whole South America continental perfectly. CSIRO-RCA4 is the most credible one, however it can't approximate the temperature of es-

pecially coastal. Interior lands are well projected by not only CSIRO-RCA4, but also MIROC-RCA4 which is in the cluster of unreliable model combinations. ICHEC-RCA4 is again the most unrepresentative model combination over South America since it doesn't procreate confidential outcomes over the majority of the observed region (Figure 5.60 and 5.61).

Table 5.36. The coefficients of The Most Representative Models

GCM - RCM Model Combination	**Coefficient**
CSIRO-QCCCE-CSIRO-Mk3-6-0-SMHI-RCA4-v3	0.36578
MIROC-MIROC5-SMHI-RCA4-v3	0.34683

Table 5.37. The coefficients of The Unrepresentative Models

GCM - RCM Model Combination	**Coefficient**
CCCma-CanESM2-SMHI-RCA4-v3	0.29522
ICHEC-EC-EARTH-SMHI-RCA4-v3	0.12368
IPSL-IPSL-CM5A-MR-SMHI-RCA4-v3	0.26422
MOHC-HadGEM2-ES-SMHI-RCA4-v3	0.16732
MPI-M-MPI-ESM-LR-SMHI-RCA4-v3	0.25459
NCC-NorESM1-M-SMHI-RCA4-v3	0.23849
NOAA-GFDL-GFDL-ESM2M-SMHI-RCA4-v3	0.25489

5.1.20. Evaluation Of Statistical Methodologies Over South America Temperature

CCCma, CSIRO, ICHEC, IPSL, MIROC, MOHC, MPI, NCC and NOAA are equally applied GCMs over South America in CORDEX Project and CSIRO is the most successful one overall Central America is taken consideration. RCA4 is the unique RCM, using in the GCM-RCM model combinations in simulations over South America and 16.6 % of them is successful in the simulations. Because of the uniqueness of RCM, applying in the simulations over South America in CORDEX project, it can't be concluded that using RCA4 as RCM is useful or not over this domain. On the other

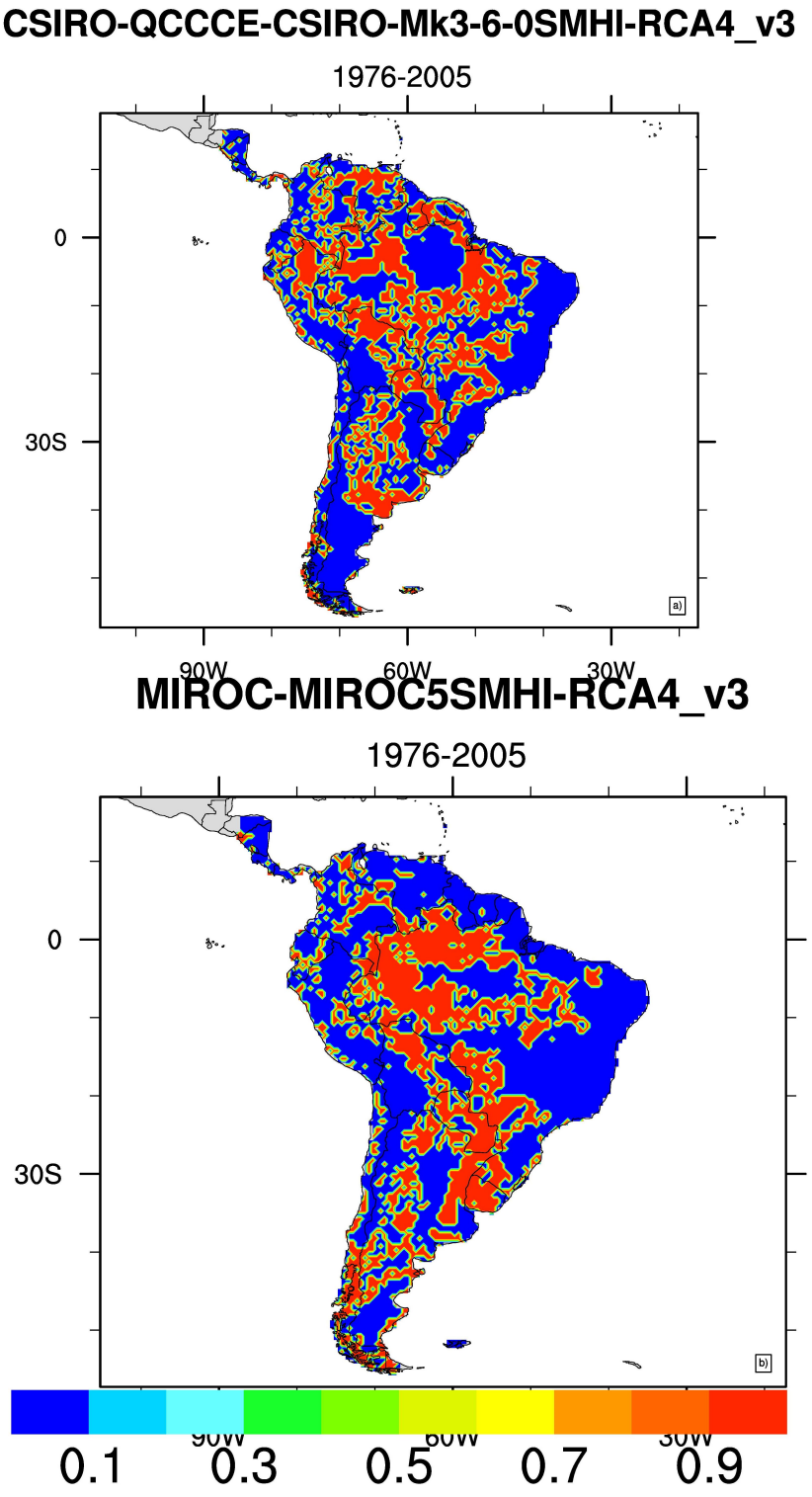

Figure 5.60. The "DSDAEE of the Most Representative Model Combinations in Statistical Methodology 4 in the period between the years 1976 and 2005

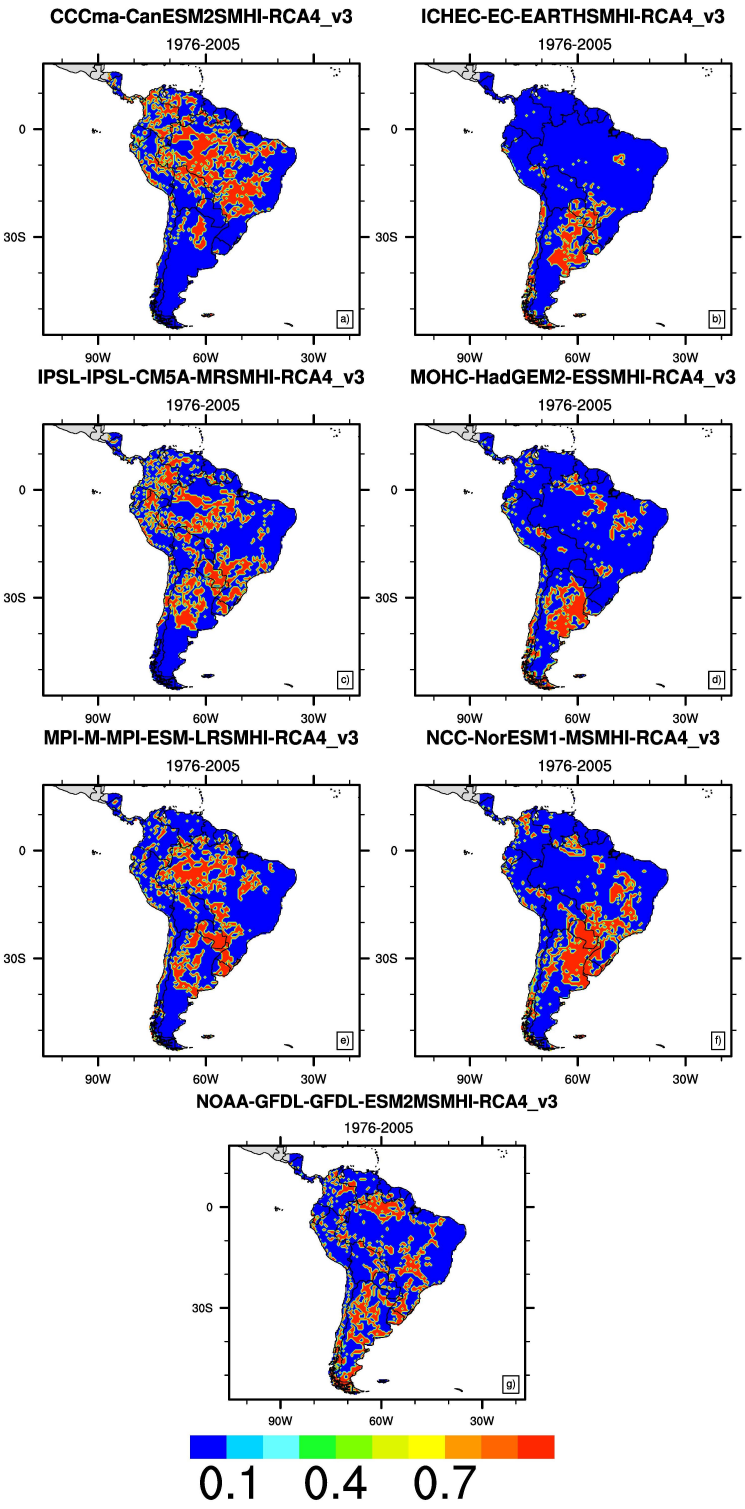

Figure 5.61. The "DSDAEE of the Unrepresentative Model Combinations in Statistical Methodology 4 in the period between the years 1976 and 2005

hand, it can be claimed that CSIRO is the most convenient GCM for temperature projections of South America (Table 5.38).

Table 5.38. The Amount of Total and successful GCM – RCMs

GCM	**TOTAL**	**successful**	**RCM**	**TOTAL**	**successful**
CCCma	4	2 (50 %)	RCA4	36	6 (16.6 %)
CSIRO	4	3 (75 %)	REGCM	16	3 (18.75%)
ICHEC	4	0			
IPSL	4	0			
MIROC	4	1 (25 %)			
MOHC	4	0			
MPI	4	0			
NCC	4	0			
NOAA	4	0			

5.1.21. Application of Statistical Methodology 1 to the Monthly Temperature Data: The Case of West Asia

As shown in Table 5.39 and 5.40, CSIRO-RCA4 and IPSL-RCA4 combinations are the successful ones over South America. 79 % of the grid points in CSIRO-RCA4 model combination and 75 % of the grid points in IPSL-RCA4 are higher than WSDAAE. MIROC-RCA4, MOHC-RCA4 and CCCma-RCA4, defining in unrepresentative model combinations, have the maximum percentage with 68 %, 67 % and 67 % respectively which are at least 7 % smaller than the model combinations, defined in the most representative ones and it is second in order to simulate the temperature patterns of South America.

CSIRO-RCA4 is well enough to figure out the temperature properties of the observed area, except Turkmenistan, Oman, Somalia, Vietnam, Thailand, Cambodia, western coastal of India. IPSL-RCA4 demonstrates the temperature patterns of observed area except Tajikistan, Kyrgyzstan, Central China, East Mediterranean Coastal, Egypt, Aegen Sea Coastal and eastern part of Turkey. CCCma-RCA4 is also successful

to show temperature patterns of the whole area, except Arabian Peninsula and Egypt. MIROC-RCA4 is an unrepresentative model combination for southern India, Egypt, Somalia, Oman, coastal borders of Turkmenistan and Kazakhstan to Caspian Sea. MOHC-RCA4 is demonstrative for temperature projections except Eastern coastal of Red Sea, Chinese eastern land borders and western Arabian Sea. NOAA-RegCM and NOAA-RCA4 is very unsuccessful and it will be jeopardous to use these model combinations for West Asia temperature simulations (Figure 5.62 and 5.63).

Table 5.39. The coefficients of The Most Representative Models

GCM - RCM Model Combination	**Coefficient**
CSIRO-QCCCE-CSIRO-Mk3-6-0-SMHI-RCA4-v2	0.79787
IPSL-IPSL-CM5A-MR-SMHI-RCA4-v2	0.75776

Table 5.40. The coefficients of The Unrepresentative Models

GCM - RCM Model Combination	**Coefficient**
CCCma-CanESM2-IITM-RegCM4-4-v5	0.44417
CCCma-CanESM2-SMHI-RCA4-v2	0.67812
CNRM-CERFACS-CNRM-CM5-IITM-RegCM4-4-v5	0.25284
CNRM-CERFACS-CNRM-CM5-SMHI-RCA4-v2	0.38038
CSIRO-QCCCE-CSIRO-Mk3-6-0-IITM-RegCM4-4-v5	0.60050
ICHEC-EC-EARTH-historical-r12i1p1-SMHI-RCA4-v2	0.22709
IPSL-IPSL-CM5A-LR-IITM-RegCM4-4-v5	0.47111
MIROC-MIROC5-SMHI-RCA4-v2	0.68004
MOHC-HadGEM2-ES-SMHI-RCA4-v2	0.67638
MPI-M-MPI-ESM-LR-MPI-CSC-REMO2009-v1	0.52513
MPI-M-MPI-ESM-LR-SMHI-RCA4-v2	0.61371
MPI-M-MPI-ESM-MR-IITM-RegCM4-4-v5	0.40570
NCC-NorESM1-M-SMHI-RCA4-v2	0.49089
NOAA-GFDL-GFDL-ESM2M-IITM-RegCM4-4-v5	0.20869
NOAA-GFDL-GFDL-ESM2M-SMHI-RCA4-v2	0.10943

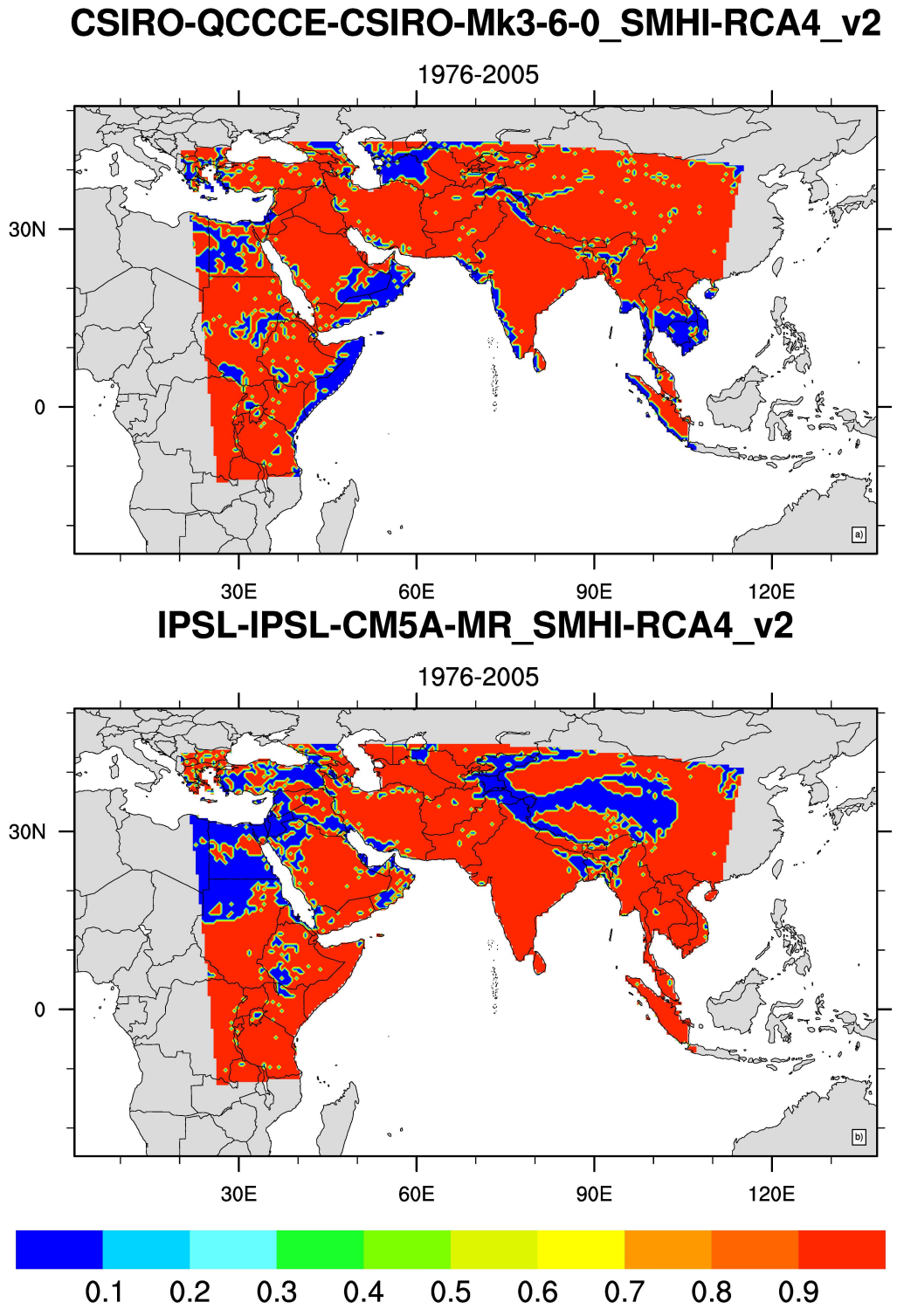

Figure 5.62. The "DSDAEE of the Most Representative Model Combinations in Statistical Methodology 1 in the period between the years 1976 and 2005

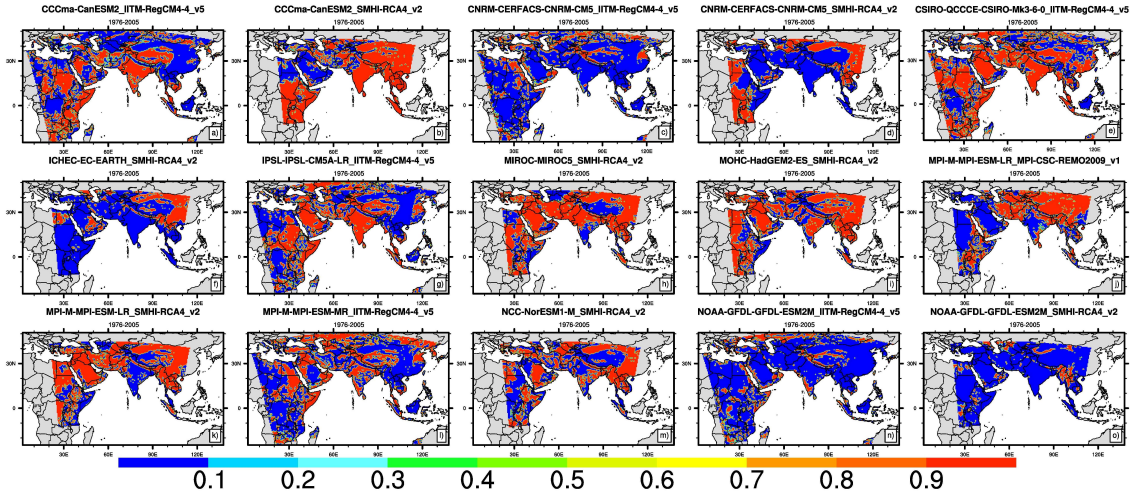

Figure 5.63. The "DSDAEE of the Unrepresentative Model Combinations in Statistical Methodology 1 in the period between the years 1976 and 2005

5.1.22. Application of Statistical Methodology 2 to the Monthly Temperature Data: The Case of West Asia

As shown in Table 5.41 and 5.42, CCCma-RCA4, CSIRO-RCA4 IPSL-RCA4, MIROC-RCA4 and MOHC-RCA4 combinations are the successful ones over West Asia. 70 % of the grid points in CCCma-RCA4 model combination, 82 % of the grid points in CSIRO-RCA4, 76 % of the grid points in IPSL-RCA4, 70 % of the grid points in MIROC-RCA4, and 69 % of the grid points in MOHC-RCA4 are higher than WSDAAE. MPI-RCA4, defining in unrepresentative model combinations, have the maximum percentage with 63 % which are at least 6 % smaller than the model combinations, defined in the most representative ones and it is second in order to simulate the temperature patterns of West Asia.

CCCma-RCA4 originates temperature patterns over observed region very well except Arabian Peninsula, Egypt, Northern Sudan, Eastern Mediterranean Coastal, Iraq, Afghanistan, Pakistan and India border, Chinese western border. CSIRO-RCA4 portrays temperature patterns over observed region very well excluding Somalia, Oman, Vietnam, Kampuchea, Turkmenistan, and eastern India. IPSL-RCA4 is good at rep-

resenting temperature accomplishedly except Arabian Peninsula, Egypt, Northern Sudan, Eastern Mediterranean Coastal, Iraq, Afghanistan, Pakistan and India border, Chinese western border, Turkey and Central China. MIROC-RCA4 indicates featly the temperature design of West Asia except Oman, South-western China, Kazakhstan and Turkmenistan border of Caspian Sea coastal, Egypt, India, Somali and Malaysia. MOHC-RCA4 generates temperature data very well over whole region except Somalia, Red Sea Coastal, Oman, Yemen, Arabian Sea Coastal, south-western India, Malaysia, Central China, Tajikistan, Caspian Sea coastal of Kazakhstan and Eastern Anatolia of Turkey. MPI-RCA4, falling in to unsuccessful model combinations, is good at presenting temperature over region except India, Pakistan, Nepal, Southern China, Caspian Sea coastal of Kazakhstan and Turkmenistan, Indian Ocean coastal of Tanzania, Kenya and Somali. NOAA-RegCM and NOAA-RCA4 is also very unsuccessful and wouldn't be applied to project West Asia temperature (Figure 5.64 and 5.65).

Table 5.41. The coefficients of The Most Representative Models

GCM - RCM Model Combination	**Coefficient**
CCCma-CanESM2-SMHI-RCA4-v2	0.70891
CSIRO-QCCCE-CSIRO-Mk3-6-0-SMHI-RCA4-v2	0.82525
IPSL-IPSL-CM5A-MR-SMHI-RCA4-v2	0.76159
MIROC-MIROC5-SMHI-RCA4-v2	0.70425
MOHC-HadGEM2-ES-SMHI-RCA4-v2	0.69735

5.1.23. Application of Statistical Methodology 3 to the Monthly Temperature Data: The Case of West Asia

As shown in Table 5.43 and 5.44, CSIRO-RegCM, IPSL-RegCM and CSIRO-RCA4 model combinations are the successful ones over West Asia. 38 % of the grid points in CSIRO-RegCM model combination, 33 % of the grid points in IPSL-RegCM, 32 % of the grid points in CSIRO-RCA4 are higher than WSDAAE. IPSL-RCA4, defining in unrepresentative model combinations, have the maximum percentage with 31 % which are at least 1 % smaller than the model combinations, defined in the most representative ones and it is second in order to simulate the temperature patterns of

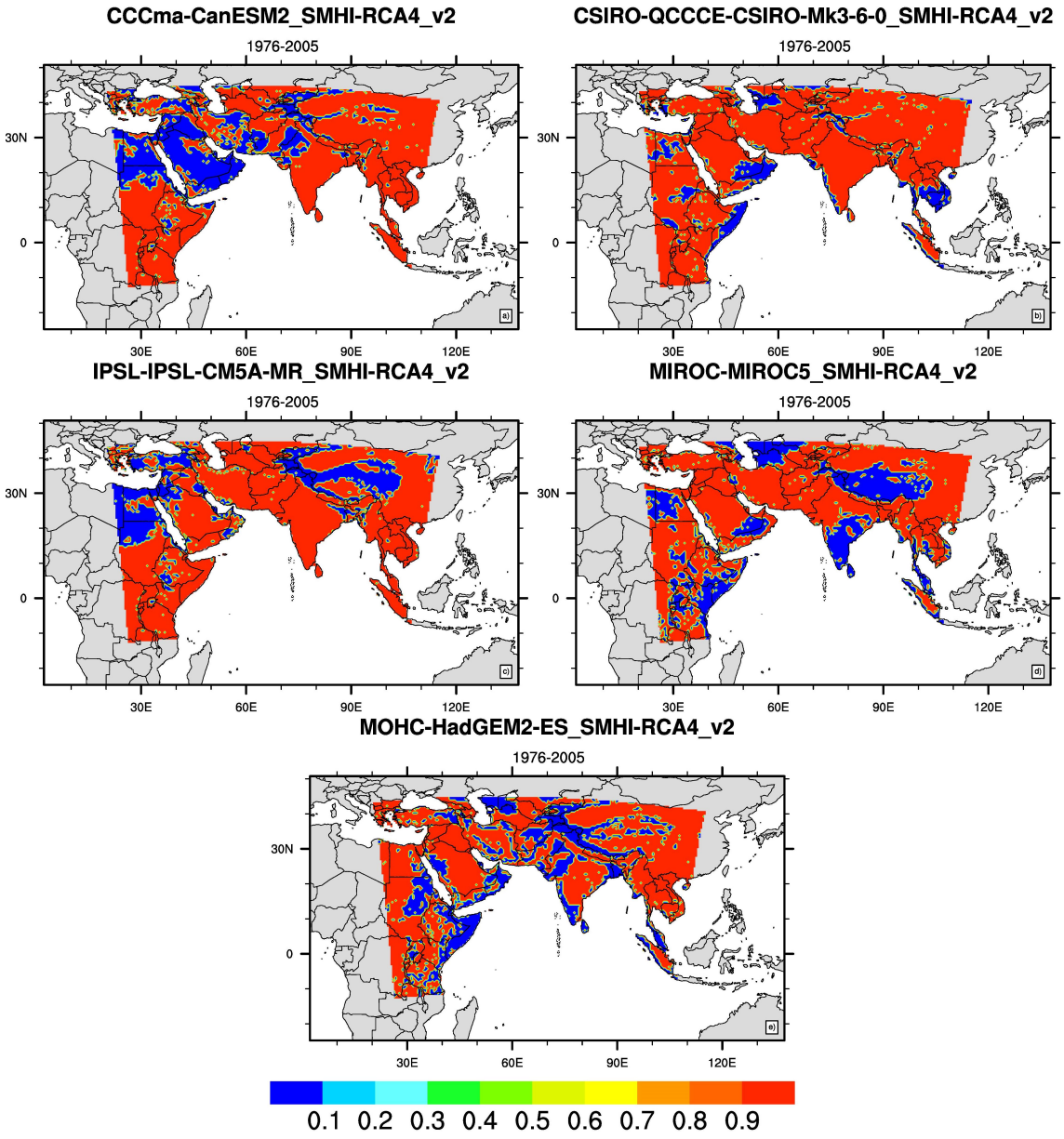

Figure 5.64. The "DSDAEE of the Most Representative Model Combinations in Statistical Methodology 2 in the period between the years 1976 and 2005

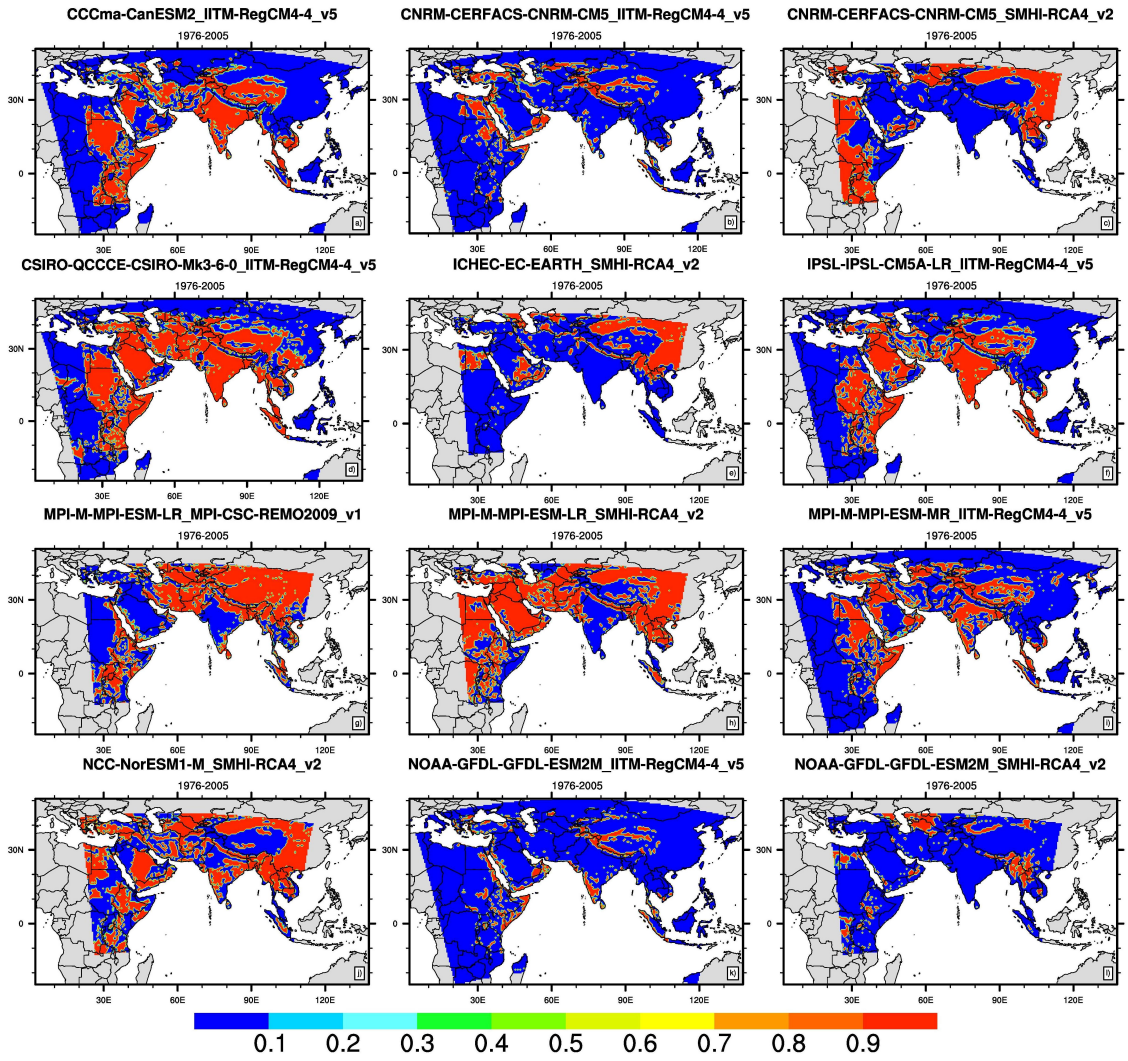

Figure 5.65. The "DSDAEE of the Unrepresentative Model Combinations in Statistical Methodology 2 in the period between the years 1976 and 2005

Table 5.42. The coefficients of The Unrepresentative Models

GCM - RCM Model Combination	**Coefficient**
CCCma-CanESM2-IITM-RegCM4-4-v5	0.30811
CNRM-CERFACS-CNRM-CM5-IITM-RegCM4-4-v5	0.13436
CNRM-CERFACS-CNRM-CM5-SMHI-RCA4-v2	0.38778
CSIRO-QCCCE-CSIRO-Mk3-6-0-IITM-RegCM4-4-v5	0.42670
ICHEC-EC-EARTH-SMHI-RCA4-v2	0.24332
IPSL-IPSL-CM5A-LR-IITM-RegCM4-4-v5	0.31667
MPI-M-MPI-ESM-LR-MPI-CSC-REMO2009-v1	0.53204
MPI-M-MPI-ESM-LR-SMHI-RCA4-v2	0.63402
MPI-M-MPI-ESM-MR-IITM-RegCM4-4-v5	0.25515
NCC-NorESM1-M-SMHI-RCA4-v2	0.50936
NOAA-GFDL-GFDL-ESM2M-IITM-RegCM4-4-v5	0.097685
NOAA-GFDL-GFDL-ESM2M-SMHI-RCA4-v2	0.12424

West Asia.

The majority of the grid points in the region couldn't pass T-test. CSIRO-RegCM is more successful over eastern Arabian Peninsula, Northern Africa, India, Northern Asia and southern part of observed Africa continental. IPSL-RegCM is successful over Western Turkey, Northern Sudan and India, southern Egypt, eastern China, Turkmenistan, Uzbekistan and Tajikistan. CSIRO-RCA4 produces comparably good results over Red Sea coastal and interior lands of Eastern Africa, Saudi Arabia, Northern India and Northern Asia (Figure 5.66 and 5.67).

Table 5.43. The coefficients of The Most Representative Models

GCM - RCM Model Combination	**Coefficient**
CSIRO-QCCCE-CSIRO-Mk3-6-0-IITM-RegCM4-4-v5	0.38316
CSIRO-QCCCE-CSIRO-Mk3-6-0-SMHI-RCA4-v2	0.32945
IPSL-IPSL-CM5A-LR-IITM-RegCM4-4-v5	0.33490

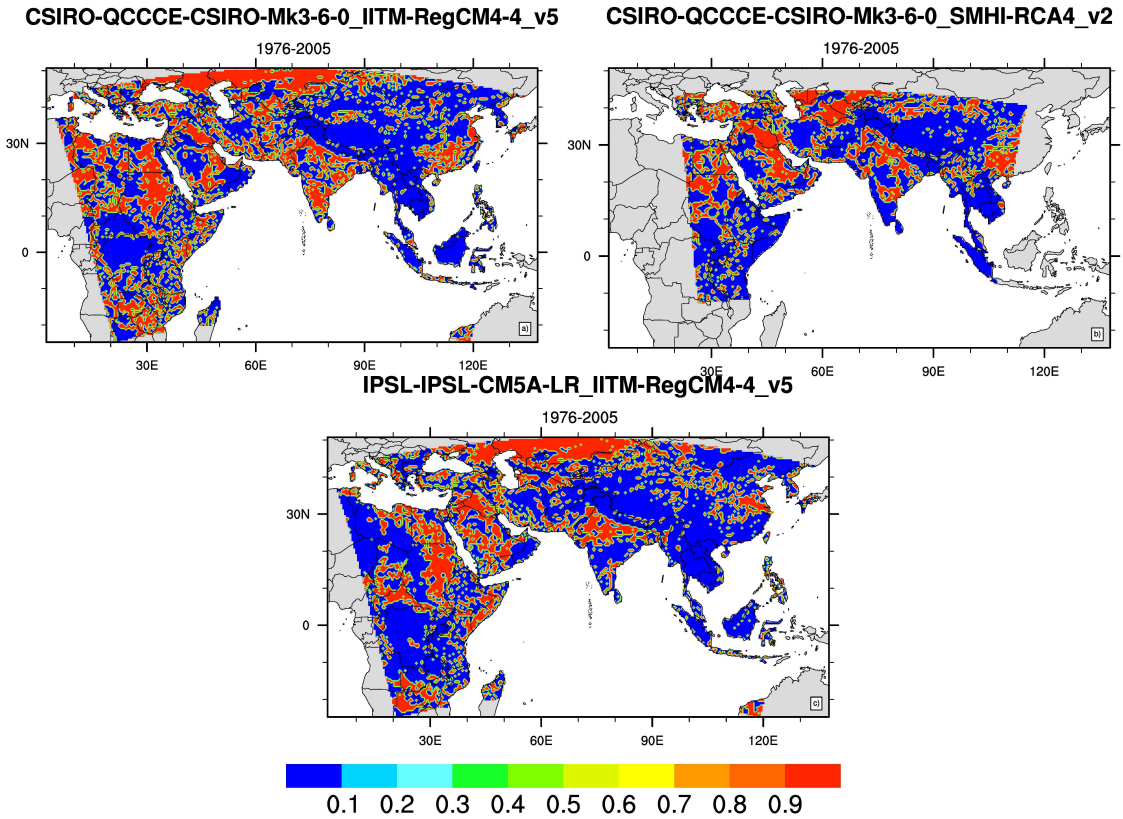

Figure 5.66. The "DSDAEE of the Most Representative Model Combinations in Statistical Methodology 3 in the period between the years 1976 and 2005

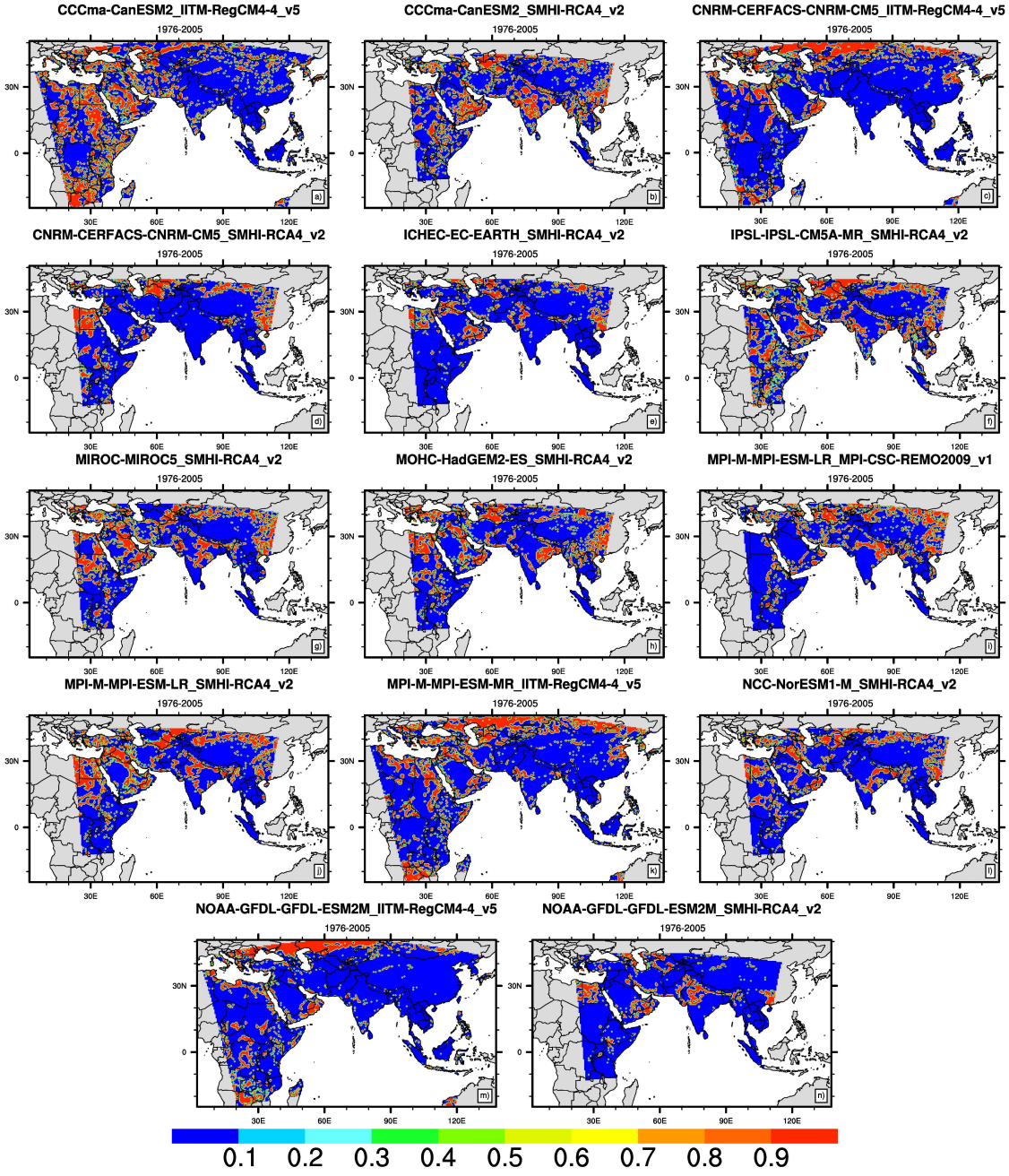

Figure 5.67. The "DSDAEE of the Unrepresentative Model Combinations in Statistical Methodology 3 in the period between the years 1976 and 2005

Table 5.44. The coefficients of The Unrepresentative Models

GCM - RCM Model Combination	Coefficient
CCCma-CanESM2-IITM-RegCM4-4-v5	0.28947
CCCma-CanESM2-SMHI-RCA4-v2	0.29333
CNRM-CERFACS-CNRM-CM5-IITM-RegCM4-4-v5	0.22180
CNRM-CERFACS-CNRM-CM5-SMHI-RCA4-v2	0.18981
ICHEC-EC-EARTH-SMHI-RCA4-v2	0.15062
IPSL-IPSL-CM5A-MR-SMHI-RCA4-v2	0.31896
MIROC-MIROC5-SMHI-RCA4-v2	0.27927
MOHC-HadGEM2-ES-SMHI-RCA4-v2	0.26521
MPI-M-MPI-ESM-LR-MPI-CSC-REMO2009-v1	0.23132
MPI-M-MPI-ESM-LR-SMHI-RCA4-v2	0.27586
MPI-M-MPI-ESM-MR-IITM-RegCM4-4-v5	0.25581
NCC-NorESM1-M-SMHI-RCA4-v2	0.21528
NOAA-GFDL-GFDL-ESM2M-IITM-RegCM4-4-v5	0.17826
NOAA-GFDL-GFDL-ESM2M-SMHI-RCA4-v2	0.11658

5.1.24. Application of Statistical Methodology 4 to the Monthly Temperature Data: The Case of West Asia

As shown in Table 5.45 and 5.46, CSIRO-RegCM and IPSL-RegCM model combinations are the successful ones over West Asia. 39 % of the grid points in CSIRO-RegCM model combination and 34 % of the grid points in IPSL-RegCM are higher than WSDAAE. IPSL-RCA4, defining in unrepresentative model combinations, have the maximum percentage with 33 % which are at least 1 % smaller than the model combinations, defined in the most representative ones and it is second in order to simulate the temperature patterns of West Asia.

The majority of the grid points in the region couldn't pass T-test. CSIRO-RegCM is more successful over eastern and northern Arabian Peninsula, Northern Africa, India, Northern Asia and southern part of observed Africa continental. IPSL-RegCM is successful over eastern Africa, Somali and Northern Asia (Figure 5.68 and

5.69).

Table 5.45. The coefficients of The Most Representative Models

GCM - RCM Model Combination	Coefficient
CSIRO-QCCCE-CSIRO-Mk3-6-0-IITM-RegCM4-4-v5	0.39407
IPSL-IPSL-CM5A-LR-IITM-RegCM4-4-v5	0.34761

Table 5.46. The coefficients of The Unrepresentative Models

GCM - RCM Model Combination	Coefficient
CCCma-CanESM2-IITM-RegCM4-4-v5	0.31149
CCCma-CanESM2-SMHI-RCA4-v2	0.31314
CNRM-CERFACS-CNRM-CM5-IITM-RegCM4-4-v5	0.23281
CNRM-CERFACS-CNRM-CM5-SMHI-RCA4-v2	0.19364
CSIRO-QCCCE-CSIRO-Mk3-6-0-SMHI-RCA4-v2	0.32820
ICHEC-EC-EARTH-historical-r12i1p1-SMHI-RCA4-v2	0.15087
IPSL-IPSL-CM5A-MR-SMHI-RCA4-v2	0.33486
MIROC-MIROC5-SMHI-RCA4-v2	0.29117
MOHC-HadGEM2-ES-SMHI-RCA4-v2	0.26696
MPI-M-MPI-ESM-LR-MPI-CSC-REMO2009-v1	0.23748
MPI-M-MPI-ESM-LR-SMHI-RCA4-v2	0.28118
MPI-M-MPI-ESM-MR-IITM-RegCM4-4-v5	0.27267
NCC-NorESM1-M-SMHI-RCA4-v2	0.22418
NOAA-GFDL-GFDL-ESM2M-IITM-RegCM4-4-v5	0.19112
NOAA-GFDL-GFDL-ESM2M-SMHI-RCA4-v2	0.12366

5.1.25. Evaluation of Statistical Methodologies Over West Asia Temperature

MPI is most frequently applied GCMs over South Asia in CORDEX Project and CSIRO is the most successful one overall Central America is taken consideration. RCA4 is the applied and successful RCM, using in the GCM-RCM model combinations in simulations over West Asia it can't be concluded that using RCA4 as RCM is useful or not over this domain. Hence, simulating CSIRO as GCM and using it's outcomes

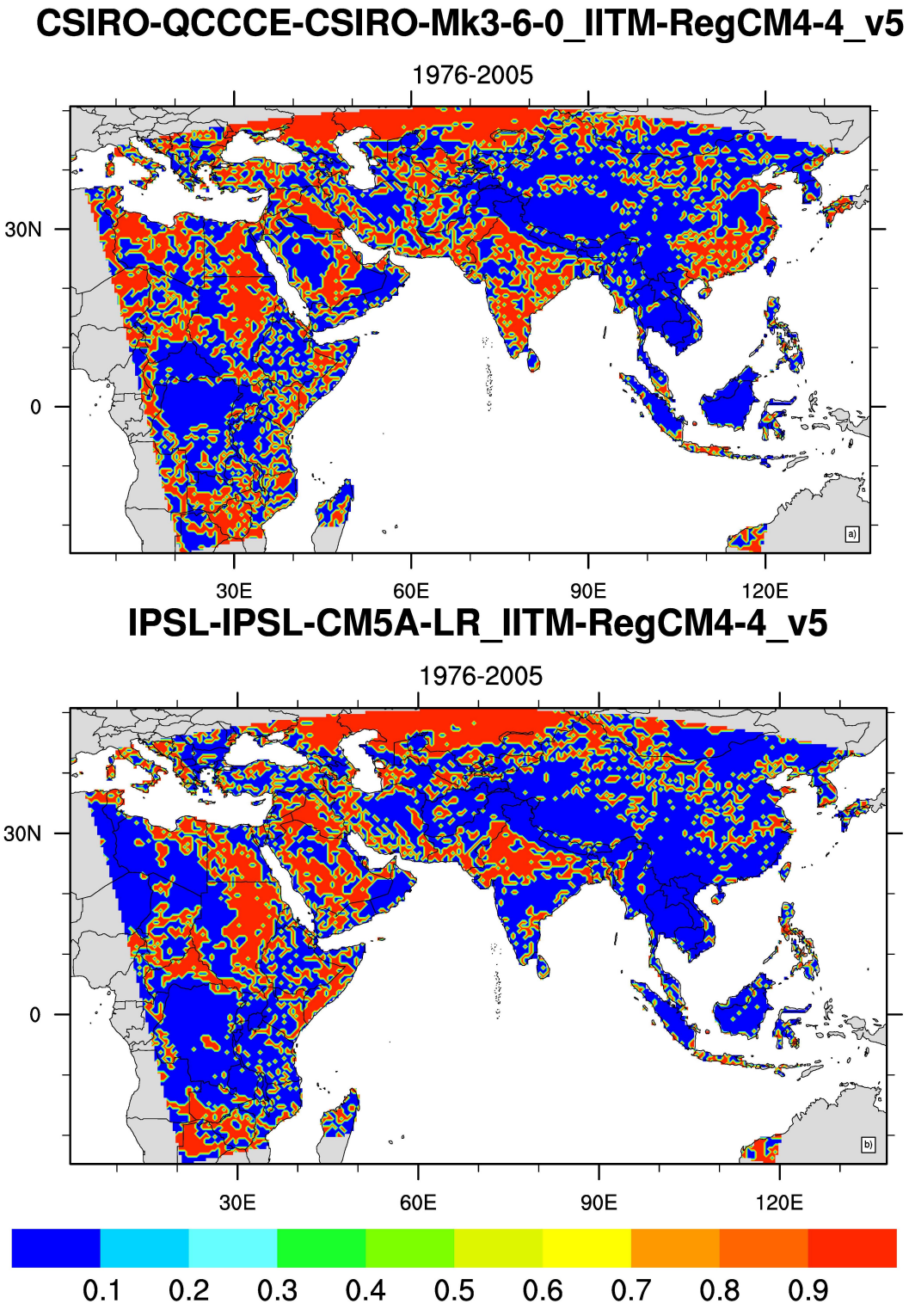

Figure 5.68. The "DSDAEE of the Most Representative Model Combinations in Statistical Methodology 4 in the period between the years 1976 and 2005

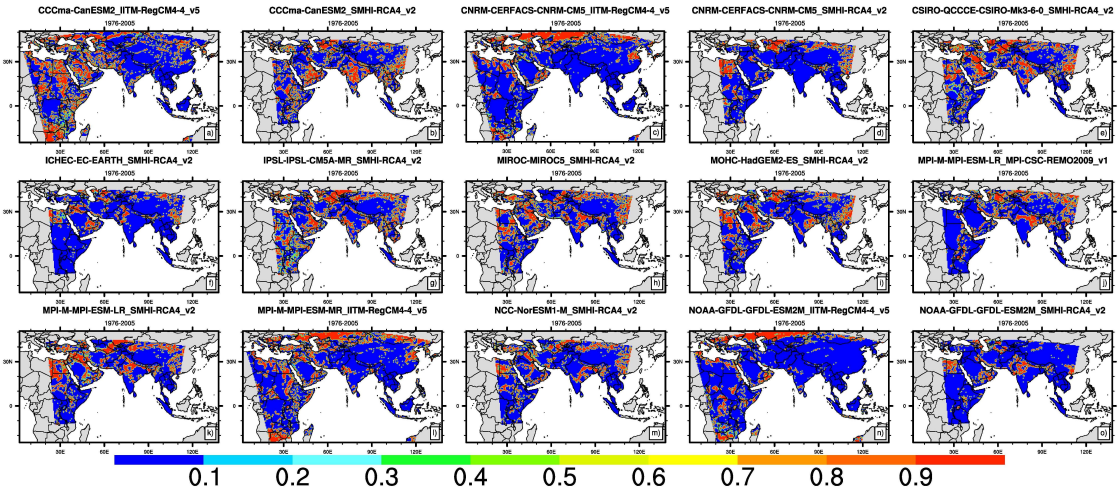

Figure 5.69. The "DSDAEE of the Unrepresentative Model Combinations in Statistical Methodology 4 in the period between the years 1976 and 2005

as initial conditions- boundary conditions in the RCA4 is the most convenient choice to project overall West Asia temperature (Table 5.47).

5.1.26. Overall Evoluation Application of Statistical Methodologies

There are mainly four Methodologies (each GCM-RCM model combination is used for four times over a region) applied over five regions in this thesis. For example, it is shown that CSIRO as a GCM is used for 24 times. This amount corresponds to six model combinations using four times for each methodologies. It seems that 12 of these applications are successful. Similarly, CNRM is applied CSIRO is the most successful GCM and MPI is the most applied one over these five regions (5.48). CLM is the most successful RCM and RCA4 is the most applied regional climate model. Hence, it can be suggested that using CSIRO-CLM (CSIRO as GCM and CLM as RCM) model combination is one of the most meaningful and convenient one to simulate the temperature in climate studies (Table 5.49).

Table 5.47. The Amount of Total and successful GCM – RCMs

GCM	**TOTAL**	**successful**	**RCM**	**TOTAL**	**successful**
CCCma	8	1 (12.5 %)	REMO	4	0
CNRM	8	0	RegCM	24	4(16.6 %)
CSIRO	8	5(62.5 %)	RCA4		
ICHEC	4	0			
IPSL	8	4 (50 %)			
MIROC	4	1 (25 %)			
MOHC	4	1 (25 %)			
MPI	12	0			
NCC	4	0			
NOAA	8	0			

Table 5.48. The Amount of Total and successful GCMs

GCM	**TOTAL**	**successful**	**PERCENTAGE**
CSIRO	24	12	50
CCCma	24	9	37.5
MPI	64	21	32.81
MIROC	28	8	28.57
MOHC	48	11	22.92
IPSL	32	7	21.88
NCC	24	2	8.33
CNRM	40	0	0
ICHEC	56	0	0
NOAA	28	0	0

Table 5.49. The Amount of Total and successful RCMs

RCM	TOTAL	successful	PERCENTAGE
CLM	40	13	32.5
REMO	36	9	25
UQAM	8	2	25
RCA4	200	39	19.5
REGCM	40	7	17.5
CNRM	4	0	0
DMI	12	0	0
HMS	4	0	0
IPSL	4	0	0
KNMI	24	0	0
RMIB	4	0	0

5.2. Future Projection of Temperature

5.2.1. Future Projection of Temperature: The Case for Europe

In the following five sections, the difference of the average temperature between 2050s / 2080s (in the period between 2036 and 2065 / 2066 and 2095) and reference period (between 1976 and 2005) is calculated in each season with respect to RCP 2.6, RCP 4.5 and RCP 8.5. The outputs of RCPs (2.6, RCP 4.5 and RCP 8.5) are obtained by forming ensemble with respect to Test7 of Methodology 3 and using better representative model combinations.

In the winter season in 2050s, there isn't a serious temperature increase over Western Europe with respect to the increase over the remaining part of the Europe with respect to RCP 2.6, RCP 4.5 and RCP 8.5 scenario. Moreover, a small decline up to -0.4°C in temperature over Ireland is estimated. Decrease in temperature scatters through the Portugal with respect to RCP 8.5. In the same scenario, the smallness in alteration spans through whole Europe and North Africa. East-northern Russia is the hotspot in Europe. The most augmentation in temperature is seen over this

region in winter, spring and autumn seasons with respect to all of the Representative Concentration Pathways. Scandinavian countries come in second order in the intensity of the increase in temperature. There has been slightly small increase over Central and Northern Europe. The augmentation in temperature increases across the southern Europe and Northern Africa and pass 3°C.

In 2080s, the increase in the temperature over especially Northern Europe reaches up to 5°C except the summer season. A small decline in temperature is expected over United Kingdom in winter season. Mediterranean coastal is the second most risky area in especially spring and summer season with regards to temperature increases (Figure 5.70 and 5.71).

5.2.2. Future Projection of Temperature: The Case for Africa

Over Africa, the alteration of the temperature exhibits four main patterns, each being particular to one of four sub-regions.These subregions are Northern Africa (NA), Sub-Saharan Africa (SSA), Central Africa (CA) and Southern Africa (SA). In 2050s, augmentation in temperature is up to 2.1°C over NA and SA in the winter season. It is estimated that the increase in temperature reaches to 1.5°C over SSA and CA. In spring season, increment in temperature mounts up to 2°C over most of the Africa. It is more surplus over SSA than the remaining part of the observed area especially with respect to RCP 8.5 scenario. In summer season, NA and SSA are the regions which are adversely affected from temperature rise since it isn't smaller than 1.5°C. It is smaller than this amount over SA and CA with respect to RCP 4.5 scenario. Summer and autumn seasons are the hotspot since the most excrescence temperature rise in 2050s is seen in this season over almost every sub regions with respect to all of the Representative Concentration Pathways. It even reaches up to 2.5°C over SSA, SA and NA in RCP 2.6. Western SSA, SA and Arabian Peninsula are the regions where temperature will be at least 3°C more than today in 2050s. The distribution of the temperature alteration patterns is sharper than the one in 2080s. The amount of the rise of temperature changes in this period is more than the range between 0.5°C and 2.5°C than 2050s (Figure 5.72 and 5.73)..

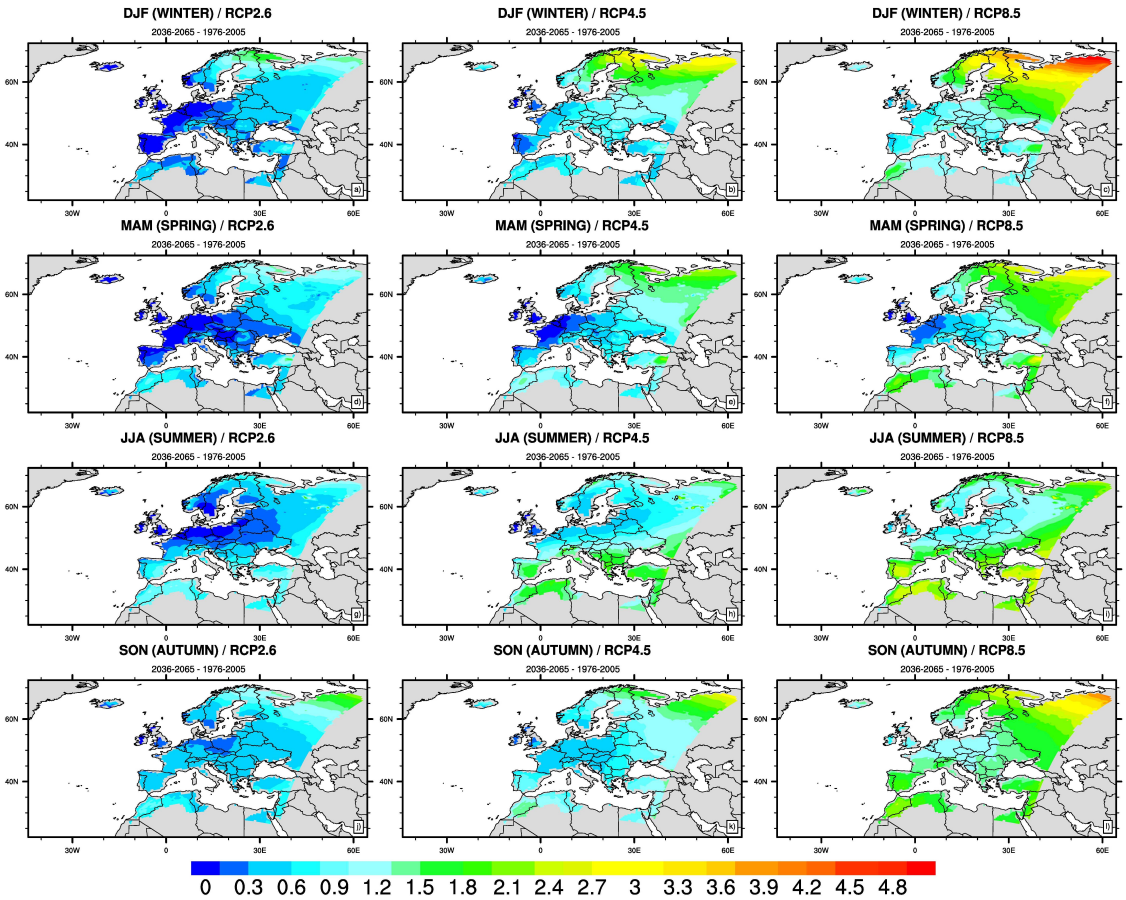

Figure 5.70. The map of spatial distribution of differences of monthly temperature averages of Europe region in seasons (Winter; Spring; Summer and Autumn) for 2050s (2036-2065 - 1976 – 2005) according to RCP 2.6, RCP 4.5 and RCP 8.5 Scenario

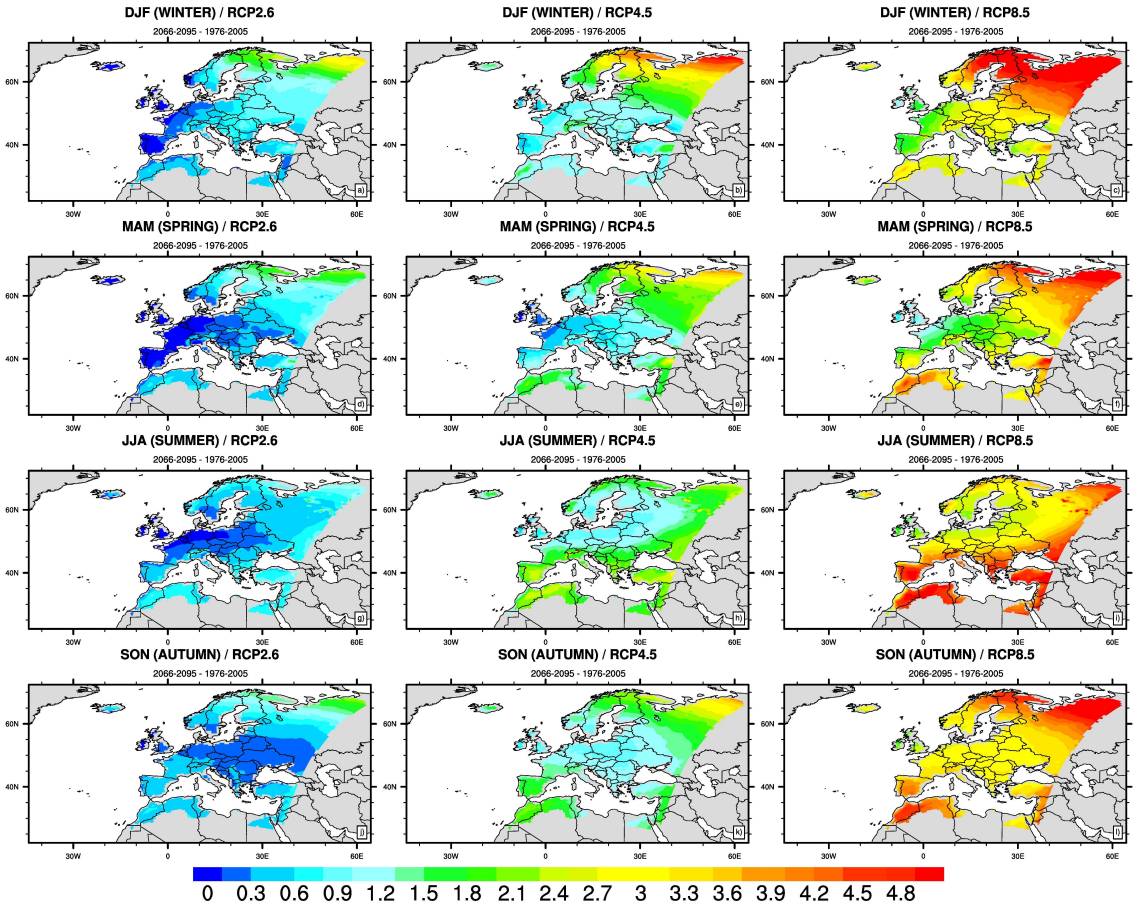

Figure 5.71. The map of spatial distribution of differences of monthly temperature averages of Europe region in seasons (Winter; Spring; Summer and Autumn) for 2080s (2066-2095 - 1976 – 2005) according to RCP 2.6 , RCP 4.5 and RCP 8.5 Scenario

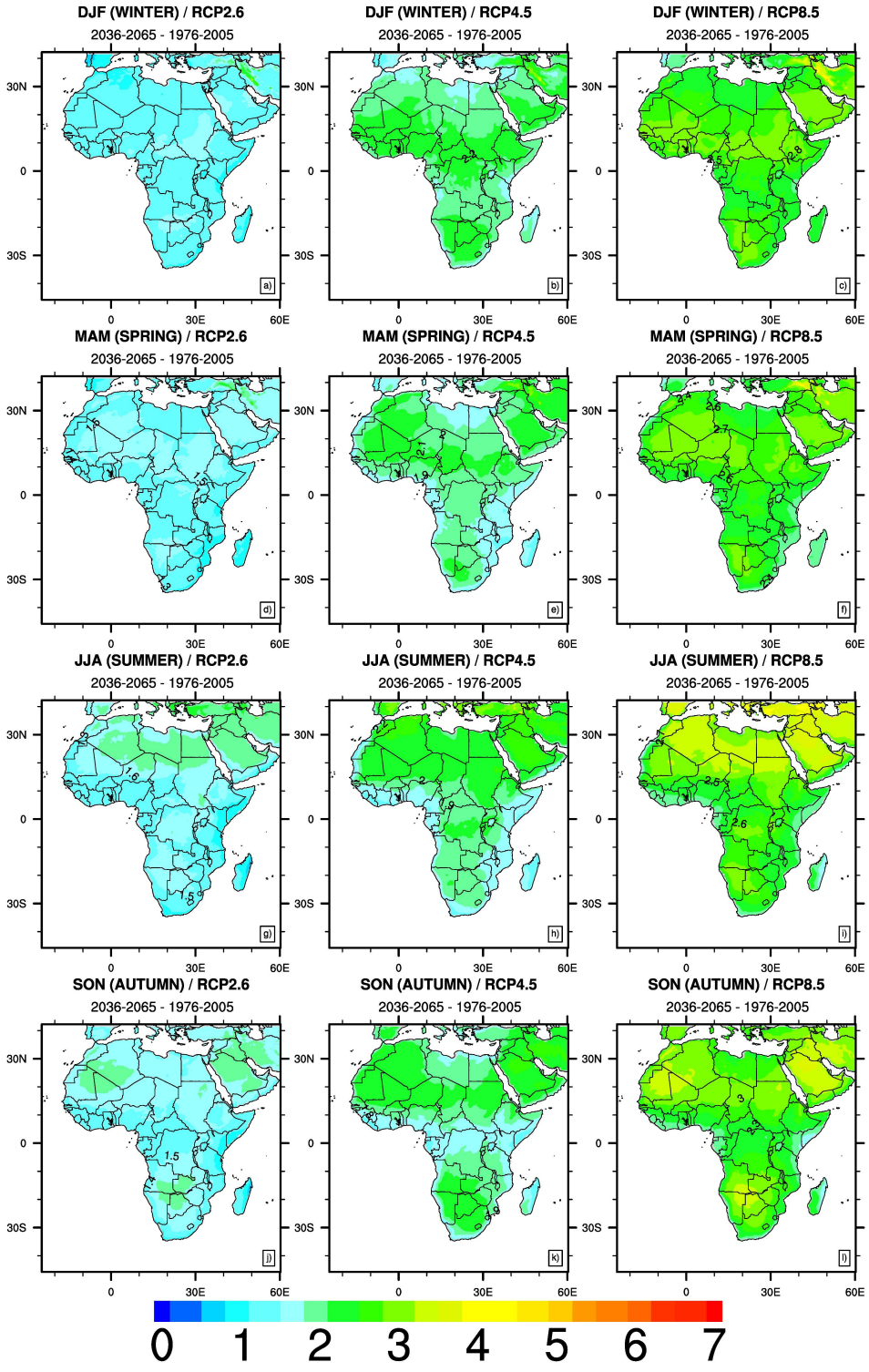

Figure 5.72. The map of spatial distribution of differences of monthly temperature averages of Africa region in seasons (Winter; Spring; Summer and Autumn) for 2050s (2036-2065 - 1976 – 2005) according to RCP 2.6, RCP 4.5 and RCP 8.5 Scenario

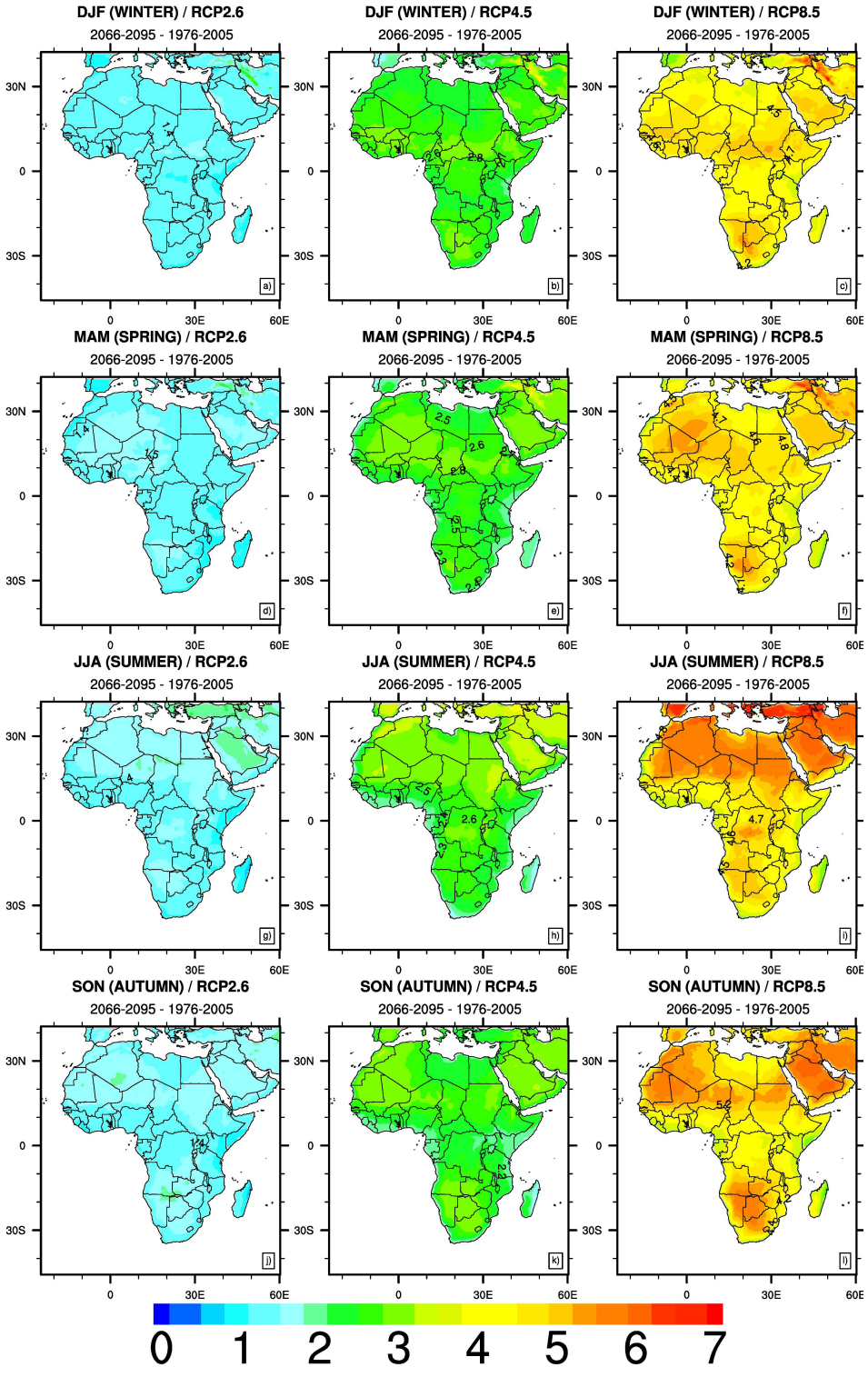

Figure 5.73. The map of spatial distribution of differences of monthly temperature averages of Africa region in seasons (Winter; Spring; Summer and Autumn) for 2080s (2066-2095 - 1976 – 2005) according to RCP 2.6 , RCP 4.5 and RCP 8.5 Scenario

5.2.3. Future Projection of Temperature: The Case for Central America

In the winter season, the most seen increases can be seen in the Northern part of the observed area. It reaches up to 4°C in both 2050s and 2080s. In the remaining part, it changes between 1°C (in Brazil – Peru border with respect to RCP 2.6 scenario) and 2.8°C (over Southern Colombia and North-western Brazil with respect to RCP 4.5 and RCP 8.5 scenario). In the spring, the patterns of the temperature differences are very similar to the one in winter. Florida, Georgia and Colombia coastal, Colombia-Brazil-Peru border feel less temperature increase (1.6°C) with respect to RCP 2.6 scenario. In spring season, the augmentation in temperature over the continent of South America with respect to RCP 4.5 is visibly bigger than the one with respect to RCP 2.6 scenario. In summer season, the rise in temperature reaches up to 4°C especially over the observed part of South America. The smallest elevation can be seen over Guetelema with respect to RCP 2.6 scenario. On the other hand, the difference between the temperature of 2050s and reference period will not be smaller than 1°C except RCP 2.6. The augmentation in the northern part of the observed are will be higher than the one over Central part of the observed domain. The distribution of temperature increase in 2080s is approximately 2.7°C with respect to RCP 4.5 and nearly 5°C with respect to RCP 8.5. The overall temperature increase in 2080s is approximately 1°C higher than the one in 2050s (Figure 5.74 and 5.75).

5.2.4. Future Projection of Temperature: The Case for South America

According to our observations over South America, the region splits into two main subregions. These arethe domains lying above and below of the Argentina-Brazil border. The augmentation in temperature reaches up to 2°C in the northern part (NSA) in winter season with respect to RCP 4.5 and RCP 8.5. The rise in temperature difference between 2050s and reference period descends through the southern part (SSA) and the temperature rise is nearly 1.2°C. The temperature increases up to 2.6°C in the Colombia-Brazil border. In the spring season, the amount of the temperature increase differs from $1-1.5$°C in RCP 2.6 scenario to $4-5$°C in RCP 8.5 scenario over the NSA. In the south of the SSA, it has the smallest value and 1°C and reaches up to

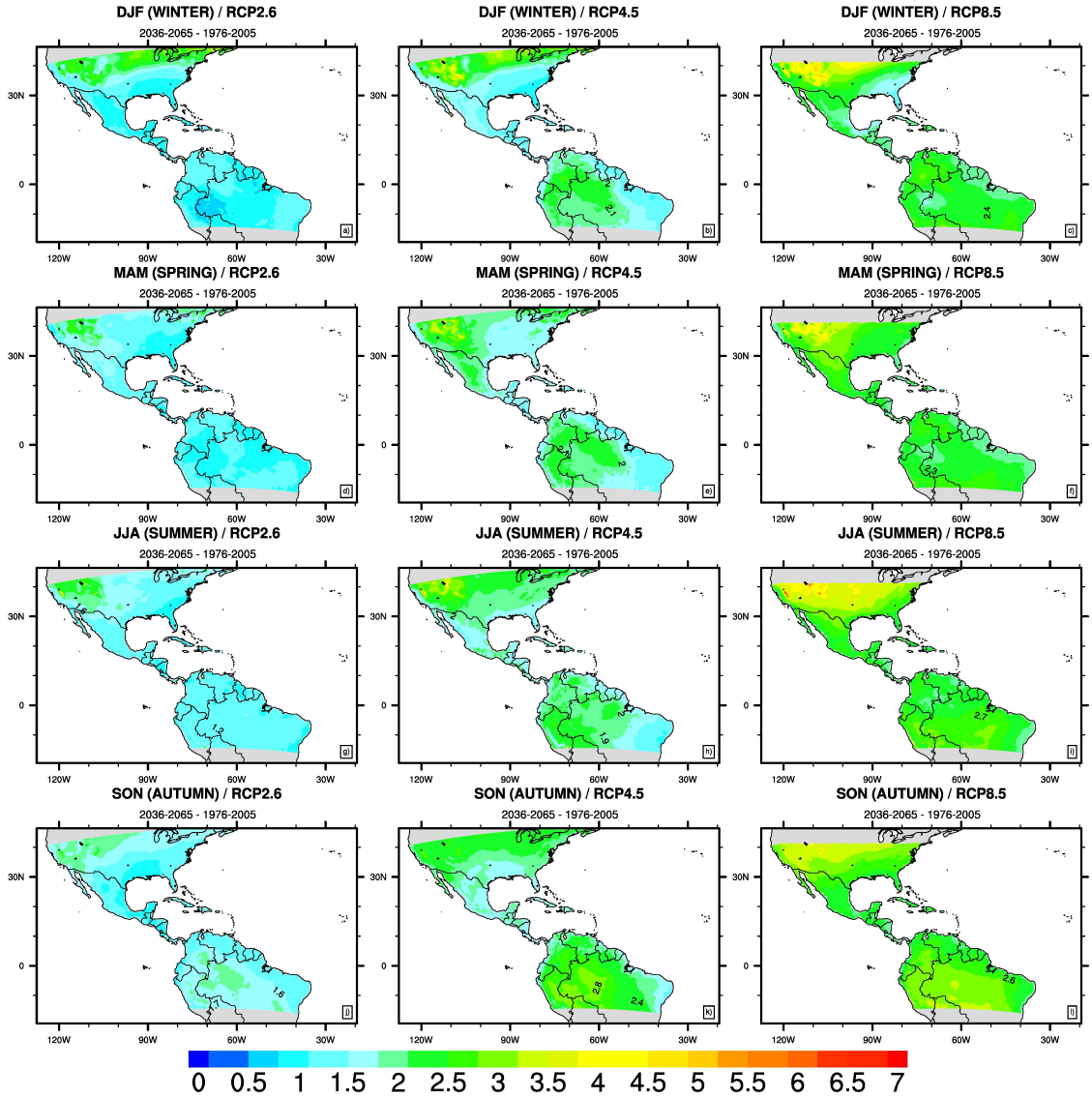

Figure 5.74. The map of spatial distribution of differences of monthly temperature averages of Central America region in seasons (Winter; Spring; Summer and Autumn) for 2050s (2036-2065 - 1976 – 2005) according to RCP 2.6, RCP 4.5 and RCP 8.5 Scenario

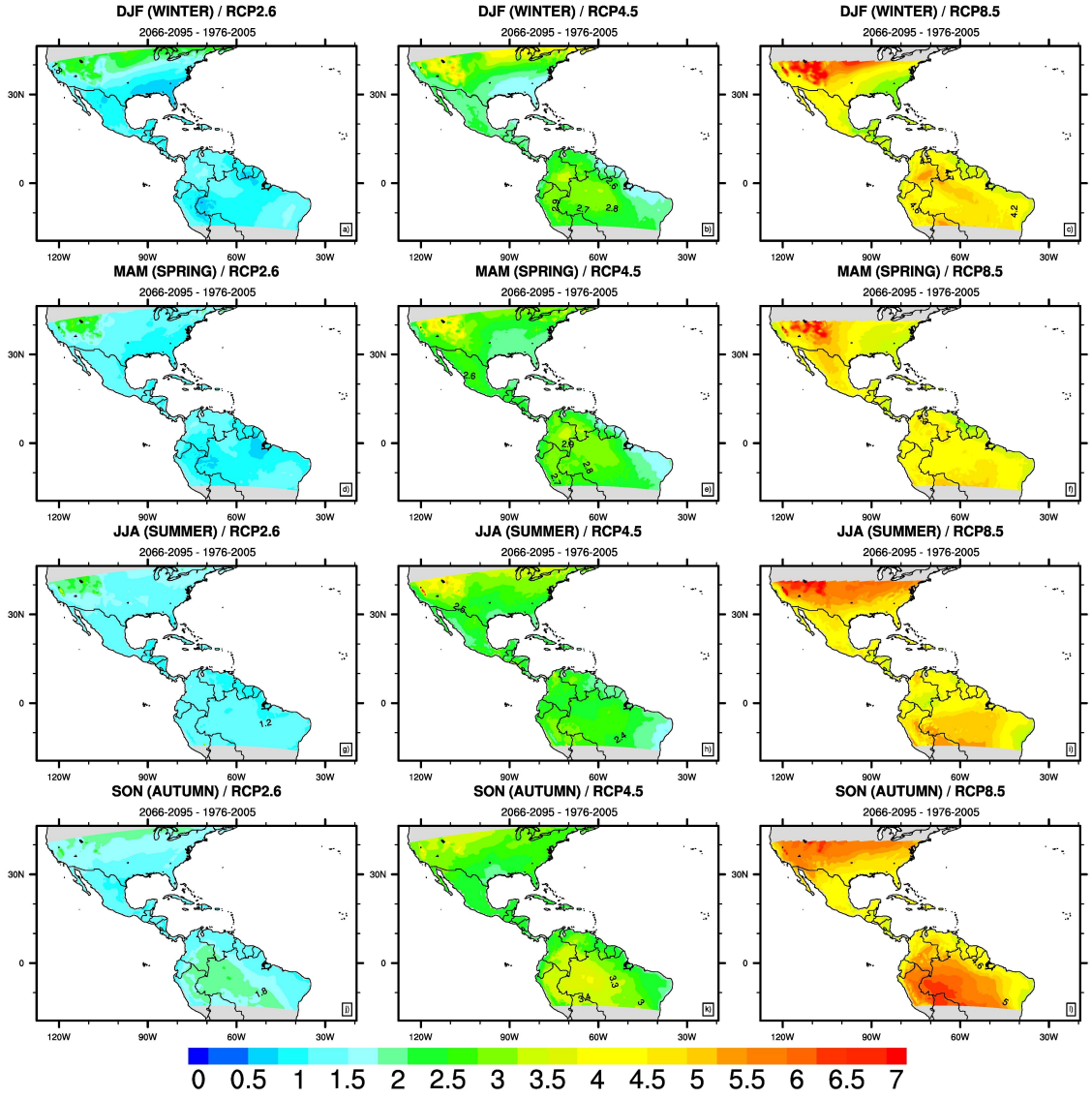

Figure 5.75. The map of spatial distribution of differences of monthly temperature averages of Central America region in seasons (Winter; Spring; Summer and Autumn) for 2080s (2066-2095 - 1976 – 2005) according to RCP 2.6 , RCP 4.5 and RCP 8.5 Scenario

2°C just above the Argentina. In the summer season, the general temperature variation tendency is same with the other seasons over SSA and the amount of variation is exactly same. On the other hand, the temperature rise is approximately 0.5°C smaller than the one in autumn season. It elevates to 3°C in the center of NSA. Autumn season is in the first order in the sense of the temperature augmentation. It is estimated that the temperature of 2050s will be $2 - 3.5$°C higher than the reference period especially over NSA. The alteration in the level of temperature over SSA is very similar to the aforementioned season. The patterns of temperature augmentation in 2080s are very similar to the one in 2050s. The main difference is in the amount. The temperature rise in 2080s is higher than the one in 2050s (Figure 5.76 and 5.77).

5.2.5. Future Projection of Temperature: The Case for West Asia

There are various sub regions in West Asia. In winter, there has been at least 1°C temperature increase according to RCP 2.6 scenario. This amount rises to the 2.5°C over western borders of Chına and also 3°C over the southern China. The western Turkey, Syria coastal, Indonesia, Vietnam, Sri Lanka and south-eastern coastal of India and Tanzania coastal are the ones where temperature rises (approximately 0.6°C) are smaller than the remaining part of the observed region with respect to RCP 4.5 and RCP 8.5. The difference between 2050s and reference period is more than 4°C over the borders of south- western China. In spring season, the raise of temperature in spring season is nearly $1.5 - 2$°C more than the one in winter season. Afghanistan and the countries enclosure Afghanistan are the most risky one in the sense of the augmentation in temperature since this augmentation will reach up to 5°C. In general the northern part of the West Asia is in more danger than the southern part with regards to adverse effects of temperature increment. In summer, there isn't a significant difference between the temperature outcomes of Representative Concentration Pathways. Temperature augmentation in 2050s will be nearly 3°C over especially north-western part of the domain and it isn't smaller than 1°C over the remaining part of the observed area. In autumn, temperature increase across the western china border is sharper than the remaining part. Temperature augmentation reaches up to 6°C over this region and

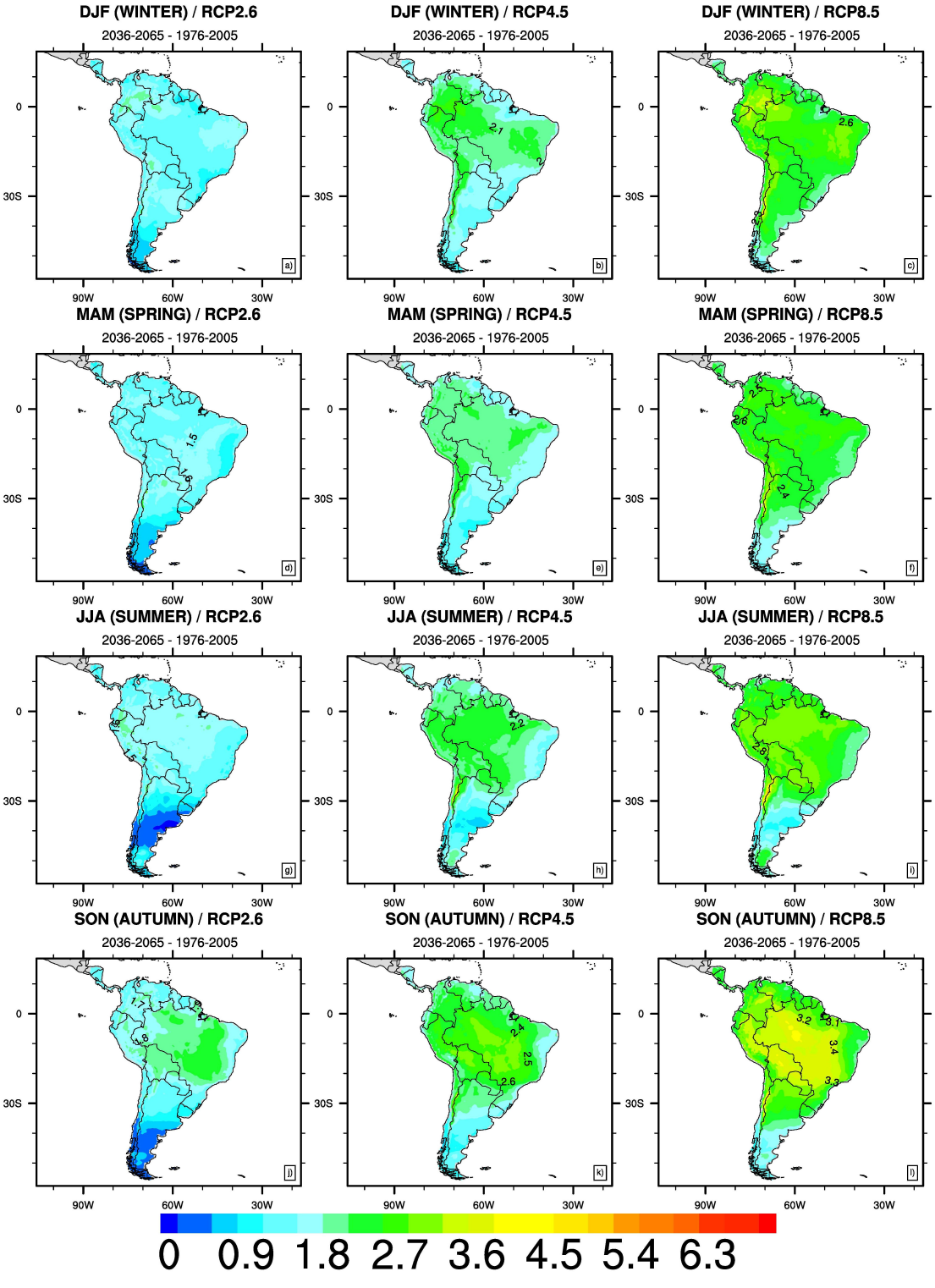

Figure 5.76. The map of spatial distribution of differences of monthly temperature averages of South America region in seasons (Winter; Spring; Summer and Autumn) for 2050s (2036-2065 - 1976 – 2005) according to RCP 2.6, RCP 4.5 and RCP 8.5 Scenario

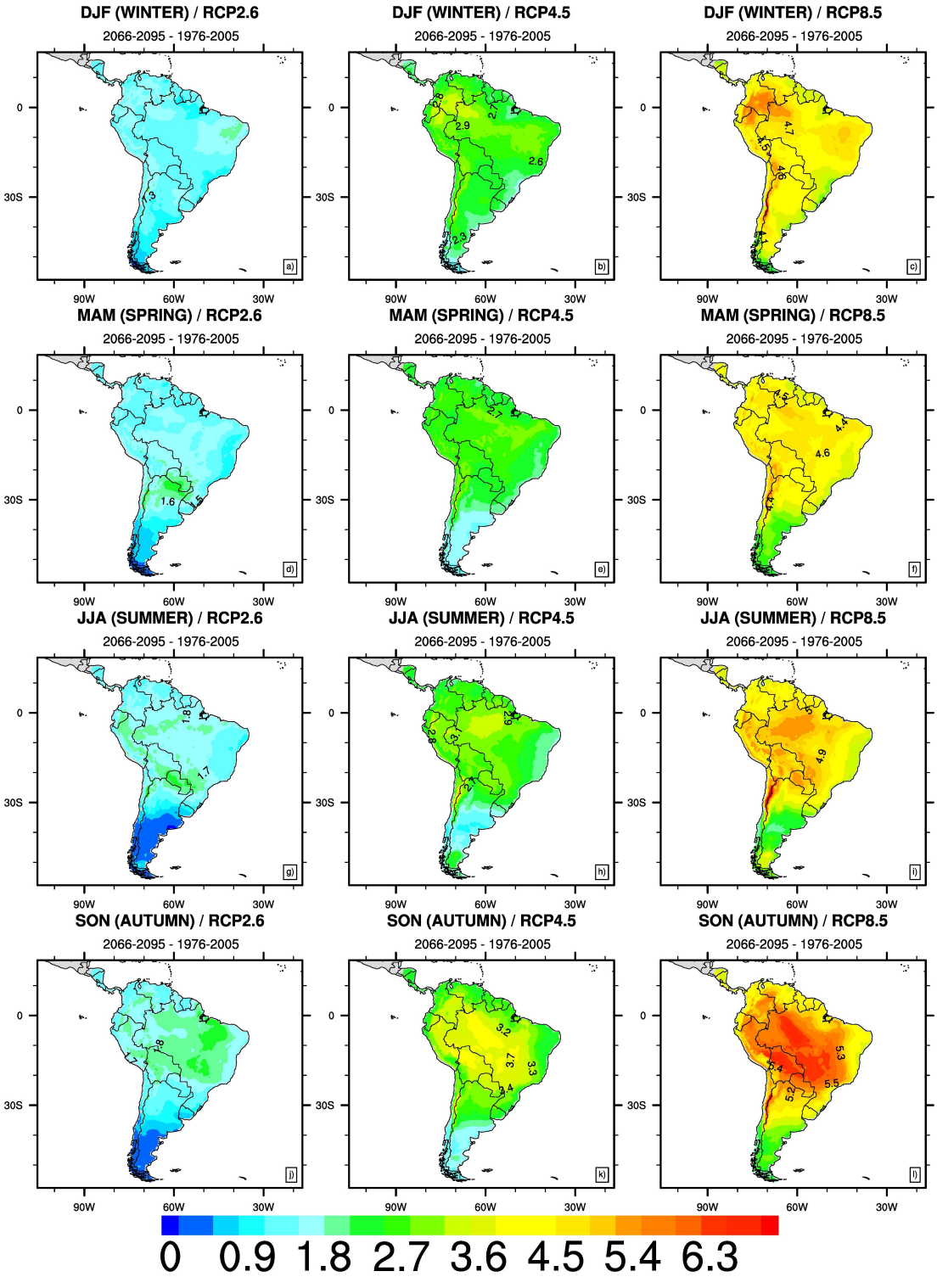

Figure 5.77. The map of spatial distribution of differences of monthly temperature averages of South America region in seasons (Winter; Spring; Summer and Autumn) for 2080s (2066-2095 - 1976 – 2005) according to RCP 2.6 , RCP 4.5 and RCP 8.5 Scenario

southern Iraq, northern Arabia and southern China are second in order with regards to temperature rise. It is forecasted that the temperature of these regions will be at least 4.5°C warmer than today. India, Somali, Malaysia, Indonesia are the regions in which minimum temperatures of the observed domain are estimated. In 2080s, there isn't a significant change in the patterns of temperature patterns. On the other hand, it is estimated that the temperature in 2080s will be approximately 1.5°C higher than the one in 2050s (Figure 5.78 and 5.79).

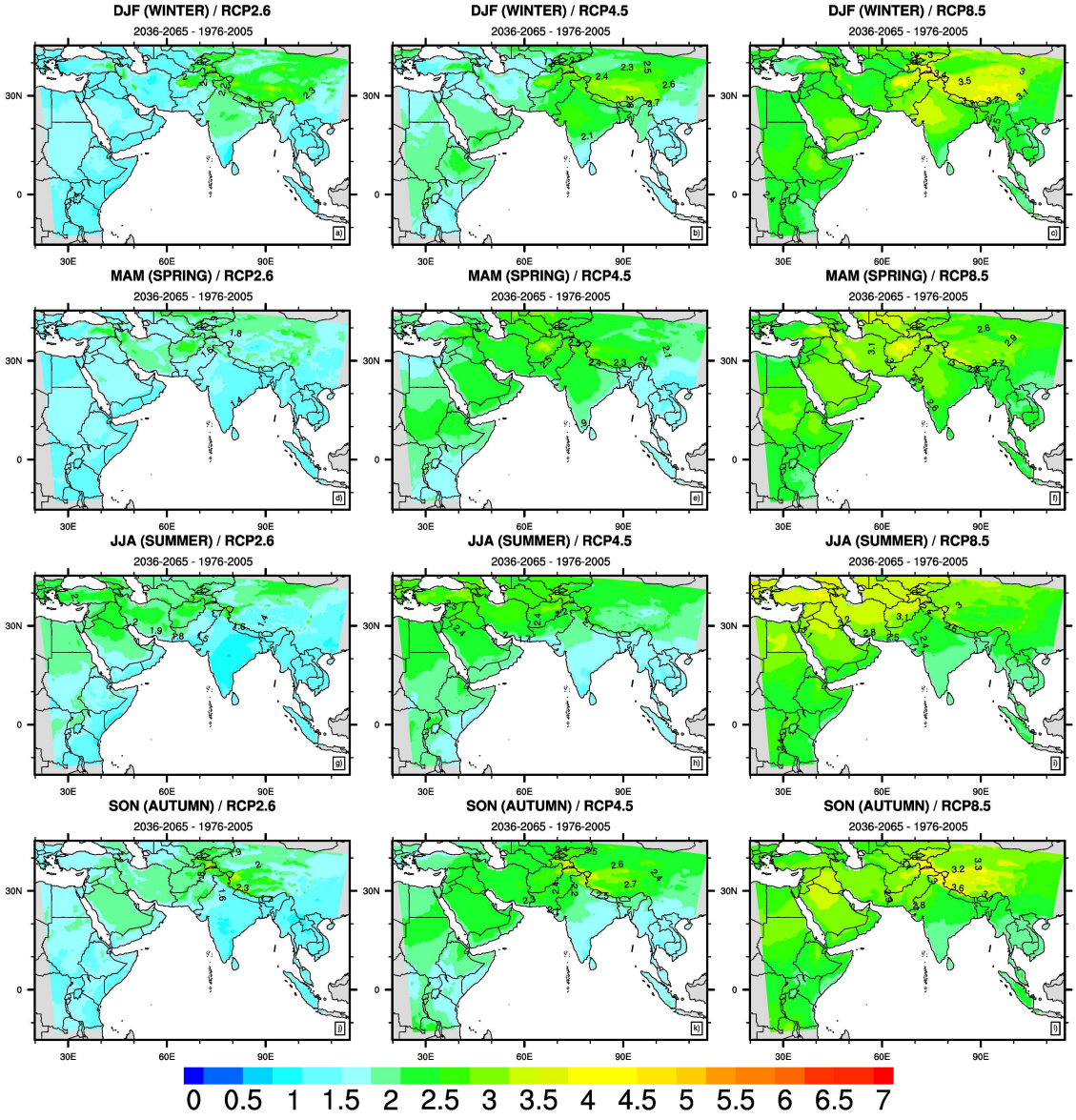

Figure 5.78. The map of spatial distribution of differences of monthly temperature averages of West Asia region in seasons (Winter; Spring; Summer and Autumn) for 2050s (2036-2065 - 1976 – 2005) according to RCP 2.6, RCP 4.5 and RCP 8.5 Scenario

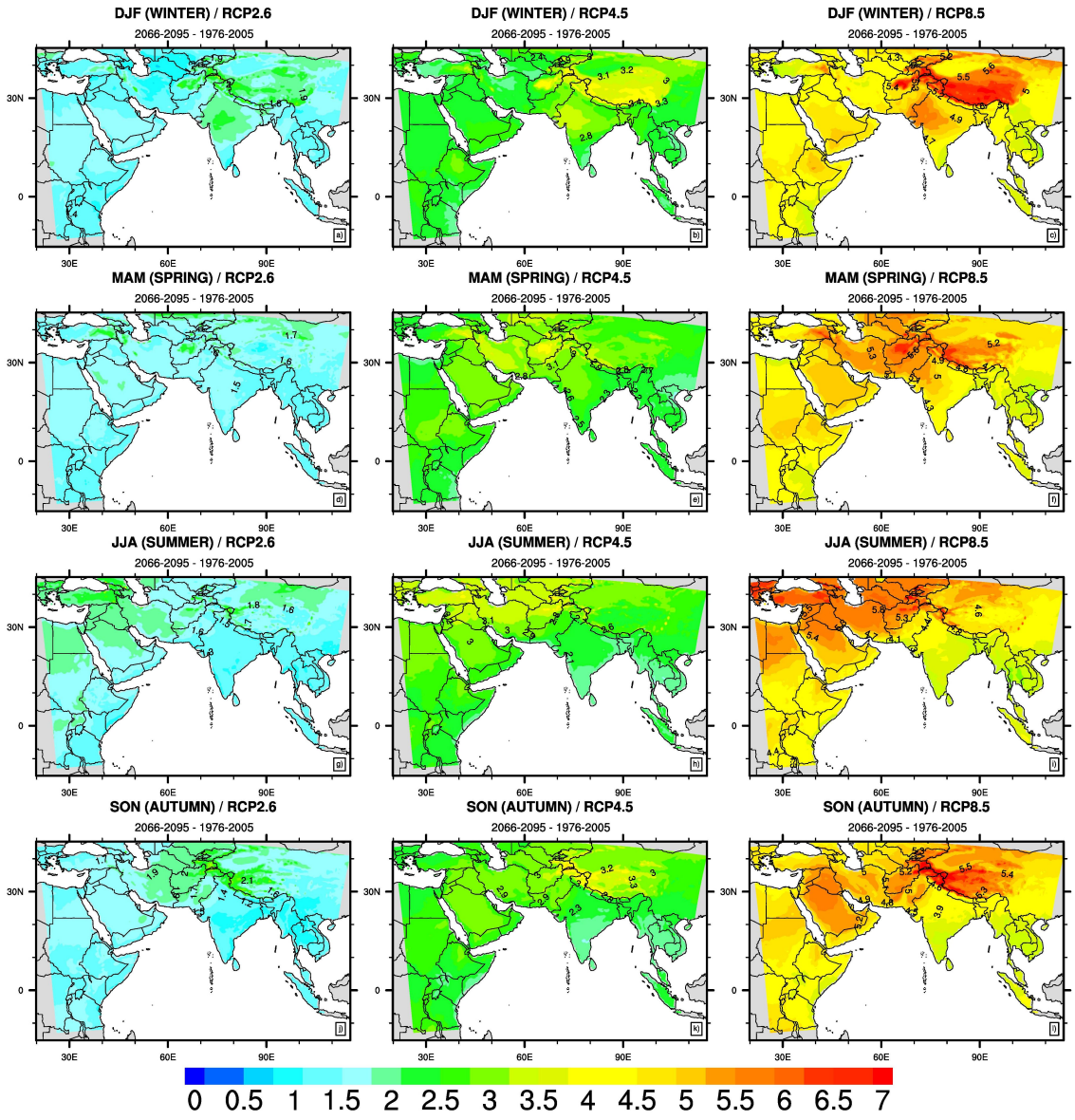

Figure 5.79. The map of spatial distribution of differences of monthly temperature averages of West Asia region in seasons (Winter; Spring; Summer and Autumn) for 2080s (2066-2095 - 1976 – 2005) according to RCP 2.6 , RCP 4.5 and RCP 8.5 Scenario

5.3. Application of the Methodology of Daily Maximum Temperature Selection

5.3.1. Application of the Methodology of Daily Maximum Temperature Selection: The Case of Europe

In this section, the numbers of extremely hot days (EHD) in a year in 2050s (between the years 2036 and 2065) and in 2080s (between the years 2066 and 2095) are calculated for each season. The definition of the extremely hot day is as follows. If the maximum temperature in a day is bigger than the maximum value of maximum temperatures of the reference, this day is said to be an extremely hot day. Moreover, the consecutive periods (CPHD), having at least 5 consecutive hot days, in a year are also calculated in each season in the aforementioned future periods.

The maximum temperature data sets, used in extreme event analysis in this thesis, are determined by using the necessary calculations defined in Section 4.3. By applying this methodology, the resemblance of the observed data set and model combination is measured by taking in consideration a great majority of percentile values of model and model combination data set. The comparison of the minimum value, 1 %, 5 %, 10 % , 25 % ,32 %, 45 %, 50 %, 55 %, 68 %, 75 %, 90 %, 95 %, 99 % and maximum value of maximum temperature percentile of observed data set and model combinations are performed by calculated the absolute differences of them. Then the averages of these absolute differences are found and are attained to the corresponding model combinations. The ones having lower value than the mean of the sum of averages and standard deviation of absolute differences of models are collected as “most representative models”. Further operations to calculate EHD and CPHD are carried out by using the outputs of “most representative models” (Table 5.50 and 5.51).

For Europe, the most representative models are MIROC-RCA4, MOHC-KNMI, MOHC- RCA4 and MPI-RCA4. MPI-RCA4 and MIROC-RCA4 are the best ones of these “most representative models”. The coefficients of these model combinations, obtained after spplying the aforementioned operations, are listed in 5.50. The equally

weighted averages of the max. temp. data, spanning the 2050s and 2080s, of these four model combinations are used to estimate future EHD and CPHD over Europe. ICHEC-DMI and NOAA-RCA4 are the worst ones and it is jeopardous to apply to these two models for heat wave analysis since one may end up with incorrect outcomes (Figure 5.80, 5.81, 5.82 and 5.83).

It is estimated that there will be at least 6 etremely hot days in a year in Scandinavian countries in winter.This number may even reach to 12 days with respect to RCP 4.5. The European part of the Russia, Switzerland, Austria, Czech Republic and Mediterranean coastal are also adversely affected by climate change where approximately 7 days in a year will be extremely hot days. Turkey and the European part of Russia are added in the class in which heat waves will be more frequently observed in 2080s with respect to RCP 8.5 scenario.

It is estimated that at least 5 days in a year will be extremely hot day over Scandinavian countries and European part of Russia in spring of 2050s with respect to RCP 4.5. Turkey, North Africa and Northern France are also hazardously affected by high temperature records where approximately 8 days in a year will be extremely hot days. Central Europe is the least affected region in spring season from high temperature. The amounts of heat waves in 2080s increases approximately 3-4 days in a year and the regions being exposed to the heat waves with respect to RCP 4.5 scenario. The critical regions are similar but the amount of the heat waves will be increased by 1-2 days in 2050s and are nearly same in 2080s compared to RCP 8.5 scenario. European part of Russia and Central Turkey are the regions which have 2-3 more extremely hot days in 2050s compared to 2080s. Heat wave amounts in Central Europe increases from 1-2 days in 2050s to 2-3 days in 2080s.

Mediterranean Coastal of Turkey and Syria and Southern United Kingdom are the regions in which heat waves will occur much more in autumn of 2050s according to RCP 4.5 scenario. It is foreseen that approximately 2-4 extremely hot days will be seen over the most of the remaining part of the observed domain in 2080s. The general tendency of the distribution and intensity of heat waves in 2080s with respect to the

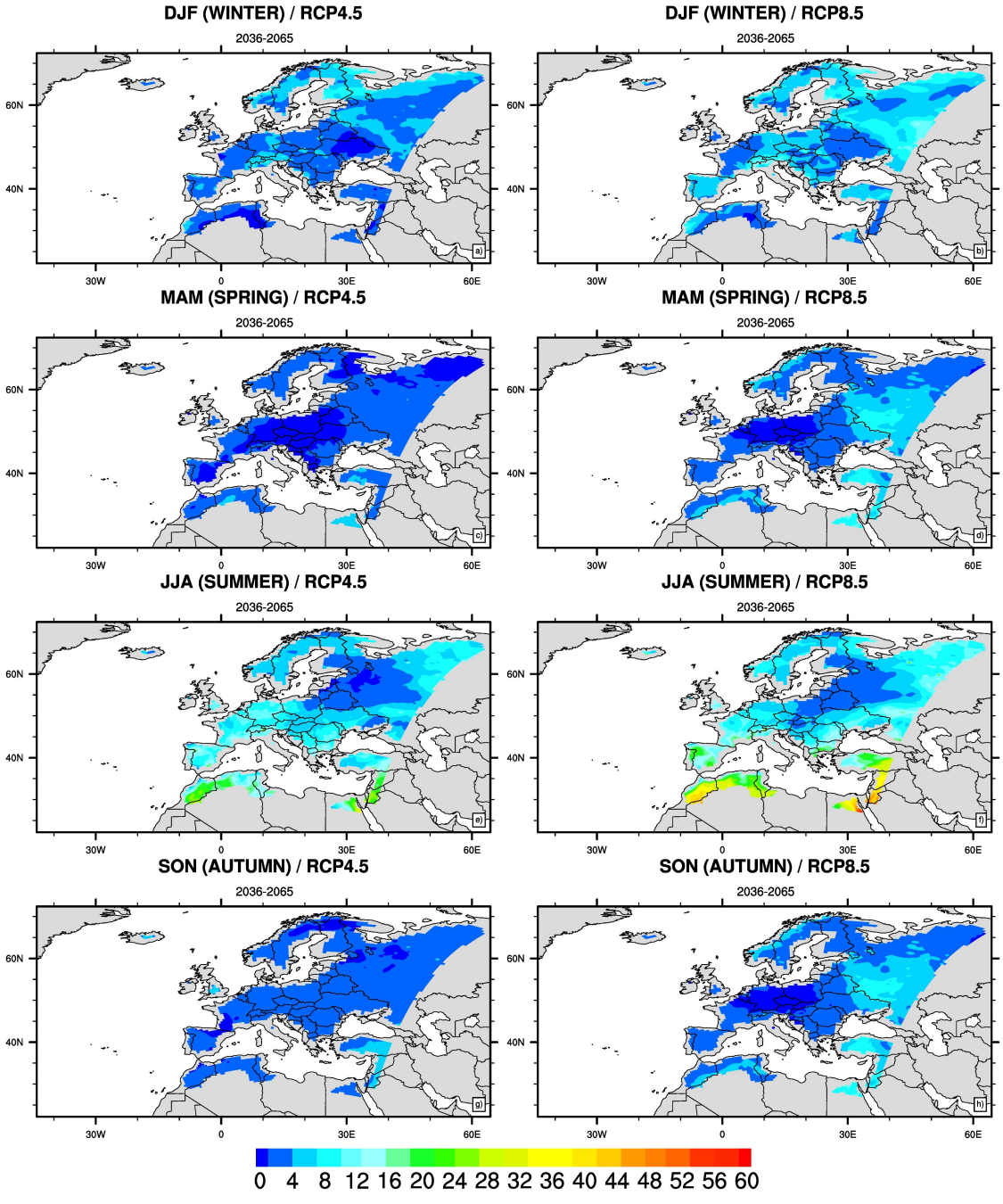

Figure 5.80. Extremely Hot Day Amounts in a year over Europe in 2050s with respect to RCP4.5 and RCP8.5 scenario

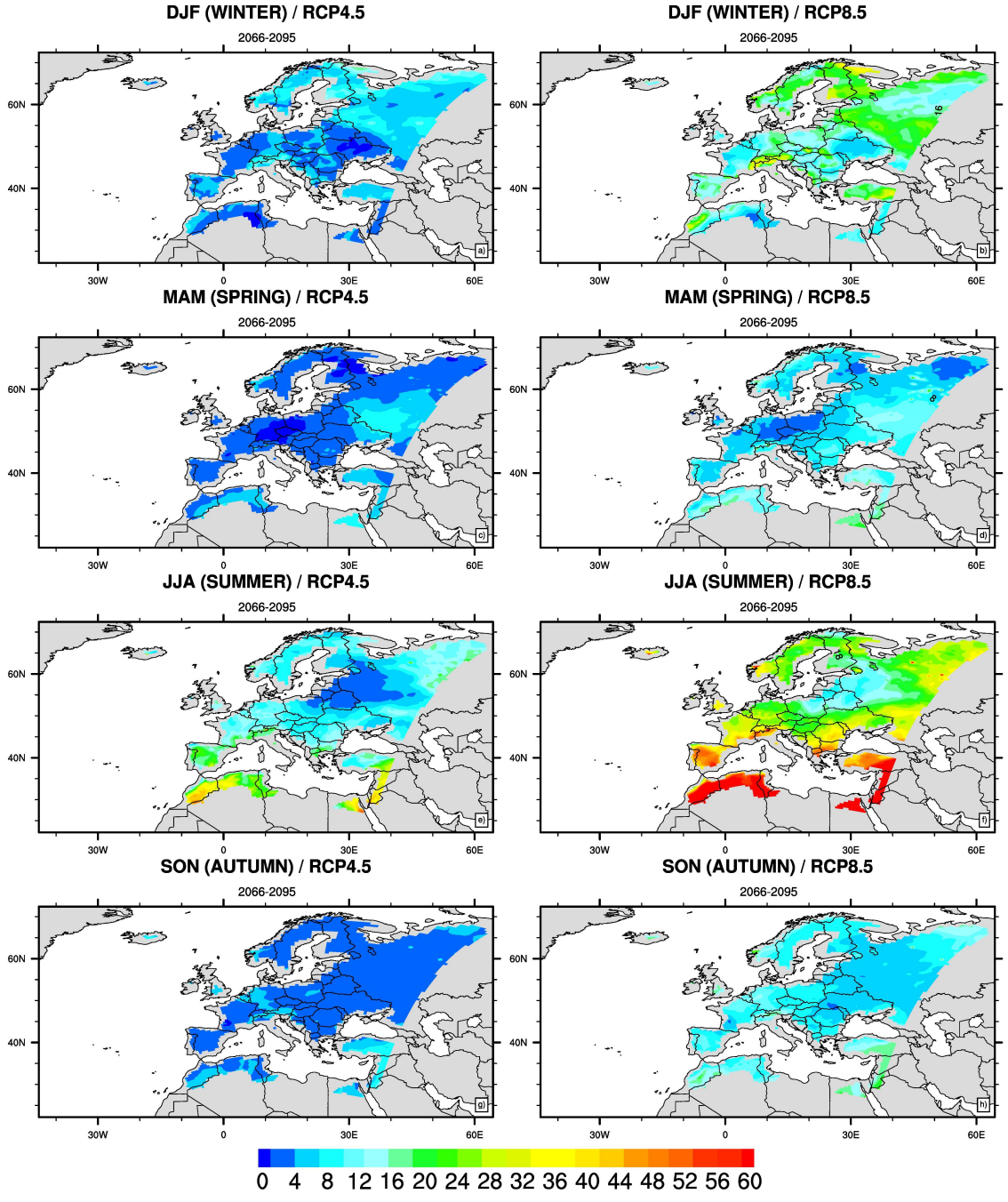

Figure 5.81. Extremely Hot Day Amounts in a year over Europe in 2080s with respect to RCP4.5 and RCP8.5 scenario

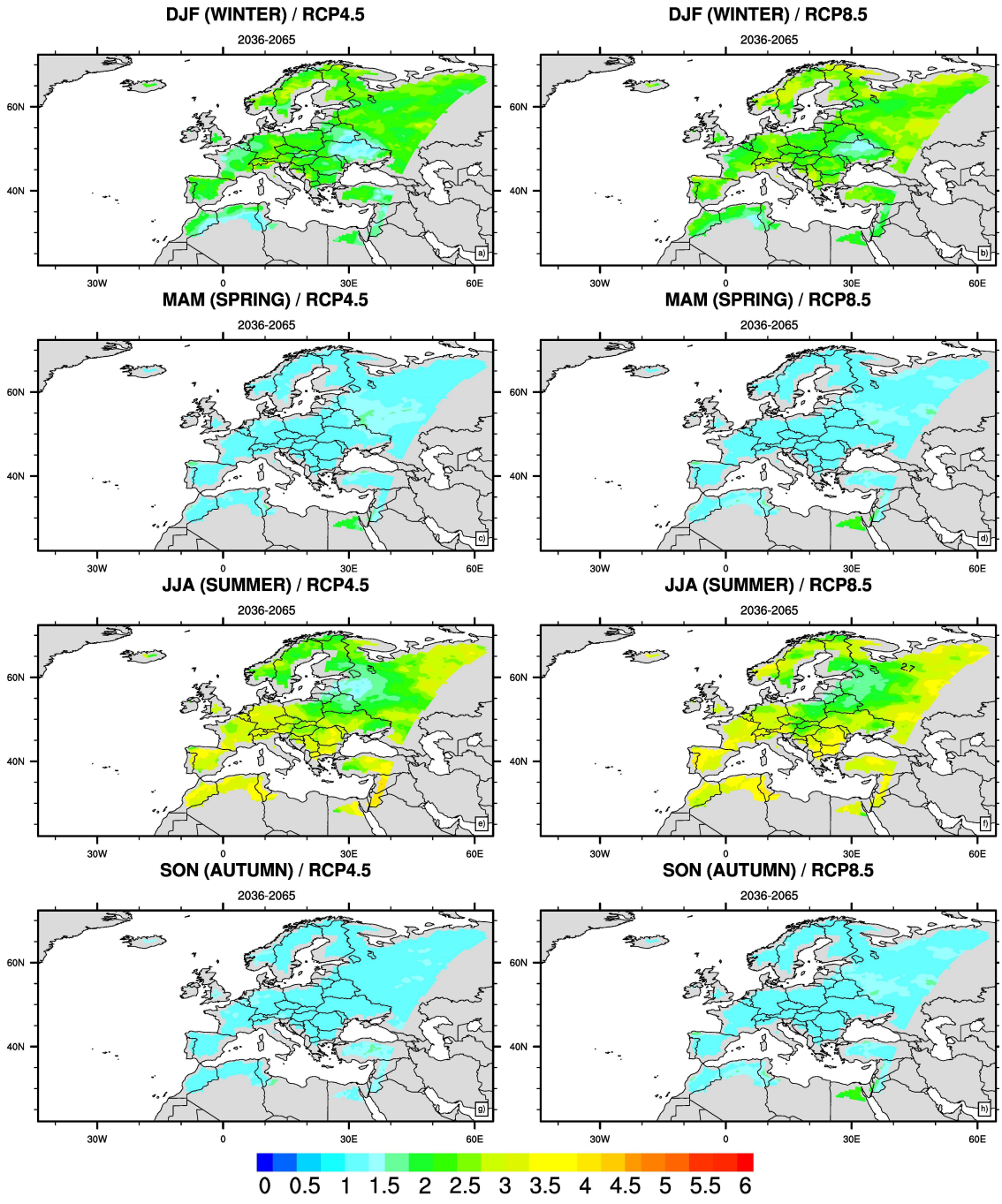

Figure 5.82. Consecutive Extremely Hot Day Amounts in a year over Europe in 2050s with respect to RCP4.5 and RCP8.5 scenario

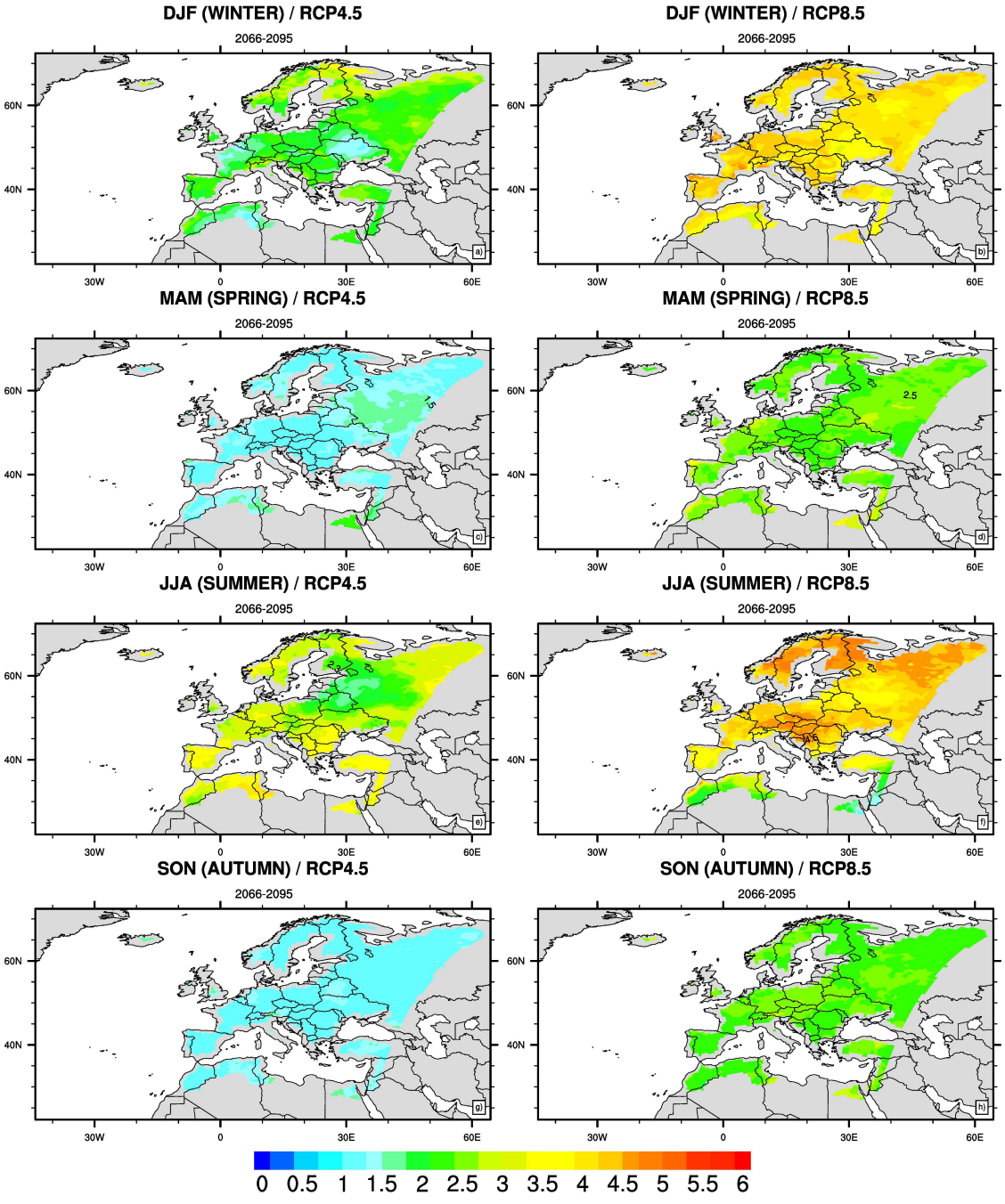

Figure 5.83. Consecutive Extremely Hot Day Amounts in a year over Europe in 2080s with respect to RCP4.5 and RCP8.5 scenario

RCP 8.5 scenario are similar to the ones with respect to RCP 4.5 scenario. At least 8 extremely hot days will occur in a year over south-western Russia and Central Turkey in 2050s according to RCP 8.5 scenario in autumn season.

It is estimated that at least 4-5 consecutive periods of heat waves in two years will occur over Europe, even reach up to 6 consecutive periods of heat waves in two years over Scandinavian countries in winter season in 2050s with respect to RCP 4.5. Ukraine and Northern France are the exceptions and the amount of consecutive periods is 6 in five years. Turkey and Northern part of Scandinavian have one more consecutive period of heat waves in 2080s compared to 2050s with respect to RCP 4.5. The distribution of the consecutive periods of heat wave patterns in RCP 8.5 is very similar to the ones for RCP 4.5 in 2050s. However, it reaches up to 10 in three years over Spain, France, Germany, United Kingdom, northern Scandinavian countries and some parts of Russia in 2080s with respect to RCP 8.5 scenario.

The distribution and intensity of consecutive period of heat waves over Europe in summer season is very similar to the ones in winters of both 2050s and 2080s with respect to RCP 4.5 RCP 8.5. The unique exception occurs in 2080s with respect to RCP 8.5 scenario, since at least 10 consecutive periods of heat waves are estimated over Europe, excluding Turkey and Northern Africa.

Eastern Belarus and Ukraine, Southern Russia, North Africa, Northern France and Germany and Scandinavian countries are the regions which have at least 3 consecutive periods of heat wave in two year and the remaining part have at least 1 consecutive period of heat wave in one year in spring of 2050s with respect to RCP 4.5 and RCP 8.5 scenario. The area, having approximately 3 consecutive period of heat wave enlarges from both sides with respect to RCP 4.5 scenario and covers the whole map with respect to RCP 8.5 scenario in 2080s.

The amount of consecutive period of heat waves in autumn season alters between 3 and 5 in both 2050s and 2080s with respect to RCP 4.5 scenario. Moreover, It reaches up to 6-7 over Turkey. On the other hand, there is a keen increase in the amount of

consecutive periods of heat wave from 2050s to 2080s with respect to RCP 8.5 scenario. In 2050s, this amount changes between 3 and 5 in three years in 2050s in the observed area, but it goes up to 6-8 in 2080s.

Table 5.50. The coefficients of The Most Representative Models

GCM - RCM Model Combination	**Coefficient**
MIROC-MIROC5-SMHI-RCA4-v1	0.824570
MOHC-HadGEM2-ES-KNMI-RACMO22E-v2	0.794590
MOHC-HadGEM2-ES-SMHI-RCA4-v1	0.796730
MPI-M-MPI-ESM-LR-SMHI-RCA4-v1	0.829830

5.3.2. Application of the Methodology of Daily Maximum Temperature Selection: The Case of Africa

For Africa, the most representative models are CSIRO-RCA4, MIROC-RCA4, IPSL-RCA4, MOHC- RCA4 and MPI-RCA4. CSIRO-RCA4 is the best one of these "most representative models" (Table 5.52 and 5.53). The equally weighted averages of these five models maximum temperature data set, spanning the 2050s and 2080s are used to estimate future EHD and CPHD over Africa. ICHEC-DMI and ICHEC-KNIMI1 and ICHEC-KNMI2 are the worst one and it is jeopardous to apply to these two models for heat wave analysis since incorrect outcomes can be obtained at the conclusion (Figure 5.84, 5.85, 5.86 and 5.87).

Table 5.51. The coefficients of The Unrepresentative Models

GCM - RCM Model Combination	**Coefficient**
CCCma-CanESM2-SMHI-RCA4-v1	0.741820
CCCma-CanESM2-UCAN-WRF341I-v2	0.520440
CNRM-CERFACS-CNRM-CM5-CLMcom-CCLM5-0-6-v1	0.383960
CNRM-CERFACS-CNRM-CM5-SMHI-RCA4-v1	0.554710
CSIRO-QCCCE-CSIRO-Mk3-6-0-SMHI-RCA4-v1	0.511680
ICHEC-EC-EARTH-CLMcom-CCLM5-0-6-v1	0.269470
ICHEC-EC-EARTH-DMI-HIRHAM5-v1	0.076713
ICHEC-EC-EARTH-KNMI-RACMO22E-v1	0.571070
ICHEC-EC-EARTH-KNMI-RACMO22E-v2	0.510320
ICHEC-EC-EARTH-SMHI-RCA4-v1	0.685940
IPSL-IPSL-CM5A-MR-SMHI-RCA4-v1	0.600660
MIROC-MIROC5-CLMcom-CCLM5-0-6-v1	0.260510
MOHC-HadGEM2-ES-CLMcom-CCLM5-0-6-v1	0.728780
MPI-M-MPI-ESM-LR-CLMcom-CCLM4-8-17-v1	0.557240
MPI-M-MPI-ESM-LR-CLMcom-CCLM5-0-6-v1	0.465730
MPI-M-MPI-ESM-LR-MPI-CSC-REMO2009-v1	0.717290
MPI-M-MPI-ESM-LR-MPI-CSC-REMO2009-v2	0.620720
NCC-NorESM1-M-SMHI-RCA4-v1	0.682630
NOAA-GFDL-GFDL-ESM2M-SMHI-RCA4-v1	0.150900

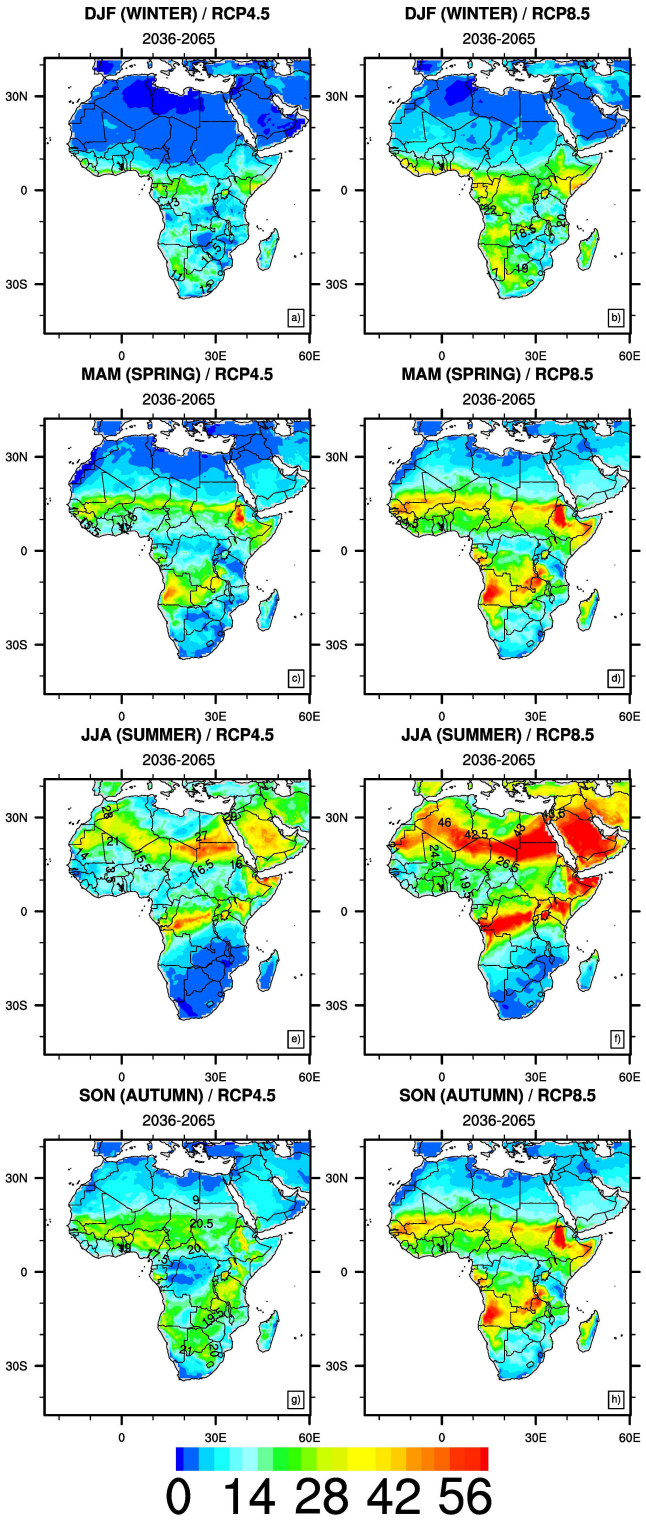

Figure 5.84. Extremely Hot Day Amounts in a year over Africa in 2050s with respect to RCP4.5 and RCP8.5 scenario

It is estimated that at least 5 days in a year will be extremely hot day over Northern part of the observed area, including Northern Africa, Turkey and Arabian Peninsula, in winter and spring seasons in 2050s with respect to RCP 4.5. Starting from the middle sub Saharan countries, the heat wave amounts starts to increase and goes up to 50 days in a year in the remaining part of Africa. The distribution and intensity of heat waves in 2050s with respect to RCP 8.5 is very similar to the ones in 2080s of RCP 4.5 scenario. However, the intensity increases to 40 days over the southern part of the Africa and even two of three days in 2080s will be extremely hot day over same regions. Extremely hot day amounts elevates to 30 days over some parts of northern part of the observed area, including Turkey.

Mauritania, Mali, Southern Algeria, Chad, Southern Egypt, Northern Sudan, Central Arabian Peninsula, Somali, Yemen, Democratic Republic of the Congo, Kenya and Uganda will be the most effected regions from extremely hot temperature since at least one of two days will be extremely hot in 2050s and 2080s with respect to RCP 4.5 and in 2050s according to RCP 8.5 in summer. This amount extends to 70 days in a year in 2080s with respect to RCP 8.5 over the aforementioned regions. Southern Africa will be less affected from the adverse outcomes of extremely hot temperature since the amount of extremely hot days change between 10 and 15 in a year over Southern Africa, except 2080s with respect to RCP 8.5.

It is projected that Sub Saharan and southern countries except Democratic Republic of the Congo will have more extremely hot days in 2050s and 2080s in autumn season with respect to both RCP 4.5 and RCP 8.5 . The amount of the hot days will be approximately 60 days in a year with respect to RCP 8.5 in 2080s. It alters between 15 and 20 days in a year over the remaining part of the observed area.

Consecutive period of heat wave will occur at least three times in two years over the northern part of the domain. This amount enlarges to seven in two years over the southern part of the observed area in winter season in 2050s with respect to RCP 4.5. It is at least five times in two years over the northern part in 2080s and similarly seven in two years over the southern Africa with respect to RCP 4.5. This is same in 2050s

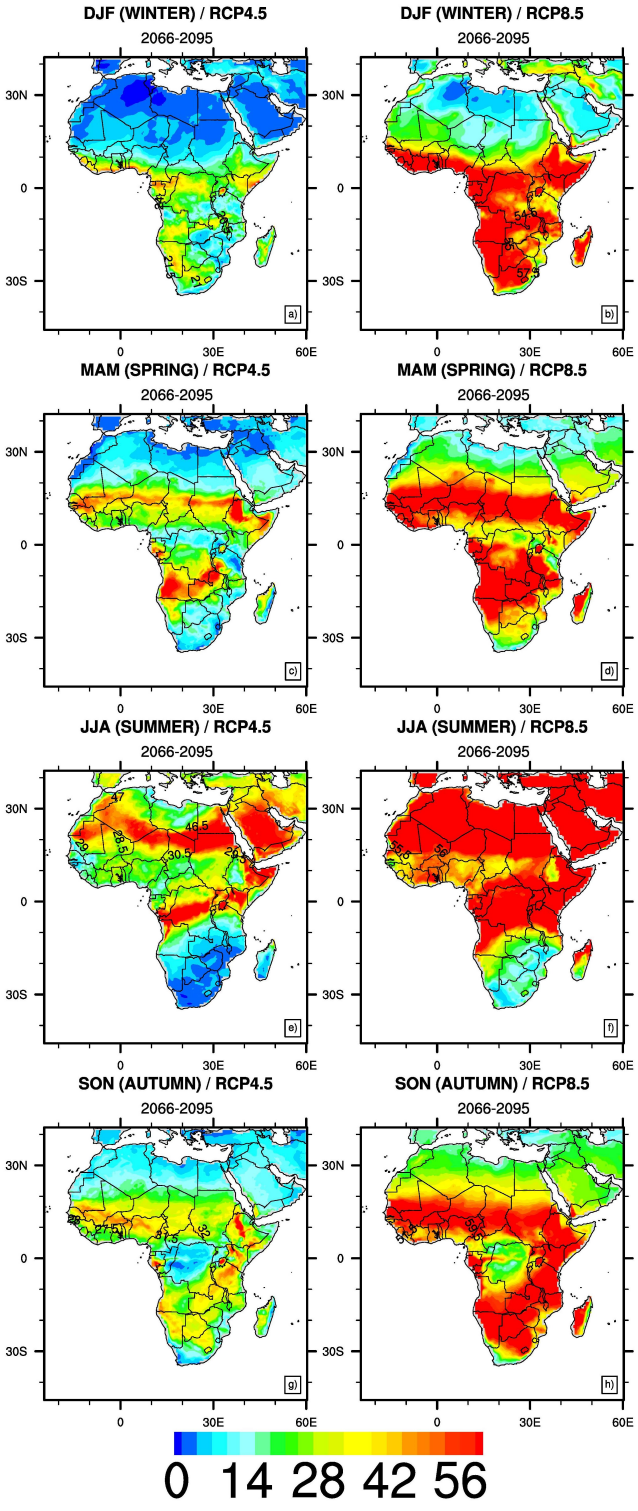

Figure 5.85. Extremely Hot Day Amounts in a year over Africa in 2080s with respect to RCP4.5 and RCP8.5 scenario

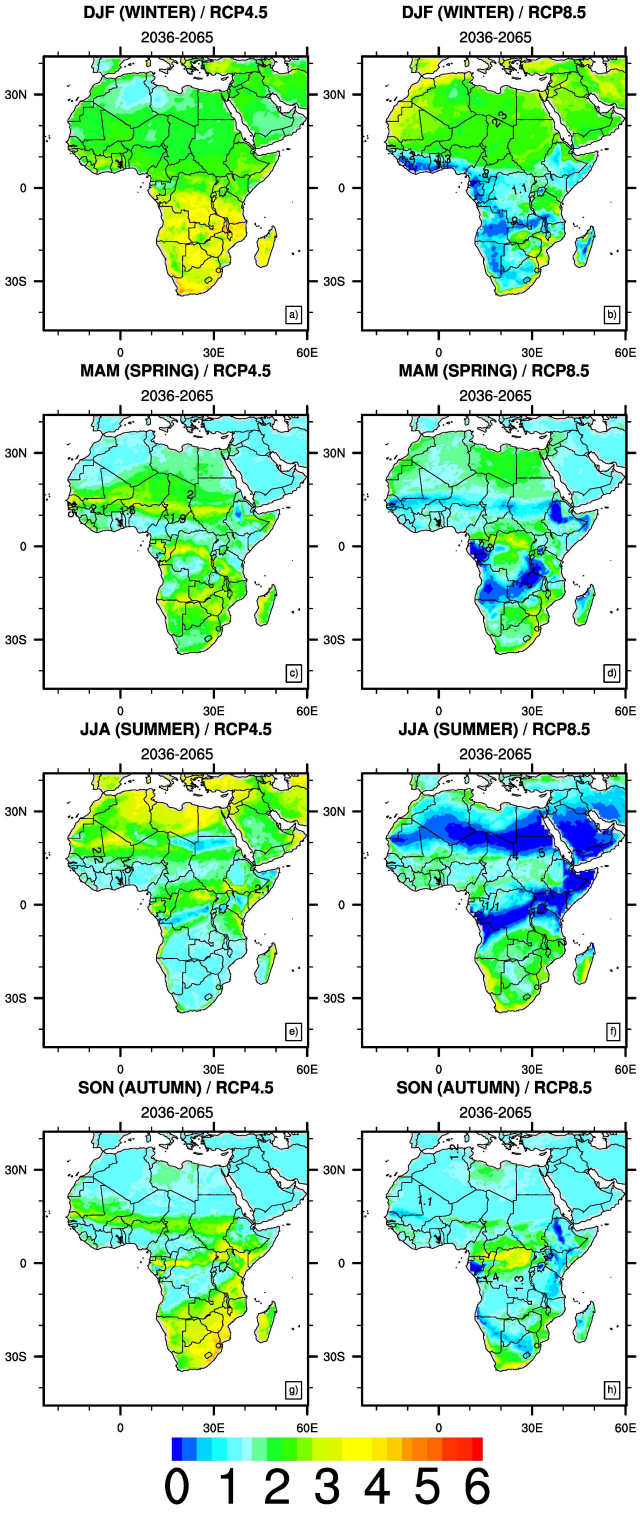

Figure 5.86. Consecutive Extremely Hot Day Amounts in a year over Africa in 2050s with respect to RCP4.5 and RCP8.5 scenario

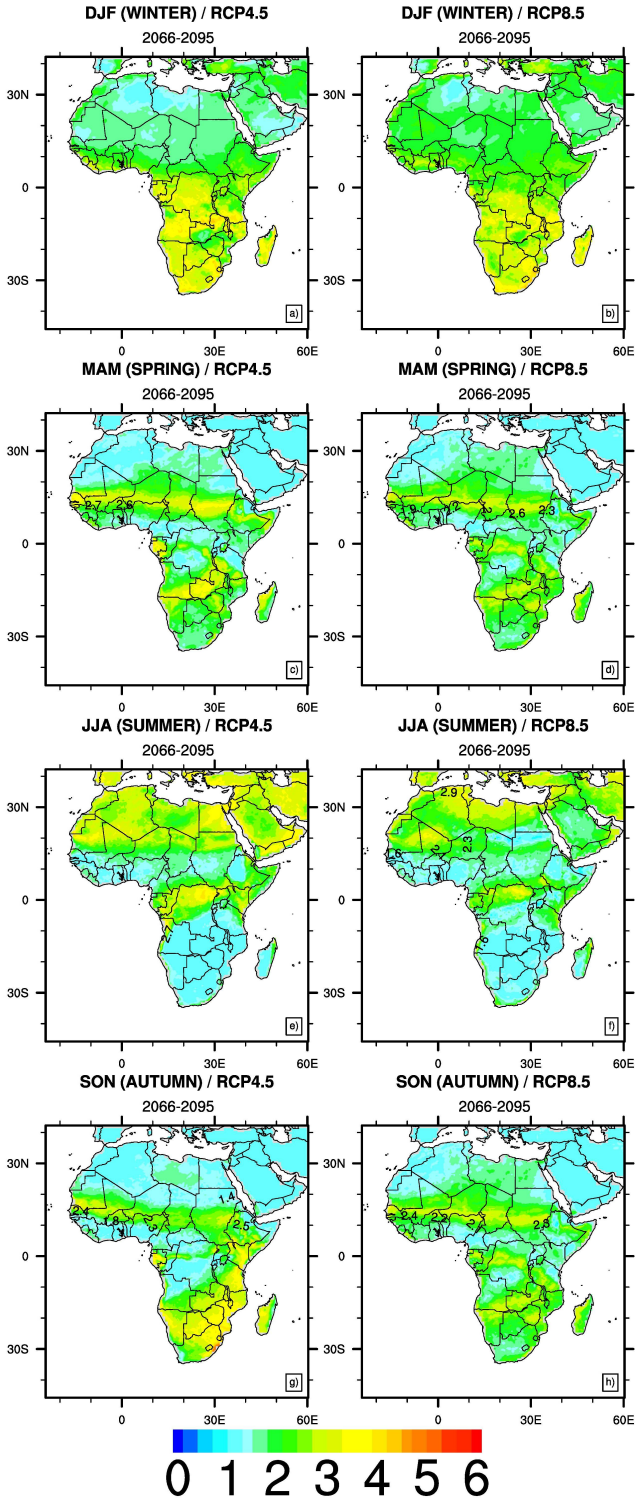

Figure 5.87. Consecutive Extremely Hot Day Amounts in a year over Africa in 2080s with respect to RCP4.5 and RCP8.5 scenario

with respect to RCP 8.5. On the other hand, it will decrease to the three times in two years over the south part of the observed area in2080s with respect to RCP 8.5 scenario.

In spring season, consecutive period of heat wave will occur at least three times in a year over the Sub Saharan Africa. In the northern and southern part this amount will decrease to three times in two years in 2050s with respect to RCP 4.5. In 2080s, consecutive period of heat waves will extend to the at least two times n a year in the majority of the observed area which have similar distribution and intensity in 2050s with respect to RCP 8.5. In 2080s, approximately one more consecutive period of heat wave will be seen with respect to RCP 8.5.

In summer season, the intensity of consecutive period of heat wave with respect to RCP 4.5 is different. The observed area can be separated to three parts which are North Africa, Sub Saharan Africa and Southern Africa. Approximately three consecutive period of heat wave will occur in a year over the Northern Africa, three one will occur in two years over Sub Saharan and Southern Africa. It is three times in two years over Sub Saharan and Southern Africa and six times in two years over Northern Africa in 2050s with respect to RCP 4.5 and in 2080s with respect to RCP 8.5. This amount will decrease over the Northern and Sub Saharan Africa and will increase over Southern Africa in 2080s with respect to RCP 8.5.

In autumn season, the consecutive period of heat wave will be higher over the Southern Africa and will be approximately 2 or 3 times in a year and 1 or 2 times in a year over Northern Africa in both 2050s and 2080s.

5.3.3. Application of the Methodology of Daily Maximum Temperature Selection: The Case of Central America

For Central America, the most representative models are MOHC-RegCM and MPI-RegCM (Table 5.54 and 5.55). The maximum temperature data sets of MPI-RegCM with respect to RCP 2.6, RCP 4.5 and RCP 8.5 aren't available in the CORDEX

Table 5.52. The coefficients of The Most Representative Models

GCM - RCM Model Combination	**Coefficient**
CSIRO-QCCCE-CSIRO-Mk3-6-0-SMHI-RCA4-v1	0.93093
IPSL-IPSL-CM5A-MR-SMHI-RCA4-v1	0.84654
MIROC-MIROC5-SMHI-RCA4-v1	0.89231
MOHC-HadGEM2-ES-SMHI-RCA4-v1	0.83160
MPI-M-MPI-ESM-LR-SMHI-RCA4-v1	0.88484

Table 5.53. The coefficients of The Unrepresentative Models

GCM - RCM Model Combination	**Coefficient**
CCCma-CanESM2-SMHI-RCA4-v1	0.79172
CCCma-CanESM2-UQAM-CRCM5-v1	0.74852
CNRM-CERFACS-CNRM-CM5-CLMcom-CCLM4-8-17-v1	0.11993
CNRM-CERFACS-CNRM-CM5-SMHI-RCA4-v1	0.66727
ICHEC-EC-EARTH-DMI-HIRHAM5-v2	0.17104
ICHEC-EC-EARTH-KNMI-RACMO22T-v1	0.16891
ICHEC-EC-EARTH-KNMI-RACMO22T-v2	0.17839
ICHEC-EC-EARTH-MPI-CSC-REMO2009-v1	0.38145
ICHEC-EC-EARTH-SMHI-RCA4-v1	0.47055
IPSL-IPSL-CM5A-LR-GERICS-REMO2009-v1	0.42955
MIROC-MIROC5-GERICS-REMO2009-v1	0.74030
MOHC-HadGEM2-ES-CLMcom-CCLM4-8-17-v1	0.49749
MOHC-HadGEM2-ES-GERICS-REMO2009-v1	0.66740
MOHC-HadGEM2-ES-KNMI-RACMO22T-v2	0.39884
MPI-M-MPI-ESM-LR-CLMcom-CCLM4-8-17-v1	0.38447
MPI-M-MPI-ESM-LR-MPI-CSC-REMO2009-v1	0.71116
MPI-M-MPI-ESM-LR-UQAM-CRCM5-v1	0.69383
NCC-NorESM1-M-DMI-HIRHAM5-v1	0.58345
NCC-NorESM1-M-SMHI-RCA4-v1	0.76542
NOAA-GFDL-GFDL-ESM2G-GERICS-REMO2009-v1	0.32695
NOAA-GFDL-GFDL-ESM2M-SMHI-RCA4-v1	0.44010

Project. Hence, maximum temperature data set of MOHC-RegCM is the unique choice and the outcomes of this model combination, spanning the 2050s and 2080s are used to estimate future EHD and CPHD over Central America. CSIRO-RCA4 and MIROC-RCA4 are the worst one and it is jeopardous to apply to these two models for heat wave analysis since incorrect outcomes can be obtained at the conclusion (Figure 5.88 and 5.89).

The available data set of the most representative models for future projections of over Central America is MOHC-RegCM1 with respect to RCP 8.5. Hence all of the following outcomes are the ones obtained from the projection of this model combination with respect to RCP 8.5. It is estimated that at least two days in a year will be extremely hot day over Northern part of Central America in winter season in both 2050s and 2080s. The amount of heat wave over the Southern part of the Central America will alter between 6 and 15 days in a year in 2050s and 30-60 days in a year in 2080s. In spring season, this amount will change between 2 and 10 in the northern part of Central America and will increase up to 30 days over the southern part of Central America in 2050s. In 2080s, the distribution of the extremely hot days is very similar to the one in 2050s but the amount of extremely hot days in 2080s will be approximately 35-40 days higher than the one in 2050s. In summer and autumn seasons, the amount of extremely hot days in 2050s will change between 15 and 30 in a year and will be more in southern part than in the northern part. In 2080s, it will tremendously elevate and reach up to one of the two days in each season over especially south-eastern part of the observed area.

Consecutive period of heat wave will change between one and four in a year over the observed area in future. In 2050s, it will be one or two times in a year in winter, spring and autumn season over Northern part of the observed area and it will occur between one and three times over southern Central America. The amount of consecutive period of heat wave in summer season will be more than other seasons and alter between five and nine in three years in 2050s. In 2080s, consecutive period of heat wave will occur between 3 and 6 times in two years in each season.

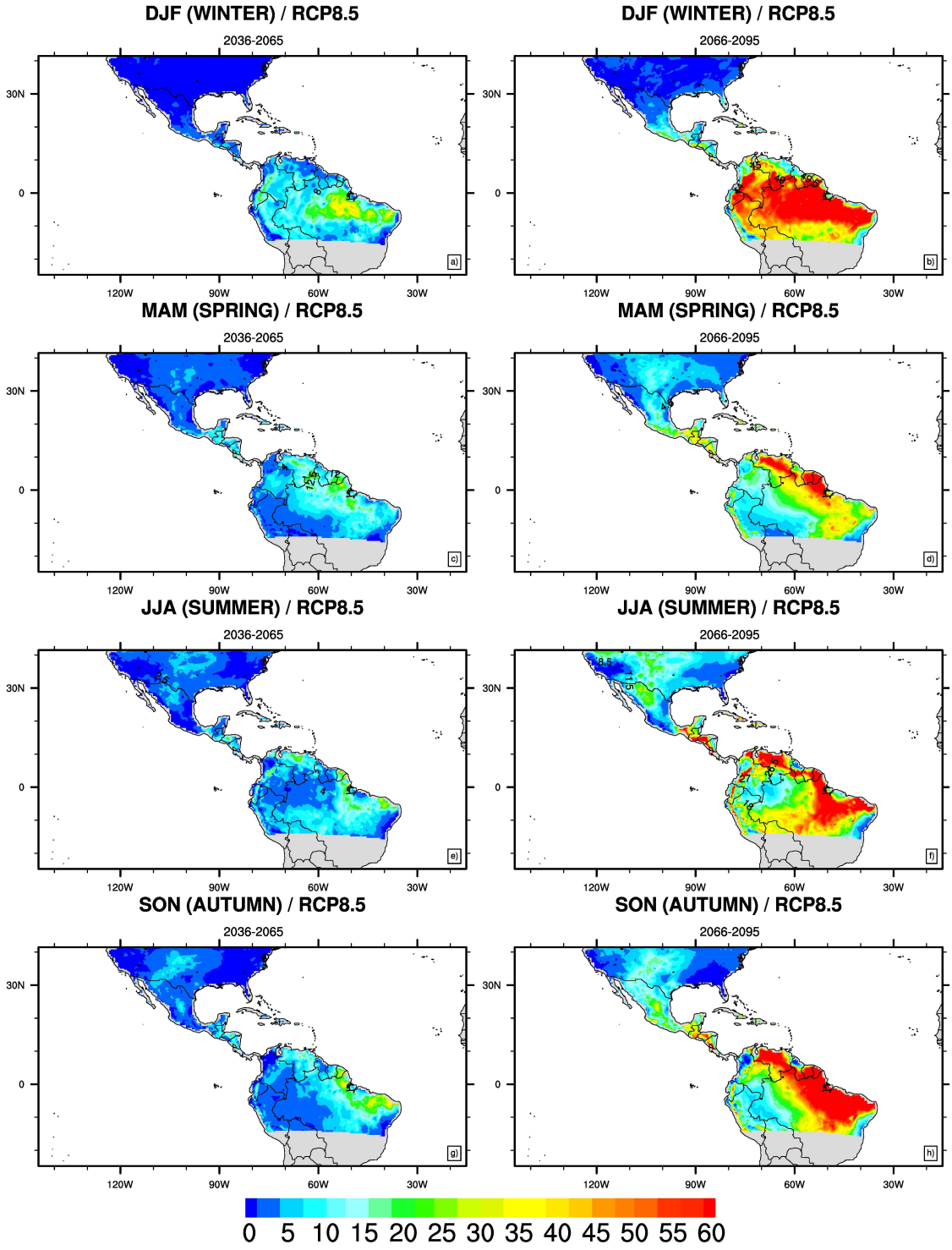

Figure 5.88. Extremely Hot Day Amounts in a year over Central America in 2050s and 2080s with respect to RCP8.5 scenario

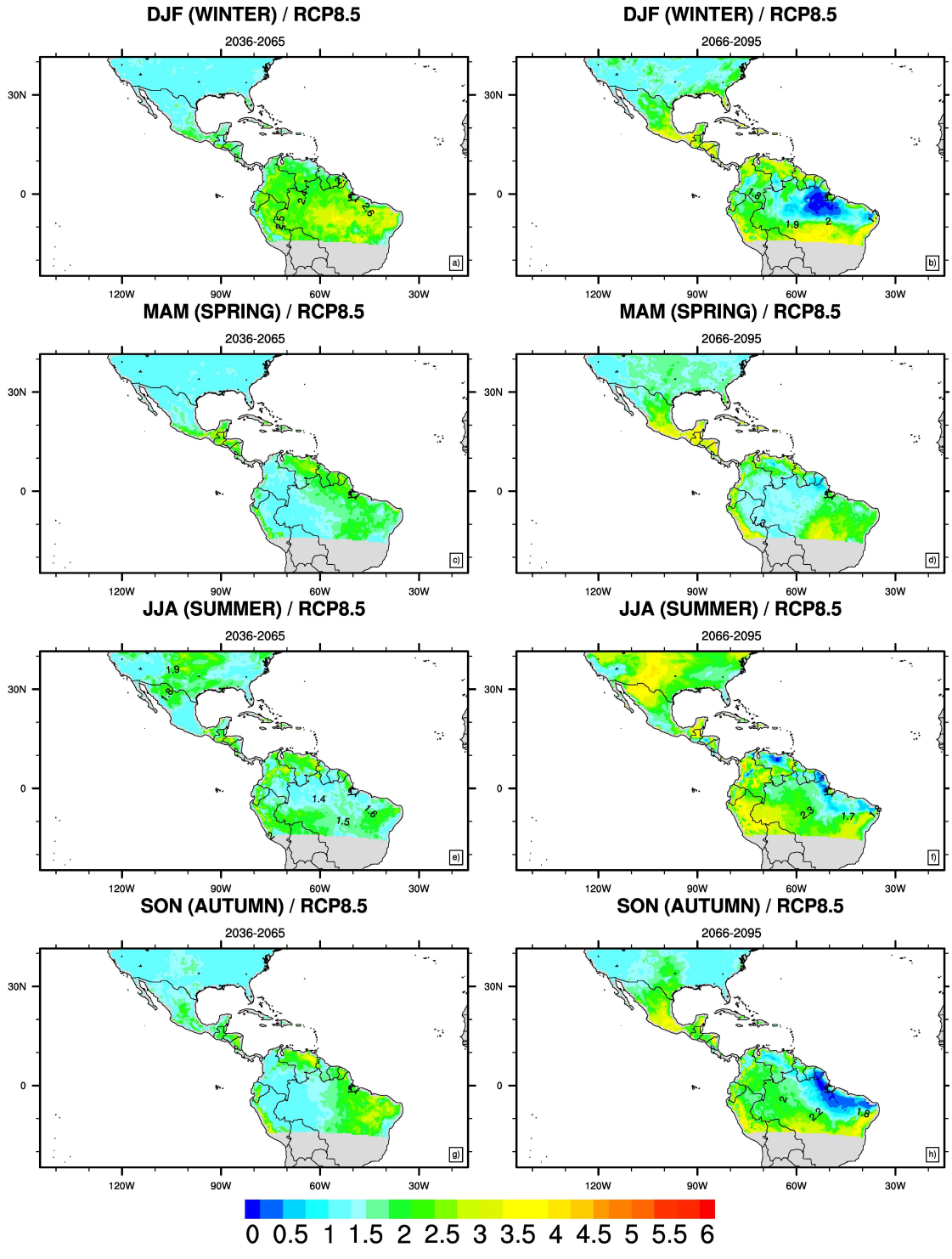

Figure 5.89. Consecutive Extremely Hot Day Amounts in a year over Central America in 2050s and 2080s with respect to RCP8.5 scenario

Table 5.54. The coefficients of The Most Representative Models

GCM - RCM Model Combination	**Coefficient**
MPI-M-MPI-ESM-MR-ICTP-RegCM4-3-v2	0.79819
MOHC-HadGEM2-ES-ICTP-RegCM4-3-v2	0.80524

Table 5.55. The coefficients of The Unrepresentative Models

GCM - RCM Model Combination	**Coefficient**
CCCma-CanESM2-SMHI-RCA4-v1	0.45269
CNRM-CERFACS-CNRM-CM5-SMHI-RCA4-v1	0.72556
CSIRO-QCCCE-CSIRO-Mk3-6-0-SMHI-RCA4-v1	0.34281
ICHEC-EC-EARTH-SMHI-RCA4-v1	0.66917
IPSL-IPSL-CM5A-MR-SMHI-RCA4-v1	0.44555
MIROC-MIROC5-SMHI-RCA4-v1	0.36363
MOHC-HadGEM2-ES-ICTP-RegCM4-3-v4	0.72055
MOHC-HadGEM2-ES-SMHI-RCA4-v1	0.67280
MPI-M-MPI-ESM-LR-SMHI-RCA4-v1	0.68224
MPI-M-MPI-ESM-MR-ICTP-RegCM4-3-v4	0.50465
NCC-NorESM1-M-SMHI-RCA4-v1	0.70414
NOAA-GFDL-GFDL-ESM2M-SMHI-RCA4-v1	0.21212

5.3.4. Application of the Methodology of Daily Maximum Temperature Selection: The Case of South America

For South America, the most representative model is MIROC-RCA4 (Table 5.56 and 5.57). Hence, maximum temperature data set of MIROC-RCA4 is the unique choice and the outcomes of this model combination, spanning the 2050s and 2080s are used to estimate future EHD and CPHD over South America. IPSL-RCA4 and NOAA-RCA4 are the worst one and it is jeopardous to apply to these two models for heat wave analysis since incorrect outcomes can be obtained at the conclusion (Figure 5.90, 5.91, 5.92 and 5.93).

It is estimated that at least one day (reach up to 15 days in some parts) in a year will be extremely hot day over South America in winter season in both 2050s and 2080s. The amount of heat wave over the South America will alter between 2 and 20 days in a year in 2050s and will enlarge to 50 days in a year in 2080s with respect to both scenarios in spring, summer and autumn season. Extremely hot days over the southern part of South America in spring and autumn season and eastern part of the observed domain in summer season will be lower than the remaining part of the domain.

Consecutive period of heat wave will change between one and four in a year over the observed area in future. In 2050s, it will be one or three times in a year in whole seasons over the observed area with respect to RCP 4.5 and it will occur between three and eight times in two years in 2050s with respect to RCP 8.5. The amount of consecutive period of heat wave in all of the seasons in 2080s with respect to RCP 4.5 will be nearly same the ones in 2050s with respect to RCP 8.5. In 2080s, consecutive period of heat waves will occur at least two times in a year over the majority of the observed area for all seasons in 2080s with respect to RCP 8.5.

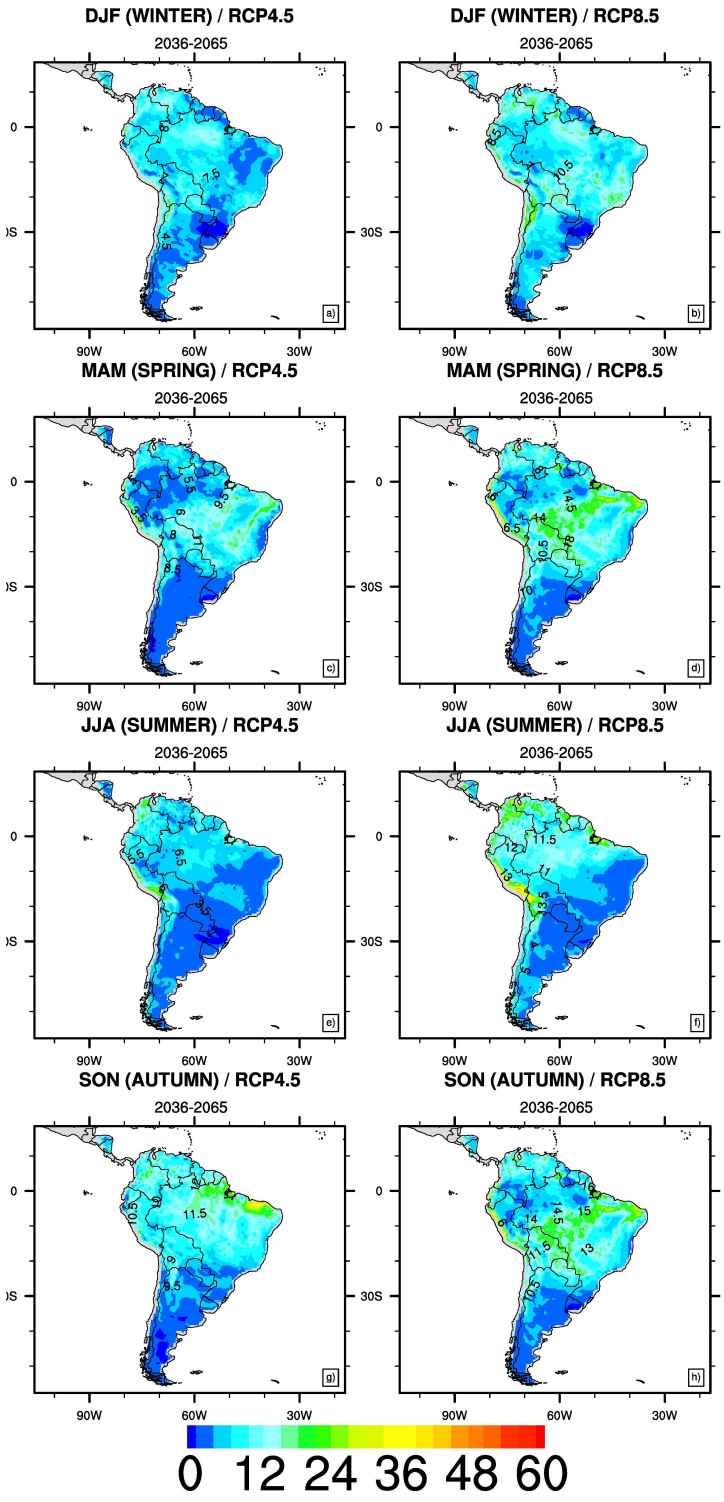

Figure 5.90. Extremely Hot Day Amounts in a year over South America in 2050s with respect to RCP4.5 and RCP8.5 scenario

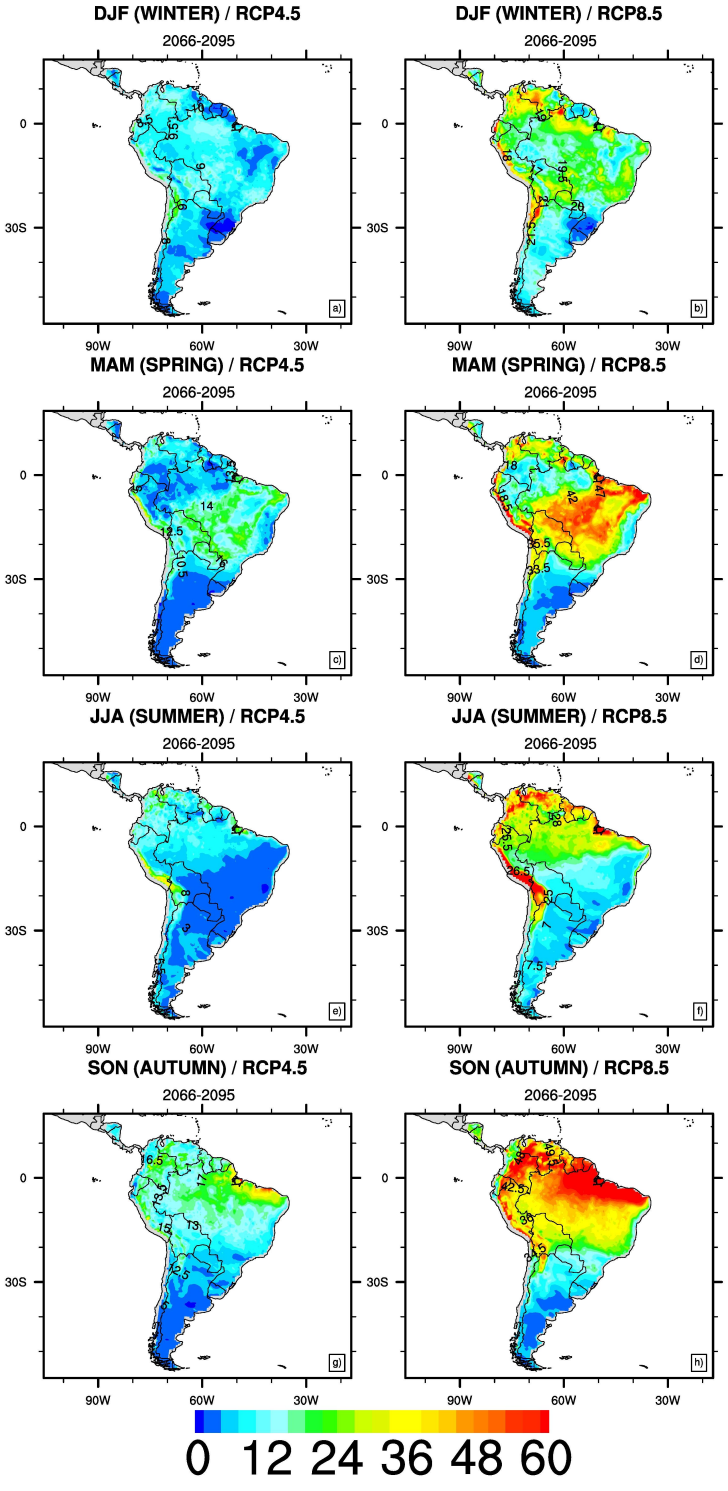

Figure 5.91. Extremely Hot Day Amounts in a year over South America in 2080s with respect to RCP4.5 and RCP8.5 scenario

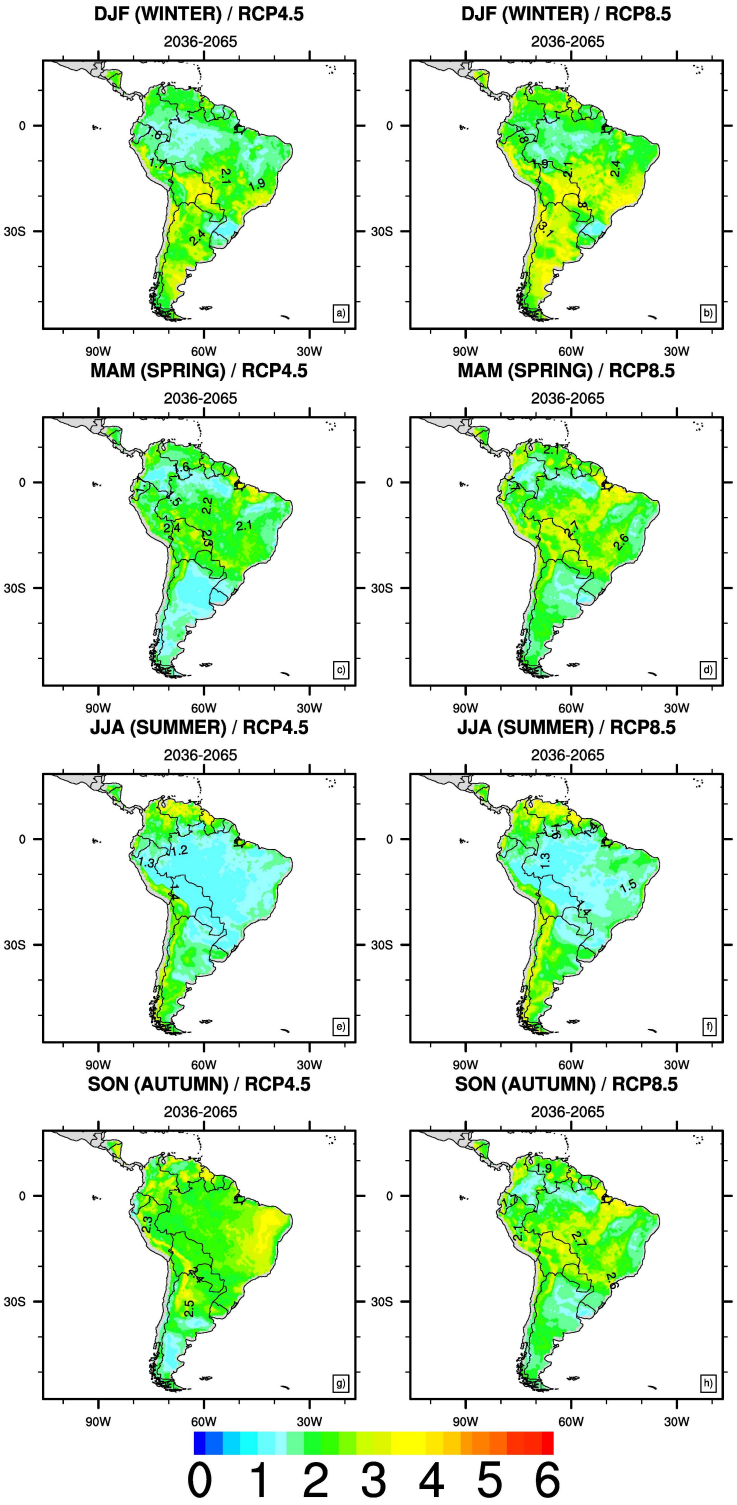

Figure 5.92. Consecutive Extremely Hot Day Amounts in a year over South America in 2050s with respect to RCP4.5 and RCP8.5 scenario

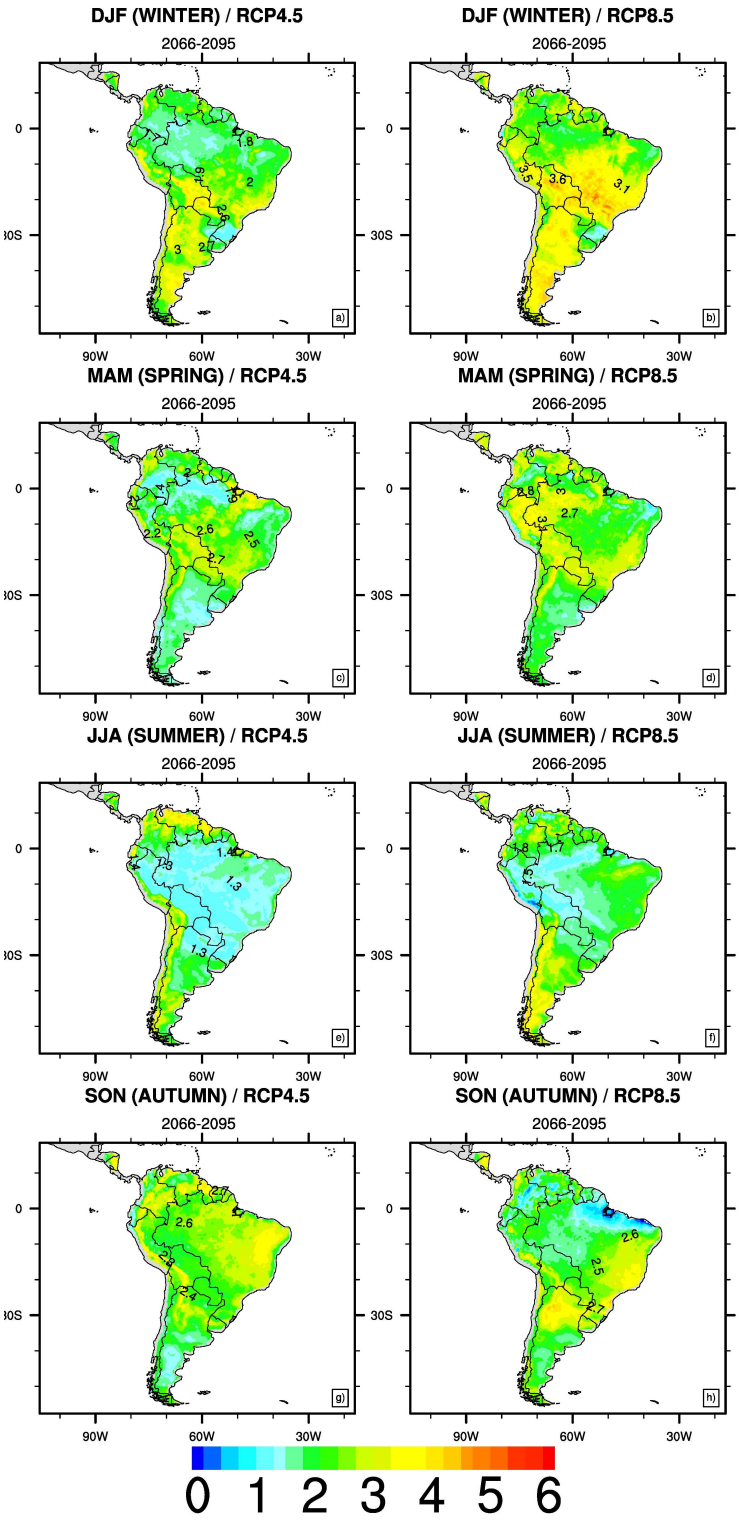

Figure 5.93. Consecutive Extremely Hot Day Amounts in a year over South America in 2080s with respect to RCP4.5 and RCP8.5 scenario

Table 5.56. The coefficients of The Most Representative Models

GCM - RCM Model Combination	Coefficient
MIROC-MIROC5-SMHI-RCA4-v3	0.81425

Table 5.57. The coefficients of The Unrepresentative Models

GCM - RCM Model Combination	Coefficient
CCCma-CanESM2-SMHI-RCA4-v3	0.58420
CSIRO-QCCCE-CSIRO-Mk3-6-0-SMHI-RCA4-v3	0.41336
ICHEC-EC-EARTH-SMHI-RCA4-v3	0.55805
IPSL-IPSL-CM5A-MR-SMHI-RCA4-v3	0.28506
MOHC-HadGEM2-ES-SMHI-RCA4-v3	0.73296
MPI-M-MPI-ESM-LR-SMHI-RCA4-v3	0.68622
NCC-NorESM1-M-SMHI-RCA4-v3	0.68961
NOAA-GFDL-GFDL-ESM2M-SMHI-RCA4-v3	0.33234

5.3.5. Application of the Methodology of Daily Maximum Temperature Selection: The Case of West Asia

For West Asia, the most representative model is CSIRO-RCA4 (Table 5.58 and 5.59). Hence, maximum temperature data set of CSIRO-RCA4 is the unique choice and the outcomes of this model combination, spanning the 2050s and 2080s are used to estimate future EHD and CPHD over West Asia. ICHEC-RCA4 and NOAA-RCA4 are the worst one and it is jeopardous to apply to these two models for heat wave analysis since incorrect outcomes can be obtained at the conclusion (Figure 5.94, 5.95, 5.96 and 5.97).

West Asia will be the less affected region according to projection outcomes. It is estimated that at most one day in a year will be extremely hot day over especially Northern part of observed area in whole seasons in both 2050s and 2080s with respect to RCP 4.5 and RCP 8.5. The amount of heat wave over the Sudan, Etiophia, Kenya,

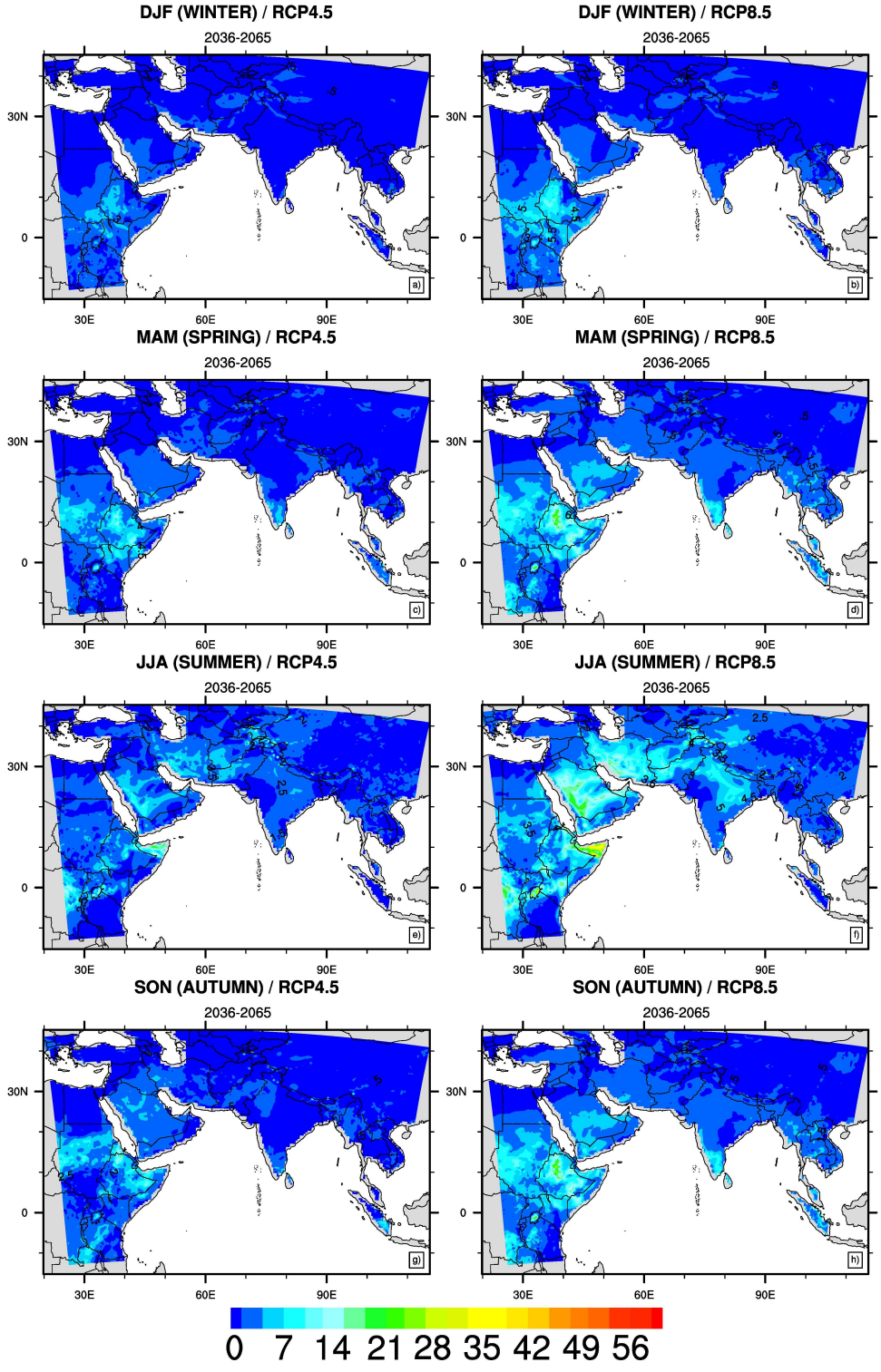

Figure 5.94. Extremely Hot Day Amounts in a year over West Asia in 2050s with respect to RCP4.5 and RCP8.5 scenario

Somali and Saudi Arabia will alter between 2 and 4 days in a year in 2050s and 2080s with respect to both Representative Concentration Pathways. Extremely hot days will enlarge to 7 days in a year in 2080s with respect to RCP 8.5 in spring, summer and autumn season.

Consecutive period of heat wave in 2050s and 2080s with respect to RCP 4.5 and in 2050s with respect to RCP 8.5 have similar distributions and intensity for both seasons. It will change between 2 and 7 in three years over the observed region and will be higher over the southern part than the northern part of the observed area and will reach its maximum value in summer season. In 2080s, it will not be lower than 3 times in two years over the observed area with respect to RCP 8.5.

Table 5.58. The coefficients of The Most Representative Models

GCM - RCM Model Combination	**Coefficient**
CSIRO-QCCCE-CSIRO-Mk3-6-0-SMHI-RCA4-v2	0.82671

Table 5.59. The coefficients of The Unrepresentative Models

GCM - RCM Model Combination	**Coefficient**
CCCma-CanESM2-SMHI-RCA4-v2	0.70132
CNRM-CERFACS-CNRM-CM5-SMHI-RCA4-v2	0.35977
ICHEC-EC-EARTH-SMHI-RCA4-v2	0.19825
IPSL-IPSL-CM5A-MR-SMHI-RCA4-v2	0.66377
MIROC-MIROC5-SMHI-RCA4-v2	0.69720
MOHC-HadGEM2-ES-SMHI-RCA4-v2	0.69975
MPI-M-MPI-ESM-LR-MPI-CSC-REMO2009-v1	0.61130
MPI-M-MPI-ESM-LR-SMHI-RCA4-v2	0.64458
NCC-NorESM1-M-SMHI-RCA4-v2	0.31202
NOAA-GFDL-GFDL-ESM2M-SMHI-RCA4-v2	0.10815

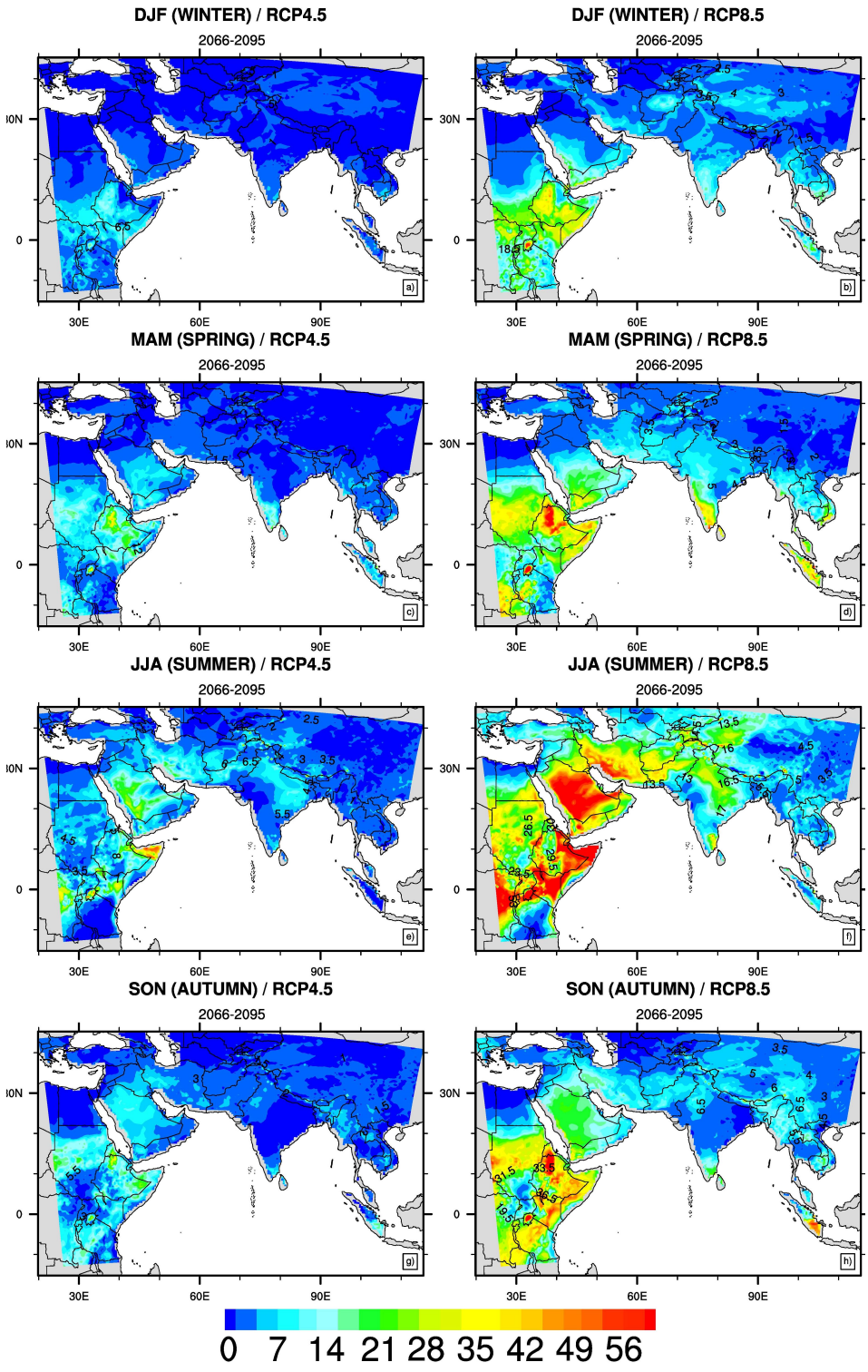

Figure 5.95. Extremely Hot Day Amounts in a year over West Asia in 2080s with respect to RCP4.5 and RCP8.5 scenario

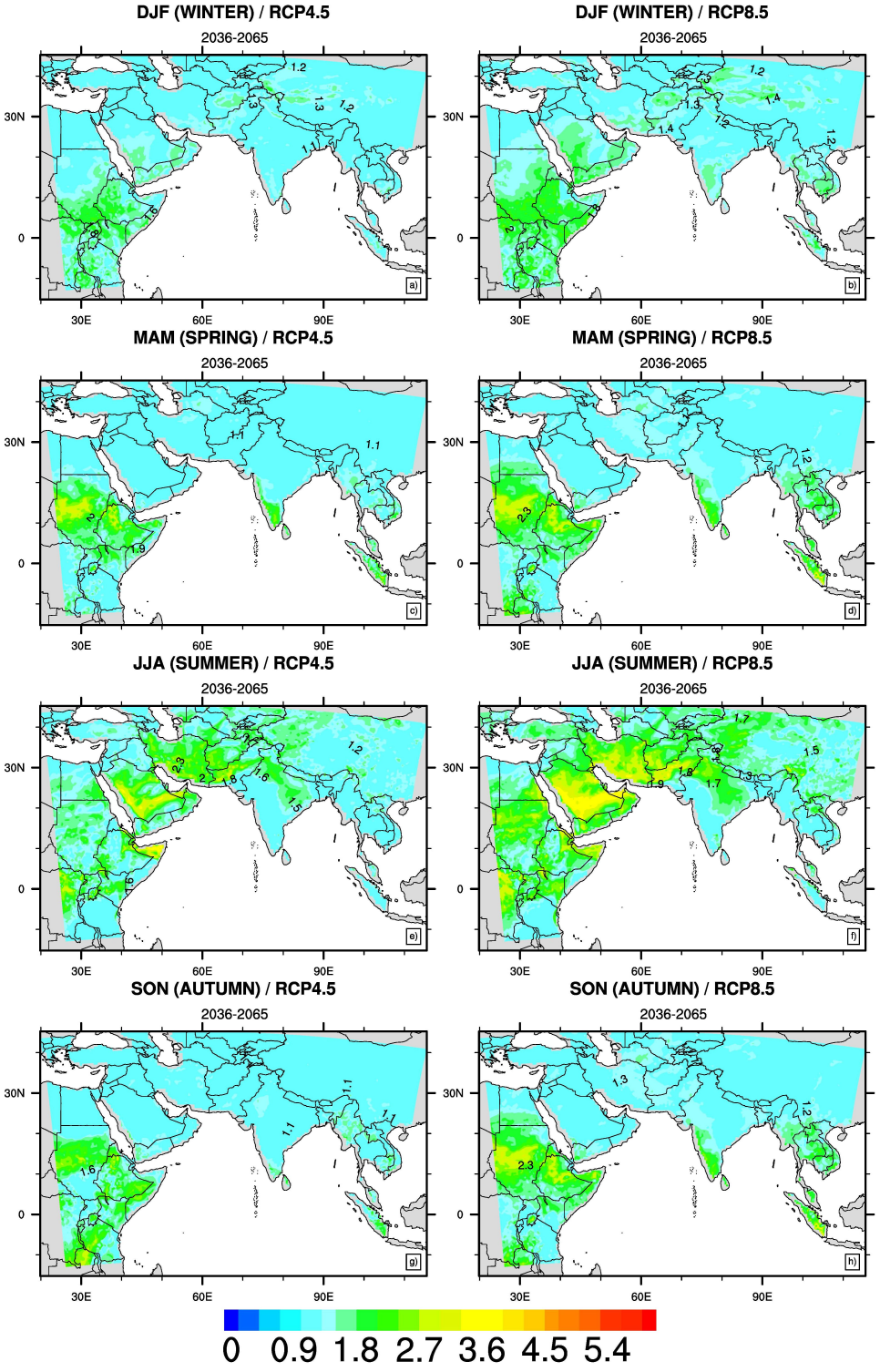

Figure 5.96. Consecutive Extremely Hot Day Amounts in a year over West Asia in 2050s with respect to RCP4.5 and RCP8.5 scenario

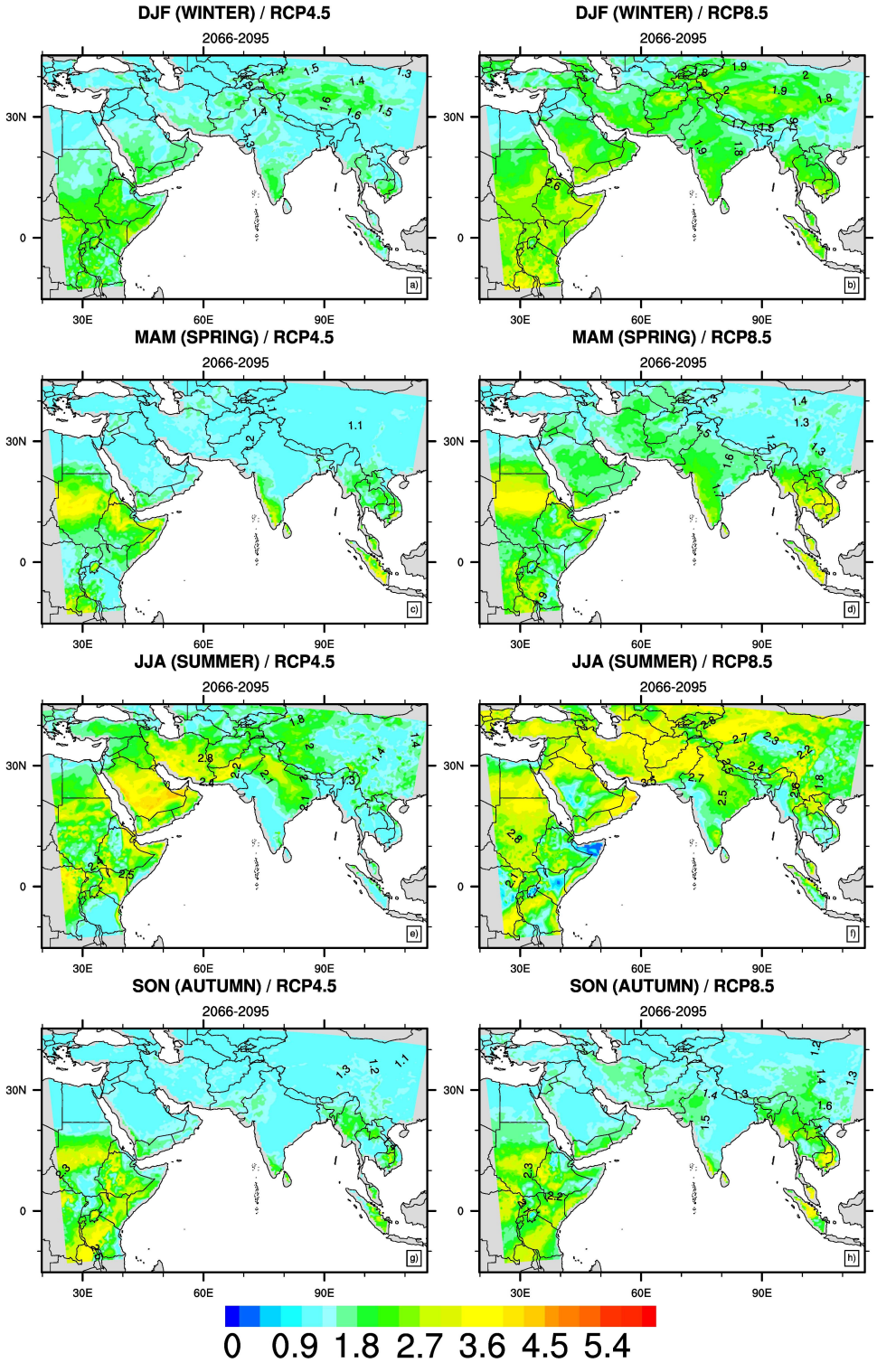

Figure 5.97. Consecutive Extremely Hot Day Amounts in a year over West Asia in 2080s with respect to RCP4.5 and RCP8.5 scenario

5.4. WBGT and Labor Productivity Alteration

5.4.1. WBGT and Labor Productivity Alteration: The Case of Europe

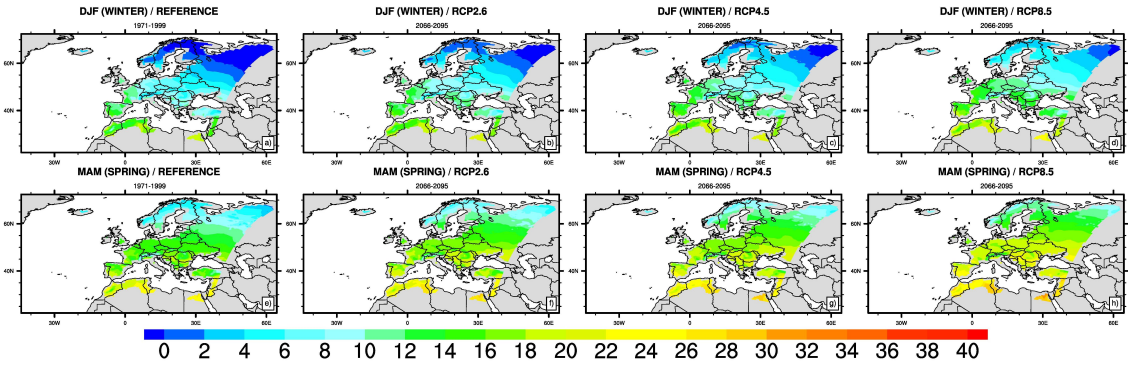

Figure 5.98. The map of spatial distribution of WBGT averages in Europe region in a year in Winter and Spring in each period (1976 - 2005 and 2066 – 2095) according to RCP 2.6s, RCP 4.5 and RCP 8.5 Scenario

In the following part, WBGT is calculated by using the most representative models maximum temperature and relative humidity outputs. Labor productivity is attained with regards to projected WBGTs over aforementioned five regions. The average values of critical days in which WBGT is over the determined temperature limits were calculated over the observed area. Winter is the most riskless season in whole observed periods in the sense of thermal discomfort and labor productivity losses over Europe. On the other hand, summer; as it is expected; is the riskiest season in each period. Autumn is in the second order according to the thermal discomfort. Figure 5.98 illustrates the spatial distribution of the percentages of aforementioned critical days over Europe. In the northern part of the Europe, these percentages are really small. Mediterranean coastal were adversely affected from hot days. The percentage of the days which have risky WBGT values is high over especially Portugal, Spain, Italy, Turkey, Greece and France coastal in summer.

No labor productivity losses were foreseen in all periods in winter over Continental Europe. Imperceptible losses were estimated over the Northern Africa, southern coastal

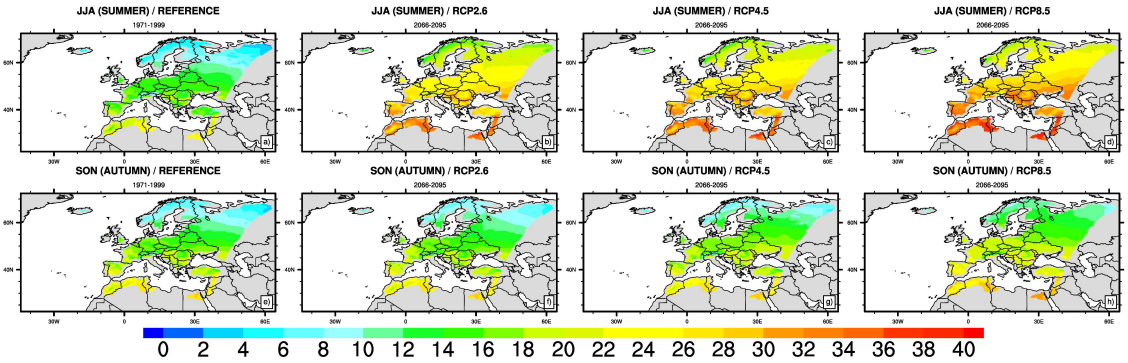

Figure 5.99. The map of spatial distribution of WBGT averages in Europe region in a year in Summer and Autumn in each period (1976 - 2005 and 2066 – 2095) according to RCP 2.6 , RCP 4.5 and RCP 8.5 Scenario

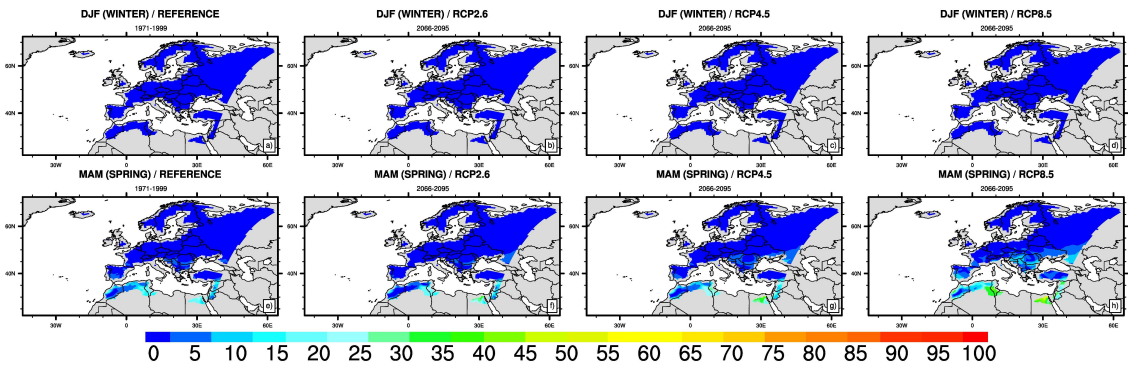

Figure 5.100. The reduction in labor productivity in Europe region in a year in Winter and Spring in each period (1976 - 2005 and 2066 – 2095) according to RCP 2.6 , RCP 4.5 and RCP 8.5 Scenario

of Spain and Portugal in spring and autumn. As it is expected, most losses were foreseen in summer. The percentage of losses can be reached up to 60 % over Mediterranean coastal of Europe. In the northern part of observed Europe was less influenced from the destructive effects of hot weather (Figure 5.98, 5.99, 5.100 and 5.101).

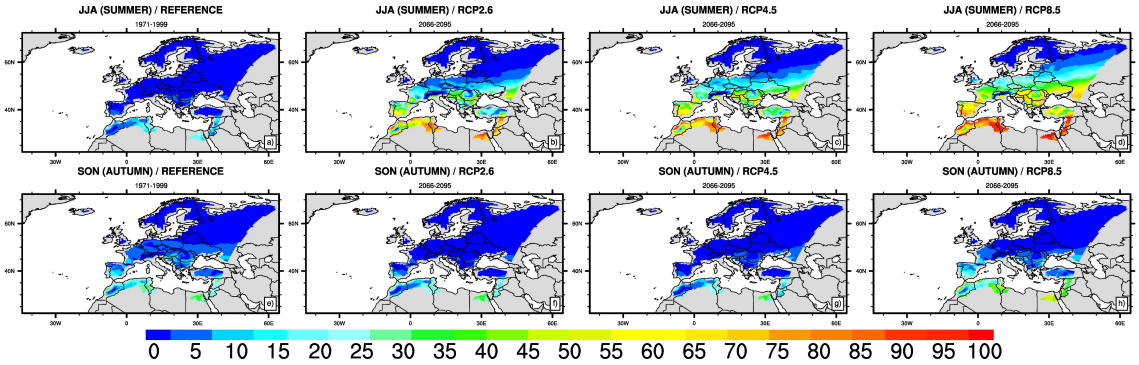

Figure 5.101. The reduction in labor productivity in Europe region in Summer and Autumn in each period (1976 - 2005 and 2066 – 2095) according to RCP 2.6 , RCP 4.5 and RCP 8.5 Scenario

5.4.2. WBGT and Labor Productivity Alteration: The Case of Africa

The observed are can be separated to three main areas to research the foreseen WBGT and labor productivity alteration. These areas can be basically defined as the Northern Africa (NA), the domain between just above the Ecuador line and northern part of the observed area; Middle Africa (MA), the domain between just below and above the Equator line and Southern Africa (SA), the domain between just below the Ecuador line and southern part of the observed area.

The risk coefficients of these areas (NA, MA and SA) are very different from each other but similar in each season. WBGT will change between 20°C and 28°C over NA, 30°C and 40°C over MA and 16°C and 28°C over SA. Summer is the riskiest season and winter has the lowest risk in sense of projected WBGT.

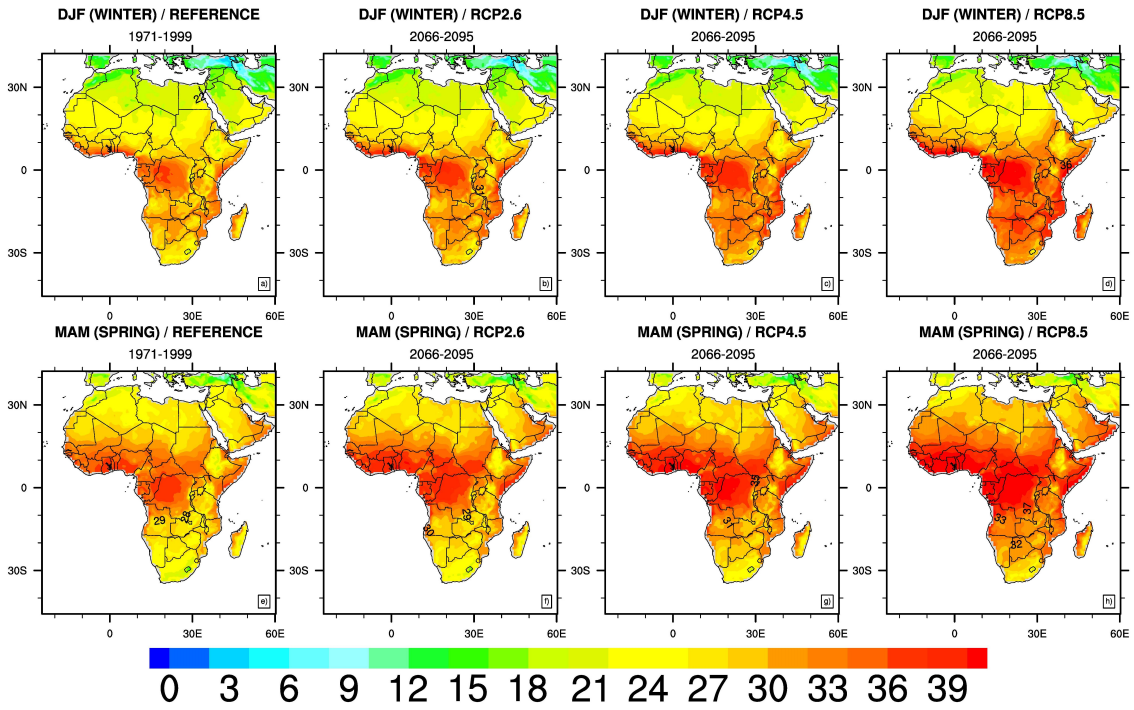

Figure 5.102. The map of spatial distribution of WBGT averages in Africa region in a year in Winter and Spring in each period (1976 - 2005 and 2066 – 2095) according to RCP 2.6 , RCP 4.5 and RCP 8.5 Scenario

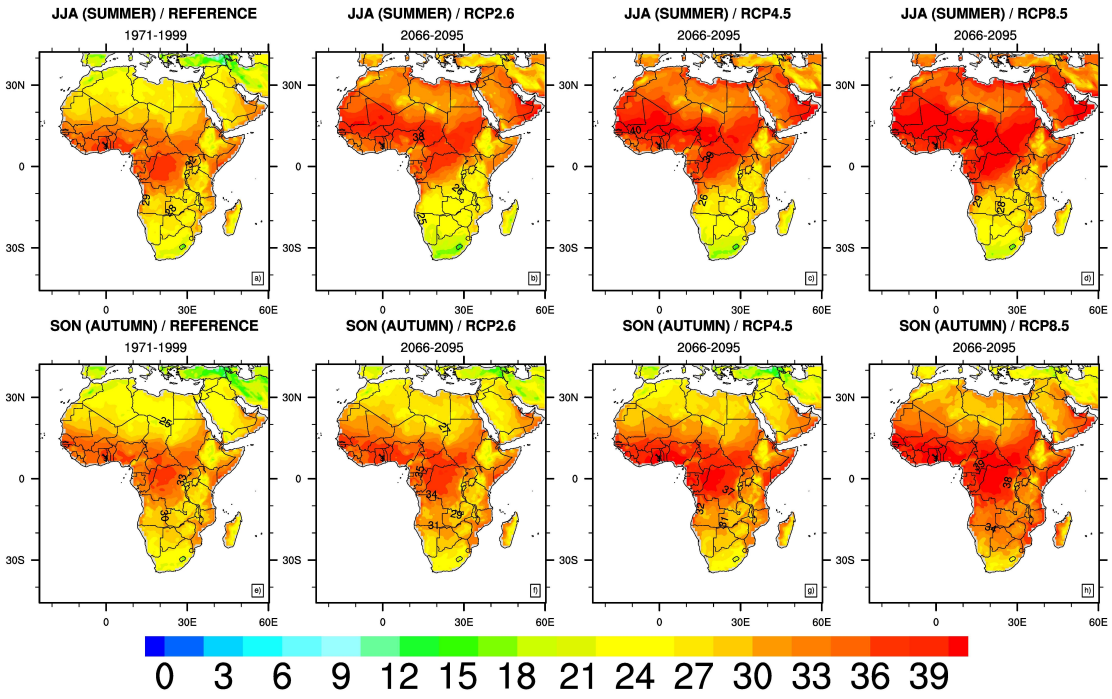

Figure 5.103. The map of spatial distribution of WBGT averages in Africa region in a year in Summer and Autumn in each period (1976 - 2005 and 2066 – 2095) according to RCP 2.6, RCP 4.5 and RCP 8.5 Scenario

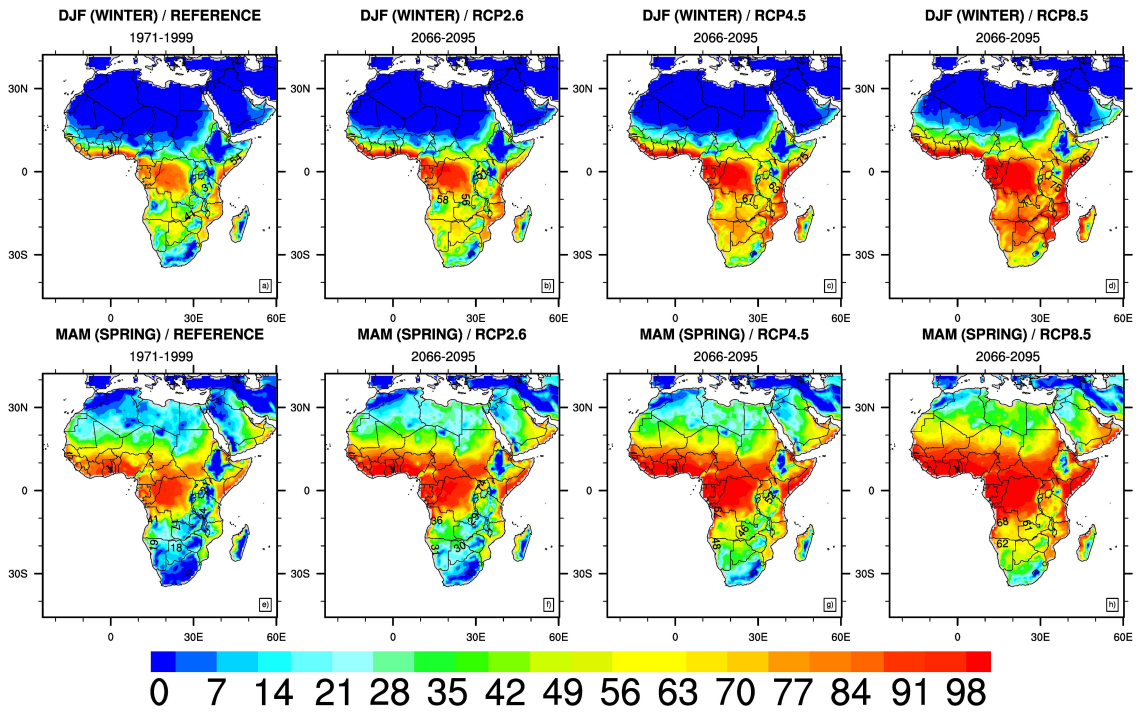

Figure 5.104. The reduction in labor productivity in Africa region in a year in Winter and Spring in each period (1976 - 2005 and 2066 – 2095) according to RCP 2.6 , RCP 4.5 and RCP 8.5 Scenario

NA is the most riskless domain in whole observed periods in the sense of thermal discomfort and labor productivity losses over Africa. Labor productivity will not be higher than 2 % over this domain in winter season. It will reach up to 40 % in other seasons except summer season. In summer season, the labor productivity will reach up to 98 % over the majority of the NA in especially 2080s with respect to RCP 8.5. MA is the most risky domain over Africa. The labor productivity over the majority of MA will not be lower than 50 % and will reach up to 98 % over the majority of the domain in each season with respect to both scenarios in both 2050s and 2080s. The labor productivity will be the lowest value in summer season and the maximum value in winter season over SA (Figure 5.102, 5.103, 5.104 and 5.105).

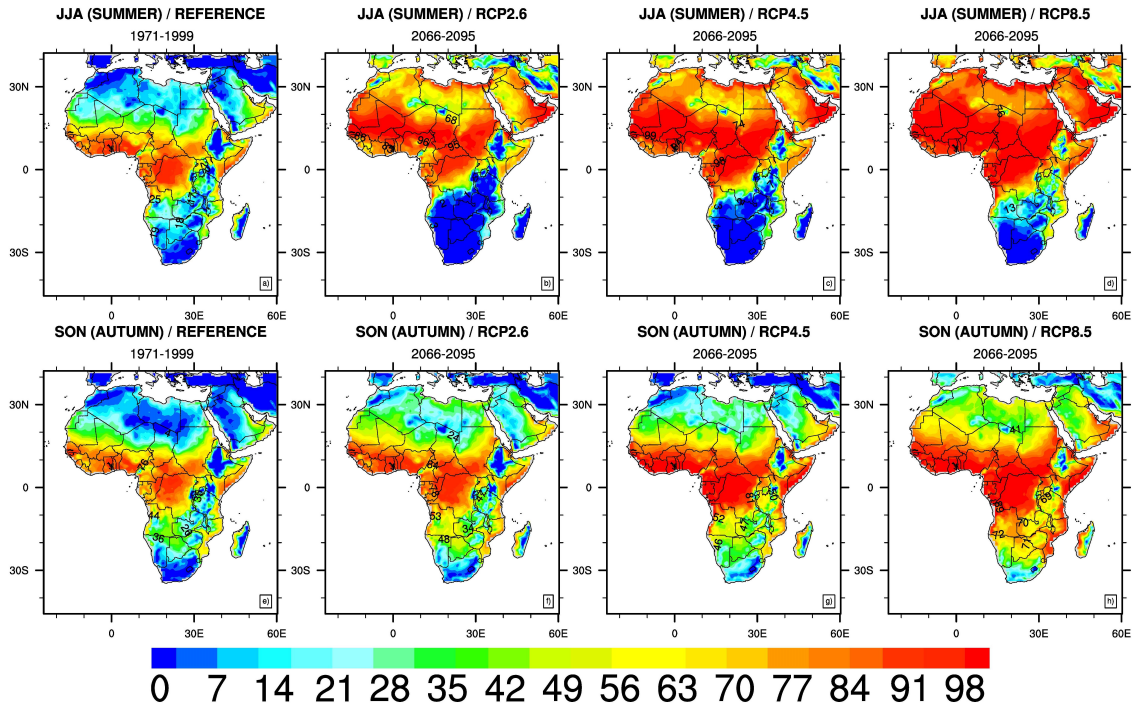

Figure 5.105. The reduction in labor productivity in Africa region in a year in Summer and Autumn in each period (1976 - 2005 and 2066 – 2095) according to RCP 2.6 , RCP 4.5 and RCP 8.5 Scenario

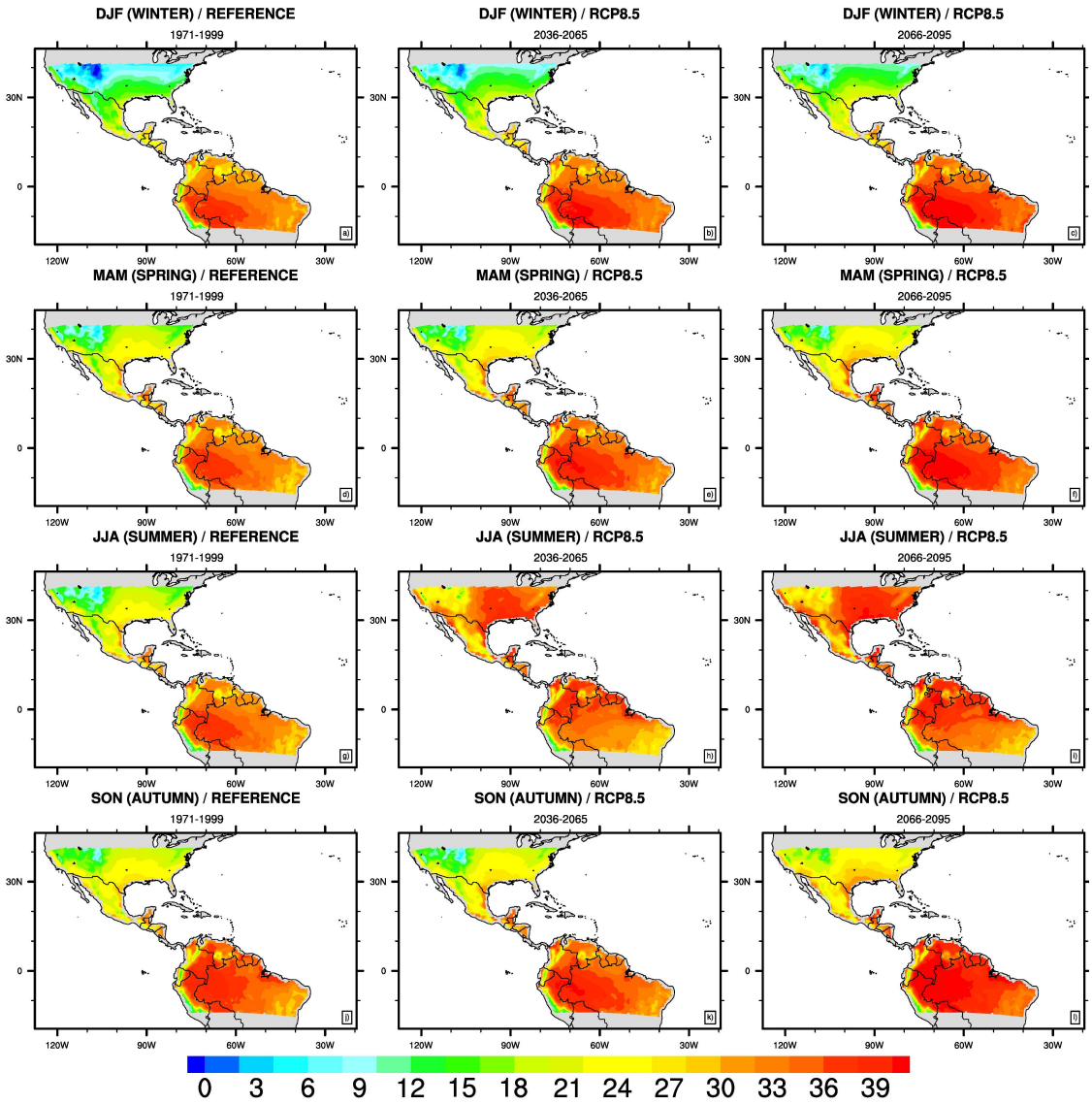

Figure 5.106. The map of spatial distribution of WBGT averages in Central America region in a year in seasons (Winter, Spring, Summer and Autumn) in each period (1976 - 2005; 2036 - 2065 and 2066 – 2095) according to RCP 8.5 Scenario

5.4.3. WBGT and Labor Productivity Alteration: The Case of Central America

The observed are can be separated to two main areas to research the foreseen WBGT and labor productivity alteration. These areas can be basically defined as the Northern Central America (NCA) and Southern Central America (SCA). The risk coefficients of these two areas (NCA and SCA) are very different from each other. WBGT will change between 24°C and 39°C over SCA, 3°C and 27°C over NCA, except summer season. Summer is the riskiest season and winter has the lowest risk in sense of projected WBGT with respect to RCP 8.5.

NCA is the most riskless domain in whole observed periods in the sense of thermal discomfort and labor productivity losses over Central America. Labor productivity will not be higher than 5 % over this domain in winter season. It will reach up to 35 % in other seasons except summer season. In summer season, the labor productivity will reach up to 90 % over the eastern part of the NCA. SCA is the most risky domain over Central America. The labor productivity over the majority of SCA will not be lower than 35 % and will reach up to 95 % over the majority of the domain in each season, except western coastal (Figure 5.106 and 5.107).

5.4.4. WBGT and Labor Productivity Alteration: The Case of South America

The observed are can be separated to four main areas to research the foreseen WBGT and labor productivity alteration. These areas can be basically defined as the North-western South America (NWSA), Middle Eastern South America (MESA), Southern South America (SSA) and Western coastal of South America (WCSA). The risk coefficients of these four areas (NWSA, MESA, SSA and WCSA) are very different from each other but very similar in each season and period with respect to both seasons. WBGT will change between 30°C and 40°C over NWCA, 25°C and 35°C over MESA, 7°C and 19°C over SSA and 10°C and 19°C over ESA. Winter is the riskiest season and summer has the lowest risk in sense of projected WBGT with respect to both RCP

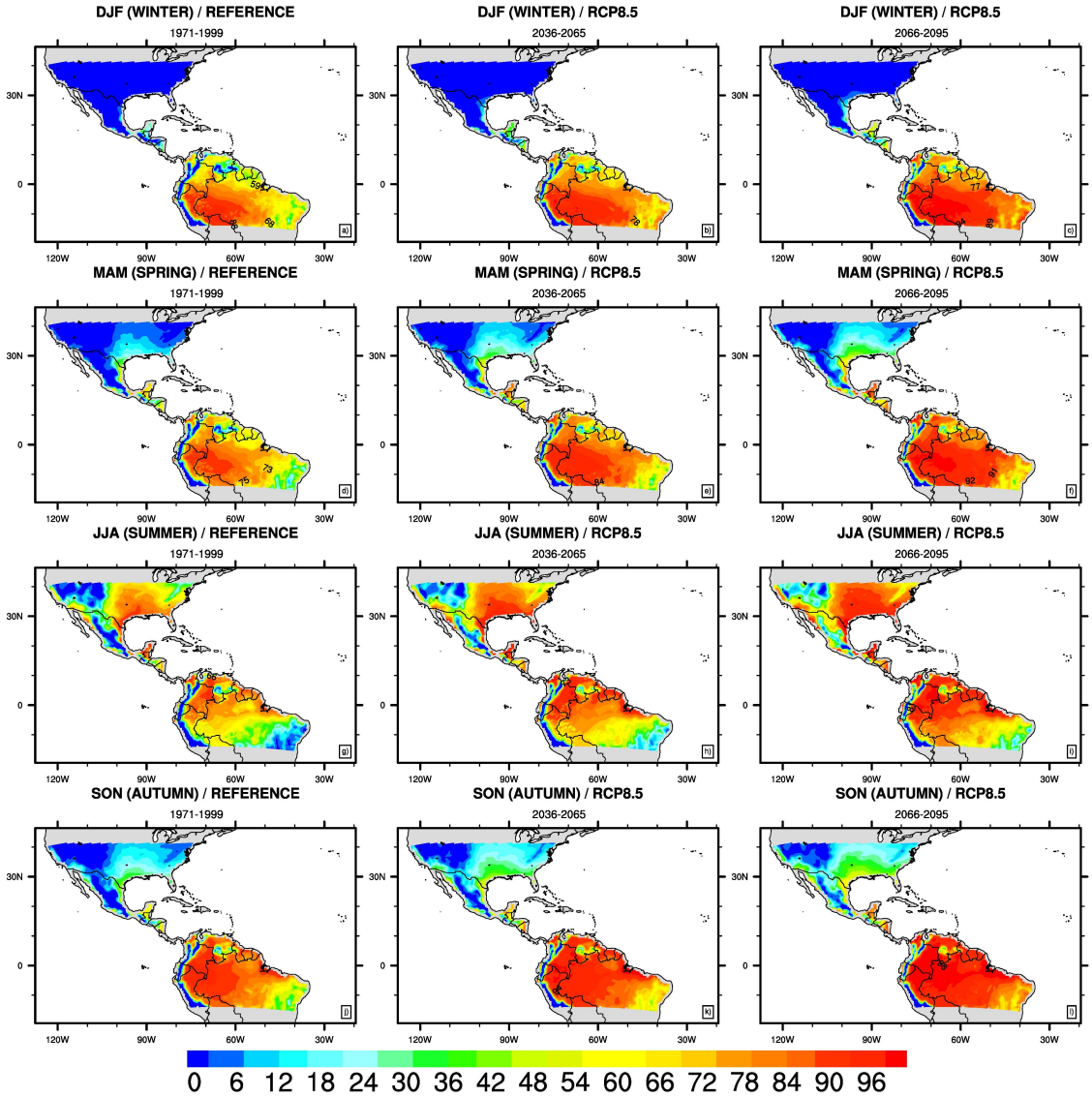

Figure 5.107. The reduction in labor productivity in Central America region in a year in seasons (Winter, Spring, Summer and Autumn) in each period (1976 - 2005; 2036 - 2065 and 2066 – 2095) according to RCP 8.5 Scenario

4.5 and RCP 8.5.

SSA is the most riskless domain in whole observed periods in the sense of thermal discomfort and labor productivity losses over South America.The loss in labor productivity will not be higher than 3 % over this domain. The labor productivity will reach up to 94 % over the NWSA and NWSA is the most risky domain over South America. The labor productivity over the majority of MESA will not be lower than 50 % and will reach up to 75 % over the majority of the domain in each season. The labor productivity over ESA change between 3 and 35 % (Figure 5.108, 5.109, 5.110 and 5.111).

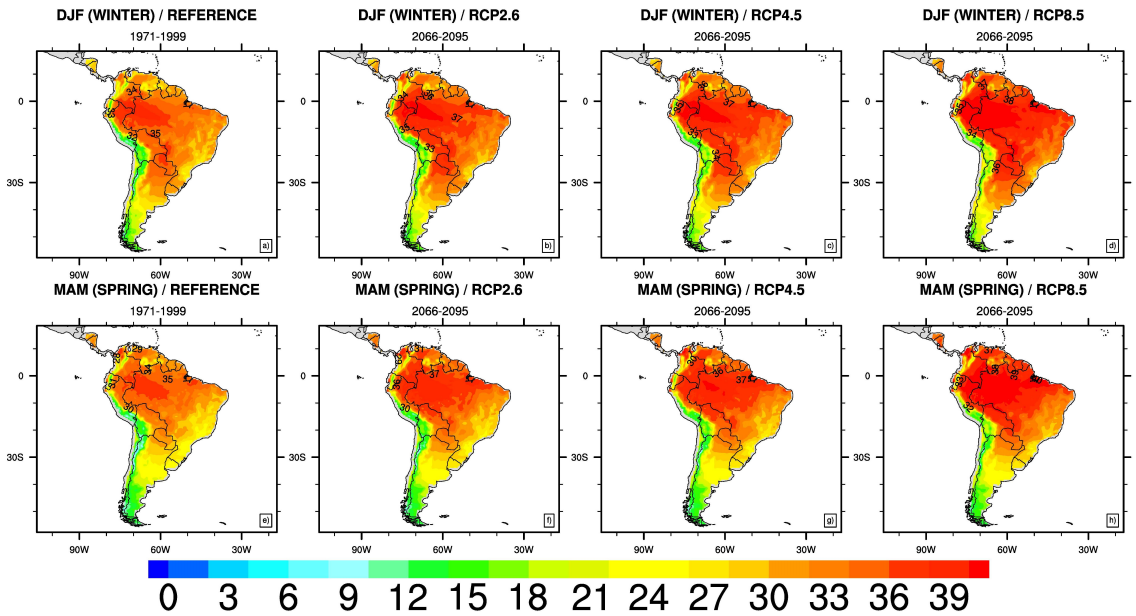

Figure 5.108. The map of spatial distribution of WBGT averages in South America region in a year in Winter and Spring in each period (1976 - 2005 and 2066 – 2095) according to RCP 2.6 , RCP 4.5 and RCP 8.5 Scenario

5.4.5. WBGT and Labor Productivity Alteration: The Case of West Asia

The observed are can be separated to three main areas to research the foreseen WBGT and labor productivity alteration. These areas can be basically defined as the Northern West Asia (NWAS), East Africa (EAF) and South West Asia (SWAS). The

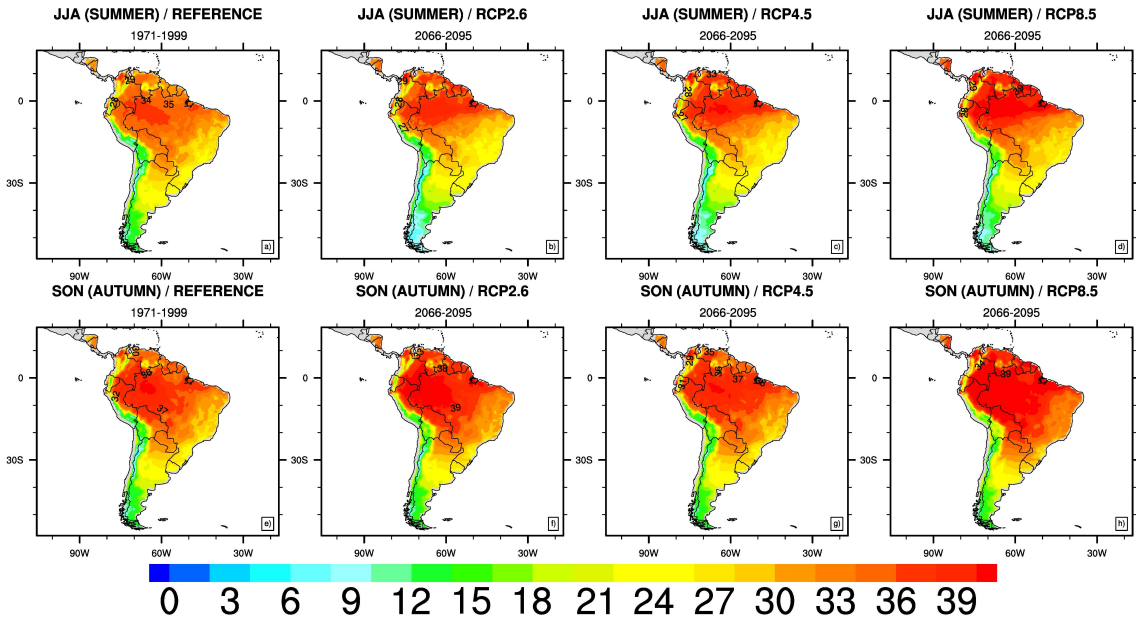

Figure 5.109. The map of spatial distribution of WBGT averages in South America region in a year in Summer and Autumn in each period (1976 - 2005 and 2066 – 2095) according to RCP 2.6 , RCP 4.5 and RCP 8.5 Scenario

risk coefficients of these three areas (NWAS, EAF and SWAS) are very similar in each season and period. WBGT will change between 0°C and 24°C over NWAS, 21°C and 40°C over EAF and 18°C and 40°C over SWAS. Summer is the riskiest season and winter has the lowest risk in sense of projected WBGT with respect to both RCP 4.5 and RCP 8.5.

NWAS is the most riskless domain in whole observed periods in the sense of thermal discomfort and labor productivity losses over West Asia. Labor productivity will not be higher than 27 % over this domain. The labor productivity will reach up to 94 % over the EAF and SWAS. EAF is the most risky domain over Wes Asia. The labor productivity over the majority of EAF and SWAS will not be lower than 60 % and will reach up to 94 % over the majority of the domain in each season, except winter (Figure 5.112 and 5.113).

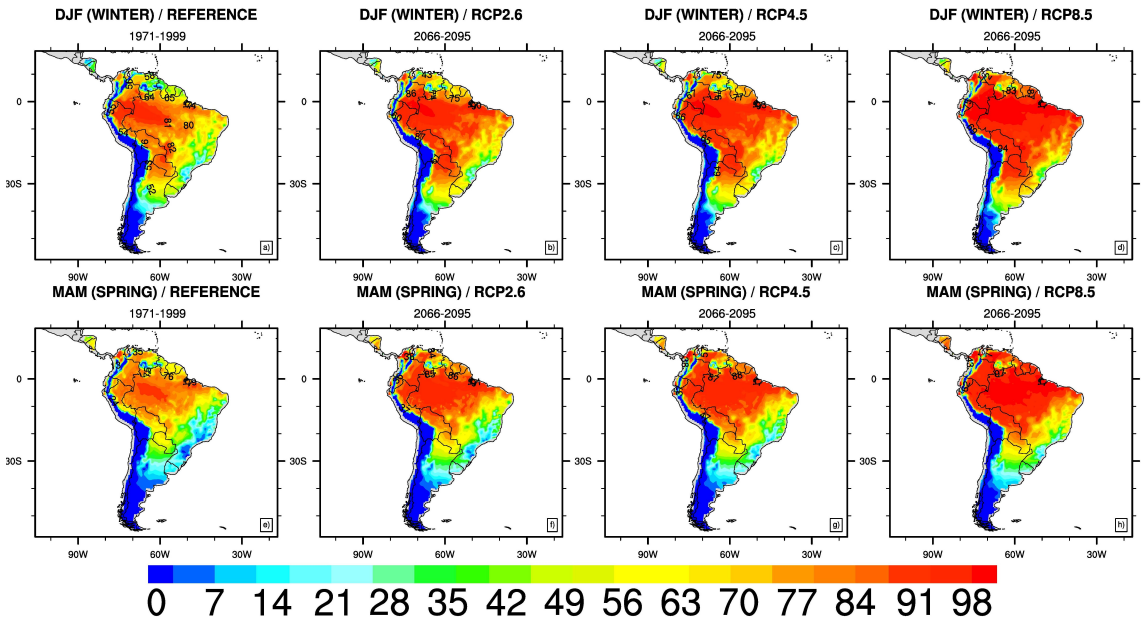

Figure 5.110. The reduction in labor productivity in South America region in a year in Winter and Spring in each period (1976 - 2005 and 2066 – 2095) according to RCP 2.6 , RCP 4.5 and RCP 8.5 Scenario

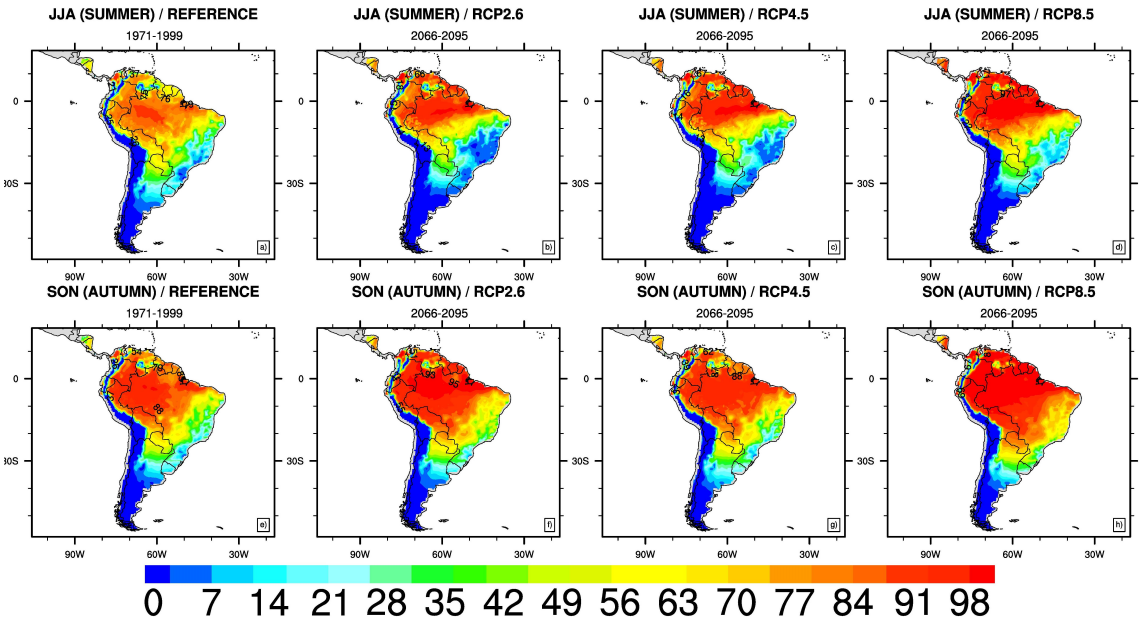

Figure 5.111. The reduction in labor productivity in South America region in a year in Summer and Autumn in each period (1976 - 2005 and 2066 – 2095) according to RCP 2.6 , RCP 4.5 and RCP 8.5 Scenario

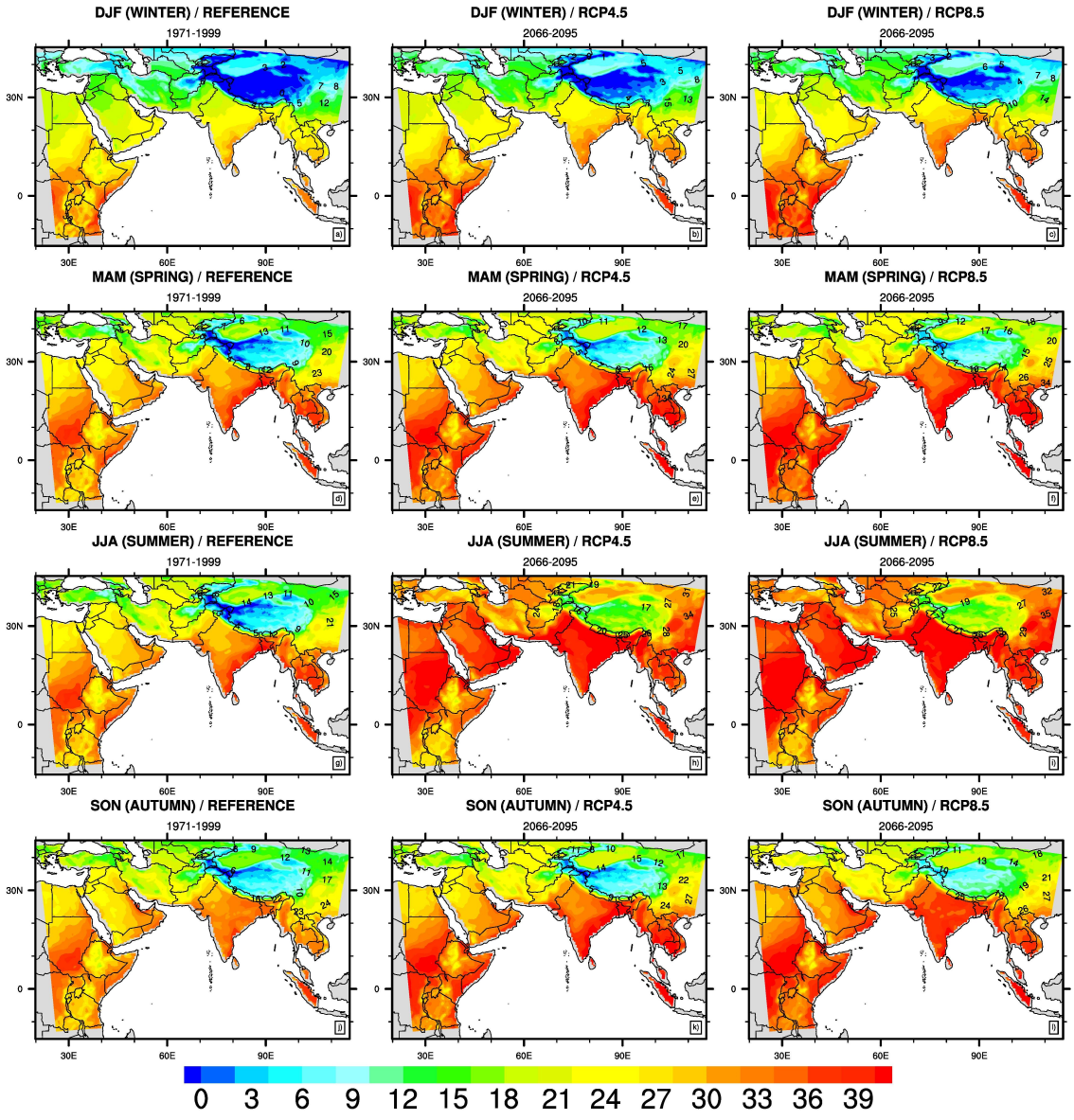

Figure 5.112. The map of spatial distribution of WBGT averages in West Asia region in a year in seasons (Winter, Spring, Summer and Autumn) in each period (1976 - 2005 and 2066 – 2095) according to RCP 4.5 and RCP 8.5 Scenario

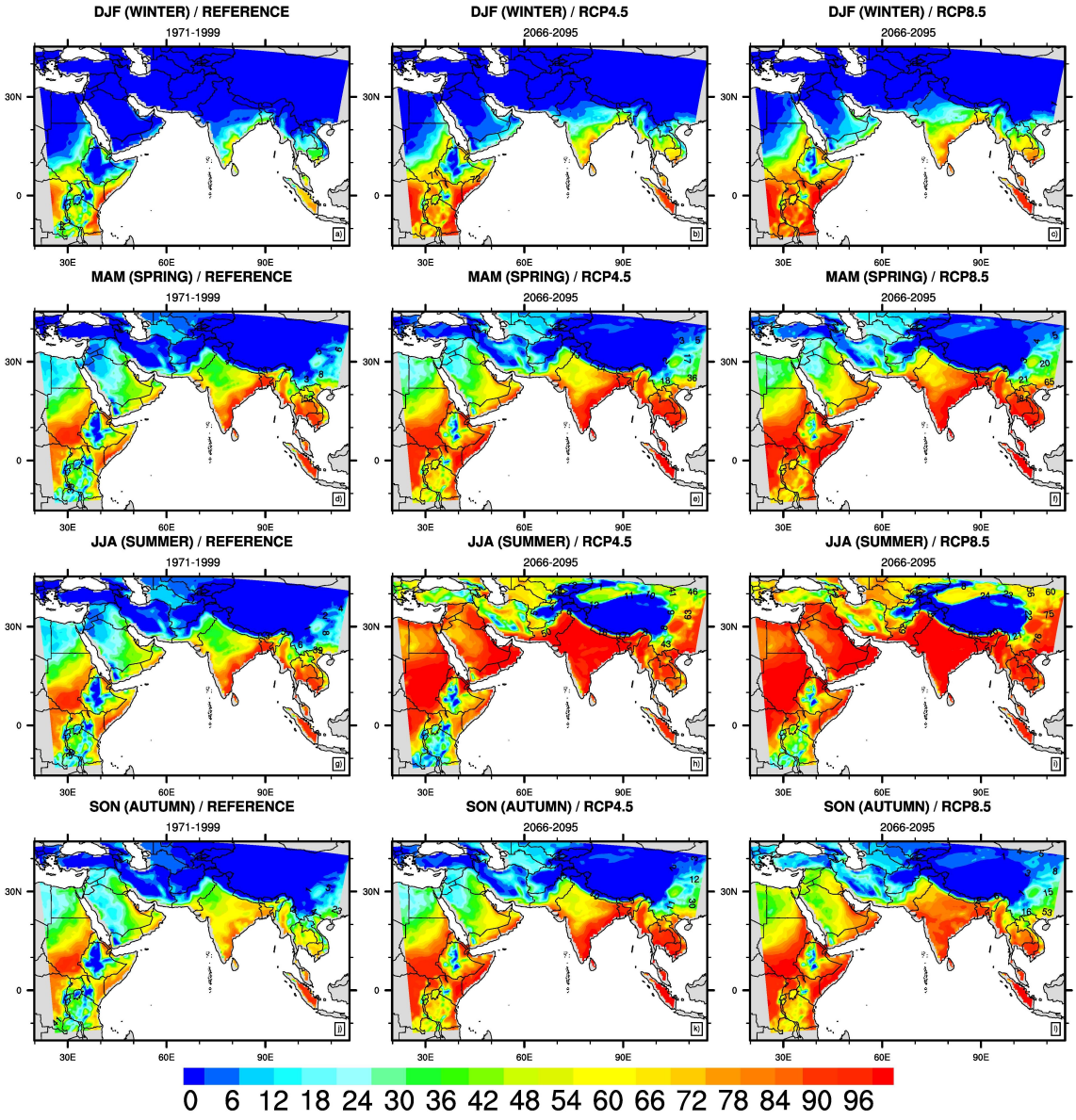

Figure 5.113. The reduction in labor productivity in West Asia region in a year in seasons (Winter, Spring, Summer and Autumn) in each period (1976 - 2005 and 2066 – 2095) according to RCP 4.5 and RCP 8.5 Scenario

6. CONCLUSION

One of the most sensitive spot in this research is finding the most accurate multi-model combination to use in the future projections over the observed region. Therefore, the performances of model combinations are evaluated by analyzing their time series in the reference period. The first observed variable is the monthly temperature over regions of Europe, Africa, West Asia, Central and South America and the data sets are obtained from CORDEX Project. The performances of each model combinations are determined by our new proposed methodology.

It is found that PES produces temperature results approximately 1 C better than EWA. MPI is the best representative GCM and REMO is the best representative RCM over Europe. In our methodologies, MPI is used in 20 trials as GCM over five domains. According to the our findings, MPI is defined as the GCM of representative model combinations in 14 of these trials. Similarly, REMO is used in 8 trials as RCM over five domains. According to the our findings, REMO is defined as the RCM of representative model combinations in 6 of these trials. CSIRO is the best representative GCM and RCA4 is the best representative RCM over Africa. MPI is used 4 times as GCM and it takes place every time in the cluster of successful model combinations. Similarly, RCA4 is used 40 times as RCM and it is coexisted 15 times in the cluster of successful model combinations. NCC and IPSL are the best representative GCMs and RCA4 is the best representative RCM over Central America. NCC and IPSL are both used 4 times as GCM and they both take place 2 times in the cluster of successful model combinations. Similarly, RCA4 is used 40 times as RCM and it is takes place 8 times in the cluster of successful model combinations. CSIRO is the best representative GCM and RCA4 is the best representative RCM over South America. CSIRO is used 4 times as GCM and it takes place 3 times in the cluster of successful model combinations. Similarly, RCA4 is used 36 times as RCM and it takes place 6 times in the cluster of successful model combinations. CSIRO is the best representative GCM and RCA4 is the best representative RCM over West Asia. CSIRO is used 8 times as GCM and it takes place 5 times in the cluster of successful model combinations. Similarly, RCA4 is

used 40 times as RCM and it is takes place 8 times in the cluster of successful model combinations.

According to our analysis, the most convenient climate model projection to simulate temperature should be performed by running MPI-REMO combination over Europe, CSIRO-RCA4 combination over Africa, NCC-RCA4 and IPSL-RCA4 over Central America, CSIRO-RCA4 over South America and CSIRO-RCA4 over West Asia in the CORDEX Project. RCA4 is the unique RCM running over South America and it can be concluded that other RCM combinations with CSIRO GCM may produce better results than CSIRO-RCA4 combination does. In general, CSIRO is the best GCM because it is used 24 times as GCM and takes place 12 times in the cluster of successful model combinations. Similarly, CLM is the best RCM because it is used 40 times as RCM and takes place 13 times in the cluster of successful model combinations.

There are limited numbers of GCM-RCM combinations in the CORDEX Project. All of the combinations weren't simulated over every domains. On the other hand, it is the most comprehensive and recent one in its field. According to the outcomes of this thesis, performing climate model simulations of running CLM as RCM driven by the outputs of CSIRO GCM is the most reliable combination. This conclusion is attained after spanning the majority of model combinations which encompasses nearly the whole World. Hence, this model combination (CSIRO-CLM) will generate more reliable results than a randomly selected one over any unexamined sub-regions in the world.

The quality and capability of further efforts like future projections, heat wave analysis and WBGT calculations depends on the accuracy of GCMs and RCMs. Continuing with unreliable model combinations leads researchers to obtain incorrect results. Hence, it is essential to determine the most accurate model combinations to represent the climate of an observed area.

Proposed methodologies produce at least 1°C better temperature outcomes than EWA does. Hence, using our suggested methodologies generates more reliable results

than EWA does in climate studies to project the temperature patterns. It is found that a temperature augmentation up to 5°C will be seen over some regions in the World. The Northern Africa, the Northern Europe, Brazil and its eastern neighbors, Iran, Afghanistan, Arabian Peninsula and the eastern Turkey are the hotspots in the sense of temperature increase because these aforementioned regions will encounter approximately 5°C augmentations in temperature in the future.

Another significant advantage of our methodology is that it gives chance to researchers to look deeply and in detail to the smaller regions of observed continentals. By viewing the outcomes of the errors of all seasons in a single figure, researchers can easily decide the most suitable model combinations at first glance. More confidential model combination selections can also be carried out by applying our suggested methodology over the selected small region.

The accuracy of model combinations, used in the heat wave analysis in the literature, focuses on the 90 % (95 % or 99 %) percentile values of daily maximum temperature. If this value of a model combination and the observation data set is similar to each other (have small differences), than it is alleged that the selected model combination is convenient to perform Heat Wave analysis. This sort of approach disregards the capability and the performance of model combination in producing the daily maximum temperature in the whole range. However, it isn't reliable to decide the success of a model combination by analyzing a unique value on its probability density function. Because of this fact, a new methodology is suggested. The comparison is carried out by regarding the full range of the probability density functions of model combinations and the observation data set. This methodology starts to compare the values from minimum one to maximum one in its distribution and generates a single value symbolizing the accuracy of the model combination. Heat wave, WBGT and labor productivity analysis are performed by using these successful model combinations. Moreover, a simple definition of the extremely hot day is proposed in this thesis. It searches the full range of the past and finds the maximum value of the daily maximum temperature. This maximum value is assigned as the minimum temperature of the "extremely hot day". Selecting the limit value for "extremely hot day" with this

definition heals the breach in the literature about the intensity of destructiveness of extreme weather events in the future. It can be easily claimed that this intensity will be higher in the future than the one in recent history.

Northern Europe, Mediterranean Coastal, Sub-Saharan Africa, Brazil, eastern Africa coastal, southern Arabian Peninsula, Iran and Pakistan are the critical regions in the sense of heat waves because number of extremely hot day and consecutive extremely hot day periods will be higher than the ones in the other observed regions of the World. The alteration in the labor productivity is also examined with the help of the WBGT index, calculated in this thesis, and limit values which are determined by NIOSH.

Mediterranean Coastal, Sub-Saharan Africa, Central America, northern part of South America, northern part of South Africa, southern coastal of Indian Ocean and eastern coastal of Africa are the most risky regions in terms of the decrease of the labor productivity. The decreases will reach up to 98 % in agriculture and construction sectors in the future. These decreases either trigger the economic losses or increase the jeopardy of health problems of workers.

REFERENCES

1. van Vuuren, D., J. Edmonds, M. Kainuma and *et al.*, "The representative concentration pathways: an overview", *Climatic Change*, Vol. 109,5, 2011.

2. Steele, K. and C. Werndl, "Climate models, calibration, and confirmation", *The British Journal for the Philosophy of Science*, Vol. 64(3), 609-635, 2013.

3. Steele, K. and C. Werndl, "Model−Selection Theory: The Need for a More Nuanced Picture of Use−Novelty and Double−Counting", *The British Journal for the Philosophy of Science*, Vol. axw024, 2016.

4. Aflatooni, M. and J. Aghajanzadeh, "Comparison of Different Global Climate Models and Statistical Downscaling Methods to Forecast Temperature Changes in Fars Province of Iran", *Environment and Pollution*, Vol. 2(4), 135, 2013.

5. Pierce, D. W., T. P. Barnett, B. D. Santer and P. J. Gleckler, "Selecting global climate models for regional climate change studies", *Proceedings of the National Academy of Sciences*, Vol. 106(21), 8441-8446, 2009.

6. A., R. S. M. and A. Hind, "Statistical framework for evaluation of climate model simulations by use of climate proxy data from the last millennium−Part 1: Theory", *Climate of the Past*, Vol. 8(4), 1339-1353, 2012.

7. Lee, J. K. and Y. O. Kim, "Selection of representative GCM scenarios preserving uncertainties", *Journal of Water and Climate Change*, Vol. 8(4), 641-651, 2017.

8. Murphy, A. H., "General decompositions of MSE−based skill scores: measures of some basic aspects of forecast quality", *Monthly Weather Review*, Vol. 124, 2353–2369, 1996.

9. Gleckler, P. J., K. E. Taylor and C. Doutriaux, "Performance metrics for climate

models", *Journal of Geophysical Research*, Vol. 113, D06104, 2008.

10. Pitman, A. J. and S. E. Perkins, "Regional projections of future seasonal and annual changes in rainfall and temperature over Australia based on skill-selected AR4 models", *Earth International*, Vol. 12, 2008.

11. Chiew, F. H. S., J. Teng, J. Vaze and D. G. C. Kirono, "Influence of global climate model selection on runoff impact assessment", *Journal of Hydrology*, Vol. 379, 172–180, 2009.

12. Winter, C. L. and D. Nychka, "Forecasting skill of model averages", *Stochastic Environmental Research and Risk Assessment*, Vol. doi:10.1007/s00477-009-0350-y, 2009.

13. Murphy, A. H., "Skill scores based on the mean-square error and their relationships to the correlation coefficient", *Monthly Weather Review*, Vol. 116, 2417–2424, 1989.

14. Epstein, E. S. and A. M. Murphy, "Skill scores and correlation coefficients in model verification", *Monthly Weather Review*, Vol. 117, 572–581, 1989.

15. Michaels, P. J., P. C. Knappenberger, J. R. Christy and *et al.*, "Assessing the consistency between short−term global temperature trends in observations and climate model projections", *arXiv*, Vol. 1309.5164, 2013.

16. Vano, J. A., J. B. Kim, D. E. Rupp and P. W. Mote, "Selecting climate change scenarios using impact−relevant sensitivities", *Geophysical Research Letters*, Vol. 42(13), 5516-5525, 2015.

17. Deidda, R., M. Marrocu, G. Caroletti and *et al.*, "Regional climate models' performance in representing precipitation and temperature over selected Mediterranean areas", *Hydrology and Earth System Sciences*, Vol. 17(12), 5041, 2013.

18. Gupta, H., S. Sorooshian, P. O. Yapo and *et al.*, "Status of Automatic Calibration for Hydrologic Models: Comparison with Multilevel Expert Calibration", *Journal of Hydrologic Engineering*, Vol. 4:2(135), 1999.

19. Matsuura, C. W. K., "Advantages of the Mean Absolute Error (MAE) over the Root Mean Square Error (RMSE) in assessing average model performance", *Climate Research*, Vol. 30,79–82, 2005.

20. Legates, D. R. and G. M. Jr, "Evaluating the use of goodness−of−fit measures in hydrologic and hydro climatic model validation", *water resources research*, Vol. 35:1,233-241, 1999.

21. Shalby, A., M. Elshemy and B. A. Zeidan, "Selecting of Regional Climate Model Simulations for Modeling Climate Change Impacts on the Water Quality Status of Lake Burullus, Egypt", *IWTC20*, 2017.

22. Anagnostopoulos, G. G., D. Koutsoyiannis, A. Christofidesand and *et al.*, "A comparison of local and aggregated climate model outputs with observed data", *Hydrological Sciences Journal−Journal des Sciences Hydrologiques*, Vol. 55(7), 1094-1110, 2010.

23. Evans, J. P., F. Ji, C. Lee and *et al.*, "Design of a regional climate modelling projection ensemble experiment–NARCliM", *Geoscientific Model Development*, Vol. 7(2), 621-629, 2014.

24. Overland, J. E., M. Wang, N. A. Bond and *et al.*, "Considerations in the selection of global climate models for regional climate projections: The Arctic as a case study", *Journal of Climate*, Vol. 24(6), 1583-1597, 2011.

25. Reifen, C. and R. Toumi, "Climate projections: Past performance no guarantee of future skill?", *Geophys. Res. Lett.*, Vol. 36, L13704, 2009.

26. Kotlarski, S., K. Keuler, O. B. Christensen, A. Colette, M. Déqué, A. Gobiet,

and G. Nikulin, "Regional climate modeling on European scales: a joint standard evaluation of the EURO - CORDEX RCM ensemble", *Geoscientific Model Development*, Vol. 7(4), 1297-1333, 2014.

27. Flaounas, E., P. Drobinski, M. Borga, J. C. Calvet, G. Delrieu, E. Morin and R. Toffolon, "Assessment of gridded observations used for climate model validation in the Mediterranean region: the HyMeX and MED - CORDEX framework", *Environmental Research Letters*, Vol. 7(2), 2012.

28. Raymond, F., A. Ullmann, P. Camberlin, P. Drobinski and C. C. Smith, "Extreme dry spell detection and climatology over the Mediterranean Basin during the wet season", *Geophysical Research Letters*, Vol. 43(13), 7196-7204, 2016.

29. Lhotka, O., *Long-term variability of heat waves and cold spells in Central Europe*, Ph.D. Thesis, Charles Unıversıty in Prague, Faculty of Scıence, Department of Physical Geography and Geoecology, 2016.

30. Madsen, M. S., P. L. Langen, F. Boberg and J. H. Christensen, "Inflated Uncertainty in Multimodel - Based Regional Climate Projections", *Geophysical Research Letters*, Vol. 44(22), 2017.

31. Luca, A. D., D. Argüeso, J. P. Evans, R. Elía and R. Laprise, "Quantifying the overall added value of dynamical downscaling and the contribution from different spatial scales", *Journal of Geophysical Research: Atmospheres*, Vol. 121(4), 1575-1590, 2016.

32. Andreas, F. P., L. Wolfgang, F. Giorgia, F. Andrew, B. Nikolina, G. Klaus, K. Michael and T. Merja, "A review on regional convection permitting climate modeling Demonstrations, prospects and challenges", *Reviews of geophysics*, Vol. 53(2), 323-361, 2015.

33. Altinsoy, H., T. Ozturk, M. Turkes and M. L. Kurnaz, *Analysis of the effect of climate change on the yield of crops in Turkey using a statistical approach*,

Springer, Berlin, Heidelberg, 2013.

34. Kurt, C., A. R. Muş, H. Altinsoy and M. L. Kurnaz, *İklim Değişikliğinin Türkiye Tarım Ürünlerinin Verimi Üzerine Etkisi*, Istanbul-Turkey, 2011.

35. Kurt, C., A. R. Muş, H. Altinsoy and M. L. Kurnaz, *İklim Değişkenlerinin ve Nüfusun Türkiye Tarım Ürünlerinin Verimi Üzerine Etkisi*, Istanbul-Turkey, 2010.

36. Apostolakis, A., K. Wagner, I. N. Daliakopoulos, N. N. Kourgialas and I. K. Tsanis, "Greenhouse Soil Moisture Deficit under Saline Irrigation and Climate Change", *Procedia engineering*, Vol. 162, 537-544, 2016.

37. Møller, L. R., M. Drews and M. A. D. Larsen, "Simulation of Optimal Decision-Making Under the Impacts of Climate Change", *Environmental management*, Vol. 60(1), 104-117, 2017.

38. Im, E. S. and E. A. Eltahir, "Enhancement of rainfall and runoff upstream from irrigation location in a climate model of West Africa", *Water Resources Research*, Vol. 50(11), 8651-8674, 2014.

39. Altinsoy, H., A. Yuncu and M. L. Kurnaz, *The Precipitation and Temperature Regime Over Three European Sub-regions as a Result of Climate Change*, Springer, Berlin, Heidelberg, 2013.

40. Türkeş, M., M. L. Kurnaz, T. Öztürk and H. Altınsoy, *Climate changes versus 'security and peace'in the Mediterranean macroclimate region: are they correlated*, Istanbul-Turkey, 2011.

41. Altınsoy, H., T. Öztürk, M.Türkeş and M. L. Kurnaz, *Projections of future air temperature and precipitation changes in the Mediterranean Basin by using the global climate model*, Istanbul-Turkey, 2011.

42. Bucchignani, E., P. Mercogliano, H. J. Panitz and M. Montesarchio, "Climate change projections for the Middle East-North Africa domain with COSMO-CLM at different spatial resolutions", *Advances in Climate Change Research*, Vol. 9(1), 66-80, 2018.

43. Ozturk, T., M. T. Turp, M. Türkeş and M. L. Kurnaz, "Future projections of temperature and precipitation climatology for CORDEX - MENA domain using RegCM4. 4.", *Atmospheric Research*, Vol. 206, 87-107, 2018.

44. Öztürk, T., H. Altınsoy, M. Türkeş and M. L. Kurnaz, *Simulation of extreme events for the Central Asia cordex domain by using the RegCM 4.0*, 5th Atmospheric Science Symposium Proceedings Book, 2011.

45. Altinsoy, H., T. Ozturk, M. Turkes and M. L. Kurnaz, *Simulating the climatology of extreme events for the central Asia domain using the RegCM 4.0 regional climate model*, Springer, Berlin, Heidelberg, 2013.

46. ilvina A. Solman, E. Sanchez, P. Samuelsson, R. P. da Rocha, L. Li, J. Marengo, N. L. Pessacg, A. R. C. Remedio, S. C. Chou, H. Berbery, H. L. Treut, M. de Castro and D. Jacob, "Evaluation of an ensemble of regional climate model simulations over South America driven by the ERA - Interim reanalysis: model performance and uncertainties.", *Climate Dynamics*, Vol. 41(5-6), 1139-1157, 2013.

47. Pielke, R. A., A. Pitman, D. Niyogi, R. Mahmood, C. Mcalpine, F. Hossain, K. K. Goldewijk, U. Nair, R. Betts and S. Fall, "Land use - land cover changes and climate: modeling analysis and observational evidence", *Wiley Interdiscip. Rev. Clim. Change*, Vol. 2 828–850, 2011.

48. Davidson, E. A., A. C. de Araújo and P. A. *et al.*, "The Amazon basin in transition", *Nature*, Vol. 481 321–328, 2012.

49. Lawrence, D. and K. Vandecar, "Effects of tropical deforestation on climate and agriculture", *Nature Climate Change*, Vol. 5 27–36, 2015.

50. Wu, M., G. Schurgers, A. Ahlström, M. Rummukainen, P. A. Miller, B. Smith and W. May, "Impacts of land use on climate and ecosystem productivity over the Amazon and the South American continent", *Environmental Research Letters*, Vol. 12(5), 2017.

51. Fernandez, J. P., S. H. Franchito, V. B. Rao and M. Llopart, "Changes in Koppen-Trewartha climate classification over South America from RegCM4 projections", *Atmospheric Science Letters*, Vol. 18(11), 427-434, 2017.

52. Šeparović, L., A. Alexandru, R. Laprise, A. Martynov, L. Sushama, K. Winger, K. Tete and M. Valin, "Present climate and climate change over North America as simulated by the fifth - generation Canadian regional climate model", *Climate dynamics*, Vol. 41(11-12), 3167-3201, 2013.

53. Parker, L. E. and J. T. Abatzoglou, "Projected changes in cold hardiness zones and suitable overwinter ranges of perennial crops over the United States", *Environmental Research Letters*, Vol. 11(3), 2016.

54. Fahad, G. R., R. Nazari, J. Daraio and D. J. Lundberg, "Regional Study of Future Temperature and Precipitation Changes Using Bias Corrected Multi-Model Ensemble Projections Considering High Emission Pathways", *J Earth Sci Clim Change*, Vol. 8(409), 2, 2017.

55. Fuentes-Franco, R., E. Coppola, F. Giorgi, E. G. Pavia, G. T. Diro and F. Graef, "Inter - annual variability of precipitation over Southern Mexico and Central America and its relationship to sea surface temperature from a set of future projections from CMIP5 GCMs and RegCM4 CORDEX simulations", *Climate Dynamics*, Vol. 45(1-2), 425-440, 2015.

56. Winter, J. M., P. J. F. Yeh, X. Fu and E. A. Eltahir, "Uncertainty in modeled and observed climate change impacts on American Midwest hydrology", *Water Resources Research*, Vol. 51(5), 3635-3646, 2015.

57. Wu, C., X. Liu, Z. Lin, A. M. Rhoades, P. A. Ullrich, C. M. Zarzycki and S. R. R. Esfarjani, "Exploring a Variable Resolution Approach for Simulating Regional Climate in the Rocky Mountain Region Using the VR - CESM", *Journal of Geophysical Research: Atmospheres*, Vol. 122(20), 2017.

58. Kim, J., D. E. Waliser, C. A. Mattmann, C. E. Goodale, A. F. Hart, P. A. Zimdars, D. J. Crichton, C. Jones, G. Nikulin, B. Hewitson, C. Jack, C. Lennard and A. Favre, "Evaluation of the CORDEX - Africa multi - RCM hindcast: systematic model errors", *Climate dynamics*, Vol. 42(5-6), 1189-1202, 2014.

59. Creese, A. and R. Washington, "Using qflux to constrain modeled Congo Basin rainfall in the CMIP5 ensemble", *Journal of Geophysical Research: Atmospheres*, Vol. 121(22), 2016.

60. Mutayoba, E. and J. J. Kashaigili, "Evaluation for the Performance of the CORDEX Regional Climate Models in Simulating Rainfall Characteristics over Mbarali River Catchment in the Rufiji Basin, Tanzania", *Journal of Geoscience and Environment Protection*, Vol. 5(04), 139, 2017.

61. Onyutha, C., H. Tabari, A. Rutkowska, P. Nyeko-Ogiramoi and P. Willems, "Comparison of different statistical downscaling methods for climate change rainfall projections over the Lake Victoria basin considering CMIP3 and CMIP5", *Journal of Hydro-environment Research*, Vol. 12, 31-45, 2016.

62. Shongwe, M. E., C. Lennard, B. Liebmann, E. A. Kalognomou, L. Ntsangwane and I. Pinto, "An evaluation of CORDEX regional climate models in simulating precipitation over Southern Africa", *Atmospheric Science Letters*, Vol. 16(3), 199-207, 2015.

63. Ogega, O. M., L. Ojwang, C. Oludhe and J. Mbugua, "An integrated climate change adaptation framework for coastal small-holder farmers in Kenya", .

64. James, R., R. Washington and R. Jones, "Process - based assessment of an en-

semble of climate projections for West Africa", *Journal of Geophysical Research: Atmospheres*, Vol. 120(4), 1221-1238, 2015.

65. Erfanian, A., G. Wang, M. Yu and R. Anyah, "Multimodel ensemble simulations of present and future climates over West Africa: Impacts of vegetation dynamics", *Journal of Advances in Modeling Earth Systems*, Vol. 8(3), 1411-1431, 2016.

66. Sylla, M. B., F. Giorgi, E. Coppola and L. Mariotti, "Uncertainties in daily rainfall over Africa: assessment of gridded observation products and evaluation of a regional climate model simulation", *International Journal of Climatology*, Vol. 33(7), 1805-1817, 2013.

67. Kling, H., P. Stanzel and M. Fuchs, "Regional assessment of the hydropower potential of rivers in West Africa", *Energy Procedia*, Vol. 97, 286-293, 2016.

68. Brands, S., S. Herrera, J. Fernández and J. M. Gutiérrez, "How well do CMIP5 Earth System Models simulate present climate conditions in Europe and Africa?", *Climate dynamics*, Vol. 41(3-4), 803-817, 2013.

69. Hauser, M., L. Gudmundsson, R. Orth, A. Jézéquel, K. Haustein, R. Vautard, J. van Oldenborgh Geert, L. Wilcox and S. I. Seneviratne, "Methods and model dependency of extreme event attribution: the 2015 European drought", *Earth's Future*, Vol. 5(10), 1034-1043, 2017.

70. Rajczak, J. and C. Schär, "Projections of future precipitation extremes over Europe: A multimodel assessment of climate simulations.", *Journal of Geophysical Research: Atmospheres*, Vol. 122(20), 2017.

71. Vries, H., G. Lenderink and E. Meijgaard, "Future snowfall in western and central Europe projected with a high - resolution regional climate model ensemble", *Geophysical Research Letters*, Vol. 41(12), 4294-4299, 2014.

72. Saeed, S., E. Brisson, M. Demuzere, H. Tabari, P. Willems and N. P. van Lipzig,

"Multidecadal convection permitting climate simulations over Belgium: sensitivity of future precipitation extremes", *Atmospheric Science Letters*, Vol. 18(1), 29-36, 2017.

73. Wouters, H., K. D. Ridder, L. Poelmans, P. Willems, J. Brouwers, P. Hosseinzadehtalaei and M. Demuzere, "Heat stress increase under climate change twice as large in cities as in rural areas: A study for a densely populated midlatitude maritime region", *Geophysical Research Letters*, Vol. 44(17), 8997-9007, 2017.

74. Vautard, R., T. Noël, L. Li, M. Vrac, E. Martin, P. Dandin and S. Joussaume, "Climate variability and trends in downscaled high - resolution simulations and projections over Metropolitan France", *Climate dynamics*, Vol. 41(5-6), 1419-1437, 2013.

75. Verfaillie, D., M. Lafaysse, M. Déqué, N. Eckert, Y. Lejeune and S. Morin, "Multicomponent ensembles of future meteorological and natural snow conditions for 1500 m altitude in the Chartreuse mountain range, Northern French Alps", *The Cryosphere*, Vol. 12(4), 1249, 2018.

76. Hackenbruch, J., G. Schädler and J. W. Schipper, "Added value of high-resolution regional climate simulations for regional impact studies", *Meteorologische Zeitschrift*, Vol. 25, No. 3, pp. 291–304, 06 2016, `http://dx.doi.org/10.1127/metz/2016/0701`.

77. Imbery, F., S. Plagemann and J. Namyslo, "Processing and analysing an ensemble of climate projections for the joint research project KLIWAS", *Advances in Science and Research*, Vol. 10(1), 91-98, 2013.

78. Stott, P. and C. Forest, "Ensemble climate predictions using climate models and observational constraints", *Phil. Trans. R. Soc. A*, Vol. 365, 2029–2052, 2007.

79. Christensen, J., E. Kjellstrom, F. Giorgi, G. Lenderink and M. Rummukainen, "Weight assignment in regional climate models", *Climate Research*, Vol. 44,

179–194, 2010.

80. Deque, M. and S. Somot, "Weighted frequency distributions express modelling uncertainties in the ENSEMBLES regional climate experiments", *Climate Research.*, Vol. 44, 195–209, 2010.

81. Giorgi, F., C. Jones and G. R. Asrar, "Addressing climate information needs at the regional level: the CORDEX framework", *WMO Bulletin*, Vol. 58, 175–183, 2009.

82. Piniewski, M., A. Mezghani, M. Szcześniak and Z. W. Kundzewicz, "Regional projections of temperature and precipitation changes: Robustness and uncertainty aspects", *Meteorol. Z*, Vol. 26, 223-234, 2017.

83. Della-Marta, P. M., J. Luterbacher and H. W. *et al.*, "Summer heat waves over western Europe 1880 - 2003, their relationship to large-scale forcings and predictability", *Climate Dynamics*, Vol. 29,251–275, 2007.

84. Kysely, J., "Recent severe heat waves in central Europe: how to view them in a long-term prospect?", *International Journal Climatology*, Vol. 30,89-109, 2010.

85. Barriopedro, D., E. M. Fischer, J. Luterbacher and *et al.*, "The hot summer of 2010: redrawing the temperature record map of Europe", *Science*, Vol. 332,220-224, 2011.

86. Bono, A. D., G. Giuliani, S. Kluser and P. Peduzzi, "Impacts of summer 2003 heat wave in Europe", *UNEP/DEWA/GRID-Europe Environ Alert Bull*, Vol. 2,1-4, 2004.

87. Beniston, M., D. B. Stephenson, O. B. Christensen and *et al.*, "Future extreme events in European climate: an exploration of regional climate model projections", *Climate Change*, Vol. 81,71–95, 2007.

88. Langousis, A., A. Mamalakis, R. Deidda and M. Marrocu, "Assessing the relative effectiveness of statistical downscaling and distribution mapping in reproducing rainfall statistics based on climate model results", *Water Resources Research*, Vol. 52(1), 471-494, 2016.

89. Davin, E. L., E. Maisonnave and S. I. Seneviratne, "Is land surface processes representation a possible weak link in current Regional Climate Models?", *Environmental Research Letters*, Vol. 11(7), 2016.

90. Montesarchio, M., A. L. Zollo, E. Bucchignani, P. Mercogliano and S. Castellari, "Performance evaluation of high - resolution regional climate simulations in the Alpine space and analysis of extreme events", *Journal of Geophysical Research: Atmospheres*, Vol. 119(6), 3222-3237, 2014.

91. Torma, C., F. Giorgi and E. Coppola, "Added value of regional climate modeling over areas characterized by complex terrain-Precipitation over the Alps", *Journal of Geophysical Research: Atmospheres*, Vol. 120(9), 3957-3972, 2015.

92. Liu, S., W. Gao and X. Z. Liang, "A regional climate model downscaling projection of China future climate change", *Climate dynamics*, Vol. 41(7-8), 1871-1884, 2013.

93. Arini, E. Y., R. Hidayat and A. Faqih, "Rainfall simulation using RegCM4 model in Kalimantan during El Nino Southern Oscillation", *Procedia Environmental Sciences*, Vol. 24, 70-86., 2015.

94. Zhang, D. F., Z. Y. Han and Y. Shi, "Comparison of climate projections between driving CSIRO-Mk3. 6.0 and downscaling simulation of RegCM4. 4 over China", *Advances in Climate Change Research*, Vol. 8(4), 245-255, 2017.

95. Tang, J., X. Niu, S. Wang, H. Gao, X. Wang and J. Wu, "Statistical downscaling and dynamical downscaling of regional climate in China: Present climate evaluations and future climate projections", *Journal of Geophysical Research: At-*

mospheres, Vol. 121(5), 2110-2129, 2016.

96. Zhang, D. F., X. J. Gao, A. Zakey and F. Giorgi, "Effects of climate changes on dust aerosol over East Asia from RegCM3", *Advances in Climate Change Research*, Vol. 7(3), 145-153, 2016.

97. Mishra, V., D. Kumar, A. R. Ganguly, J. Sanjay, M. Mujumdar, R. Krishnan and R. D. Shah, "Reliability of regional and global climate models to simulate precipitation extremes over India", *Journal of Geophysical Research: Atmospheres*, Vol. 119(15), 9301-9323, 2014.

98. Sabeerali, C. T., S. A. Rao, A. R. Dhakate, K. Salunke and B. N. Goswami, "Why ensemble mean projection of south Asian monsoon rainfall by CMIP5 models is not reliable?", *Climate Dynamics*, Vol. 45(1-2), 161-174., 2015.

99. Mishra, V., "Climatic uncertainty in Himalayan water towers", *Journal of Geophysical Research: Atmospheres*, Vol. 120(7), 2689-2705, 2015.

100. Dimri, A. P., D. Kumar, A. Choudhary and P. Maharana, "Future changes over the Himalayas: Mean temperature", *Global and Planetary Change*, Vol. 162, 235-251, 2018.

101. Dimri, A. P., D. Kumar, A. Choudhary and P. Maharana, "Future changes over the Himalayas: Mean temperature", *Global and Planetary Change*, Vol. 162, 235-251, 2018.

102. Anand, J., M. Devak, A. K. Gosain, R. Khosa and C. T. Dhanya, "Spatial Extent of Future Changes in the Hydrologic Cycle Components in Ganga Basin using Ranked CORDEX RCMs", *Hydrol. Earth Syst. Sci. Discuss.*, Vol. https://doi.org/10.5194/hess-2017-189, 2017.

103. Öztürk, T., H. Altinsoy and M. L. Kurnaz, *İstatistiksel Metotlar Kullanılarak İklim Değişkenlerinin Uç Olaylar Analizi*, Istanbul-Turkey, 2011.

104. Altinsoy, H., C. Kurt, H. A. Yildirim and A. Öztopal, *Future heat wave analysis over Aegean coastal regions by using ensemble project results*, Brussels-Belgium, 2013.

105. Öztürk, T., H. Altınsoy and M. L. Kurnaz, *Climate Variable Extreme Event Analysis by Using Statistical Methods*, Istanbul-Turkey, 2010.

106. der Linden, P. V. and J. E. Mitchell, "ENSEMBLES: Climate change and its impacts-Summary of research and results from the ENSEMBLES project", *ENSEMBLES*, Vol. 1, 2009.

107. Giorgi, F. and P. Lionello, "Climate change projections for the Mediterranean region", *Global and planetary change*, Vol. 63(2-3), 90-104, 2008.

108. Sánchez, E., C. Gallardo, M. Gaertner, A. Arribas and M. Castro, "Future climate extreme events in the Mediterranean simulated by a regional climate model: a first approach", *Global and Planetary Change*, Vol. 44, 1-4, 163-180, 2004.

109. Yildirim, H. A. and H. Altinsoy, "Chaos and trend analysis of monthly precipitation over Arabian Peninsula and Eastern Mediterranean", *Arabian Journal of Geosciences*, Vol. 10(2),21, 2017.

110. Öztürk, T., H. Altinsoy, M. Türkeş and M. L. Kurnaz, *RegCM4.0 Experiments for Central Asia CORDEX Domain*, Trieste- Italy, 2011.

111. Öztürk, T., H. Altinsoy and M. L. Kurnaz, *The Precipitation and Temperature Regime over Turkey as a Result of Climate Change*, Trieste- Italy, 2010.

112. Yüncü, A., T. Öztürk, H. Altinsoy and M. L. Kurnaz, *Türkiye'de Yüzyılın 2070-2100 Yılları için Sıcaklık ve Yağış Rejimi Tahminleri*, Istanbul-Turkey, 2011.

113. Altinsoy, H., A. Öztopal and H. A. Yildirim, *21th century precipitation projection over the Eastern Mediterranean by using RegCM 4.1.1*, Brussels-Belgium, 2013.

114. Altinsoy, H., C.Kurt, H. A.Yildirim and A.Öztopal, *Projection of air temperature over Turkey by using multi-model ensemble approach*, Brussels-Belgium, 2013.

115. Altınsoy, H., A. Yüncü, T. Öztürk and M. L. Kurnaz, *Projection of 21st Century Turkey Precipitation and Temperature*, Istanbul-Turkey, 2010.

116. Yıldırım, H. A., H. Altinsoy and C. İkiel, *Küresel Iklim Modelleri Sonuçlarina Göre Türkiye'nin Sicaklik Trend Analizi*, Istanbul-Turkey, 2013.

117. Hadjinicolaou, P., C. Giannakopoulos, C. Zerefos, M. A. Lange, S. Pashiardis and J. Lelieveld, "Mid - 21st century climate and weather extremes in Cyprus as projected by six regional climate models", *Regional Environmental Change*, Vol. 11(3), 441-457, 2011.

118. Orlowsky, B. and S. I. Seneviratne, "Global changes in extreme events: regional and seasonal dimension", *Climatic Change*, Vol. 110(3-4), 669-696, 2012.

119. Diffenbaugh, N. S. and F. Giorgi, "Climate change hotspots in the CMIP5 global climate model ensemble", *Climatic change*, Vol. 114(3-4), 813-822, 2012.

120. Kostopoulou, E. and P. D. Jones, "Assessment of climate extremes in the Eastern Mediterranean", *Meteorology and Atmospheric Physics*, Vol. 89.1-4:69-85, 2005.

121. Flocas, H. A., M. Hatzaki, K. Tolika, C. Anagnostopoulou, E. Kostopoulou, C. Giannakopoulos, ... and I. Tegoulias, "Ability of RCM - GCM couples to represent the relationship of large scale circulation to climate extremes over the Mediterranean region", *Climate Research*, Vol. 46(3), 197-209, 2011.

122. Fischer, E. M. and R. Knutti, "Anthropogenic contribution to global occurrence of heavy-precipitation and high-temperature extremes", *Nature Climate Change*, Vol. 5.6:560, 2015.

123. Nikulin, G., E. Kjellström, U. L. F. Hansson, G. Strandberg and A. Ullerstig,

"Evaluation and future projections of temperature, precipitation and wind extremes over Europe in an ensemble of regional climate simulations", *Tellus A*, Vol. 63(1), 41-55, 2011.

124. Altinsoy, H. and H. A.Yildirim, "Wet bulb globe temperature across Western Turkey according to the ENSEMBLES project", *International Journal of Global Warming*, Vol. 9(1),66-80, 2016.

125. Yildirim, H. A. and H. Altinsoy, "Nonlinear dynamics of monthly temperature data set in the Northwestern (Marmara region) Turkey", *International Journal of Global Warming*, Vol. 14(1),97-117, 2018.

126. Altinsoy, H., A. Öztopal and H. A. Yildirim, *Projections of labor productivity over Eastern Mediterranean region by using ReGCM4.1.1*, Brussels-Belgium, 2013.

127. Yıldırım, H. A., H. Altinsoy and C. İkiel, *Trakya'daki Günlük Yağış Verisinin Kaotik Davranışı*, Istanbul-Turkey, 2013.

128. Yıldırım, H. A. and H. Altinsoy, *ISO 7730 ve 7246 Standartlarina Göre Termal Konfor Programı*, Ankara-Turkey, 2016.

129. Altinsoy, H., *Termal Konfor İndisleri Ve Türkiye Üzerine Uygulamaları*, Istanbul-Turkey, 2014.

130. Altinsoy, H., A. Aslantaş, O. Doğru, H. Kılınç and K. Kadiroğulları, *Ofis Ortamındaki Odaların Sıcaklıklarına Göre Gruplandırılması*, Istanbul-Turkey, 2014.

131. Altinsoy, H., *Türkiye'de Ölçülen Sicaklik Ve Bağil Nem Verilerinin Analizi*, Istanbul-Turkey, 2014.

132. Altinsoy, H. and H. A. Yildirim, *Türkiye'nin Batisindaki Işçi Verimliliğinin Projeksiyonu*, Istanbul-Turkey, 2014.

133. Altinsoy, H. and H. A. Yildirim, *Türkiye'nin Sel Kaynaklı Önlenemeyen İş*

Kazaları Risk Haritası, Istanbul-Turkey, 2014.

134. Kadiroğulları, K., H. Altınsoy, O. Doğru and A. Aslantaş, *Ofis Ortamında Kişi Başına Ortalama WBGT Hesaplanması*, Istanbul-Turkey, 2014.

135. Ozturk, T., H. Altinsoy, M. Turkes and M. L. Kurnaz, "Simulation of Temperature and Precipitation Climatology for the Central Asia Cordex Domain by Using RegCM 4.0", *Climate Research*, Vol. 52,63-76, 2012.

136. Bedia, J., S. Herrera, A. Camia, J. M. Moreno and J. M. Gutiérrez, "Forest fire danger projections in the Mediterranean using ENSEMBLES regional climate change scenarios", *Climatic Change*, Vol. 122(1-2), 185-199, 2014.

137. ÇSGB, *Çalışanların Gürültü ile İlgili Risklerden Korunmalarına Dair Yönetmelik*, 2013, `http://www.resmigazete.gov.tr/eskiler/2013/07/20130728-11.htm`, accessed at June 2018.

138. ÇSGB, *Çalışanların Titreşim ile İlgili Risklerden Korunmalarına Dair Yönetmelik*, 2013, `http://www.resmigazete.gov.tr/eskiler/2013/08/20130822-2.htm`, accessed at June 2018.

139. ÇSGB, *Tozla Mücadele Yönetmeliği*, 2013, `http://www.resmigazete.gov.tr/eskiler/2013/11/20131105-9.htm`, accessed at June 2018.

140. ÇSGB, *İş Hijyeni Ölçüm Test ve Analizi Yapan Laboratuvarlar Hakkında Yönetmelik*, 2013, `http://www.resmigazete.gov.tr/eskiler/2013/08/20130820-3.htm`, accessed at June 2018.

141. Altinsoy, H. and H. A. Yıldırım, "Doğu Akdeniz Bölgesindeki Hırham Modeli Sonuçlarının İşçi Verimliliği Projeksiyonu", *3. TÜRKİYE İKLİM DEĞİŞİKLİĞİ KONGRESİ TİKDEK2013*, Vol. 3−5 Haziran,2013,İtü, İstanbul, 2013.

142. NIOSH, *Criteria for a Recommended Standard: Occupational Exposure to Hot*

Environments (Revised Criteria 1986), National Institute for Occupational Safety and Health, Washington DC, 1986.

143. Moran, D. S., Y. Shapiro, Y. Epstein and *et al.*, *A modified discomfort index (MDI) as an alternative to the wet bulb globe temperature (WBGT)*, Environmental Ergonomics 8, J.A. Hodgdon and J.H. Heaney and M.J. Buono (Eds.), 1998.

144. Altinsoy, H. and H. A. Yildirim, "Labor productivity losses over western Turkey in the twenty−first century as a result of alteration in WBGT", *International journal of biometeorology*, Vol. 59.4,463−471, 2015.

145. Kjellstrom, T., R. S. Kovats, S. J. Lloyd, T. Holt and R. S. J. Tol, "The direct impact of climate change on regional labor productivity", *Arch Environ Occup Health*, Vol. 64(4):217–227, 2009.

146. Pandolf, S. D. M. K. B., Y. Shapiro and *et al.*, "An environmental stress index (ESI) as a substitute for the wet bulb globe temperature (WBGT)", *Journal of Thermal Biology*, Vol. 26.4: 427−431, 2001.

147. Pandolf, D. S. M. K. B., A. Vitalis and *et al.*, "Evaluation of the environmental stress index (ESI) for the southern hemisphere", *Journal of Thermal Biology*, Vol. 29.7: 535−538, 2004.

148. Moran, D. S., K. B. Pandolf, Y. Shapiro and *et al.*, "Evaluation of the environmental stress index for physiological variables", *Journal of thermal biology*, Vol. 28.1: 43−49, 2003.

149. Gubernot, D. M., G. B. Anderson and K. L. Hunting, "The epidemiology of occupational heat exposure in the United States: a review of the literature and assessment of research needs in a changing climate", *International journal of biometeorology*, Vol. 58.8:1779−1788, 2014.

150. Tanaka, M., "Heat stress standard for hot work environments in Japan", *Industrial health*, Vol. 45.1: 85−90, 2007.

151. Haruyama, Y., Y. Muto, H. Matsuzuki and *et al.*, "Evaluation of subjective thermal strain in different kitchen working environments using subjective judgment scales", *Industrial health*, Vol. 48.2:135−144, 2010.

152. Islam, M. Z., *Influence of gender on heart rate and core temperature at critical wbgt for five clothing ensembles at three levels of metabolic rate*, Ph.D. Thesis, Unıversıty of South Florida, 2005.

153. Öztürk, T., H. Altınsoy, M. Türkeş and M. L. Kurnaz, "Simulation of Temperature and Precipitation Climatology for the Central Asia Cordex Domain by Using RegCM 4.0", *Climate Research*, Vol. 52, 63−76, 2012.

154. Bi, P., S. Loughnan, M. Lloyd and *et al.*, "The effects of extreme heat on human mortality and morbidity in Australia: implications for public health", *Asia−Pacific Journal of Public Health*, Vol. doi:1010539510391644, 2011.

155. Kerslake, D. M., *The stress of hot environments(no.29)*, Cambridge University Press, UK, 1972.

156. Ramsey, J., "Effects of workplace thermal conditions on safe working behaviour", *J Saf Res*, Vol. 14:105–114, 1983.

157. Dawson, N., *Body temperature and exercise performance*, The Physiological Challenge, Auckland, 1993.

158. Lundgren, K., K. K. and V. Venugopal, "Occupational heat stress and associated productivity loss estimation using the PHS model (ISO 7933): a case study from workplaces in Chennai, India", *Global health action*, Vol. 7, 2014.

159. Kjellstrom, T., T. Lembe, B. Hyatt and *et al.*, "Climate change and occupational

health: A South African perspective", *SAMJ: South African Medical Journal*, Vol. 104.8:586−587, 2014.

160. Rowlinson, S. and A. J. Yunyan, "Construction accident causality: An institutional analysis of heat illness incidents on site", *Safety Science*, Vol. 78:179−189, 2015.

161. Pryor, R. R., D. J. Casa, J. C. Holschen and *et al.*, "Exertional heat stroke: strategies for prevention and treatment from the sports field to the emergency department", *Clinical Pediatric Emergency Medicine*, Vol. 14.4:267−278, 2013.

162. Burke, L. M., "Nutritional needs for exercise in the heat", *Comparative Biochemistry and Physiology Part A: Molecular and Integrative Physiology*, Vol. 128.4:735−748, 2001.

163. Sahu, S., S. Moumita and T. Kjellstrom, "Heat exposure, cardiovascular stress and work productivity in rice harvesters in India: implications for a climate change future", *Industrial health*, Vol. 51.4:424−431, 2013.

164. Lan, L., W. Pawel and L. Zhiwei, "Quantitative measurement of productivity loss due to thermal discomfort", *Energy and Buildings*, Vol. 43.5:1057−1062, 2011.

165. Kosonen, R. and F. Tan, "The effect of perceived indoor air quality on productivity loss", *Energy and Buildings*, Vol. 36.10:981−986, 2004.

166. Sawka, M. N., J. M. Scott and A. L. William, "Hydration effects on thermoregulation and performance in the heat", *Comparative Biochemistry and Physiology Part A: Molecular and Integrative Physiology*, Vol. 128.4:679−690, 2001.

167. Burke, L. M., "Nutritional needs for exercise in the heat", *Comparative Biochemistry and Physiology Part A: Molecular and Integrative Physiology*, Vol. 128.4:735−748, 2001.

168. Horie, S., "Prevention of heat stress disorders in the workplace", *JMAJ*, Vol. 56:186−192, 2013.

169. Cortez, O. D., "Heat stress assessment among workers in a Nicaraguan sugarcane farm", *Global Health Action*, Vol. 2, 2009.

170. Wesseling, J. C. C., B. R. Solano and *et al.*, "Heat exposure in sugarcane harvesters in Costa Rica", *American journal of industrial medicine*, Vol. 56.10:1157−1164, 2013.

171. Hargreaves, M., "Physiological limits to exercise performance in the heat", *Journal of Science and Medicine in Sport*, Vol. 11.1:66−71, 2008.

172. Tian, Z., N. Zhu, G. Zheng and *et al.*, "Experimental study on physiological and psychological effects of heat acclimatization in extreme hot environments", *Building and Environment*, Vol. 46.10:2033−2041, 2011.

173. Lan, L., Z. Lian, L. Pan and *et al.*, "Neurobehavioral approach for evaluation of office workers' productivity: The effects of room temperature", *Building and Environment*, Vol. 44.8:1578−1588, 2009.

174. Nag, P. K., D. Priya and N. Anjali, "Critical body temperature profile as indicator of heat stress vulnerability", *Industrial health*, Vol. 51.1:113−122, 2013.

175. Ayyapan, R., S. Sankar, P. Rajkumar and *et al.*, "Work−related heat stress concerns in automotive industries: a case study from Chennai, India", *Global Health Action*, Vol. 2, 2009.

176. Arbury, S., B. Jacklitsch, O. Farquah and *et al.*, "Heat illness and death among workers−United States, 2012−2013", *Morbidity and Mortality Weekly Report*, Vol. 63:661−665, 2014.

177. Adelakun, A., "Occupational heat exposure", *Applied occupational and environ-*

mental hygiene, Vol. 14.3:153−154, 1999.

178. Sett, M. and S. Subhashis, "Effects of occupational heat exposure on female brick workers in West Bengal, India", *Global health action*, Vol. 7, 2014.

179. Hunt, A. P., A. W. Parker and I. B. Stewart, "Symptoms of heat illness in surface mine workers", *International archives of occupational and environmental health*, Vol. 86.5:519−527, 2013.

180. Wallace, R. F., D. Kriebel, L. Punnett and *et al.*, "Prior heat illness hospitalization and risk of early death", *Environmental Research*, Vol. 104.2:290−295, 2007.

181. Noakes, T. D., "A modern classification of the exercise−related heat illnesses", *Journal of Science and Medicine in Sport*, Vol. 11.1:33−39, 2008.

182. Perry, A. G., M. J. Korenberg, G. G. Hall and *et al.*, "Modeling and syndromic surveillance for estimating weather−induced heat−related illness", *Journal of environmental and public health*, Vol. 2011, 2011.

183. Lu, S. and Z. Neng, "Experimental research on physiological index at the heat tolerance limits in China", *Building and Environment*, Vol. 42.12:4016−4021, 2007.

184. Zhao, J., Z. Neng and L. Shilei, "Productivity model in hot and humid environment based on heat tolerance time analysis", *Building and environment*, Vol. 44.11:2202−2207, 2009.

185. Yi, W. and A. P. Chan, "Optimizing work–rest schedule for construction rebar workers in hot and humid environment", *Building and Environment*, Vol. 61:104-113, 2013.

186. Dash, S. K. and T. Kjellstrom, "Workplace heat stress in the context of rising

temperature in India", *Current Science*, Vol. 101.4496−503, 2011.

187. Langkulsen, U., V. Nuntavarn and T. Sasitorn, "Health impact of climate change on occupational health and productivity in Thailand", *Global Health Action*, Vol. 3, 2010.

188. Bricknell, M. C. M., "Heat illness in the army in Cyprus", *Occupational medicine*, Vol. 46.4304−312, 1996.

189. Chad, K. E. and J. M. M. Brown, "Climatic stress in the workplace: its effect on thermoregulatory responses and muscle fatigue in female workers", *Applied ergonomics*, Vol. 26.1:29−34, 1995.

190. Yamamoto, S., M. Iwamoto, M. Inoue and *et al.*, "Evaluation of the effect of heat exposure on the autonomic nervous system by heart rate variability and urinary catecholamines", *Journal of occupational health*, Vol. 49.3:199−204, 2007.

191. Lan, L., L. Zhiwei and L. Pan, "The effects of air temperature on office workers' well−being, workload and productivity−evaluated with subjective ratings", *Applied ergonomics*, Vol. 42.1:29−36, 2010.

192. Niemelä, R., M. Hannula, S. Rautio and *et al.*, "The effect of air temperature on labour productivity in call centres−a case study", *Energy and Buildings*, Vol. 34.8:759−764, 2002.

193. Chan, A. P. C., W. Yi, D. P. Wong and *et al.*, "Determining an optimal recovery time for construction rebar workers after working to exhaustion in a hot and humid environment", *Building and environment*, Vol. 58:163−171, 2012.

194. Chen, M. L., C. J. Chen, W. Y. Yeh and *et al.*, "Heat stress evaluation and worker fatigue in a steel plant", *AIHA Journal*, Vol. 64.3:352−359, 2003.

195. Jay, O. and P. K. Glen, "Heat exposure in the Canadian workplace", *American*

journal of industrial medicine, Vol. 53.8:842−853, 2010.

196. Gomes, J., O. Lloyd and N. Norman, "The health of the workers in a rapidly developing country: effects of occupational exposure to noise and heat", *Occupational medicine*, Vol. 52.3:121−128, 2002.

197. Singh, L. P., A. Bhardwaj, K. K. Deepak and *et al.*, "Occupational heat exposure in extreme weather conditions in small and medium enterprises (SME) in India", *International journal of human geography and environmental studies*, Vol. 1.1:32−38, 2009.

198. Ismail, A. R., M. R. A. Rani, Z. K. M. Makhbul and *et al.*, "A study of relationship between wbgt and relative humidity to worker performance", *World Academy of Science, Engineering and Technology*, Vol. 51:209−214, 2009.

199. Biradar, C. I. and P. Naveen, "Study of Occupational Risks to Personnel in an Air Force Station", *Ind J Aerospace Med*, Vol. 57:2, 2013.

200. Nag, P. K., P. Dutta and A. Nag, "Industrial health", *Critical body temperature profile as indicator of heat stress vulnerability*, Vol. 51.1:113−122, 2013.

201. A., M. and J. Rukijkanpanich, "A participatory approach to health promotion for informal sector workers in Thailand", *Journal of injury and violence research*, Vol. 2.2:111, 2010.

202. Bernard, T. E. and R. R. Cross, "Heat stress management: Case study in an aluminum smelter", *International journal of industrial ergonomics*, Vol. 23:5-6: 609-620, 1999.

203. Logan, P. W. and T. E. Bernard, "Heat stress and strain in an aluminum smelter", *American Industrial Hygiene Association Journal*, Vol. 60.5:659−665, 1999.

204. Leung, M., I. Y. S. Chan and J. Yu, "Preventing construction worker injury in-

cidents through the management of personal stress and organizational stressors", *Accident Analysis and Prevention*, Vol. 48:156−166, 2012.

205. ECA&D, *ECA&D Project E-OBS Data Set*, 2018, `http://www.ecad.eu`, accessed at June 2018.

206. ENSEMBLES, *ENSEMBLES Project Data Set*, 2009, `http://ensembles-eu.metoffice.com`, accessed at June 2018.

207. Adam, J. C. and D. P. Lettenmaier, "Adjustment of global gridded precipitation for systematic bias", *Journal of Geophysical Research: Atmospheres*, Vol. 108(D9), 2003.

208. Harris, I. P. D. J., P. D. Jones, T. J. Osborn and D. H. Lister, "Updated high−resolution grids of monthly climatic observations−the CRU TS3.10 Dataset", *International Journal of Climatology*, Vol. 34(3), 623-642, 2014.

209. Levent, K. M. and H. Altınsoy, *Correlation Analysis of Housing Prices and Economic Indicators: An application of econophysics to housing prices*, Lambert Academic Publishing, Germany, 2009.

210. Epstein, Y. and D. S. Moran, "Thermal comfort and the heat stress indices", *Ind Health*, Vol. 44(3):388–398, 2006.

211. Youglou, C. P. and D. Minard, "Control of heat casualties at military training centers", *AMA Arch Ind Health*, Vol. 16(4):302-316, 1957.

212. ACSM, "Prevention of thermal injuries during distance running", *American College Sports Medicine Medical J Australia*, Vol. 141:876-879, 1984.

213. Kjellstrom, T., I. Holmer and B. Lemke, "Workplace heat stress, health and productivity−an increasing challenge for low and middleincome countries during climate change", *Global Health Action*, Vol. 2, 2009.

214. ISO, "Hot environments estimation of the heat stress on working man, based on the WBGT−index (wet bulb globe temperature). ISO Standard 7243", *International Standards Organization*, Vol. Geneva, 1989.